The role of individual subunits in the formation and function of presynaptic Kv3 potassium channels

Thesis submitted for the degree of
Doctor of Philosophy
at the University of Leicester

By

Amy Richardson BSc

Department of Neuroscience, Psychology and Behaviour
University of Leicester

September 2019

0.1 Abstract

The role of individual subunits in the formation and function of presynaptic Kv3 potassium channels

Amy Richardson

Kv3 potassium channels, composed of four subunits, mediate fast action potential (AP) repolarisation. In the auditory brainstem they enable neurons to faithfully follow high-frequency sound stimuli with temporal precision, vital for binaural integration and sound localisation. Of four Kv3 subunits, only Kv3.1 and Kv3.3 are present in the auditory brainstem. A neurodegenerative disease (spinocerebellar ataxia type 13, SCA13) associated with impaired sound localisation, is caused by mutations of Kv3.3, highlighting the importance of these subunits in this system.

The contributions of specific subunits to pre and post- synaptic Kv3 channels was examined in this thesis, with a particular focus given to presynaptic Kv3 channels (at the giant calyx of Held terminal) and their ability to modulate transmitter release from the synapse. Whole-cell patch clamp was conducted on *in vitro* brainstem slices from wildtype, Kv3.1 and Kv3.3 knockout mice, in combination with histology. Experiments were repeated in mice harbouring an SCA13 mutation (R420H) that has been linked with auditory deficits in humans. Lastly, whole-cell patch clamp was used in expression systems to determine whether different Kv3 subunits could form heteromers.

These studies showed Kv3.1 and Kv3.3 had equal importance for AP repolarisation in neurons of the medial nucleus of the trapezoid body (MNTB) while Kv3.3 subunits dominated in neurons of the lateral superior olive (LSO) and at the presynaptic calyx of Held terminal. Kv3.3 was required at this synapse to limit AP duration, preventing excessive transmitter release, particularly during high-frequency stimulation. AP durations in MNTB and LSO neurons of the SCA13 mouse model were identical to those in Kv3.3 knockouts showing that the edited subunits do not form functional channels. Lastly, co-expression studies in CHO cells revealed that Kv3.3 subunits can form heteromeric channels with Kv3.1 but not with Kv3.4.

0.2 Acknowledgements

Firstly, I would like to thank both of my supervisors, Ian for giving me the opportunity to conduct this research, for his guidance, enthusiasm and useful discussion throughout the whole PhD. Secondly, Vincenzo for his endless patience, kindness and willingness to answer every one of the countless questions that I asked. I truly appreciate the time you have both dedicated to teaching me and the knowledge I have gained from you during the past four years.

I'd also like to thank the members of Autifony Therapeutics who made me feel incredibly welcome and part of a family during my three-month stay in Italy. Thanks in particular to Manuela for teaching me cell culture, Michele for his help with electrophysiology and to Nadia for her guidance throughout the project.

Thank you to the various lab members that have come and gone in the past 4 years and made life in the lab enjoyable. In particular Sherylanne Newton, for providing not only a lot of laughs but also a strong role model when I started my PhD and Michelle Anderson for her constant encouragement (both inside the lab and out) and for her help with immunohistochemistry. Additionally, the members of office 330, past and present for providing me with cake and good company.

Lastly, I'd like to thank my family for their endless support and encouragement, without whom I wouldn't have made it this far, my brother for providing the competitive drive needed to motivate me throughout, and the BBSRC and Autifony Therapeutics Srl for the funding that made this project possible.

0.3 Declarations

The work presented throughout this thesis is my own unless declared otherwise. Below is a summary of work contributed by others:

- Some immunohistochemistry images used throughout this thesis were taken by Michelle Anderson using a confocal microscope although the immunohistochemistry and analysis was performed by myself.
- Immunohistochemistry performed by Sherylanne Newton using Kv3.2 and Kv3.4 is presented in chapter 1.
- ABRs performed on knockout mice discussed in chapter 3 were done by Sherylanne Newton in my presence.
- Immunohistochemistry and co-immunoprecipitation performed on CHO cells was done with the help of Manuela Marabita at Autifony Therapeutics
- Some electrophysiology recordings performed on CHO cells were done by Michele Speggiorin at Autifony Therapeutics, although all analysis was done by myself.

Contents

0.1 Abstract 1

0.2 Acknowledgements 2

0.3 Declarations 3

0.4 List of Abbreviations 19

1 Introduction **21**

1.1 Anatomy of the auditory brainstem 22

1.2 Function of the Superior Olivary Complex (SOC) 23

1.3 Medial Nucleus of the Trapezoid Body (MNTB) 24

1.4 Calyx of Held 24

1.5 Ionic conductances at the Calyx of Held terminal 26

1.6 Lateral superior olive (LSO) 26

1.7 Medial superior olive (MSO) 27

1.8 Sound localisation 27

1.9 Potassium channel structure and function 30

1.10 Kv channel activation 33

1.11 Kv channel function 33

1.12 Kv channel inactivation 34

1.13 High-voltage activated Kv3 channels 35

1.14 Tissue expression of Kv3 subunits 36

1.15 Regulation of Kv3 activity 36

1.16 Kv3 pharmacology 37

1.17 Kv3 in the auditory brainstem 38

1.18 Kv3 in disease 39

1.19 Synaptic transmission at the calyx of Held 40
1.20 Glutamate receptors at the Calyx-MNTB synapse 43
1.21 Glycine receptors at the MNTB-LSO synapse 43
1.22 Hypothesis 44

2 Methods **45**

2.1 Experimental animals 45
2.2 Genotyping 46
2.2.1 Genotyping solutions 46
2.2.2 Genotyping protocol 46
2.3 Cell culture 48
2.3.1 Solutions 48
2.3.2 Defrosting cells 48
2.3.3 Seeding and counting cells 49
2.3.4 CHO cell tranfection with Kv3 plasmids 49
2.4 Immunohistochemistry 50
2.4.1 Solutions 51
2.4.2 Protocol 52
2.4.3 Analysis 54
2.4.4 Immunohistochemistry of CHO cells 54
2.5 Western blotting 54
2.5.1 Solutions (Brain tissue) 55
2.5.2 Protein extraction (brain tissue) 56
2.5.3 Running and transferring gels 57
2.5.4 Antibody labelling 57
2.5.5 Protein extraction for CHO cells 60
2.5.6 Running and transferring (CHO) 60
2.6 Coimmunoprecipitation (Co-IP) 61
2.6.1 Protocol 61
2.7 Patch clamp electrophysiology 63
2.7.1 Electrical properties of a cell 63

2.7.2 Recording apparatus 64
2.7.3 Recording circuitry - operational amplifier 65
2.7.4 The problem of series resistance 65
2.7.5 Liquid junction potential 67
2.7.6 Solutions 68
2.7.7 Brain slice preparation 70
2.7.8 Whole cell patch clamp 70
2.7.9 Analysis 71
2.8 Statistics 72

3 Kv3 channels in the superior olivary complex (SOC) are composed of Kv3.3 and Kv3.1 73

3.1 Immunohistochemical labelling (IHC) of Kv3 subunits in the SOC . . 75
3.2 Kv3 potassium currents in the MNTB and LSO 77
3.3 Contribution of Kv3.1 and Kv3.3 subunits to Kv3 current in the MNTB and LSO 82
3.4 Histological validation of knockout mice 84
3.5 Discussion 87
3.5.1 MNTB and LSO neurons possess significant Kv3 currents . . . 87
3.5.2 Kv3 subunit composition in the MNTB 88
3.5.3 Kv3 subunit composition in the LSO 89
3.5.4 Subcellular targeting of Kv3.1b and Kv3.3 89
3.5.5 Subcellular distribution of Kv3.1 and Kv3.3 may reflect different molecular interactions 90
3.5.6 Heteromers vs homomers 90
3.5.7 Both Kv3.1 and Kv3.3 contribute to fast AP repolarisation in the MNTB 91
3.5.8 Why are expression patterns of Kv3.1 and Kv3.3 in the MNTB and LSO different? 91
3.5.9 Contribution by Kv3.1a 93
3.5.10 No functional protein is present in either knockout 94

3.5.11 Summary 95

4 Kv3 channels in the calyx of Held terminal 96

4.1 Methods 97

4.2 Kv3 currents in the calyx of Held terminal 99

4.3 Kv3 currents modulate presynaptic action potential waveform 101

4.4 Kv3.1 and Kv3.3 subunits are present in the calyx of Held terminal . 105

4.5 Contribution of Kv3.1 and Kv3.3 to presynaptic action potential repolarisation 109

4.6 Discussion 113

4.6.1 Calyces possess TEA-sensitive currents 113

4.6.2 Kv3 channels are responsible for modulating presynaptic AP waveform 114

4.6.3 Subunits forming presynaptic Kv3 channels 115

4.7 summary 117

5 The role of presynaptic Kv3 channels in modulating synaptic transmission 118

5.1 Methods 120

5.2 Simultaneous recordings at the calyx-MNTB synapse 123

5.3 EPSCs at the MNTB are AMPA-mediated 124

5.4 EPSC amplitudes are larger in Kv3.3 KO animals 126

5.5 Blocking presynaptic Kv3 has a smaller effect on EPSC amplitude in Kv3.3 KO animals 128

5.6 Short term depression of EPSC amplitudes is much quicker and larger in Kv3.3 KO mice 131

5.7 Quantal amplitudes are decreased in Kv3.3 KO mice 142

5.8 Changes in the rate of vesicle replenishment were not observed in Kv3.1 KOs 147

5.9 The tonotopic gradient of the MNTB does not influence transmitter release in CBA WT, Kv3.3 KOs or Kv3.1 KOs 152

5.10 Kv3.3 subunits appear to dominate at other auditory synapses 154
5.11 Discussion 156
5.11.1 EPSCs in adult MNTB neurons are incredibly rapid 156
5.11.2 Kv3.3 subunits are required to sustain high frequency transmission at the calyx of Held 157
5.11.3 The mystery of resistance to synaptic depression in Kv3.1 KO animals 159
5.12 Importance of Kv3.3 subunits appears to hold true at other auditory synapses 160
5.13 Consequences on auditory function 161
5.14 Summary 164

6 Kv3.3 and spinocerebellar ataxia type 13 (SCA13) 165

6.1 Potassium currents in MNTB and LSO neurons expressing Kv3.3^{R420H} are similar to those in the Kv3.3 KO 167
6.2 Action potential duration is increased in MNTB and LSO neurons of Kv3.3^{R420H} mice 170
6.3 EPSCs at the calyx-MNTB synapse of Kv3.3^{R420H} mice are large and resistant to short term depression 173
6.4 Potassium currents are increased in MNTB neurons of old Kv3.3^{R420H} mice 176
6.5 Action potential duration is unchanged in neurons of the MNTB and LSO of old Kv3.3^{R420H} mice 179
6.6 Kv3.1b and Kv3.3 subunit protein expression increases with age . . . 181
6.7 Discussion 183
6.7.1 The Kv3.3^{R420H} mutation produces current and action potentials identical to those in Kv3.3 KOs 183
6.7.2 Why is there no Kv3.3 current in Kv3.3^{R420H} mice? 184
6.7.3 Age-dependent changes in Kv3 channels of the MNTB and LSO 187
6.7.4 Changes to AP cannot account for decreased auditory function in old Kv3.3 KO mice 188

6.7.5 Age-dependent increase in Kv3 protein expression 189
6.7.6 High frequency transmission is enhanced in Kv3.3^{R420H} mice . 189
6.8 Summary 190

7 Can Kv3 subunits form heteromeric channels? 191

7.1 Methods 193
7.2 Kinetics of Kv3.3 channels 194
7.2.1 Activation 194
7.2.2 Steady-state inactivation 197
7.3 Kinetics of Kv3.1b channels 198
7.3.1 Activation 199
7.3.2 Steady-state inactivation 201
7.4 Kinetics of Kv3.4a channels 202
7.4.1 Activation 202
7.4.2 Steady-state inactivation 202
7.5 Co-expression of Kv3.3 and Kv3.4a 205
7.5.1 Kv3.3-like cells 206
7.5.2 Kv3.4-like cells 208
7.5.3 Kv3.3 + Kv3.4 cells 210
7.5.4 Kv3.3/Kv3.4 fast 214
7.5.5 Kv3.3/Kv3.4 slow cells 217
7.5.6 Kv3.4 does not co-immunoprecipitate with Kv3.3 221
7.5.7 Kv3.3 and Kv3.4 are not colocalised 223
7.6 Co-expression of Kv3.3 and Kv3.1b 224
7.6.1 Steady-state inactivation 228
7.6.2 Kv3.1 co-immunoprecipitates with Kv3.3 230
7.7 Discussion 232
7.7.1 Properties of Kv3.3, Kv3.1b and Kv3.4a homomeric channels 232
7.7.2 Do Kv3.3 subunits form heteromeric channels? 233
7.8 Summary 235

8 Final conclusions and future directions **236**

8.1 Main findings 237

8.2 Role of Kv3 channels in cell excitability 238

8.3 Role of Kv3 in modulating transmission 238

8.4 Kv3 channel composition in auditory brainstem neurons 240

8.5 SCA13 mouse model 241

8.6 Limitations 242

8.7 Future directions 243

8.7.1 Chapter 3 243

8.7.2 Chapter 4 and 5 244

8.7.3 Chapter 6 244

8.7.4 Chapter 7 245

9 References **246**

List of Tables

2.1 **Primary antibody concentrations used in immunohistochemistry and western blotting** 58

2.2 **Secondary antibody concentrations used in immunohistochemistry and western blotting** 59

2.3 **Primary antibody and IgG isotype volumes used in co-IP** . . 62

2.4 **Composition of normal and slicing artificial cerebrospinal fluid (acsf)** 69

2.5 **Composition of intracellular patch solution for K^+ recordings** 69

5.1 **EPSC parameters in CBA wildtype, Kv3.3 KO and Kv3.1 KO animals in response to 100, 200 or 600Hz stimulation.** . . 138

5.2 **Percentage of cells recorded from in each part of the MNTBs tonotopic axis** 153

5.3 **Initial EPSC amplitudes in cells recorded from the medial, middle and lateral portions of the MNTB** 153

7.1 **CHO cells co-expressing hKv3.3 an hKv3.4a can be divided into 5 distinct populations based on their current kinetics.** . 205

List of Figures

1.1 **Schematic depicting nuclei of the superior olivary complex (SOC) and their projections.** 23

1.2 **Giant Calyx of Held synapse in the medial nucleus of the trapezoid body (MNTB).** 25

1.3 **Interaural timing and level differences used for binaural processing arise due to the separation of ears on either side of the head.** 28

1.4 **Response profiles of neurons in the lateral and medial superior olive (LSO and MSO) in response to binaural inputs.** . . 29

1.5 **Divisions of potassium channel subunits based on number of transmembrane domains (TMDs).** 31

1.6 **Structure of a Kv subunit.** 32

1.7 **Current kinetics of delayed rectifying Kv channels.** 34

1.8 **Kv3 currents recorded from CHO cells expressing human Kv3.1b, 3.2, 3.3d or 3.4a.** 35

1.9 **Only Kv3.1 and Kv3.3 subunits are present in the medial nucleus of the trapezoid body (MNTB) and lateral superior olive (LSO).** 39

1.10 **Vesicle pools at the calyx of Held** 42

2.1 **Bürker grid for counting cells.** 50

2.2 **Components of the electrophysiology set-up.** 65

2.3 **Simplified diagram of amplifier circuit connected to a cell during whole cell patch clamp.** 66

2.4 **Effect of series resistance on membrane potential (V_m).** . . . 68

3.1 **Kv3.3 and Kv3.1 are expressed in MNTB neurons but only Kv3.3 is present in the LSO soma.** . . . 76
3.2 **Kv3.2 and Kv3.4 are absent in the MNTB.** . . . 77
3.3 **Analysis of paired TEA perfusion experiments.** . . . 78
3.4 **MNTB principal neurons possess a TEA-sensitive current.** . . . 79
3.5 **Potassium current amplitudes in MNTB neurons do not change with time** . . . 80
3.6 **LSO neurons possess a TEA-sensitive current.** . . . 81
3.7 **Potassium current amplitudes in LSO neurons do not change with time.** . . . 81
3.8 **Potassium currents in MNTB neurons are not changed in Kv3.3 and Kv3.1 KO mice aged P21-P25.** . . . 83
3.9 **Potassium currents in LSO principal neurons are decreased in Kv3.3 KO mice but not Kv3.1 KOs.** . . . 83
3.10 **Kv3.1b and Kv3.3 protein is absent in Kv3.1 and Kv3.3 KOs, respectively.** . . . 85
3.11 **No Kv3.1b or Kv3.3 staining is observed in Kv3.1 and Kv3.3 KO mice, respectively.** . . . 86
3.12 **Action potential duration is increased in MNTB and LSO neurons of Kv3.1 KO and Kv3.3 KO mice.** . . . 92

4.1 **Calyx of Held terminals of mice possess a TEA-sensitive K^+ current** . . . 100
4.2 **TEA decreases the afterhyperpolarisation amplitude of action potentials at the calyx of Held.** . . . 102
4.3 **1mM TEA increases action potential duration at the calyx terminal.** . . . 103
4.4 **TEA significantly increases AP rise and decay times in the calyx terminal.** . . . 104

4.5 **Kv3.1b and Kv3.3 are present in the presynaptic calyx terminal.** . . . 106
4.6 **Both Kv3.1b and Kv3.3 colocalise with presynaptic marker.** 107
4.7 **Presynaptic expression of Kv3.1b and Kv3.3 does not change in Kv3.3 and Kv3.1 KO mice, respectively.** . . . 108
4.8 **Afterhyperpolarisation amplitude of action potentials is decreased in Kv3.3 KO mice.** . . . 110
4.9 **Presynaptic AP duration is significantly increased in Kv3.3 KOs but not Kv3.1 KOs.** . . . 112

5.1 **Placement of stimulation electrode for EPSC and IPSC recordings in MNTB and LSO, respectively.** . . . 122
5.2 **Simultaneous recordings from the calyx of Held terminal and an MNTB principal neuron in a brainstem section of a CBA wildtype mouse aged P11.** . . . 124
5.3 **EPSCs recorded from MNTB neurons of adult mice are fast with large amplitudes.** . . . 125
5.4 **EPSCs recorded from MNTB neurons are AMPA-dependent.** 125
5.5 **EPSC amplitudes are larger in Kv3.3 KO mice.** . . . 127
5.6 **Block of presynaptic Kv3 channels by 1mM TEA is smaller in Kv3.3 KO mice.** . . . 129
5.7 **Blocking BK channels has no effect on EPSC amplitude.** . . . 130
5.8 **High frequency stimulation train protocol.** . . . 132
5.9 **EPSC responses in MNTB neurons of Kv3.3 KO animals show faster short term depression during 100, 200 and 600Hz stimulation.** . . . 134
5.10 **Short term depression of EPSC amplitudes in increased in Kv3.3 KOs and decreased in Kv3.1 KOs.** . . . 137
5.11 **Increase in asynchronous release in Kv3.3 KOs during 600Hz stimulation.** . . . 139
5.12 **Total vesicle release is increased in Kv3.1 KOs.** . . . 140

5.13 **The readily releasable vesicle pool (RRP) is unchanged in Kv3.3 and Kv3.1 KOs.** . . . 141
5.14 **Miniature excitatory post-synaptic currents recorded in MNTB neurons of CBA wildtype, Kv3.3 KO and Kv3.1 KO mice.** . 144
5.15 **mEPSC amplitude is decreased in Kv3.3 KOs.** . . . 146
5.16 **Recovery curve stimulation protocol.** . . . 148
5.17 **Recovery of EPSC amplitudes after high-frequency stimulation occurs within 10s.** . . . 150
5.18 **Recovery from short term depression in EPSC amplitude occurs at a faster rate in Kv3.3 KO mice.** . . . 151
5.19 **Position of recorded neurons in the tonotopic map of the MNTB.** . . . 152
5.20 **1mM TEA does not affect IPSC amplitudes in Kv3.3 KO mice.** . . . 155
5.21 **Kv3.3 KOs display decreased wave IV amplitude in auditory brainstem response recordings (ABRs) at 24kHz.** . . . 163

6.1 **Mutations in the Kv3.3 subunit identified in Spinocerebellar ataxia type 13.** . . . 166
6.2 **Potassium currents are unchanged in MNTB neurons expressing Kv3.3^{R420H} subunits.** . . . 168
6.3 **Potassium currents are dramatically reduced in LSO neurons expressing Kv3.3^{R420H} subunits.** . . . 169
6.4 **Action potentials are significantly longer in MNTB neurons of Kv3.3^{R420H} mice.** . . . 171
6.5 **Action potential duration is significantly increased in LSO neurons of Kv3.3^{R420H} mice.** . . . 172
6.6 **EPSC amplitudes are significantly larger in MNTB neurons of Kv3.3^{R420H} mice.** . . . 174
6.7 **EPSC amplitudes in the MNTB of Kv3.3^{R420H} mice are resistant to short-term depression** . . . 175

6.8 **Potassium currents in MNTB neurons of Kv3.3^{R420H} mice were significantly increased at 6 months of age compared to young animals.** . . . 177
6.9 **Potassium currents in LSO neurons of Kv3.3^{R420H} and Kv3.3 KO mice were significantly increased at 6 months of age compared to young animals.** . . . 178
6.10 **Action potential duration in MNTB neurons does not change in old Kv3.3^{R420H} mice.** . . . 180
6.11 **Action potential duration in LSO neurons does not change in old Kv3.3^{R420H} mice.** . . . 180
6.12 **Kv3.3 and Kv3.1b expression increases with age.** . . . 182
6.13 **Kv3.3 protein is retained in the cytoplasm of MNTB but not LSO neurons in Kv3.3^{R420H} mice.** . . . 186
6.14 **No neurodegeneration is observed in Kv3.3 KOs** . . . 188

7.1 **Kv3.3 currents are partially inactivated at a holding potential of -70mV** . . . 194
7.2 **Kv3.3 currents exhibit slow-inactivation in CHO cells** . . . 196
7.3 **Activation parameters for Kv3.3 channels expressed in CHO cells** . . . 197
7.4 **Kv3.3 channels show steep steady-state inactivation in CHO cells** . . . 198
7.5 **Kv3.1b currents show very little inactivation in CHO cells** . 200
7.6 **Activation parameters for Kv3.1b channels expressed in CHO cells** . . . 200
7.7 **Kv3.1b channels show steep steady-state inactivation in CHO cells** . . . 201
7.8 **Kv3.4a channels show very fast inactivation when expressed in CHO cells** . . . 203
7.9 **Activation curve parameters for Kv3.4a channels expressed in CHO cells** . . . 203

7.10 **Kv3.4a channels completely inactivate by 0mV in CHO cells** 204
7.11 **Co-expression of Kv3.3 and Kv3.4 subunits in CHO cells generates five distinct types of Kv3 current.** 206
7.12 **Kv3.3-like cells have near identical currents to Kv3.3 WT.** . 207
7.13 **Kv3.4-like cells have identical currents to Kv3.4 WT.** 209
7.14 **Kv3.3 + Kv3.4 cells display current kinetics intermediate to both Kv3.3 and Kv3.4 WT** 211
7.15 **Inactivation of Kv3.3 + Kv3.4 currents at +50mV has three components** 212
7.16 **Steady-state currents of Kv3.3 + Kv3.4 cells are not different to those in Kv3.3 WT** 213
7.17 **Kv3.3/Kv3.4 fast cells display current kinetics similar to Kv3.4 WT** 215
7.18 **Inactivation of Kv3.3/Kv3.4 fast currents at +50mV has three components.** 216
7.19 **Kv3.3/Kv3.4 slow cells display current kinetics similar to Kv3.3 WT** 218
7.20 **Inactivation of Kv3.3/Kv3.4 slow currents at +50mV has three components.** 219
7.21 **Steady-state currents of Kv3.3/Kv3.4 slow cells are not different to those in Kv3.3 WT.** 220
7.22 **Kv3.4 protein does not co-immunoprecipitate with Kv3.3.** . . 222
7.23 **Kv3.3 and Kv3.4 subunits do not co-localise.** 223
7.24 **Kv3.1/Kv3.3 slow and fast cells display current kinetics similar to both Kv3.3 and Kv3.1 WT** 225
7.25 **Kv3.1/Kv3.3 slow cells have a similar inactivation time constant to Kv3.1 WT and Kv3.1/Kv3.3 fast cells have similar time constants to Kv3.3 WT.** 226
7.26 **Steady-state currents of Kv3.1/Kv3.3 slow and fast cells are not different to those in Kv3.3 or Kv3.1 WT** 227

7.27 **Inactivation curves of Kv3.1/Kv3.3 fast and slow cells are shifted to more negative potentials compared to both Kv3.3 and Kv3.1 WT cells.** 229
7.28 **Kv3.1b is co-immunoprecipitated with Kv3.3 in CHO cells.** . 231

0.4 List of Abbreviations

ABR - Auditory Brainstem Response

aCSF - Artificial Cerebrospinal Fluid

AHP - Afterhyperpolarisation

AIS - Axon Initial Segment

AMPA - α-amino-3-hydroxy-5-methyl-4-isoxazolepropionic acid

AR - Antigen Retrieval

aVCN - Anteroventral Cochlear Nucleus

CHO - Chinese Hamster Ovary cells

Co-IP - Co-immunoprecipitation

CN - Cochlear Nucleus

DAP - Depolarising Afterpotential

ddH_2O - Double Distilled Water

EPSC - Excitatory Postsynaptic Current

EPSP - Excitatory Postsynaptic Potential

GABA - γ- Aminobutyric Acid

GBC - Globular Bushy Cell

HRP - Horseradish Peroxidase

IC - Inferior Colliculus

ILD - Interaural Level Difference

IPSC - Inhibitory Postsynaptic Current

IPSP - Inhibitory Postsynaptic Potential

ITD - Interaural Timing Difference

Kv - Voltage-activated Potassium Channel

Kv3 - Voltage-activated potassium channel of the Kv3 family

Kv3.1 KO - CBA mouse lacking KCNC1 gene

Kv3.3 KO - CBA mouse lacking KCNC3 gene

Kv3.3^{R420H} - CBA mouse homozygous for an arginine to histidine mutation at position 420 in the KCNC3 gene

LNTB - Lateral Nucleus of the Trapezoid Body

LSO - Lateral Superior Olive

MNTB - Medial Nucleus of the Trapezoid Body

MSO - Medial Superior Olive

NMDA - N-Methyl-d-Aspartate

NoR - Nodes of Ranvier

PBS - Phosphate Buffered Saline

PBST - Phosphate Buffered Saline with 0.01% Triton X-100

PCR - Polymerase Chain Reaction

PFA - Paraformaldehyde

RNA - Ribonucleic Acid

RRP - Readily Releasable Pool

SBC - Spherical Bushy Cell

SCA13 - Spinocerebellar Ataxia Type 13

SOC - Superior Olivary Complex

SPN - Superior Paraolivary Nucleus

Tau, τ - Decay Time Constant

TBST - Tris Buffered Saline with 0.05% Tween-20

TEA - Tetraethylammonium

TMD - Transmembrane Domain

WT - Wildtype

Chapter 1

Introduction

The electrical excitability of a neuron is governed by the type of potassium channels it expresses. Expression of high voltage-activated, Kv3 potassium channels enables neurons to fire brief action potentials and sustain release of neurotransmitter at high rates. Kv3 channels are abundant in neurons of the auditory brainstem, cerebellum and fast-spiking interneurons. Within the auditory brainstem these channels are required for neurons to precisely and faithfully transmit high frequency auditory stimuli, essential for binaural processing.

Four Kv3 subunits exist (Kv3.1-3.4), encoded by the genes KCNC1-4, each with a number of isoforms. The diversity of existing subunits and isoforms in addition to the absence of specific pharmacology has meant that subunit-specific contributions to the formation and function of native Kv3 channels are not well understood.

In addition to their importance in electrical excitability, mutations in Kv3 channels have recently been linked to human neurodegenerative diseases, highlighting the importance of downstream signalling pathways of which these channels are a crucial part. In particular Kv3.1 has been linked to myoclonus epilepsy and ataxia (Muona et al. 2015) while mutations in Kv3.3 have been identified as the cause of spinocerebellar ataxia type 13 (SCA13; Waters et al. 2006).

The aim of this thesis was to investigate the composition and function of native Kv3 channels using neurons of the medial nucleus of the trapezoid body (MNTB) and lateral superior olive (LSO) within the auditory brainstem as models. A particular focus was given to understand the role of presynaptic channels in modulating

neurotransmitter release at the Calyx of Held synaptic terminal. Only two Kv3 subunits are expressed in auditory brainstem neurons, Kv3.1 and Kv3.3 and using knockout mice we aimed to dissect the contributions of these two subunits to both pre and postsynaptic Kv3 channels. The presence of only two subunits not only reduces the complexity of channel composition but when one subunit is absent in the case of knockouts, it creates a situation where only homomeric channels of a single subunit can be formed, allowing the study of a single subunit in native tissue.

In addition to investigating the composition and function of native Kv3 channels, cellular physiology of these neurons will also be examined in a mouse model harbouring a mutation within the Kv3.3 gene associated with the disease SCA13.

It is often proposed that Kv3 channels exist as heteromers in native tissue, thus the final chapter will explore the ability of different Kv3 subunits to heteromerise, using CHO cells as an expression system.

This first chapter will provide a background to topics discussed throughout this thesis including the anatomy and physiology of the auditory brainstem, Kv3 potassium channels and synaptic transmission.

1.1 Anatomy of the auditory brainstem

Sound vibrations are converted into electrical signals by hair cells of the inner ear and transmitted to the brain via spiral ganglion neurons, whose axonal branches form the vestibulocochlear nerve (VIIIth) nerve. Axons of spiral ganglion neurons terminate within the cochlear nucleus, the anterior ventral part of which (aVCN), projects to nuclei of the superior olivary complex (SOC). A number of different cell types exist in the aVCN, including spherical bushy cells (SBCs) which synapse onto the ipsilateral lateral superior olive (LSO) in addition to the ipsilateral and contralateral medial superior olive (MSO). Globular bushy cells (GBCs) instead project to the contralateral medial nucleus of the trapezoid body (MNTB; Spirou, Brownell, and Zidanic 1990) which, in turn, sends inhibitory projections to the ipsilateral MSO and LSO (Cant and Hyson 1992; figure 1.1). GBC connections to the MNTB terminate in a giant excitatory synapse known as the Calyx of Held

which ensheathes the soma of principal neurons. Neurons in each nucleus of the SOC are arranged tonotopically, such that principal neurons in more lateral portions of each nucleus respond preferentially to lower frequency stimuli whereas those in medial portions respond preferentially to higher frequencies (Sommer, Lingenhöhl, and Friauf 1993).

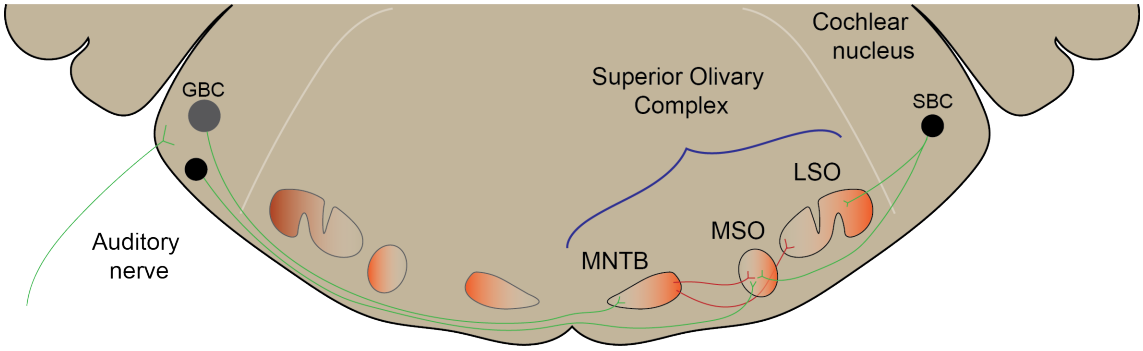

Figure 1.1: **Schematic depicting nuclei of the superior olivary complex (SOC) and their projections.** Spherical bushy cells (SBC; black circle) in the ventral cochlear nucleus (VCN) send excitatory projections to the ipsilateral lateral and medial superior olives (LSO & MSO, respectively). Globular bushy cells (GBC; grey circles) of the VCN send excitatory projections to the contralateral medial nucleus of the trapezoid body (MNTB) which in turn inhibits the ipsilateral MSO and LSO. The MNTB, LSO and MSO together form the Superior Olivary complex (also includes the superior paraolivary nucleus not shown here). Green arrows= excitatory projection; red arrows= inhibitory projections.

1.2 Function of the Superior Olivary Complex (SOC)

The SOC is the first site of binaural integration and has an important role in auditory processing, including sound source localisation and gap detection (Jenkins and Masterton 1982; Kopp-Scheinpflug et al. 2011). Neurons within the SOC are highly specialised to ensure accurate transmission of temporal information required for binaural integration. The MNTB is integral to sound localisation pathways and provides inhibition from one ear to the opposite side of the brain, essential for both processing of interaural timing (ITD) and level differences (ILD) by the MSO and LSO, respectively.

1.3 Medial Nucleus of the Trapezoid Body (MNTB)

The MNTB acts as an inhibitory relay nucleus, converting excitatory inputs from the ear to inhibitory outputs, projecting to the opposite side of the brain. Principal neurons of this nucleus are very distinct with a spherical cell soma of $\sim$20μm, very few, short dendrites and a long myelinated axon which bifurcates and projects to a number of other nuclei including the MSO and LSO (Smith, Joris, and Yin 1998; Sommer, Lingenhöhl, and Friauf 1993). Each principal cell soma is ensheathed by a single, giant, calyx of Held terminal, originating from a globular bushy cell in the cochlear nucleus (Kuwabara, DiCaprio, and Zook 1991; Smith, Joris, and Yin 1998). The function of the MNTB is to faithfully convert each excitatory, glutamatergic input (Forsythe and Barnes-Davies 1993) into an inhibitory, glycinergic output in a 1:1 ratio with minimal temporal delay ('jitter'; Brew and Forsythe 1995; Kopp-Scheinpflug et al. 2003). This is incredibly important to ensure inhibitory inputs from the MNTB arrive at the LSO simultaneously with ipsilateral excitatory inputs from the CN (Grothe 2003).

1.4 Calyx of Held

The Calyx of Held, as mentioned, is a giant, glutamatergic synapse located at the axon terminal of GBCs in the contralateral MNTB. It is one of two giant synapses in the auditory brainstem, the other of which, the Endbulb of Held, is found in the CN and synapses onto the GBCs and SBCs (Lauer et al. 2013; Sento and Ryugo 1989). An MNTB neuron only receives one calyceal input (among conventional excitatory and inhibitory synapses; Hamann, Billups, and Forsythe 2003; Albrecht et al. 2014) which wraps around its soma (figure 1.2), however, occasionally GBC axons bifurcate such that two MNTB neurons receive calyceal inputs from the same GBC (Spirou, Brownell, and Zidanic 1990; Kuwabara, DiCaprio, and Zook 1991). The large size of the calyx ensures enough transmitter is released to generate a depolarisation sufficient to produce an action potential in the post synaptic cell. In order to maximise its transmitter output, the calyx has a large number of active zones, $\sim$550-700,

(Sätzler et al. 2002; Taschenberger et al. 2002; Meyer, Neher, and Schneggenburger 2001) with a releasable vesicle pool of ∼600-5000, depending on the method used to estimate (Schneggenburger, Meyer, and Neher 1999; Scheuss, Schneggenburger, and Neher 2002; Meyer, Neher, and Schneggenburger 2001; Schneggenburger and Neher 2000; Sun and Wu 2001). Glutamate released by the terminal activates NMDA and AMPA receptors on the MNTB cell soma, resulting in a large excitatory postsynaptic potential (EPSP; Forsythe and Barnes-Davies 1993). The somatic location of the synapse on the postsynaptic cells minimises the time taken to depolarise the membrane at the site of action potential generation and increases the likelihood of generating an AP.

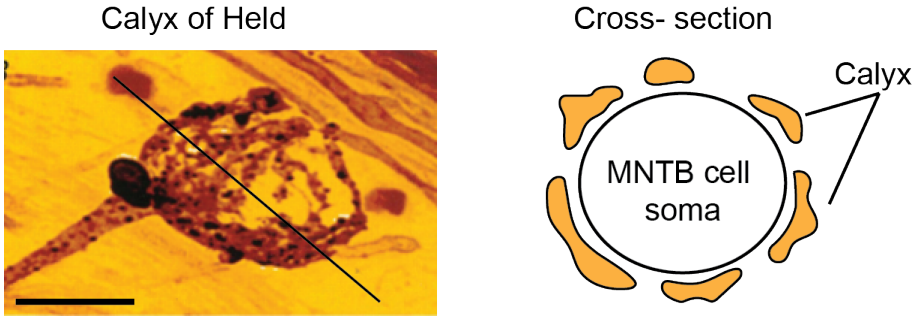

Figure 1.2: **Giant Calyx of Held synapse in the medial nucleus of the trapezoid body (MNTB). Left:** DiI (1,1'-dioctadecyl-3,3,3',3'-tetramethylindocarbocyanine perchlorate) stained calyx of Held and axon in a brainstem slice from a rat. Taken with permission from Forsythe 1994. Scale bar=10μm. **Right:** Cartoon schematic of a cross section through the calyx of Held terminal and postsynaptic MNTB neuron (indicated by black line on left). The calyx terminal wraps around the soma of MNTB principal neurons, making many synaptic contacts with the postsynaptic cell.

1.5 Ionic conductances at the Calyx of Held terminal

The calyx terminal possesses multiple ionic conductances to ensure reliable, temporally precise neurotransmitter release upon each invading AP, thereby generating a single, precise EPSP and postsynaptic AP. A switch from N, R and P-type voltage-gated Ca^{2+} channels to predominantly P-type occurs at hearing onset (Wu et al. 1999; Forsythe et al. 1998; Iwasaki and Takahashi 1998), which show tight coupling to synaptic vesicles, ensuring efficient Ca^{2+}-dependent vesicle release (Wang, Neher, and Taschenberger 2008; Wadel, Neher, and Sakaba 2007). In addition, low voltage-activated (Kv1.1 and 1.2; Dodson, Barker, and Forsythe 2002) and high voltage-activated (Kv3) potassium channels govern AP threshold and duration, respectively, limiting the number of action potentials fired, and the number of vesicles released per stimulus (Dodson et al. 2003; Wang and Kaczmarek 1998).

1.6 Lateral superior olive (LSO)

The LSO is one of the first nuclei to receive inputs from both ears and is responsible for ILD processing. In contrast to the MNTB, the neuronal population of the LSO is much more heterogenous with around 7 different morphological classes of neuron (Rietzel and Friauf 1998), although only two distinct firing patterns have been reported (Sterenborg et al. 2010). Principal neurons have an elliptical-shaped soma with a complex dendritic tree (Helfert and Schwartz 1987) and possess characteristic ionic conductances such as a large hyperpolarisation-activated potassium current (I_h; Sterenborg et al. 2010) and an absence of A-type Kvs. Glycinergic, inhibitory inputs from the MNTB and excitatory, glutamatergic inputs from SBCs in the CN converge on LSO principal neurons where their summation underlies ILD processing (Tollin 2003). Principal neurons themselves send excitatory projections to the contralateral inferior colliculus (IC) and inhibitory projections to the ipsilateral IC (Tollin 2003).

1.7 Medial superior olive (MSO)

The MSO receives bilateral excitatory inputs from SBCs in the contralateral and ipsilateral CN as well as contralateral and ipsilateral inhibition from the MNTB and LNTB, respectively (Kapfer et al. 2002; Cant and Hyson 1992; Kuwabara and Zook 1992). Neurons acts as coincidence detectors and are responsible for ITD processing. Principal neurons are bipolar with two major dendrites projecting from opposite sides of the soma (Fischl et al. 2016). Excitatory inputs from each ear synapse onto opposite dendrites, while inhibitory inputs synapse onto the soma (Kapfer et al. 2002; Smith, Owens, and Forsythe 2000). MSO neurons themselves send excitatory projections to the contralateral and ipsilateral IC (Nordeen, Killackey, and Kitzes 1983).

1.8 Sound localisation

Animals can locate the source of a sound in the azimuthal direction with remarkable precision, due to binaural processing that takes place in the SOC. The position of sound source relative to each ear creates minute differences in timing (ITD) and level of inputs (ILD) that can be detected by the MSO and LSO, respectively. ITDs arise due to the time taken (milliseconds) for a sound to travel across the width of the head, from one ear to the other. ILDs are the result of a 'shadowing' effect of the head leading to a lower sound intensity detected by the downstream ear (figure 1.3). Low (<2KHz) and high (>2KHz) frequency sounds are thought to be primarily detected via ITDs (MSO) and ILDs (LSO), respectively (Masterton et al. 1967; Boudreau and Tsuchitani 1968; Tollin 2003) and the size of an animal's head dictates which method is primarily used to locate sounds. Animals with small heads, such as rodents, that have a high frequency hearing range (16 - 100KHz; Reynolds et al. 2010) rely more on ILD processing, favouring the LSO. Those with larger heads such as humans which have a lower frequency hearing range (20Hz-20KHz; Reynolds et al. 2010), primarily use ITDs (Grothe and Pecka 2014). This preferential use of ILD processing in mice is associated with the presence of a large,

well-defined LSO structure and a much smaller MSO (Fischl et al. 2016).

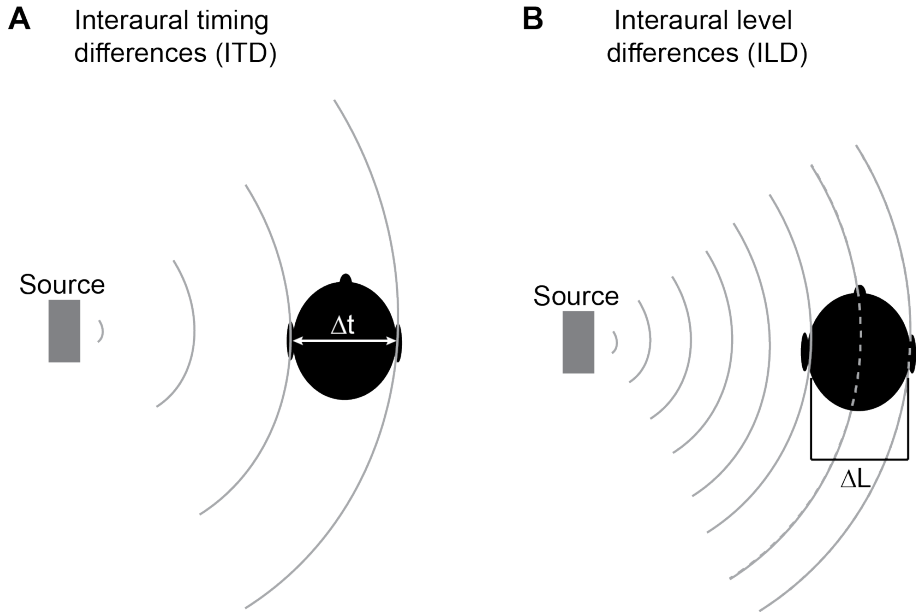

Figure 1.3: **Interaural timing and level differences used for binaural processing arise due to the separation of ears on either side of the head. A:** Interaural timing differences (ITD) arise due to the millisecond time taken for a sound to travel the distance of the head, from one ear to the other. ITDs are processed in the medial superior olive. **B:** Interaural level differences arise due to the head attenuating a sound such that it is louder in the ear closer to the source. Adapted from Grothe, Pecka, and McAlpine 2010.

ILDs are detected by the LSO via summation of the simultaneous IPSC and EPSCs arriving from the contralateral (via the MNTB) and ipsilateral ear, respectively (Moore and Caspary 1983). This creates a characteristic firing pattern of LSO neurons, in which a maximal firing rate occurs when a sound is closest to the ipsilateral ear and a complete inhibition results from a sound closest to the contralateral ear (figure 1.4). While neurons of the LSO are generally considered to respond to higher frequency sounds, there are some with low characteristic firing frequencies, in which the timing of arrival of excitatory inputs from SBCs and inhibitory inputs from the MNTB becomes very important for coincidence detection (Grothe, Pecka, and McAlpine 2010; Tollin and Yin 2005). This ability of the LSO to detect ILDs at lower frequencies may be more important in those animals with a less developed MSO, such as mice.

ITDs are processed by the MSO in the form of coincidence detection, that is

when excitatory signals from both ears arrive at the MSO neuron at the same time, it results in a depolarisation large enough to reach AP threshold. In birds this is achieved via hard-wired 'delay lines' as proposed by the Jeffress model (Jeffress 1948), in which different sized axons ('delay lines') cause inputs to simultaneously reach the coincidence detecting neurons at slightly different times, thus each neuron represents a different point in space (Joris, Smith, and Yin 1998). However, there is no good evidence for the presence of these delay lines in mammals (Smith, Joris, and Yin 1993) and the mechanism of producing delays is as yet unknown, although it has been proposed that axons of SBCs may have variable conduction velocities (Seidl and Rubel 2016; Sinclair et al. 2017). ITDs are thought to be encoded by the population of MSO neurons with an ITD function that is preferential to contralateral sounds (Grothe 2003; figure 1.4). Well-timed inhibitory inputs are important for keeping these ITD functions within a physiological range (Grothe 2003).

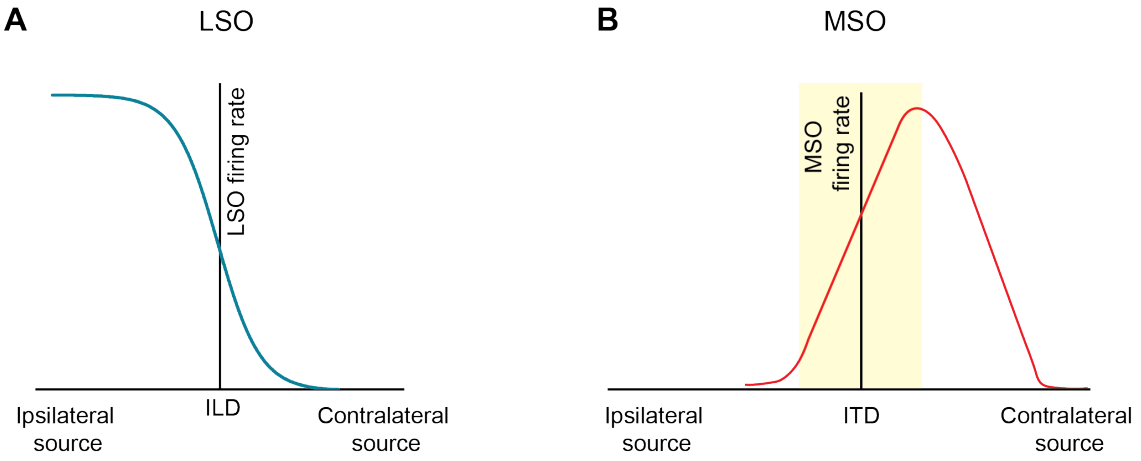

Figure 1.4: **Response profiles of neurons in the lateral and medial superior olive (LSO and MSO) in response to binaural inputs. A:** ILD function in the LSO. Firing rates in the LSO are maximal when a sound is located close to the ipsilateral ear but decrease in response to increased inhibition when a sound is located closer to the contralateral ear. **B:** ITD function in the MSO. Firing rate in the MSO is larger with contralateral sound sources with the slope of the ITD function located within a 'physiological' range (marked by yellow rectangle). Adapted from Grothe, Pecka, and McAlpine 2010.

While the MSO appears to be more important when considering timing of action potentials, being the traditional coincidence detector, the current study focuses on the LSO for a number of reasons. Firstly, the LSO is structurally more defined in mice thus locating and identifying neurons using electrophysiology was less challenging than the MSO which is much less defined, smaller and the cells less well-characterised. Secondly, mice have a preferential high-frequency hearing range and thus the LSO is likely to be more important in these animals, with these neurons responding to higher-frequency sounds. Lastly, new evidence is emerging that neurons in the LSO, particularly those that have lower characteristic firing frequencies use coincidence detection (Tollin and Yin 2005) to the same extent of the MSO and thus timing of AP firing in both the input neurons (SBCs and MNTB) and LSO neurons themselves has a significant impact on auditory function.

1.9 Potassium channel structure and function

The potassium channel family is huge with over 80 genes encoding different subunits (Trimmer 2015). These subunits form channels which can be split into three main groups based on the number of transmembrane domains (TMDs) each subunit contains: voltage-gated and calcium/sodium sensitive (Kv, KCa/KNa; 6 TMDs), inward rectifiers (Kir; 2TMDs) and two-pore domain (K2P; 4TMDs; figure 1.5).

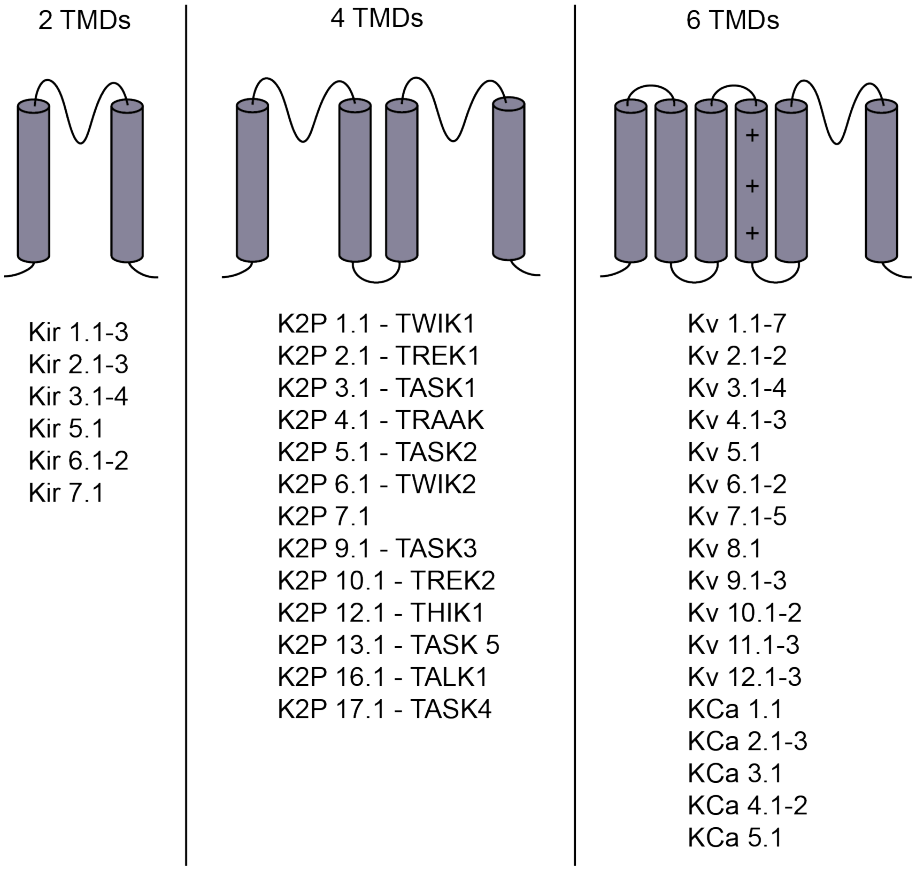

Figure 1.5: **Divisions of potassium channel subunits based on number of transmembrane domains (TMDs).** Inward rectifiers have 2 TMDs, two-pore 'leak' (K2P) channels have 4 and voltage-gated channels have 6 (Trimmer 2015.)

Functional K2P channels, otherwise known as 'leak' channels are formed of two subunits and allow the flow of potassium ions across the membrane, independent of voltage. Together with inward rectifying channels, which are formed of 4 subunits and conduct potassium ions only at negative voltages, these set the resting membrane potential of a neuron.

Delayed rectifying Kv channels (Kv1-4) instead provide the repolarising drive for action potentials (Hodgkin and Huxley 1952) as well as contributing to the resting membrane potential. Kv channels are comprised of 4 subunits, each with 6 transmembrane domains (TMD; S1-S6) and a pore-forming region (Doyle et al. 1998; figure 1.6). Each pore-forming region contains a 'GYG' repeat in the amino acid sequence which determines selectivity for potassium ions (Doyle et al. 1998), while the S4 TMD forms the voltage-sensor.

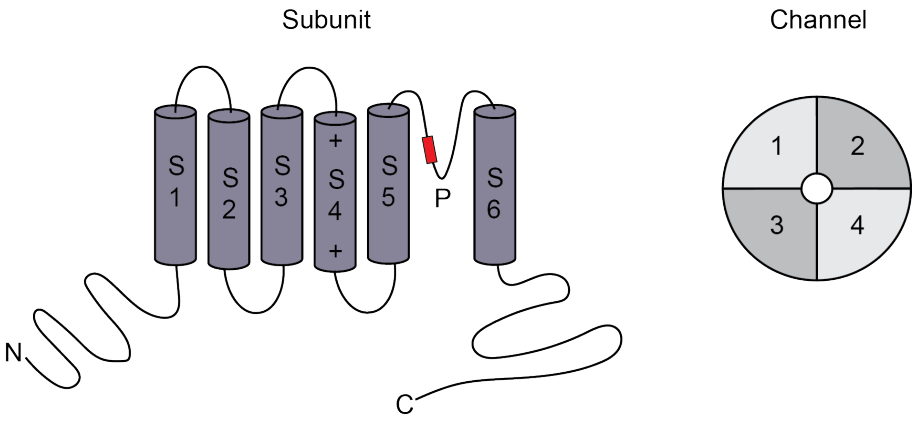

Figure 1.6: **Structure of a Kv subunit.** Each subunit is formed of 6 transmembrane domains (TMD) labelled S1-S6 and a pore-forming loop (P) containing a 'GYG' motif in the amino acid sequence (red rectangle), determining the selectivity for potassium ions. The fourth TMD, S4, is positively charged and underlies the voltage-sensing abilities of the channel. Both the N and C terminals are located inside the cell and contain motifs for binding of secondary messengers and auxiliary subunits. A channel consists of four of these subunits (right).

Subunits from the Kv1-4 families can form homotetrameric and heterotetrameric channels with other members of the same family. A tetramerisation domain, T1, located in the N-terminus, close to S1 allows subunits to join together (Kreusch et al. 1998). In addition to these, a number of other subunits are included in the Kv family (Kv5, 6, 8 and 10) which do not form functional homomeric channels themselves but can be incorporated into channels formed of subunits in the Kv1-4

families and result in altered channel properties (Post, Kirsch, and Brown 1996; Kramer et al. 1998; Ottschytsch et al. 2002).

1.10 Kv channel activation

Voltage-gated potassium channels open in response to changes in voltage across the cell membrane, typically they open upon depolarising potentials. This is due to the presence of a positively charged voltage-sensing, transmembrane domain which, upon sensing a change in potential, causes a conformational change within the protein structure leading to opening of the pore, although the exact mechanism by which this happens is still unknown (Catterall 2010).

The voltage at which Kv channels activate differs between families with Kv1 and Kv4 opening at relatively low voltages, $\sim$ -60mV - -40mV, while Kv2 and Kv3 open at relatively high voltages ($\sim$-20 - 0mV; Coetzee et al. 1999). In addition to their activation voltage, these families differ in activation kinetics, Kv1, 3 and 4 activate quickly, while Kv2s are much slower to open (Coetzee et al. 1999; Johnston, Forsythe, and Kopp-Scheinpflug 2010; figure 1.7).

1.11 Kv channel function

The function of Kv channels is also governed by their kinetics and subcellular localisation. The low activation voltage of Kv1 and the position of channels at the axon initial segment (AIS) and nodes of Ranvier (NoR) mean they have an important role in setting the threshold for AP generation and regulating excitability (Brew, Hallows, and Tempel 2003; Dodson, Barker, and Forsythe 2002). Similarly, Kv3 channels are located at the AIS, NoR, dendrites and soma, but high activation voltages and rapid gating kinetics underlie their main function in fast AP repolarisation, promoting high frequency firing (Wang et al. 1998; Macica et al. 2003; Brew and Forsythe 1995). Meanwhile, the slower activation of Kv2 combined with high activation voltages and expression at the AIS, soma and dendrites underlie its role in

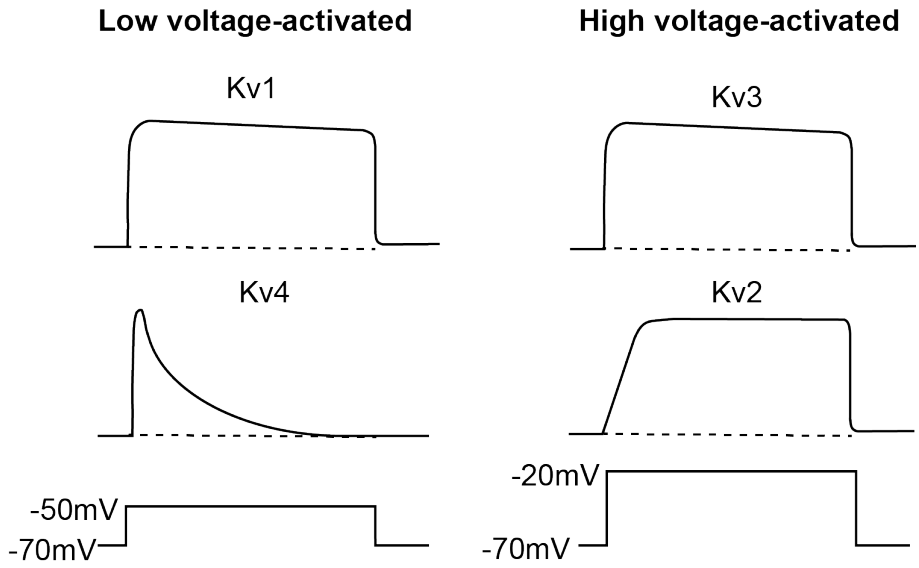

Figure 1.7: **Current kinetics of delayed rectifying Kv channels.** Kv1 and Kv4 families are low-voltage activated and activate at around -50mV. Kv4 channels require a step to hyperpolarised potentials prior to opening to relieve inactivation. Both are rapidly activating and Kv1 show little inactivation while Kv4 channels show rapid, strong N-type inactivation. Kv2 and Kv3 are high voltage activated (-20mV). Kv3 channels have rapid activation and deactivation kinetics whereas Kv2 channels are slower to activate.

AP repolarisation during prolonged activity rather than contributing to single AP repolarisation (Misonou, Mohapatra, and Trimmer 2005; Johnston et al. 2008).

1.12 Kv channel inactivation

Kv channels mainly undergo two types of inactivation, C-type and N-type. C-type is slower and involves a conformational change at the external mouth of the pore such that K^+ ions are no longer conducted (Yellen et al. 1994). N-type inactivation is usually much quicker and arises due to the presence of a positively charged N-terminal 'ball' peptide which can bind to and occlude the pore (Hoshi, Zagotta, and Aldrich 1990; Long, Campbell, and MacKinnon 2005). N-terminal peptides may be present in alpha subunits themselves such as in Kv4s, Kv3.3 and Kv3.4 or they can be provided by beta subunits bound to the inside of the channel, inducing inactivation in otherwise non-inactivating channels such as the Kv1s (Rettig et al. 1994).

1.13 High-voltage activated Kv3 channels

As mentioned, Kv3 channels are high voltage-activated with rapid gating kinetics that promote high frequency action potential firing. There are 4 genes encoding Kv3 subunits, KCNC1-4, each of which has a number of spliced variants (Rudy et al. 1999).

Each subunit has slightly different kinetics when expressed as homomers in cell lines; Kv3.1 and Kv3.2 show very little inactivation while Kv3.4 displays very rapid inactivation due to the presence of an N-terminal peptide (Hoshi, Zagotta, and Aldrich 1990; figure 1.8). Kv3.3 has a number of spliced variants, some of which contain an N-terminal peptide and produce a slow inactivation and others which lack the peptide resulting in a non-inactivating current (Fernandez et al. 2003). Importantly, splicing appears to vary in expression systems with the same RNA producing an inactivating current in oocytes but not in CHO cells (Rudy et al. 1999).

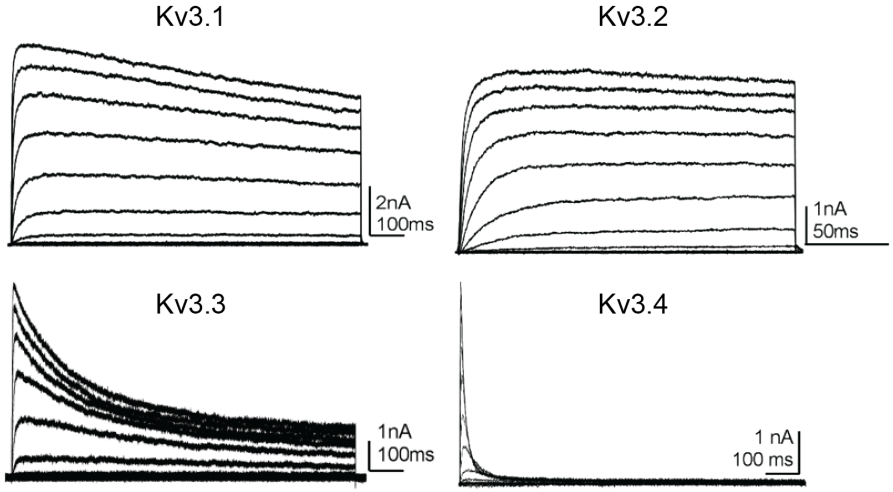

Figure 1.8: **Kv3 currents recorded from CHO cells expressing human Kv3.1b, 3.2, 3.3d or 3.4a.** Kv3.1 and Kv3.2 show very little inactivation. Kv3.3d subunits are slowly inactivating and Kv3.4a are rapidly inactivating. (Kv3.1b, Kv3.3 and Kv3.4a currents recoded by myself; Kv3.2 current recorded by Michele Speggiorin at Autifony Therapeutics).

1.14 Tissue expression of Kv3 subunits

Expression patterns of Kv3 subunits throughout the brain vary. Kv3.1 is expressed highly in numerous areas of the brain including the cerebellum, inferior colliculus, thalamic reticulum and auditory brainstem as well as in fast spiking interneurons of the cortex and hippocampus and cells in the spinal cord (Rudy et al. 1999; Weiser et al. 1994). Kv3.2 is highly expressed in the thalamus, superior colliculus and in fast-spiking interneurons, with little expression outside the brain. Kv3.3 has a similar expression pattern to Kv3.1 and is abundant in the auditory brainstem nuclei, cerebellum, thalamic reticulum and inferior colliculus as well as the spinal cord and is lowly expressed in other organs of the body including the kidney and lung (Rudy et al. 1999; Weiser et al. 1994). Kv3.4 expression is a little more scarce in the brain, present in Purkinje cells of the cerebellum, neurons of the dentate gyrus and synaptic boutons of cerebellar interneurons and fast-spiking interneurons (Rowan and Christie 2017; Baranauskas et al. 2003). Outside of the brain it is highly expressed in sympathetic ganglia and skeletal muscle (Rudy et al. 1999; Brooke et al. 2004).

Expression of more than one subunit in the same neuron often occurs, leading to the assumption that Kv3 subunits form heteromers, optimizing the kinetics of the channel for specific functions (Rudy et al. 1999; Baranauskas et al. 2003).

1.15 Regulation of Kv3 activity

Kv3 channel activity can be modulated by a number of different signalling molecules. Protein kinase C (PKC) phosphorylates Kv3.1 in the C-terminal region and Kv3.3 and Kv3.4 in the N-terminal to produce opposing effects, decreasing the amplitude of currents driven through Kv3.1 channels and removing inactivation of Kv3.3 and Kv3.4 channels thereby increasing current amplitudes (Kanemasa et al. 1995; Macica et al. 2003; Desai et al. 2008; Covarrubias et al. 1994; Beck et al. 1998). Protein kinase A (PKA) interacts with Kv3.2 and decreases current amplitudes (Moreno et al. 1995).

Ancillary subunits in the MinK-related peptide family (MiRP1-4), encoded by KCNE2-5, also form complexes with Kv3 subunits, resulting in changes to channel behaviour. MiRP2 binds Kv3.1 homomers and slows activation of the channel (McCrossan et al. 2003).

1.16 Kv3 pharmacology

In addition to these intrinsic regulators, externally applied drugs also act on Kv3 channels. The only relatively specific inhibitor that currently exists is blood depressing substance-1 (BDS-I) which significantly inhibits currents through Kv3.4 channels as well as reducing Kv3.1 and Kv3.2 mediated currents (Diochot et al. 1998; Yeung et al. 2005). It has recently been noted that BDS-I also acts on voltage-gated sodium channels, increasing currents of TTx-sensitive channels, limiting its usefulness in the study of Kv3 channels in AP repolarisation (Liu, Jo, and Bean 2012).

While not specific for Kv3 channels, low concentrations of tetraethylammonium (TEA) are a useful pharmacological tool. At 1mM TEA is relatively specific for Kv3 channels (IC_{50} $\sim$150μM), although it will also block homomeric Kv1.1 channels and BK potassium channels at this concentration, in addition to blocking most other Kv channels at higher concentrations (Coetzee et al. 1999). Low (micromolar) concentrations of 4-aminopyradine (4-AP) also block Kv3 channels and have previously been used, however these also block other Kv channels (Coetzee et al. 1999).

Novel Kv3 modulators have recently been produced which alter the gating of Kv3.1 and Kv3.2 channels. AUT1 and AUT2 shift the activation and inactivation of Kv3.1 to more negative potentials (Brown et al. 2016; Rosato-Siri et al. 2015) and can rescue firing rates of Kv3.1/Kv3.2-positive cortical interneurons treated with the blocker TEA (Rosato-Siri et al. 2015).

1.17 Kv3 in the auditory brainstem

Studies in the auditory brainstem have identified TEA-sensitive Kv3 currents in neurons of the MNTB (Brew and Forsythe 1995; Wang et al. 1998; Linley 2017), MSO (Nabel et al. 2019), CN (Olsen et al. 2018; Cao, Shatadal, and Oertel 2007) and in the calyx of Held terminal (Nakamura and Takahashi 2007). Kv3 currents create brief action potentials, allowing these neurons to fire at frequencies up to 800Hz (Wang et al. 1998; Taschenberger and Von Gersdorff 2000), when absent, as in Kv3.1 KO animals, MNTB neurons cannot sustain action potential firing above 300Hz (Wang et al. 1998). Activity-dependent modification of Kv3 channels has been noted in neurons of the MNTB, resulting in increased Kv3 activity following sound stimulation (Song et al. 2005).

Kv3 channels in these nuclei are likely composed of Kv3.1 and Kv3.3 subunits. RNA hybridisation studies have identified Kv3.1 and Kv3.3 in nuclei of the SOC (Weiser et al. 1994; Perney et al. 1992) and RNA sequencing from our own lab conducted on laser-dissected section of tissue confirmed that mRNA of only these two subunits are present in the MNTB, LSO and CN (figure 1.9).

In addition to Kv3 channels, MNTB neurons also contain significant Kv1 and Kv2- mediated potassium currents (Brew and Forsythe 1995) which limit excitability by preventing multiple action potential firing and regulate inter-AP potential during high-frequency stimulation, respectively (Dodson, Barker, and Forsythe 2002; Johnston 2007) . Kv1 currents have also been observed in the calyx of Held terminal (Dodson et al. 2003) in which they again, prevent aberrant AP firing restricting the output to one AP per stimulus.

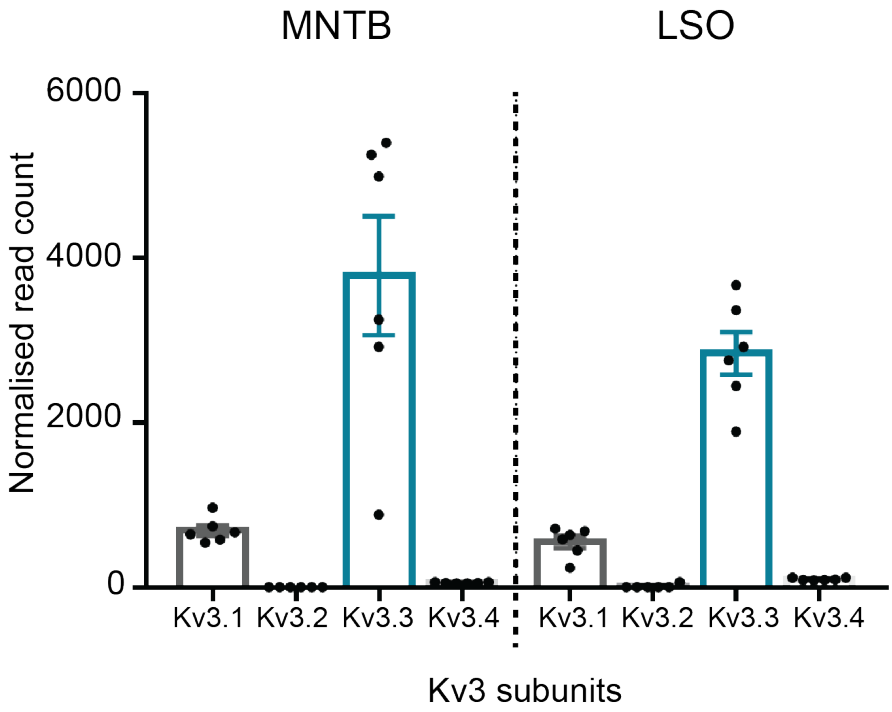

Figure 1.9: **Only Kv3.1 and Kv3.3 subunits are present in the medial nucleus of the trapezoid body (MNTB) and lateral superior olive (LSO).** Normalised mRNA levels for Kv3 subunits in laser-dissected sections of MNTB and LSO from 6 P21 CBA wildtype mice.

1.18 Kv3 in disease

Mutations in Kv3 channels have recently been described in several neurodegenerative human diseases, most notably a mutation in the gene encoding Kv3.1 (KCNC1) results in myoclonus epilepsy and ataxia (MEAK; Muona et al. 2015; Nascimento and Andrade 2016) while mutations in KCNC3, encoding Kv3.3 result in spinocerebellar ataxia type 13 (SCA13; Zhang and Kaczmarek 2016).

Interestingly both diseases are caused by mutations present in the voltage sensing domains of the subunits, resulting in a change to the amino acid sequence from an arginine to histidine (at position 320 in Kv3.1 (R320H) and both 420 (R420H) and 423 (R423H) in Kv3.3; Muona et al. 2015; Waters et al. 2006). Further mutations within other transmembrane regions as well as the N and C-terminals have since been discovered in the Kv3.3 gene, also resulting in SCA13 (Zhang and Kaczmarek 2016).

SCA13 is characterised by cerebellar ataxia, associated with degeneration of the cerebellum, but sufferers also experience cognitive and oculomotor abnormalities

(Waters et al. 2006) and seizures (Figueroa et al. 2010). The disease is either adult or early-onset depending on the mutation harboured by the patient; R420H is associated with a progressive adult-onset version while R423H causes a more severe, early-onset form (Figueroa et al. 2010) and both mutations have a dominant-negative effect on wildtype subunits.

R420H has also been linked to impaired sound localisation in human patients, with sufferers showing increased thresholds for detection of both interaural timing and level differences, highlighting the importance of Kv3.3 subunits in the auditory pathway (Middlebrooks et al. 2013).

Although the mechanism by which mutations in Kv3.3 causes neurodegeneration is not yet known, studies conducted on cell lines have shown aberrant trafficking of mutated subunits with reduced surface expression and an absence of Kv3.3-mediated current when only mutant subunits are expressed or a vast reduction in current amplitude when mutated subunits are expressed with wildtype (Gallego-Iradi et al. 2014; Waters et al. 2006; Zhao, Zhu, and Thornhill 2013). This will be discussed further in chapter 6.

1.19 Synaptic transmission at the calyx of Held

Kv3 channels are present in presynaptic terminals, including the calyx of Held (Rowan and Christie 2017; Ishikawa et al. 2003; Nakamura and Takahashi 2007). Modulation of AP waveform at the terminal could influence synaptic transmission thus synaptic function in Kv3.1 and Kv3.3 KO animals will be assessed at both the excitatory calyx of Held and inhibitory MNTB-LSO synapses of the auditory system where it is known that Kv3 channels are present (Choudhury et al, unpublished).

Neurotransmitter is released when a depolarisation of the presynaptic membrane by an invading AP opens voltage-gated calcium channels (VGCC) causing calcium influx into the synaptic terminal. This increased internal calcium concentration causes synaptic vesicles to fuse with the presynaptic membrane and release their contents into the synaptic cleft. Thus, volume of transmitter released is dictated by the duration of AP and consequent calcium influx.

Synaptic vesicles are released from the active zone, a specialised area within the terminal located directly opposite a postsynaptic density (PSD) on the postsynaptic membrane. The active zone consists of vesicles, VGCCs and a protein complex required for docking of vesicles and fusion with the membrane (Südhof 2012). The close proximity of VGCCs and vesicles within the active zone allow efficient release by minimizing the diffusion distance and thus volume of calcium ions needed for calcium-dependent exocytosis to occur (Llinas, Sugimori, and Silver 1992; Meinrenken, Borst, and Sakmann 2002). As mentioned, the calyx terminal contains a large number of active zones in order to increase the number of vesicles that can be released in one action potential, ensuring faithful release on every stimulus (Sätzler et al. 2002; Taschenberger et al. 2002).

Vesicles exist in distinct pools; those located in the active zone are referred to as the readily recyclable pool and at the calyx synapse this constitutes around 1% of the total vesicle population (figure 1.10; Rizzoli and Betz 2005). At the calyx terminal the RRP is split into two groups known as fast and slow release pools (Sakaba and Neher 2001; Lee, Ho, and Lee 2012) and estimates of RRP size range from around 600-5000 vesicles (Schneggenburger, Meyer, and Neher 1999; Sun and Wu 2001). The size of the RRP dictates how much transmitter can be released and this large RRP, mostly due to the large number of active zones, increases the amount of transmitter that can be released per AP, ensuring EPSPs in postsynaptic cells reach the threshold for action potential generation.

A recycling pool ($\sim$4% of total population) sits just outside the active zone and replenishes vesicles in the RRP once they have released their contents (De Lange, De Roos, and Borst 2003; figure 1.10). A reserve pool which constitutes around 95% of the population and is located furthest away from the release sites, replenishes vesicles in the recycling pool. Vesicles from the reserve pool are generally only recruited during intense stimulation and recruitment is much slower (De Lange, De Roos, and Borst 2003; Rizzoli and Betz 2005). Changes to either RRP and recycling pool size, number of active zones or rate of recycling will influence the amount of transmitter that can be released during repetitive stimulation, discussed in chapter

5.

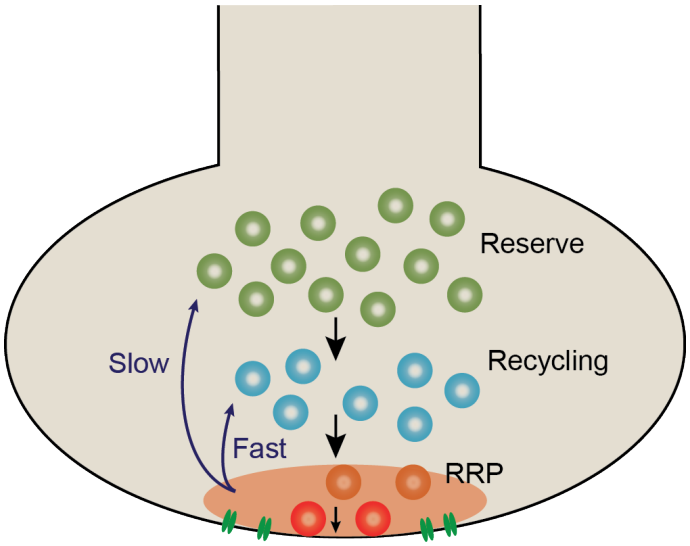

Figure 1.10: **Vesicle pools at the calyx of Held**. Calyx terminals contain 3 distinct pools of vesicles. The readily releasable pool (RRP) located in the active zone (orange area), tightly coupled to voltage gated calcium channels (green channels on membrane). The RRP can be split into two groups a fast releasing pool (red circles) and a slow releasing pool (orange circles). This RRP is replenished by vesicles from the recycling pool (blue circles) which is in turn replenished by vesicles from the reserve pool (green circles). Replenishment (recycling) via the recycling pool is fast whereas replenishment via the reserve pool is very slow and only occurs during intense stimulation. Adapted from Rizzoli and Betz 2005.

1.20 Glutamate receptors at the Calyx-MNTB synapse

Postsynaptic currents (PSCs) can be used as a read-out of transmitter release; more transmitter released means more receptors are activated and a bigger current is recorded in the postsynaptic cell. Excitatory postsynaptic currents (EPSCs), such as those recorded from MNTB neurons are generally caused by influx of positively charged ions while inhibitory (IPSCs) such as those at the MNTB-LSO synapse are usually the result of Cl^- influx. The receptor subunits expressed on a postsynaptic membrane dictate which ions the channel is permeable to, in addition to the kinetics of the PSC.

The calyx of Held-MNTB synapse is excitatory as glutamate released from the calyx binds to postsynaptic AMPA and NMDA receptors (Forsythe and Barnes-Davies 1993), resulting in an influx of positively charged ions (Na^+ and Ca^{2+}) into the postsynaptic cell and a depolarisation of the membrane known as a excitatory postsynaptic potential (EPSP).

Before hearing onset (<P14), glutamate release from the calyx of Held activates both NMDA and AMPA receptors (Steinert et al. 2010; Joshi and Wang 2002; Forsythe and Barnes-Davies 1993) and a large NMDA component results in EPSCs with a relatively slow time-course (Futai et al. 2001). At this age NMDA receptors likely contain NR2A and C subunits (Steinert et al. 2010) while AMPA receptors are likely formed of GluR1 and 2 subunits (Caicedo and Eybalin 1999). A developmental decline in NMDA receptor expression coupled with an increase in GluR4-containing AMPA receptors after hearing onset results in large EPSCs in adults with a rapid time-course (Joshi and Wang 2002; Forsythe and Barnes-Davies 1993; Caicedo and Eybalin 1999; Futai et al. 2001; Mosbacher et al. 1994).

1.21 Glycine receptors at the MNTB-LSO synapse

A developmental shift occurs at the MNTB-LSO synapse around the first postnatal week (Kandler and Friauf 1995; Kotak et al. 1998). In young animals (<P8) glycine release from the MNTB causes a depolarising potential in LSO principal neurons.

Glycine receptors are ionotropic chloride channels and opening of these results in the extrusion of Cl^- ions from LSO neurons due to a high intracellular Cl^- concentration. A developmental increase in expression of chloride transporters (KCC2) in these neurons results in a shift from high to low intracellular Cl^- concentration and thus glycinergic inputs change from a depolarising to hyperpolarising (Kakazu et al. 1999; Balakrishnan et al. 2003). A switch also occurs in transmitter release from mixed GABA/glycine to predominantly glycine in post-hearing (P14) animals (Kotak et al. 1998; Nabekura et al. 2004), although there is still debate around the function of GABA at this synapse (Fischer et al. 2019).

A switch in glycine receptor subunits expressed in LSO neurons from Glyα2 to Glyα1 is associated with an increase in receptor kinetics and decreased IPSC time-course adult mice (Pilati et al. 2016).

It is important to consider these developmental changes to both glutamatergic and glycinergic subunit expression at hearing onset when designing experiments in the auditory brainstem. This switch in subunit expression may cause changes to measured postsynaptic currents due to altered receptor kinetics, leading to increased variability if recording at the time of developmental switch and an inability to compare data gained from pre-hearing and post-hearing mice. For this reason the present study uses adult mice (above P21) for the study of synaptic physiology, at which age animals may be considered 'mature' and are likely to possess 'adult' receptor conformations.

1.22 Hypothesis

Kv3 channels provide the repolarising drive for rapid action potentials in neurons of the auditory brainstem. Thus, when present in the synaptic terminal, they limit neurotransmitter release.

Chapter 2

Methods

This chapter will provide a description of general methods used throughout the thesis. More detailed methods concerning specific experiments will be given at the beginning of each chapter. Unless otherwise stated, all chemicals were purchased from Sigma Aldrich.

2.1 Experimental animals

Animals were bred in-house during the experimental period at the university of Leicester in the preclinical research facility (PRF) under the project licence P8A3DDB49. All procedures were carried out under the above project licence and my personal licence I644BB80E, in accordance with the Animals (Scientific Procedures) Act 1986. CBA/Ca wildtype mice were used for experiments, in addition to Kv3.1 and Kv3.3 knockout mice which were backcrossed onto a CBA background for a minimum of 10 generations. Kv3.1 KO mice were acquired from Leonard Kaczmarek and generated by Rolf Joho in 1997 by insertion of a neomycin cassette into the S2-S3 linker, replacing 35bp of genomic DNA and disrupting transcription (Ho, Grange, and Joho 1997). Kv3.3 KO mice were acquired from Brian Robertson and generated by Rolf Joho in 1997 by replacing the ATG start codon with a phosphoglycerate kinase neomycin cassette, such that the resulting gene cannot be transcribed (Chan 1997).

2.2 Genotyping

Transgenic animals were bred with heterozygous parents to provide WT litter-mate controls. In order to determine the genetic status of the animals, genotpying (procedure detailed below) was carried out on ear snips taken by staff in the PRF .

2.2.1 Genotyping solutions

Ear lysis buffer (ELB)

Lysis buffer used to degrade tissue in order to extract DNA containing: Tris-HCl (100mM) at pH 8.5, ethylenediaminetetraacetic acid (EDTA; 5mM), sodium dodecyl sulphate (SDS ; 0.2% w/v) and Sodium chloride (NaCl; 200mM).

2.2.2 Genotyping protocol

DNA extraction

Tissue samples were incubated with 200μL ELB and 1μL proteinase K (20mg/mL stock) at 55^oC for 90 minutes in a thermal mixer (at 800 rpm; Eppendorf thermomixer compact) after which they were spun down in a centrifuge (Eppendorf centrifuge 5415R) for 2 minutes at 14000 RCF (relative centrifugal force). The supernatant was transferred to 200μL isopropanol and tubes were inverted a number of times until DNA formed a visible mass. Samples were spun in a centrifuge for 2 minutes at 14000 RCF, the supernatant was removed and discarded and the pellet allowed to air dry for 5 minutes. The pellet was then resuspended in 50 μL, 1x TE buffer (National diagnostics, #EC-862, diluted in distilled water) and incubated at 37^oC in a thermal mixer for 15 minutes. Samples were then run through a polymerase chain reaction (PCR) protocol to amplify DNA in the gene of interest.

PCR protocol

The presence of KCNC1 (Kv3.1) was determined using the following probes:

- 3.1X (GAAATCGAGAACGTTCGAAACGG)

- 3.1Y (TGATATTGAGGGAGTTCTTGATG)
- 3.1PPVR (CTACTTCCATTTGTCACGTCCTG)

A mix containing 5μL 2x PCR buffer (DreamTaq Green PCR master mix; Thermofisher Scientific #K1081), 0.5μL 3.1X, 0.5μL 3.1Y, 0.5μL 3.1PPVR, 2.5μL nuclease free water and 1μL sample DNA was put through the following PCR protocol using an Eppendorf thermal cycler; 94^{o}C for 5 minutes; 35 cycles of 94^{o}C, 57^{o}C and 72^{o}C each for 30 seconds followed by 5 minutes at 72^{o}C. The PCR product and DNA ladder (100bp DNA ladder, Promega #G2101) were then loaded onto a gel containing 2% w/v agarose dissolved in 1 x TAE buffer (Thermofisher Scientific, #15558042) with the addition of a DNA stain (Sybrsafe; dilution 1:10000, Thermofisher Scientific #S33102) and ran in a electrophoresis tank containing 1x TAE buffer at 100V for 40 minutes until DNA bands were separated. Bands were visualised using a UV transilluminator (UVP, model 3UV) and image analysis software, Launch DocITLS.

The presence of KCNC3 (Kv3.3) was determined using the probes:

- 3.3F (GACAGCGGTAAGATCGTGAT)
- 3.3NeoF (TCCATTTGTCACGTCCTGCA)
- 3.3R (AAACACAGACGCTTGAGCTC)

in a mix containing 10μL buffer (DreamTaq Green PCR master mix; Thermofisher Scientific cat #K1081), 1μL 3.3F, 1μL 3.3NeoF, 2μL 3.3R, 4μL nuclease free water and 1μL sample DNA. The samples were then ran on the following PCR protocol 98^{o}C for 2 minutes, 35 cycles of 98^{o}C, 62^{o}C and 72^{o}C for 25s, 35s and 65s respectively followed by 5 minutes at 72^{o}C. Samples were then loaded and ran on an agarose gel as described above.

2.3 Cell culture

While it is important to conduct research in animals to understand processes occurring in native tissues, the presence of multiple ion channels, accessory subunits and secondary messengers often complicates interpretations of data. Cell lines are therefore a useful tool to study the kinetics of single types of ion channel as well as the effects of drugs, whilst reducing confounding variables. In the present study CHO cells were used as an expression system to investigate Kv3 channel kinetics. All cell culture work should be carried out in sterile conditions using a downflow cabinet, to prevent bacterial and fungal contamination.

2.3.1 Solutions

Culture medium

Cell culture media enriched with amino acids to aid growth of Chinese hamster ovary (CHO) cells with the addition of antibiotics to prevent bacterial contamination. 1x solution containing high glucose Dulbecco's modified eagle medium (DMEM; 500ml; Sigma Aldrich, #11965084); 10% fetal bovine serum (FBS; Thermofisher); 1% penicillin/streptomycin (Thermofisher); 1% glutamine (200mM stock; Sigma); 1% non-essential amino acids (NEAA; Sigma, #M7145) and 400μg/ml G418 (Gentecin; Thermofisher).

2.3.2 Defrosting cells

Work was carried out on CHO lines, either CHO WT K1 or CHO stably expressing Kv3.3. Cells were stored in 1ml vials containing FBS and 10% dimethylsulfoxide (DMSO) in liquid nitrogen until required and new aliquots of cells were defrosted every three weeks. When required, 1ml aliquots of cells were warmed to 37^{o}C in a water bath and transferred to a sterile falcon tube. Fresh media heated to 37^{o}C was added to cells drop by drop to prevent osmotic stress. Cells were spun in a centrifuge for 10 minutes at 2000rpm until a pellet was formed. Media was removed and cells were resuspended in 5mL of fresh culture media. Media containing cells

was added to sterile T25 flasks and stored in an incubator at 37^{o}C, 95% humidity and 5% CO2 to allow cells to grow. Once cells had adhered to the flask and reached around 80% confluency they were passaged and transferred to T75 flasks, following which they were passaged according to the below protocol every 3 days.

2.3.3 Seeding and counting cells

When cells reached 80-90% confluency, media was removed from T75 flasks, cells were gently washed with 1x PBS (5mL) and detached by incubation with trypsin at 37^{o}C for 5 minutes (1mL trypsin per flask). After fresh, preheated media was added, cells were transferred to either a sterile falcon tube and centrifuged for 10 minutes at 2000rpm or to a 1mL Eppendorf for counting. In order to count cells they were added to fresh media (1:10 dilution) and were inserted into a Bürker chamber (see figure 2.1). To estimate the total number of cells in the flask, the following calculation was used:

$$Total\,cells = \frac{Cells\,in\,all\,quadrants}{Quadrants} * 10000 * 8 * 10 \tag{2.1}$$

where 10000 is the conversion factor to mL, and 8 and 10 are dilution factors. Cell pellets were resuspended in the appropriate volume of preheated media, seeded into T75 flasks for storage or plated in 6 well plates for transfection and experiments. In case of electrophysiology experiments, wells contained 4 sterile, round glass coverslips (25mm) which could be removed and placed in a recording chamber on an electrophysiology rig as required.

2.3.4 CHO cell tranfection with Kv3 plasmids

CHO-K1 and CHO cells stably expressing Kv3.3d grown to a concentration of 300,000 cells per well were transfected with plasmids containing Kv3.4a or Kv3.1b cDNA in addition to plasmids containing GFP for visualization of transfected cells. Transfection was carried out according to the Lipofectamine 2000 DNA transfection reagent protocol. As the rate of transfection into CHO cells was unknown, two

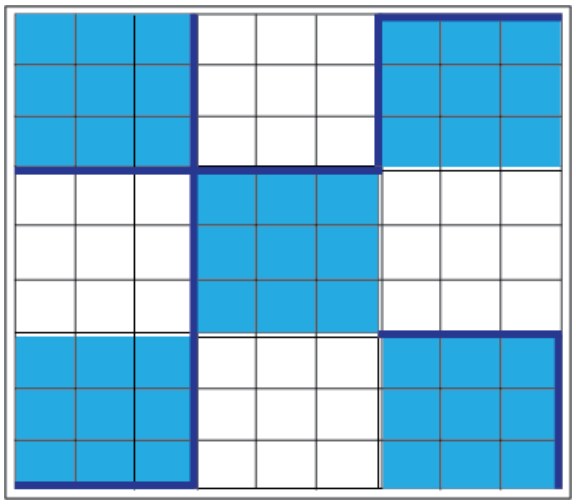

Figure 2.1: **Bürker grid for counting cells.** Cells in the light blue highlighted grids were counted, including those touching the dark blue borders only.

concentrations of Kv3.4a cDNA were used, 1ug and 2μg. GFP cDNA was added at the same concentration as Kv3.4a. cDNA and lipofectamine 2000 reagent were each diluted in 200μL Opti-MEM media in separate tubes. Care must be taken when using lipofectamine as it tends to adhere to plastic, thus it was added slowly to the media in the centre of the Eppendorf tube. The volume of lipofectamine used for transfection was 2.5x the concentration of cDNA (i.e for 1μg Kv3.4a DNA, 2.5uL lipofectamine was used). The cDNA- opti-MEM mixture was slowly added to the lipofectamine mixture and allowed to incubate for 15 minutes before being slowly added to cells seeded into a 6 well plate drop by drop with a 1mL Sterilin pipette. Media containing lipofectamine was removed after 24 hours and replaced with fresh, preheated media. As Kv3.4a had not previously been transfected into CHO cells, the expression levels of the channel on the membrane were unknown, consequently cells were used 24h, 48, 36h and 72h post-transfection to determine the optimal conditions for electrophysiological recordings. Cells expressing Kv3.1b were used 48 and 72 hours post-transfection.

2.4 Immunohistochemistry

Immunohistochemistry is a qualitative technique that can be used to determine the location of protein within tissue. It uses a primary antibody raised against the

protein of interest and a secondary antibody conjugated to a fluorescent tag that binds to the primary, allowing visualisation of the protein *in situ*.

2.4.1 Solutions

Phosphate buffered saline - Triton (PBS-T)

1 x solution of phosphate buffered saline (PBS) containing Sodium chloride (NaCl) (13.7mM); Potassium chloride (KCl) (0.3mM); Sodium orthophospate (Na_2HPO_4) (0.8mM); Potassium orthophosphate (KH_2PO_4) (0.15mM) in double distilled water with 0.1% (v/v) Triton-X100. 1 x working solution was made by dissolving 100 PBS tablets (Oxoid) in 1l of double distilled H_2O to create 10x PBS stock and diluting this 1:10 with ddH_2O. Addition of detergent, Triton-X, was used to increase permeability of cell membranes. The final solution was made to pH 7.4.

4% Paraformaldehyde (PFA)

PFA is used as a fixative to prevent tissue degradation and works by forming cross-links between proteins in the tissue. A 4% PFA solution containing 40g of PFA powder (Fisher Scientific) dissolved in 1l of 1x PBS was made by the lab technician Michelle Anderson and stored in the freezer at -20^oC until needed. When required the PFA was defrosted and stored in a Sheifferdecker at 4^oC for a number of weeks.

Blocking solution

Solution containing serum which minimises non-specific binding of antibodies to tissue. The solution is made of 1% bovine serum albumin (BSA), 10% goat serum albumin and 89% PBS-T.

Citric acid buffer

Heated citric acid buffer is used in antigen retrieval to break some of the cross-links formed during PFA fixation, giving better access to some antigens. It was a 10mM solution of citric acid in distilled water made to pH 6 using sodium hydroxide.

2.4.2 Protocol

Fixation matrix

Before using a primary antibody, it was tested using a fixation matrix to identify the best tissue fix condition. The fixation methods used were: 4% PFA; PFA with heated citric acid antigen retrieval; methanol and no fix.

Animals were humanely killed by decapitation, without anaesthesia. Brains were dissected from P21-P25 CBA mice in iced, oxygenated slicing aCSF (for composition see electrophysiology methods) and the brainstem removed using the same method as for electrophysiological experiments (see below), transferred to OCT embedding medium (Thermo Scientific) in a plastic mould with the freshly cut side placed on the bottom (spinal cord facing up) and flash frozen in a dewar containing dry ice and hexane. Frozen tissue was stored at -80^oC until required. 12 μm thick coronal sections were cut using a cryostat (Thermo Scientific CryoStar NX50) and mounted onto polylysine coated slides (Thermo Scientific). The fixation matrix protocol was as follows:

- Slides containing brainstem sections were placed in a Sheifferdecker containing either PFA for 10 minutes at 4^oC or 100% methanol for 10 minutes at -20^oC.
- Slides were transferred to a fresh Sheiefferdecker and washed 3 x 10 minutes in PBST.
- Half of the slides fixed in PFA undergo antigen retrieval so were transferred into 95^oC citric acid for 20 minutes (in a 500ml Pyrex beaker placed on a heated stage) then left to cool to 70^oC. Followed by 3 x 5 minute washes in PBST.
- Slides were partially dried and a hydrophobic (Immedge) pen was used to draw around the tissue to create a water resistant barrier. They were then placed in a humidity chamber and 300μL of blocking solution was placed onto the tissue and left for an hour to incubate at room temperature.

- Blocking solution was removed and fresh blocking solution containing primary antibodies (see table 2.1) was placed over the tissue and was left to incubate overnight at 4^oC.

- Primary antibody solution was removed and slides were washed 3 x 10 minutes in PBST.

- The following part of the protocol took place in the dark so as not to photobleach the fluorophores conjugated to the secondary antibodies. Slides were dried, placed back in the humidity chamber and incubated for 2 hours at room temperature with the secondary antibody (dilution 1:1000) in 300μL blocking solution.

- Slides were then washed 3 x 20 minutes in PBST followed by a 5 minute incubation of PBST containing Dapi stain (300nM).

- 3 x 5 minute washes in PBST were performed before slides were dried and coverslipped using hard set mounting medium (Vectorshield #H-1400).

Once optimal fixation methods were identified, immunohistochemistry was repeated on at least 2 slides from 3 different animals. Additional slides were used for peptide controls (if available), Kv3.1 and Kv3.3 KO animals and secondary only controls (primary antibody not added) which identify non-specific binding of secondary antibodies. Optimal fixation conditions for each antibody can be found in table 2.1, along with secondary antibodies in table 2.2. All sections were permeabilised using the detergent triton-X throughout the protocol, thus optimal fixation conditions reflect only those in the presence of this. The use of PBS without triton-X may change the quality of staining when antibodies are used at the optimal concentrations specified here. Although the optimal condition for Kv3.3 antibody alone was 4% PFA only, antigen retrieval was used when coimmunolabelling with Kv3.1b as this was the only fixation condition in which Kv3.1b worked well.

2.4.3 Analysis

Images were taken using a Zeiss Z1 inverted microscope, Leica DM 2500 and various confocal microscopes and were analysed using FIJI software.

2.4.4 Immunohistochemistry of CHO cells

The protocol used for staining CHO cells was as follows.

CHO cells were grown on coverslips placed in a well of a 6-well plate to a confluency of ∼70%. Media was removed from the well and cells were washed 3 times with 1xPBS (2mL) followed by a 10 minute incubation with 4% PFA (1mL) on ice. PFA was removed and cells were washed 3 x 10 minutes with 1xPBS (2mL), followed by a 30 minute blocking incubation with 0.1%BSA. Blocking solution was removed and three coverslips were incubated with 50μL blocking solution containing primary antibodies (see table 2.1) and one coverslip (secondary control) with blocking solution only (0.1%BSA) for 2 hours at room temperature, after which, all coverslips were washed 3x with 1xPBS for 5 minutes. All coverslips were then incubated with the secondary antibodies diluted in 50μL blocking solution, followed by 1x 10 minute wash with PBS, 1x 10 minute wash with PBS containing a nuclear stain (1:1000 dilution) and 1 futher 10 minute wash with PBS before being mounted onto slides with elvanol. Slides were stored in the fridge until required.

2.5 Western blotting

Western blotting is a useful tool to quantify the amount of protein present in either different animals, different areas of the brain or during different experimental conditions. Proteins are reduced, giving them a negative charge meaning they can be separated based on their molecular weight using electrophoresis. A primary antibody is used to detect the protein of interest and a secondary antibody conjugated to horse radish peroxidase (hrp) to detect the primary antibody. A reaction catalysed by hrp results in a chemical substrate (luminol) emitting a light which can be detected as a band at the molecular weight of the protein. As it is possible to normalise the

amount of target protein expressed against a universally expressed protein present in all samples, it provides a quantitative alternative to immunohistochemistry.

2.5.1 Solutions (Brain tissue)

Tris buffered saline - Tween 20 (TBS-T)

1 x buffer solution containing Tris base (50mM); Sodium chloride (NaCl) (150mM); 0.05% v/v Tween 20 and made to pH 7.6 with hydrochloric acid (HCl). A 10x TBS stock was made and diluted 1:10 in double distilled water to create 1x working solution on day of use.

Lysis Buffer

Buffer used to lyse cells in tissue preparation for protein extraction containing: Tris-HCl, pH 8.0 (20mM); NaCl (150mM); Ethylenediaminetetraacetic acid (EDTA) (5mM) and 1% v/v Triton X-100. The solution was stored at 4^{o}C until required. The following protease inhibitors were added on the day of use to prevent protein breakdown: leupeptin (10ug/mL); aprotinin (1ug/mL); antipain (10ug/mL) and Phenylmethylsulfonyl fluoride (PMSF) (1mM).

5x Running buffer

A buffer required for the proper running of proteins through both the stacking and running gels. Buffer contains Tris base (125mM); Glycine (1.25M); Sodium dodecyl sulphate (SDS) (17mM). A working solution is made by diluting 5x buffer in ddH_2O on day of use.

10x Towbins buffer

Buffer used in the transfer of negatively charged proteins to nitrocellulose membrane, consisting of Tris base (0.25M) and Glycine (1.92M) dissolved in ddH_2O. A working solution is made by diluting 10x towbins buffer with ddH_2O and methanol in 1:7:2 part ratio.

5% acrylamide stacking gel

A gel into which the protein samples are loaded for SDS-polyacrylamide gel electrophoresis. Each gel is made up of 2ml containing by volume ddH_2O (1400mL); 30% acrylamide mix (330μL); 1.0M tris pH 6.8 (250μL); 10% SDS (20μL); 10% ammonium persulphate (APS) (20μL); tetramethylethylenediamine (TEMED) (2μL).

8% acrylamide resolving gel

An 8% gel was chosen as this gave the best resolution for the chosen protein weights. 10ml of solution was made for each gel consisting of; ddH_2O (4.6mL); 30% acrylamide mix (2.7mL); 1.5M tris pH 8.8 (2.5mL); 10% SDS (100μL); 10% APS (100μL); TEMED (6μL).

2.5.2 Protein extraction (brain tissue)

Whole brainstem, cerebellum and cortex were taken from P20 CBA/Ca, Kv3.1 KO and Kv3.3 KO mice, flash frozen in round bottomed 2mL Eppendorf tubes kept in dry ice and stored at -80^{o}C until required.

Protein extraction was carried out on ice. For large samples, 100-200μL of 1% SDS solution was added to tissue followed by a brief sonication. Post-sonication, lysis buffer was added so that the final concentration of SDS was 0.1%. After homogenising, samples were spun down in a centrifuge at 13500 RMP for 30 minutes at 4^{o}C. For large samples the supernatant was carefully removed and placed in a new tube, (NB smaller samples should not contain a pellet so remain in the same tube; if a pellet remained, it was resuspended in the lysis buffer, sonicated and centrifuged for a further 20 minutes).

To determine protein concentrations, the samples were calibrated against a bovine serum albumin (BSA; 0.1%) standard at the following percentages (100μL) 0, 10 , 25, 50, 75, 100 using a protein assay. 2μL of sample was mixed well with 98μL ddH_2O and 1 mL 20% protein assay dye reagent (diluted in ddH_2O; Bio-Rad #5000006), poured into cuvettes and measured using a spectrophotometer (Janway

7300). A 'blank' containing 2μL lysis buffer (with 0.1% SDS) and 98μL ddH_2O was used as a control. In preparation for loading on gels, samples were diluted with lysis buffer and 6x sample buffer in order to make the protein concentration equal across samples.

2.5.3 Running and transferring gels

All equipment used during running and transferring of gel must be cleaned with 70% ethanol. An 8% SDS-polyacrylamide resolving gel (see solutions; TEMED must be added last) was made, poured between 1.5mm gel plates and topped with 70% ethanol. Once set, the ethanol was removed, the gel and plates rinsed with ddH_2O, dried and stacking gel (see solutions) was added with a comb placed in the top. Gels were placed in 1x running buffer, samples were loaded onto the gel at ran at 40mA (per gel) until the dye front reached the end. Proteins were then transferred onto nitrocellulose membranes (see figure) in Towbins buffer (see solutions) at 350mA for 90 minutes. Transferring must be done on ice due to the heat generated by using a large current. Presence of protein was determined using a ponceau S stain applied to the membrane for <30 seconds then washed away with ddH_2O.

2.5.4 Antibody labelling

Following this, membranes were blocked in 5% milk (in ddH_2O) for 60 minutes at room temperature on a rocker, washed in TBST for 3 x 10 minutes and incubated with the primary antibody diluted in 5% milk blocking solution overnight at 4^{o}C.

The following day membranes were washed 3 x 10 minutes in TBST then incubated with the secondary antibody (diluted in 5% milk block) for 60 minutes at room temperature. After 3 further washes in TBST, membranes were flooded with a chemiluminescence substrate for horseradish peroxidase (Amersham mild substrate; cat # GERPN2235) and imaged using a Fujifilm LAS4000 chemiluminescence imager. For a list of antibodies and dilutions used, see tables 2.1 & 2.2.

Table 2.1: **Primary antibody concentrations used in immunohistochemistry and western blotting**

Antibody	**Optimal Condition**	**Dilution IHC**	**Dilution WB**	**Supplier**
Anti-Kv3.3	PFA	1:3000	1:1000	Alomone #APC-102
Anti-Kv3.1b	AR	1:1000	1:1000	Neuromab #75-041
Anti-Kv3.2	PFA	1:200		Alomone #APC-011
Anti-Kv3.4	PFA	1:200		Alomone #APC-019
Anti-βactin			1:10000	Sigma #A5441
Anti-VGlut1	PFA	1:1000		Chemicon #AB5905
Anti-Kv3.3 (CHO)	PFA	1:100	1:500	Abcam #ab83556
Anti-βtubulin (CHO)			1:3000	Genetex #GTX101279
Anti-Kv3.4a (CHO)	PFA	1:100	1:200	Cambridge Bioscience
Anti-Kv3.1b (CHO)			1:1000	Sigma #P9732

Table 2.2: **Secondary antibody concentrations used in immunohistochemistry and western blotting**

Antibody	**Dilution IHC**	**Dilution WB**	**Supplier**
Alexafluor488 Anti-rabbit	1:1000		Thermofisher #A32731
Alexafluor488 Anti-mouse	1:1000		Thermofisher #A32723
Alexafluor546 Anti-rabbit	1:1000		Thermofisher #A11035
Alexafluor546 Anti-mouse	1:1000		Thermofisher #A11030
Alexafluor546 Anti-guinea pig	1:1000		Thermofisher #A11074
HRP-conjugated Anti-mouse		1:1000	Sigma #A8924
HRP-conjugated Anti-rabbit		1:1000	Sigma #A6154
HRP-conjugated Anti-sheep		1:1000	Bethyl Labs #A130-101P
HRP-conjugated Anti-rabbit		1:1000	CellSignalling #7074

Analysis

Images taken were saved as .tiff files and opened in FIJI software for densitometric analysis. Grey values obtained for bands from the protein of interest were normalised to those observed with β-actin to minimise differences due to loading errors.

2.5.5 Protein extraction for CHO cells

Cells were grown to $\backsim$80% confluency in a 6 well plate. Media was removed and cells were washed twice with 1x PBS (1mL). PBS was removed and 80μL lysis buffer (RIPA buffer Sigma #R0278 plus cOmplete mini protease inhibitors, Sigma #11836170001) was added per well. Cells were detached manually using a scraper, put into an Eppendorf and centrifuged at 12000rpm for 20 minutes to separate the protein from cellular debris and nuclear proteins. The supernatant, containing protein, was kept and stored at -20^{o}C until required.

2.5.6 Running and transferring (CHO)

Prior to gel loading, protein concentrations were measured using a Pierce BCA protein assay against known protein concentrations (BSA), following which, lysis buffer, sample buffer (4x Bolt LDS Sample buffer; ThermoFisher) and dithiothreitol (DTT) were added. Samples were loaded into precast 3-8% Tris-acetate gels (NuPage 10 well, 1mm; Thermofisher #EA0375) in a tank containing Tris-acetate running buffer (NuPage SDS running buffer, Thermofisher #LA0041) and ran at 100V for 20 minutes after which the voltage was increased to 150V.

Following gel electrophoresis, proteins were transferred to nitrocellulose membrane in cooled 1x transfer buffer containing 5% 20x transfer buffer (NuPage, Thermofisher #NP0006), 75% ddH_20 and 20% methanol at 350mA for 90 minutes.

After transfer to membranes, proteins were processed using the same methods as those used for brain tissue (For antibodies see tables 2.1 & 2.2).

2.6 Coimmunoprecipitation (Co-IP)

Co-immunoprecipitation is used to investigate interactions between different proteins or molecules. Tissues or cells are lysed with a weak lysis buffer that allows interactions to stay intact. Proteins are incubated with and bind to a primary antibody raised against the protein of interest. This protein-antibody complex together with any associated molecules is, in turn, attached to agarose beads forming a bead-antibody-protein complex. Unbound proteins are washed away then target proteins are detached from the bead-antibody complex and detected using western blotting.

2.6.1 Protocol

CHO cells expressing Kv3 subunits were grown in 10cm dishes until they reached 80% confluency. Media was removed and cells washed twice with 2 mL ice cold PBS. 300uL lysis buffer (Pierce IP Lysis buffer + cOmplete mini protease inhibitors) was added, cells were mechanically removed using a scraper and transferred to 1mL Eppendorf tubes. Lysates were centrifuged for 15 minutes at 12000 RPM, the supernatant transferred to a new Eppendorf and protein concentrations estimated using a Pierce BCA protein assay.

Agarose bead slurry (Pierce protein A/G agarose beads, Thermofisher Scientific) was washed prior to pre clearing of the lysate by centrifugation of bead slurry (250μL @ 1000 RCF for 1 minute), removal of the supernatant and resuspension of beads in fresh lysis buffer (500 μL). This washing stage was repeated twice. Once the bead slurry had been resuspended in lysis buffer, 100μL was added to 2mg protein lysate, incubated for 30 minutes at 4^{o}C on a rotator, then centrifuged for 10 minutes (1000 RCF) at 4^{o}C. The bead pellet was discarded and the precleared lysate separated into four tubes, two to which primary antibodies were added and two to which IgG controls were added (See table 2.3).

Antibody was incubated with protein lysates at 4^{o}C overnight. Following incubation with antibody, a further 100μL of bead slurry was added to each tube and left to incubate for 7 hours at 4^{o}C with gentle rotation.

After the incubation time was over, samples were washed 7 times to remove proteins that were not attached to the agarose beads. This was done by 1 minute centrifugations at 4^{o}C (1000 RCF), removal of the supernatant and resuspension of the beads in 250μL lysis buffer. On the last wash the supernatant was removed and beads were incubated with 50μL of 2x lamelli buffer (Sigma, #S3401) for 30 minutes at room temperature with gentle rotation, followed by centrifugation and disposal of the bead pellet. The supernatant was kept and protein detected using western blotting (see above).

Table 2.3: **Primary antibody and IgG isotype volumes used in co-IP**

Antibody	**Amount (μg)**	**Supplier**
Anti-Kv3.3	2	Abcam #ab83556
Anti-Kv3.4a	2	Cambridge Bioscience #GUNM101
Anti-Kv3.1b	2	Sigma #P9732
Sheep IgG	1.5	ThermoFisher #31243
Rabbit IgG	1.5	ThermoFisher #02-6102

2.7 Patch clamp electrophysiology

Electrophysiology is a powerful technique used to measure electrical activity both in cell culture and intact tissue. This methods section will describe electrical properties of cells, the electrophysiological set-up and the protocol for carrying out the technique.

2.7.1 Electrical properties of a cell

A neuron possesses two important electrical properties due to the nature of its lipid membrane. Firstly, the thin membrane is an insulator that separates two conductive ionic fluids, the internal and external and thus acts as a capacitor that can hold charge which, importantly, takes time to charge and discharge. In addition to this, the membrane has a certain resistance which can change when ion channels present in the membrane open, allowing the exchange of ions between fluids and thus the flow of current. This flow of current is what leads to changes in potential difference across the membrane, dictated by Ohm's law.

$$V = IR \tag{2.2}$$

A cell's capacitance is dictated by the surface area and thickness of the membrane and while it is relatively constant, small changes can be seen with the addition or subtraction of membrane as seen during vesicle release. Current will flow across a capacitor when there is a change in voltage meaning the currents measured during a voltage step are a product of both ionic flow and flow across the capacitor.

$$I_m = I_c + I_i \tag{2.3}$$

In contrast the resistance can change quite dramatically when ion channels open/close in response to changes in voltage or binding of an agonist. These properties become important in determining the time course of an electrical response within the cell to a change in voltage (such as a synaptic current) as they multiply to form a time constant τ_m.

$$\tau_m = R_m C_m \tag{2.4}$$

In addition to resistance and capacitance, the presence of two ionic solutions with an unequal distribution of ions on either side of the membrane, provides the electrochemical drive. The major constituent of the internal compartment is K^+ whereas outside, Na^+ and Cl^- dominate. As these ions carry a charge, when channels open and they move down their concentration gradient, they also create a movement of charge across the membrane, creating a potential difference, known as the membrane potential. The point at which the chemical and electrical gradients are equal is the equilibrium potential and is described by the Nernst equation.

$$Eion = \frac{RT}{zF} ln \frac{[ion]_{out}}{[ion]_{in}} \tag{2.5}$$

The Nernst equation describes the equilibrium potential only for a given ion and generally the membrane (and channels) is permeable to multiple ions, the movement of which, all contribute to the membrane potential. The Goldman-Hodgkin-Katz equation describes the reversal potential for a number of different ions each with relative permeabilities (dictated by number of open ion channels). Most often this is seen with K^+, Na^+ and Cl^- as these are the most abundant ions.

$$Erev = \frac{RT}{F} ln \frac{P_k[K]_o + P_{Na}[Na]_o + P_{Cl}[Cl]_i}{P_k[K]_i + P_{Na}[Na]_i + P_{Cl}[Cl]_o} \tag{2.6}$$

2.7.2 Recording apparatus

The electrophysiology setup consists of a recording and ground electrode connected to an amplifier (multiclamp 700A, molecular devices) via a headstage (see figure 2.2), an analogue to digital converter (Molecular Devices Digidata 1322A) and a computer running PClamp 10 and Multiclamp software used record data and control the amplifier, respectively.

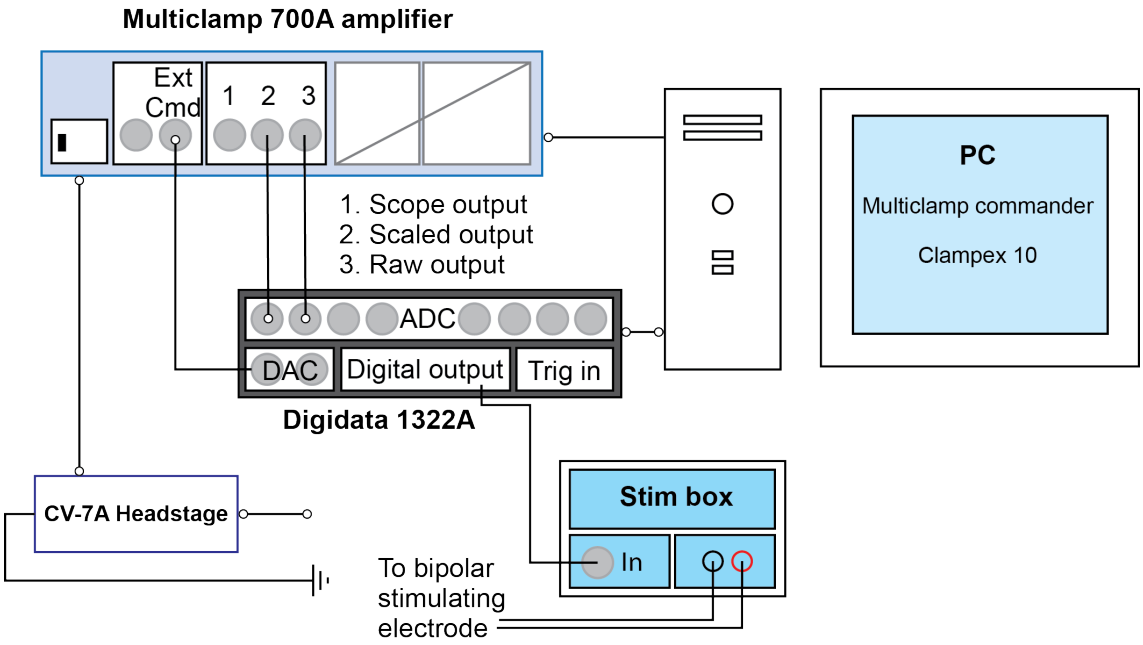

Figure 2.2: **Components of the electrophysiology set-up.** The recording and reference electrodes are connected to a headstage containing an amplifier circuit which is in turn connected to the software controlled Multiclamp 700A amplifier. Analogue acquisition signals are converted to digital signals via the digidata before being sent to the PC for visualisation in pClamp 10 software. Voltage commands generated via Clampex software are converted to analogue outputs, before being generated at the headstage. The stimulation box is controlled via digital output and Clampex 10 software.

2.7.3 Recording circuitry - operational amplifier

Whole cell recordings give researchers electrical access to the cell, required to control the potential difference across the membrane, in order to study voltage-dependent conductances. In voltage-clamp mode, this voltage control is achieved using a number of operational amplifiers (opamp), firstly to convert the recorded current to voltage, then to calculate the difference between the voltage inside the cell compared to a given command voltage (Ogden 1994). A simple schematic of the voltage-clamp circuit, during whole cell recordings can be seen in figure 2.3.

2.7.4 The problem of series resistance

Whilst this design is great as it only uses a single electrode to record and command, a number of issues arise from the circuitry. As well as the cell, the pipette also has associated capacitance and resistance. In addition to adding unwanted artefacts into recordings, this pipette resistance is in series with the cell capacitance and

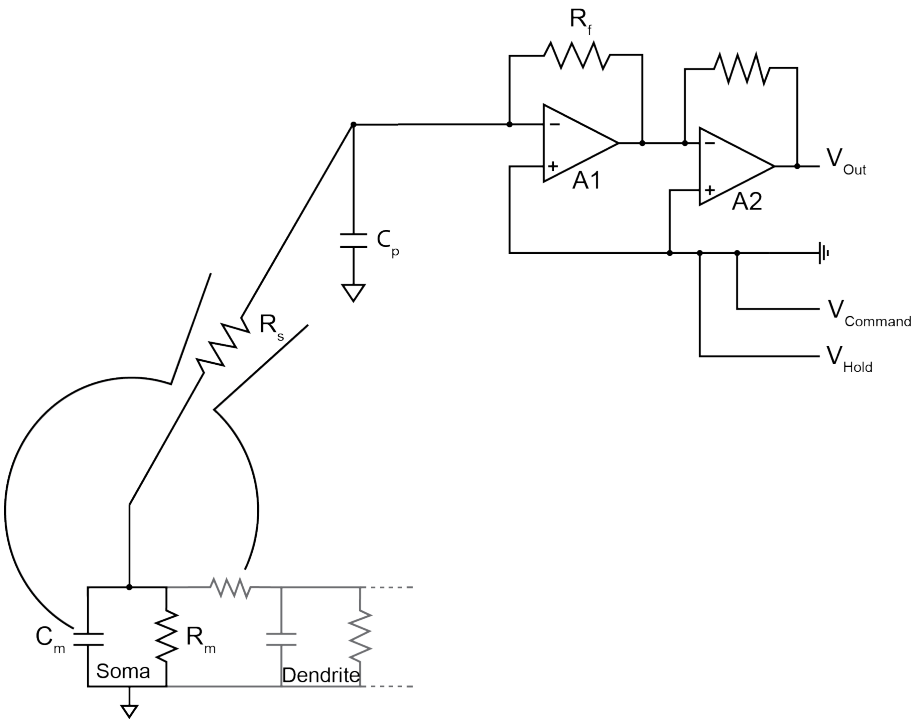

Figure 2.3: **Simplified diagram of amplifier circuit connected to a cell during whole cell patch clamp.** C_m and R_m are cell capacitance and resistance connected in parallel with membrane components of different cellular compartments connected in parallel. Series resistance (R_s) occurs at the tip of the pipette due to resistances of solutions and mainly cytoplasmic debris clogging the end of the pipette. C_p is parasitic capacitance, mostly due to pipette capacitance. A1 and A2 are operational amplifiers (op-amp) with A1 acting as a current to voltage converter and A2 as a differential amplifier. R_f is the feedback resistor used to convert current to voltage at the first op-amp, the value of which can be changed. A higher value resistor decreases noise but also decreases the maximum current that can be measured. Adapted from (Ogden 1994 and Barbour 2011).

thus forms a low-pass filter, distorting the recorded responses (figure 2.4). This pipette resistance also acts as a voltage divider creating a voltage drop, meaning the membrane voltage does not reach that of the pipette tip (i.e command voltage; figure 2.4). This creates a voltage error that, again dictated by ohms law, increases with the size of the current passed. For example, clamping a voltage at +20mV with a series resistance of 5 MΩ, producing a current of 5nA would produce a voltage error of 25mV, meaning the membrane voltage would only reach -5mV.

To overcome these issues, the amplifier contains a circuit with a variable capacitor and resistor in series, in order to neutralise the pipette and cell capacitance without affecting the behaviour of the cell itself (Ogden 1994). Similarly a positive feedback circuit is attached to the non-inverting input of the amplifier (in addition to command voltage) to compensate for some of the series resistance. In the above example, a series resistance compensated by 70% would produce an error of 7.5mV. Due to this need for compensation, recordings in which the series resistance changes dramatically (more than 10%) must be discarded as it is no longer clear if changes to the current amplitude are due to the blocking effect of a drug or simply due to an increase in uncompensated series resistance creating a bigger voltage error.

2.7.5 Liquid junction potential

Liquid junction potentials (LJP) arise due to different mobilities of ions at the junction of two liquids creating an imbalance of charge (Neher, 1992). This becomes a problem when recording in whole cell mode. During patch clamp, the pipette voltage is 'zeroed' when the pipette enters the bath and the membrane voltage is measured with respect to this zero current voltage. At this point, the solution in the pipette and bath are different, giving rise to a LJP, however when whole cell mode is entered, this is no longer the case and thus this LJP becomes another source of voltage error within the recording. The LJP was calculated (using JPCalcW in Pclamp10) to be -11mV for the experiments detailed in this thesis but was not corrected for.

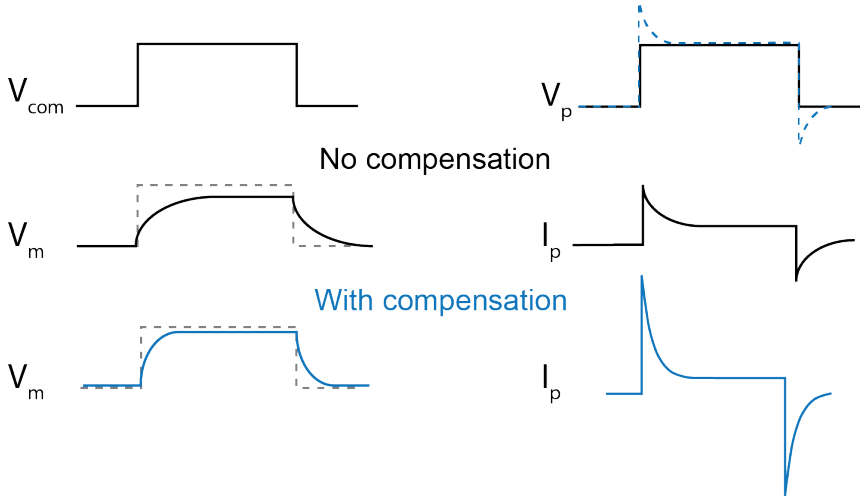

Figure 2.4: **Effect of series resistance on membrane potential (V_m).** Series resistance combines with cell capacitance, increasing the membrane time constant meaning V_m takes time to change at the onset of a voltage command. Rs acts as a voltage divider resulting in V_m never reaching the maximum voltage command. With series resistance compensation the time it takes for V_m to change at the onset of a voltage command decreases and the voltage it reaches is much closer to $V_{command}$. R_s compensation is achieved via positive feedback 'supercharging' the pipette voltage, proportional to current flow, resulting in larger current flow at $V_{command}$ onset.

2.7.6 Solutions

Brain slices were stored in and perfused with an artificial cerebrospinal fluid (aCSF) during experiments with ionic concentrations similar to those seen in extracellular fluid of the brain (pH = 7.2, osmolarity = 310-320 mOsms; Table 2.4). A similar slicing solution with low sodium and calcium was used for brain slice preparation. The osmolarity was balanced to 310mOsms using sucrose (Table 2.4).

Thick-walled, borosilicate glass pipettes (Harvard Apparatus #GC150F-7.5) were pulled to resistances of 3-4MΩ using a Narishige PC-10 vertical puller and filled with solutions that mimic the intracellular environment (high K^+, low Cl^- and Na^+). Intracellular solution composition can be found in table 2.5 (pH = 7.2 balanced with KOH, osmolarity 290 mOsms). A high chloride solution was used when recording K^+ currents (E_{Cl} = -32.7mV), however a low chloride solution (E_{Cl} = -70mV) was used for experiments investigating synaptic physiology to prevent reversal of inhibitory synaptic currents when holding neurons at -60mV. A reversal potential of -70mV ensured that activation of glycine receptors always produced a hyperpolarising IPSC (table 2.5).

Table 2.4: **Composition of normal and slicing artificial cerebrospinal fluid (acsf)**

Constituent	**Normal acsf (mM)**	**Slicing acsf (mM)**
NaCl	125	
$NaHCO_3$	26	26
Glucose	10	10
Myo-inositol	3	
KCl	2.5	2.5
Sodium pyruvate	2	
$CaCl_2$	2	0.1
NaH_2PO_4	1.25	1.25
$MgCl_2$	1	4
Ascorbic acid	0.5	0.5
Sucrose		250

Table 2.5: **Composition of intracellular patch solution for K^+ recordings. Free calcium concentration = 100nM.**

Constituent	**For I_{K^+} (mM)**	**For $I_{synaptic}$ (mM)**
K-gluconate	97.5	120
KCl	32.5	10
HEPES	40	40
EGTA	0.2	0.2
$MgCl_2$	1	1
K2- ATP	2.2	2.2
NaGTP		0.3
$CaCl_2$	0.8μL per 100mL	

2.7.7 Brain slice preparation

Mice were killed by decapitation, the brain removed from the skull and placed in ice cold slicing solution. The brain was placed with the anterior side exposed and the hindbrain removed from the forebrain with the scalpel placed at a 30^o angle to the vertical plane, towards the posterior. The hindbrain was glued to a specimen stage with the cut side down and submerged in ice cold, oxygenated slicing solution in a vibratome cutting bath (Leica biosystems, VT1200S), surrounded by ice. Slicing solution was continuously oxygenated with 95% O_2/5 %CO_2 during sectioning. Unless otherwise stated, 200μm slices were taken with a vibratome using a stainless steel blade and placed in a recovery chamber filled with normal, oxygenated aCSF, heated to 37^oC to recover for 1 hour.

2.7.8 Whole cell patch clamp

During the experiment slices were placed into a recording chamber on an upright Nikon E600FN microscope with differential interference contrast (DIC) optics and a 60x objective and cells visualised via a connected Ximea CCD, 2.8 megapixel camera (MD028MU-SY). A platinum harp with single nylon fibres attached was used to prevent the slice from moving while it was continuously perfused with oxygenated (95% O_2/5 %CO_2) acsf at a rate of 1ml/min. The perfusion system consisted of a peristaltic pump (Gilson minipuls 3) connected to a bubble trap, which serves to remove bubbles as well as electrically isolating solution flowing into the bath, and a peltier controller (Campden Instruments model 7800) which heats the solution to 35^oC. Three separate perfusion lines were connected to the rig to allow perfusion of drugs without contaminating the line carrying normal acsf. Drug application to brain slices was achieved by priming one of these lines (allowing solution to fill the line without fully reaching the bath, then unclamping the pump to prevent flow into the bath) to minimise dead time between perfusion of acsf and drug-containing acsf. When required, the line containing normal acsf was switched off and that containing the drug was switched on.

The method of patch clamp relies on the formation of a high resistance seal

between the pipette and cell membrane, typically over 1GΩ. In order to do this, positive pressure (typically 2mL with a 10mL syringe) was applied to the pipette (3-4MΩ resistance), to clean the membrane of debris that may impede the formation of a GΩ seal and the pipette moved close to the cell using a micromanipulator (sutter MP-285). The positive pressure creates a dimple in the surface of cell, indicating that the pipette is close to the surface. At this point, the pressure was slowly removed and if necessary negative pressure was applied. A negative holding potential was applied to the cell (typically -60mV), as it aided in the formation of the seal. Once a seal was formed, pipette capacitance was neutralised. All of the experiments detailed in this thesis were done using whole cell patch clamp. To achieve this mode, once the seal was formed, negative pressure was added to the pipette to break the membrane, giving electrical access to the inside of the cell. At this point, whole cell capacitance and series resistance were measured and prior to starting an experiment, series resistance was compensated using the prediction and correction parameters, set to 70%.

Unless otherwise stated, all experiments were conducted at 35^{o}C $\pm$ 1. Recordings were digitised at 100kHz and filtered at 10kHz and the bandwidth of compensation was set to 15.92Hz which is equal to 10μs lag.

2.7.9 Analysis

All electrophysiological data was analysed using Clampfit software (Pclamp 10) and graphs produced using Graphpad Prism 7.0. Current-voltage (I-V) curves were typically produced using current amplitudes towards the end of voltage steps (specified in results chapters). I-V curves in each neuron were produced from an average of 3 trials in the same cell. Action potentials analysed were generated using current steps and only the first action potential to be generated was analysed. The average values from 3 trials in the same neuron are plotted for each cell. Excitatory and inhibitory postsynaptic currents (EPSC and IPSC, respectively) were detected and parameters extracted using the template search or event detection feature of Clampfit. The data presented for each neuron are averages from 5 trials in the same

cell.

2.8 Statistics

Statistical analysis presented throughout this thesis was conducted using Graphpad Prism 7.0. Where more than 2 groups were being compared (control, Kv3.1 KO and Kv3.3 KO) an ANOVA was used with a Tukey's post hoc test for multiple comparisons. In experiments where data from the same cell was compared (control vs 1mM TEA), paired t-tests were used and in those comparing data from different cells but with only two groups (WT vs Kv3.3 KO) an unpaired t-test was carried out. In all experiments $P<0.05$ was considered a significant difference. Unless otherwise stated all variances throughout the thesis are standard error of the mean (SEM).

Chapter 3

Kv3 channels in the superior olivary complex (SOC) are composed of Kv3.3 and Kv3.1

The superior olivary complex (SOC) is an area within the auditory brainstem containing a number of nuclei, including the medial nucleus of the trapezoid body (MNTB), lateral superior olive (LSO) and medial superior olive. Among other things, these nuclei are involved in sound localisation processing. In order to accurately locate sounds, neurons must follow high frequency sound stimuli with high temporal fidelity. It has been established that Kv3 channels are responsible for fast repolarisation of action potentials, allowing neurons to fire at high frequencies, making them essential in this pathway.

The aim of this thesis was to identify subunits forming presynaptic Kv3 channels and investigate their role in modulating synaptic transmission. The experiments required making whole-cell patch recordings directly from the giant calyx of Held terminal however, due to the technical challenges involved with conducting presynaptic recordings, we started by characterising Kv3 currents in MNTB and LSO principal neurons.

Kv3 currents have been identified in nuclei of the SOC, including the MNTB and LSO (Linley 2017; Macica et al. 2003; Brew and Forsythe 1995; Wang et al. 1998). While previous work has postulated that Kv3.1b is the main constituent subunit

of these channels, it has also been suggested that Kv3.2, 3.3 and 3.4 are present in varying quantities (Johnston 2007; Wang and Kaczmarek 1998; Ishikawa et al. 2003). Contradictory to this evidence, RNA sequencing conducted in our lab shows that only Kv3.1 and Kv3.3 are present in the MNTB and LSO (figure 1.9) meaning native channels must be composed of these subunits, either as homomers, heteromers or a mixed population of both. This chapter will provide evidence that only Kv3.1 and Kv3.3 proteins are expressed in principal neurons of the SOC and they differentially contribute to Kv3 currents in the MNTB and LSO. Unless otherwise stated, all variance is stated as SEM.

3.1 Immunohistochemical labelling (IHC) of Kv3 subunits in the SOC

IHC was carried out to validate the RNA sequencing data and determine whether the mRNA is translated into functional Kv3 proteins (functional channels must be present on the membrane).

Immunohistochemical staining was conducted on brainstem sections of P21 mice using antibodies raised against Kv3.1b (dilution 1:1000), Kv3.2 (1:500), Kv3.3 (1:3000) and Kv3.4 (1:500) of which Kv3.1b and Kv3.3 have previously been validated using knockout animals (Figure 3.10). 12μm brainstem sections were post-fixed in 4% PFA and those used for Kv3.1/Kv3.3 staining underwent further antigen retrieval (see methods). Due to the lack of knockout animals for Kv3.2 and Kv3.4 subunits, these antibodies had to be validated using only the blocking peptide controls. No evidence of non-specific staining was observed in the presence of these peptides for either antibody (data not shown).

High levels of Kv3.3 and Kv3.1b staining was seen throughout the SOC, however localisation of the protein staining differed across auditory nuclei. Both proteins show apparent membrane staining in the MNTB while only Kv3.3 was present in the somata and proximal dendritic membrane of the LSO (figure 3.1). In contrast Kv3.1b protein is localised to the neuropil in the LSO, composed of synaptic boutons, dendritic spines and axons, with very little staining present in neuronal somata. Additionally, Kv3.1b appears to be localised to axon inital segments (figure 3.1 and confirmed by coimmunostaining with AIS marker Ankyrin G by another lab member) and nodes of Ranvier in MNTB principal neurons, whereas Kv3.3 is mainly somatic.

No Kv3.2 staining was observed throughout the SOC, consistent with an absence of protein. Kv3.4 however, produced discrete areas of fluorescence in both the MNTB and LSO, although it did not appear to be present in the membrane, nor was it present in principal cells (Figure 3.2). In fact, Kv3.4 staining appeared to be nuclear, often characteristic of non-specific binding of the antibody.

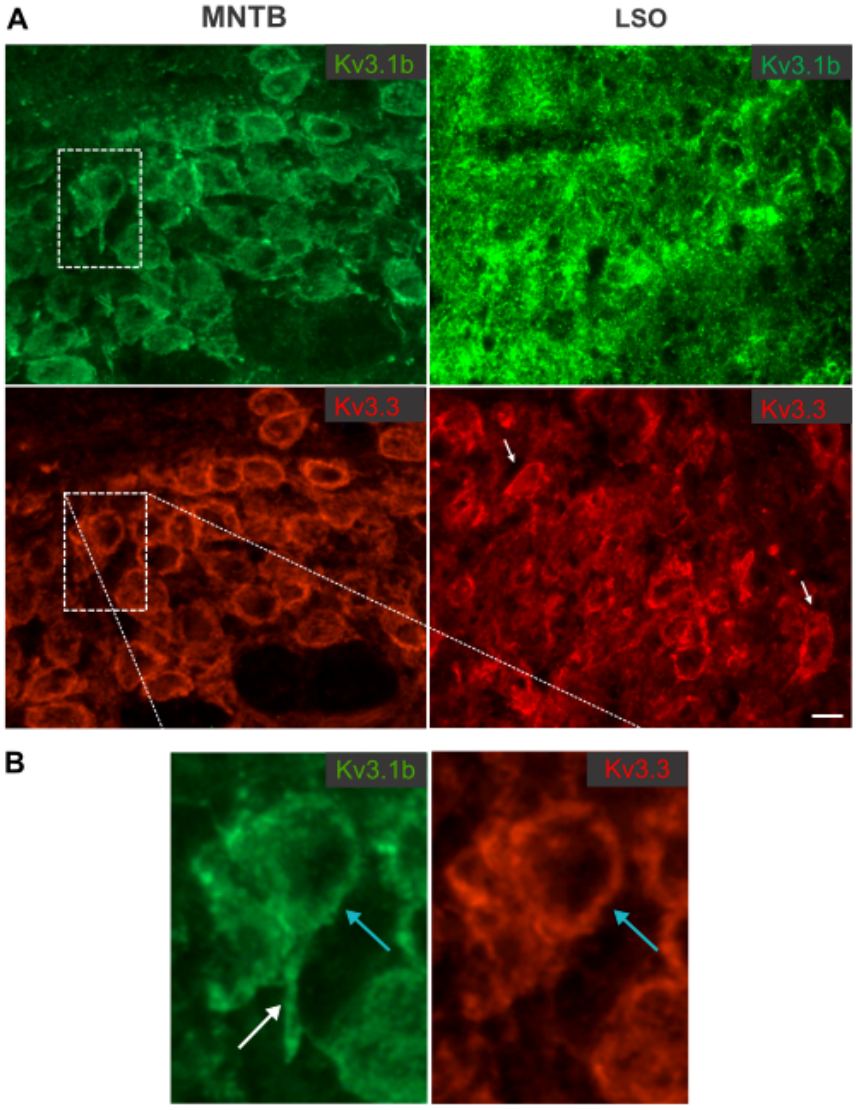

Figure 3.1: **Kv3.3 and Kv3.1 are expressed in MNTB neurons but only Kv3.3 is present in the LSO soma.** Images from a brainstem section taken from a P21 WT CBA mouse, fixed with 4% PFA and citric acid antigen retrieval. **A: Left panel** Kv3.1b (green; dilution 1:1000) and Kv3.3 (red; dilution 1:3000) staining in the MNTB.Area in white boxes are magnified in panel B. **Right panel:** The same in the LSO. White arrows indicate cell somata stained with Kv3.3. 40x magnification; Scale bar = 20μm. **B:** Magnified single MNTB neuron stained with Kv3.1b (green) and Kv3.3 (red), seen in panel A. Blue arrows indicate somatic staining; white arrow indicates axon initial segment staining with Kv3.1b. This is not seen in the same neuron stained with Kv3.3.

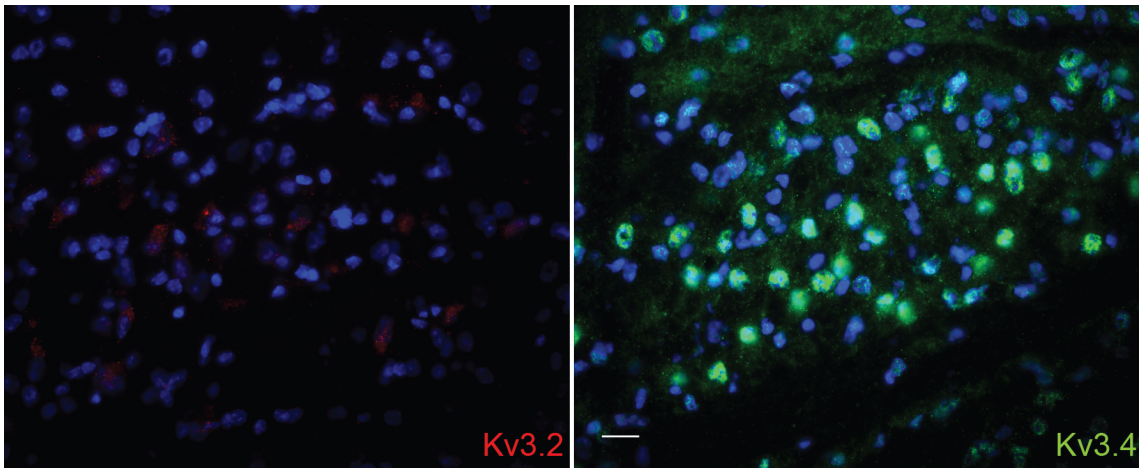

Figure 3.2: **Kv3.2 and Kv3.4 are absent in the MNTB. Left:** Kv3.2 (red; dilution 1:200) and nuclear dapi (blue) staining in the MNTB and **Right:** Kv3.4 (green; dilution 1:200) and dapi (blue) staining. Scale bar = 20μm. 20x magnification. IHC performed by Sherylanne Newton.

3.2 Kv3 potassium currents in the MNTB and LSO

Whole cell patch clamp was used to investigate whether these Kv3.1b and Kv3.3 subunit proteins form functional channels in the membrane of neurons in the MNTB and LSO, by examining the contribution of high-voltage activated conductances (Kv3) to outward potassium currents in these cells.

Kv3 currents can be isolated from other potassium currents using low concentrations of the potassium channel blocker tetraethylammonium (TEA). Paired experiments were conducted on P21-25 mice in which voltage protocols were applied to principal neurons of the MNTB or LSO during perfusion of 1mM TEA dissolved in acsf (figure 3.3). The resulting currents were plotted against command voltage in current-voltage (I-V) plots, both before and after 4 minutes of TEA application, hereafter referred to as control and 1mM TEA, respectively (Figure 3.3).

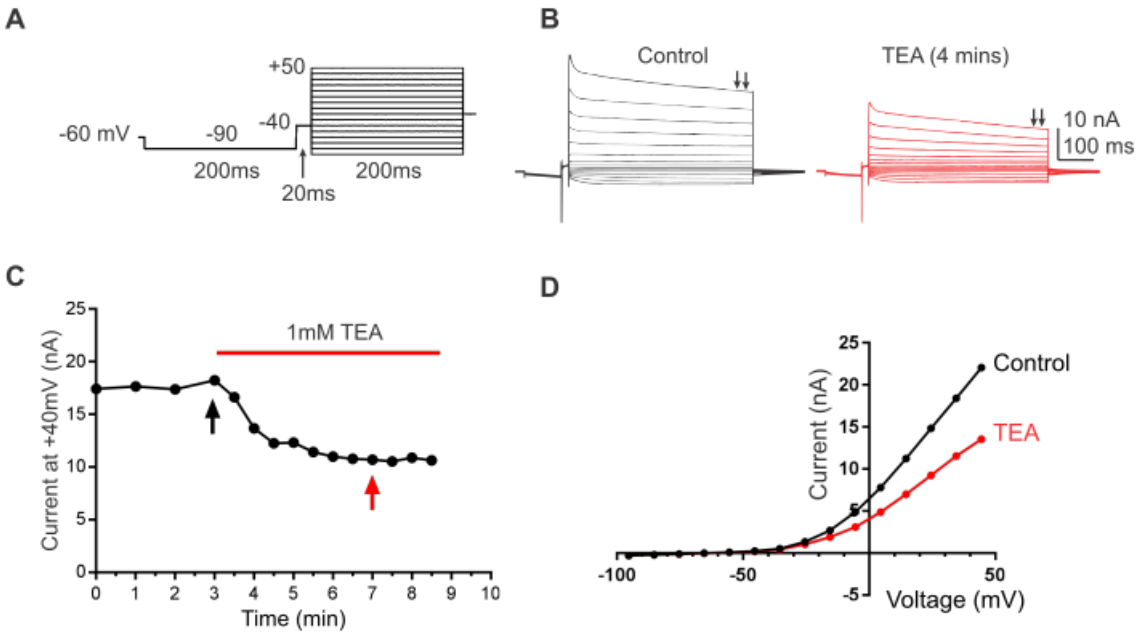

Figure 3.3: **Analysis of paired TEA perfusion experiments. A:** Voltage protocol applied to neurons from a holding potential of -60mV. A 200ms -90mV prestep was included to ensure all channels are free from inactivation, followed by a 20ms prepulse to -40mV to inactivate sodium, calcium and fast-inactivating potassium currents (Kv4). Finally a 200ms test step was applied from +50mV to -110mV in 10mV increments. **B:** Example of currents traces produced by voltage command in A, before and after TEA was applied. Arrows indicate the point of the trace that was analysed and used to generate IV plots.**C:** Current measured at +40mV before and during perfusion of 1mM TEA. Black arrow indicates time point of analysed control currents, red arrow indicates the same for 'TEA' currents. **D:** Example IV plot for control and TEA currents from one cell.

Figure 3.4 shows TEA-sensitive currents in principal cells of the MNTB. Currents above -20mV are sensitive to TEA block, consistent with its action on high voltage-activated Kv3 channels which activate around -20mV (figure 3.4B). This 'Kv3' current contributes on average 3.1 ±0.5nA of total outward current at +10mV, which is equal to 27.2 ±4.5% (n=4; figure 3.4C & D). Currents produced at this voltage are relatively small, consequently voltage errors due to series resistance are smaller and changes in current are more likely to reflect real actions of the blocker. The block produced by TEA is significant (Paired t-test; p= 0.0086, t= 6.161, df= 3) and can not be attributed to a time-dependent phenomenon such as run down as currents produced by the same protocol applied to neurons without perfusion of TEA are unaffected (figure 3.5).

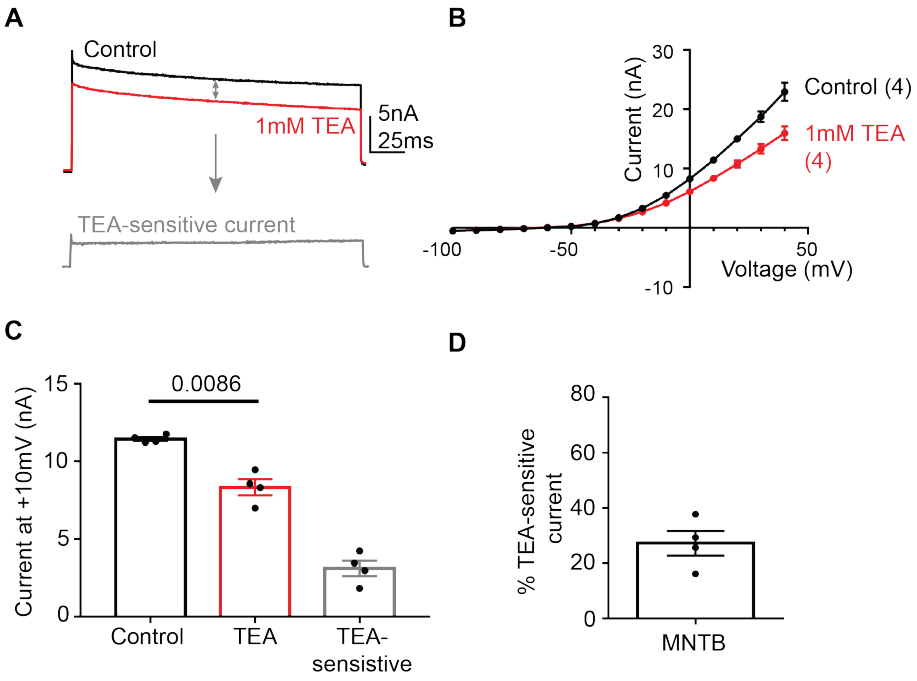

Figure 3.4: **MNTB principal neurons possess a TEA-sensitive current. A:** Example traces from one neuron at a command voltage of +40mV before (black) and after (red) application of 1mM TEA. The difference between these (marked by double ended grey arrow) shows the TEA-sensitive portion of current (grey). **B:** I-V plot of potassium currents before and after TEA perfusion. n = 4 cells from mice aged P21-25. **C:** Current amplitudes at +10mV from cells in B. The reduction in current produced by TEA is significant (Paired t-test; p= 0.0086, t= 6.161, df= 3). TEA-sensitive is defined as this difference in amplitudes between control and TEA. **D:** Percentage of TEA sensitive current calculated from C.All errors plotted are SEM.

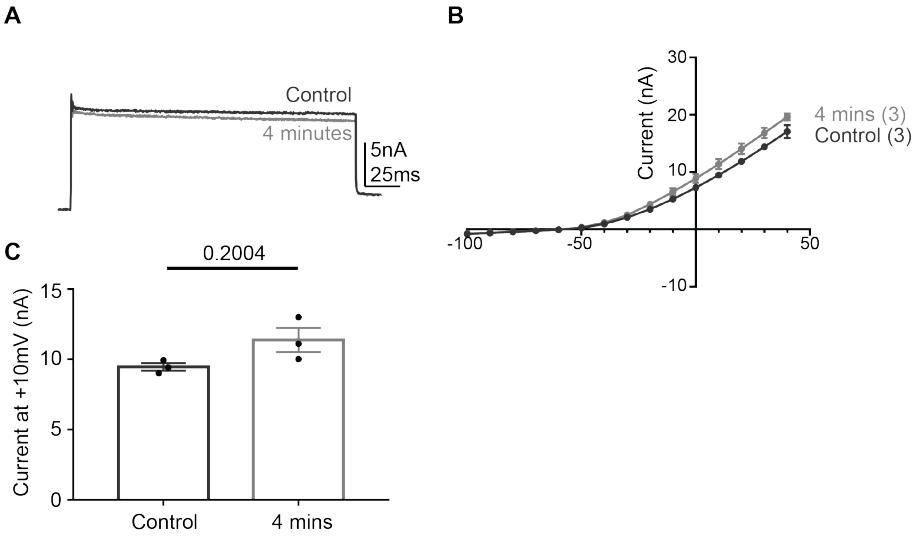

Figure 3.5: **Potassium current amplitudes in MNTB neurons do not change with time. A:** Example current traces produced at +10mV at the same time points recorded for TEA perfusion experiments. **B:** I-V plot of these potassium currents. n = 3 neurons. **C:** Current amplitudes measured at +10mV. Current amplitudes do not change significantly during 4 minutes of recording (Paired t-test; P=0.2004, t=1.883, df=2). All errors plotted are SEM.

Similar to principal cells in the MNTB, those in the LSO also possess TEA-sensitive currents (figure 3.6). Principal cells in this region were identified by their oval shape, the presence of a large hyperpolarisation-activated current and absence of a fast-inactivating A-current (Sterenborg et al. 2010). Similar to the action of TEA on MNTB neurons, TEA blocks potassium currents at potentials positive to -20mV. However, this TEA-sensitive current is larger in the LSO, contributing on average 4.8 ±0.23nA of the total current at +10mV, equal to 43 ± 5.5% (figure 3.6C & D). This TEA block is significant at +10mV and again is not affected by a time-dependent phenomenon (Control vs TEA, Paired t-test P=0.002, t=21.21, df=2; Control vs 4 minutes, Paired t-test, P=0.4121, t=1.028, df=2; figure 3.7).

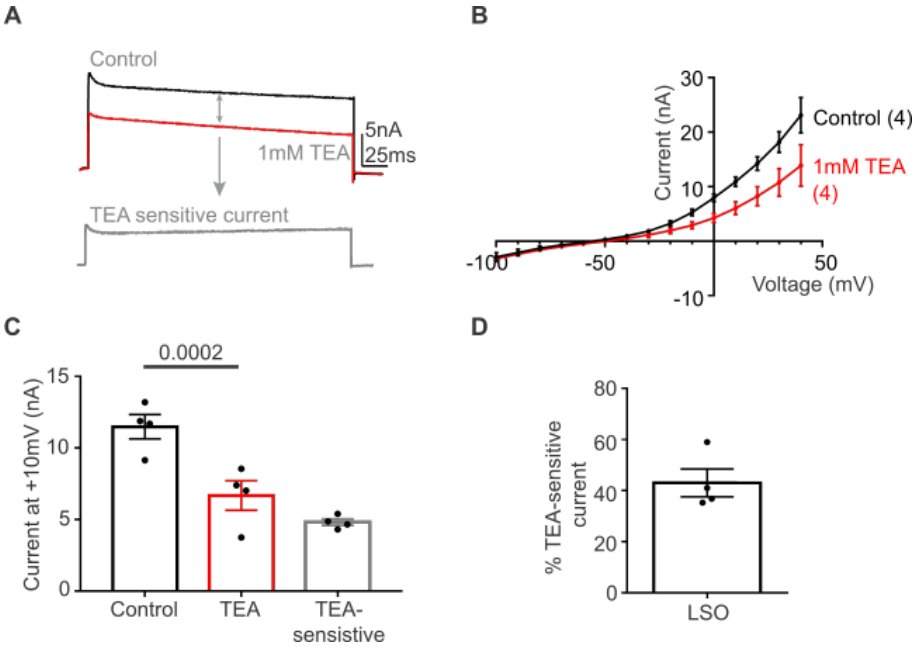

Figure 3.6: **LSO neurons possess a TEA-sensitive current. A:** Example traces from one neuron at a command voltage of +40mV before (black) and after (red) application of 1mM TEA. The difference between these (marked by double ended grey arrow) shows the TEA-sensitive portion of current (grey). **B:** I-V plot before and after TEA perfusion. n = 3 cells from mice aged P21-25. **C:** Current amplitudes at +10mV from cells in B. The reduction in current produced by TEA is significant (Paired t-test; p= 0.002, t=21.21, df= 2). 'TEA-sensitive' is defined as the difference in amplitudes between control and TEA. **D:** Percentage of TEA-sensitive current calculated from C. All errors plotted are SEM.

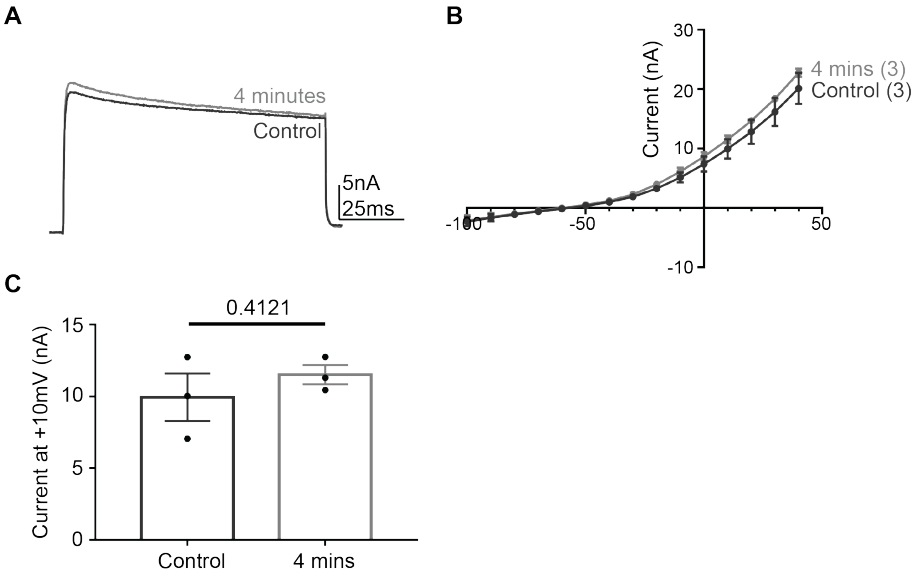

Figure 3.7: **Potassium current amplitudes in LSO neurons do not change with time. A:** Example current traces produced at +10mV at the same time points recorded for TEA perfusion experiments. **B:** I-V plot of these outward potassium currents. n=3 neurons. **C:** Current amplitudes measured at +10mV. Current amplitudes do not change significantly during 4 minutes of recording (Paired t-test; P=0.4121, t=1.028, df=2). All errors plotted are SEM.

3.3 Contribution of Kv3.1 and Kv3.3 subunits to Kv3 current in the MNTB and LSO

It has been established that principal neurons in both nuclei possess TEA-sensitive, Kv3 currents but which subunits carry this current remains unknown. Previous work has identified Kv3.1 as the sole contributor to Kv3 currents in MNTB neurons, with Kv3.1 KO mice reportedly showing a complete lack of high-voltage K^+ current (Macica et al. 2003). Utilising Kv3.1 and Kv3.3 knockout animals we show that, in contrast to these previous findings, both subunits are equally important in the MNTB, whereas Kv3.3 appears to carry the Kv3 current in LSO neurons.

Voltage clamp experiments were conducted on CBA WT, Kv3.1 KO and Kv3.3 KO mice aged P21-25 using the same voltage protocol used in TEA experiments. After entering whole-cell configuration, cells were left for 5 minutes for dialysis of internal patch solution to occur before any protocols were recorded. I-V plots for each neuron were created from an average of 3 recordings taken 1 minute apart. Figure 3.8 shows that K^+ currents in both knockouts are similar to WT. Current amplitudes at +10mV of 10.3± 1.68nA (n=12), 11.6± 2.54nA (n=7) and 9.1± 1.96nA (n=8) in WT, Kv3.1 and Kv3.3 KO, respectively are not significantly different (one-way ANOVA, $F(2,24)= 2.801$, $P=0.0806$; figure 3.8C). In contrast, current amplitudes in the LSO are reduced at voltages positive to -20mV in the Kv3.3 KO compared to both WT and Kv3.1 KOs (figure 3.9B). At +10mV average current amplitudes are significantly decreased at 6.3± 2.11nA (Kv3.3 KO n=9) compared to 11.4± 3.63nA (n=12) in WT and 11.8± 3.04nA (n=6) in Kv3.1 KO (one-way ANOVA, Tukey's post hoc, WT vs Kv3.3 KO $P=0.0028$, Kv3.1 KO vs 3.3 KO $P= 0.0062$; figure 3.9C). Potassium currents in Kv3.1 KOs however were not significantly different from wildtype principal neurons (one-way ANOVA, Tukey's post hoc, WT vs Kv3.1 KO, $P=0.9510$).

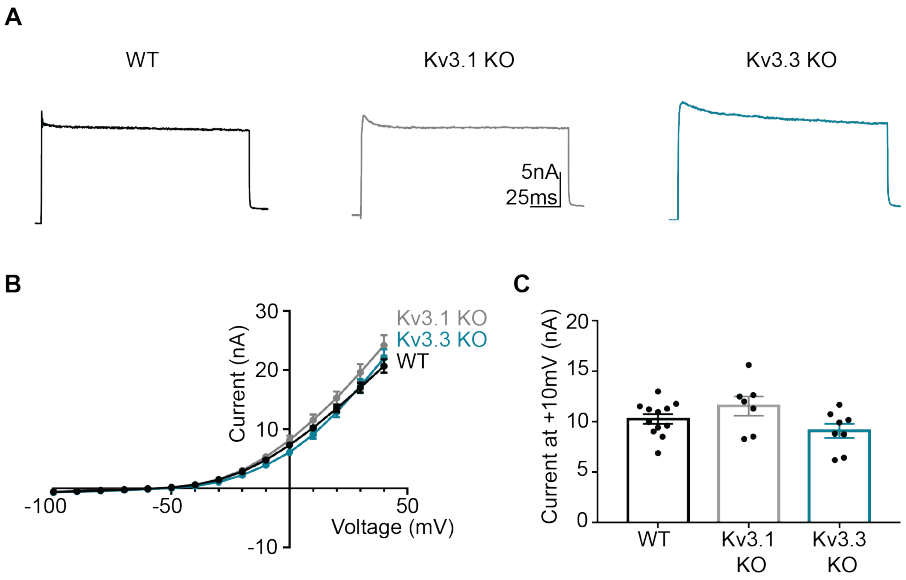

Figure 3.8: **Potassium currents in MNTB neurons are not changed in Kv3.3 and Kv3.1 KO mice aged P21-P25. A:** Example current traces generated with a +10mV voltage command from single neurons. **B:** I-V plot for K^+ currents in WT (n=12), Kv3.1 KO (n=7) and Kv3.3 KO mice (n=8). **C:** Currents measured at +10mV from recordings in B. Currents are not significantly different (one-way ANOVA, F(2,24)=2.801, P=0.0806). All errors plotted are SEM.

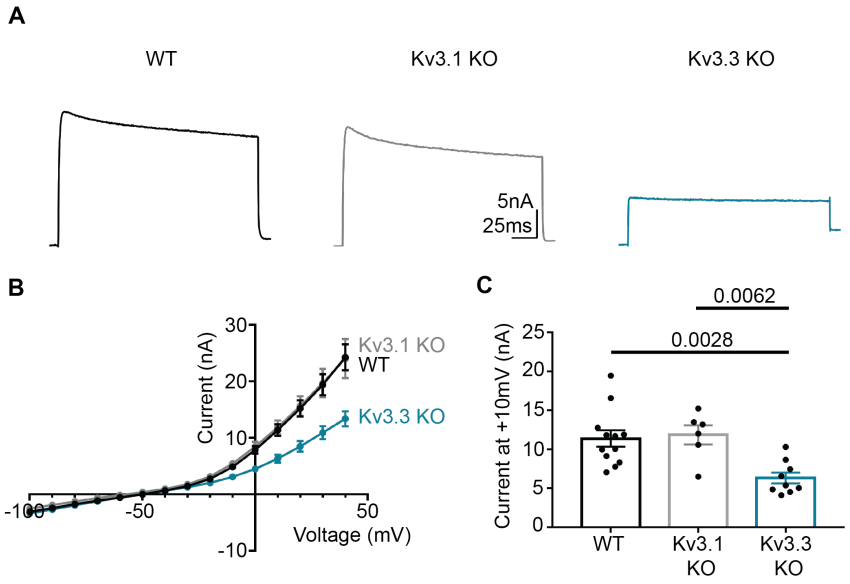

Figure 3.9: **Potassium currents in LSO principal neurons are decreased in Kv3.3 KO mice but not Kv3.1 KOs. A:** Example current traces generated with a +10mV voltage command from single neurons. **B:** I-V plot for K^+ currents in WT (n=12), Kv3.1 KO (n=6) and Kv3.3 KO mice (n=9) aged P21-P25. **C:** Currents measured at +10mV from recordings in B. Currents are significantly decreased in Kv3.3 KOs (one-way ANOVA & Tukey's post hoc, P values displayed on graph). All errors plotted are SEM.

3.4 Histological validation of knockout mice

Western blots were carried out on both knockout mice lines to confirm that no protein was present in the brain (figure 3.10). Entire brainstems were taken from three mice aged P21-22 from each knockout line and Kv3.1 and Kv3.3 protein levels were compared to those in WT mice. No Kv3.3 protein expression was detected in tissue from Kv3.3 KO mice. In contrast low levels of Kv3.1b protein were detected in Kv3.1 KO mice, although this was minimal (0.28 vs 1.80 and 2.12 in WT and 3.3KO, respectively). There was no significant difference in level of Kv3.1b protein in Kv3.3 KO animals compared to WT (one-way ANOVA & Tukey's post hoc, P = 0.6148) nor was there a significant difference in Kv3.3 protein in the Kv3.1 KOs (one-way ANOVA & Tukey's post hoc, P= 0.7973).

Since a small amount of protein expression was seen in the Kv3.1 KOs, immunohistochemistry was used to determine whether this protein was present on the membrane of neurons, indicating it may still be functional. Figure 3.11 shows there is no staining present in either knockout, while protein expression of the other subunit remains unchanged.

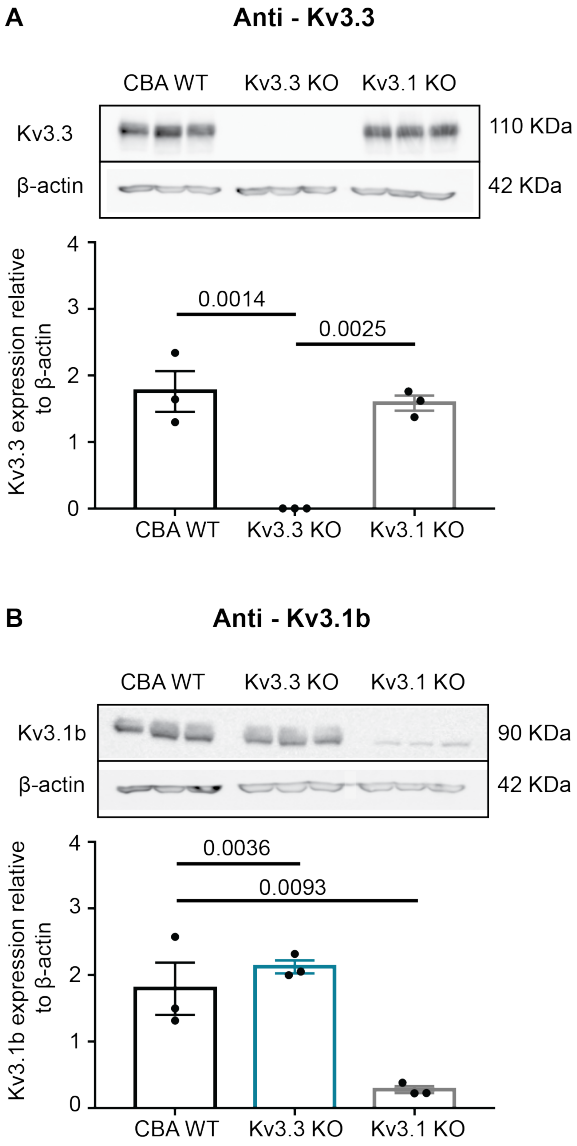

Figure 3.10: **Kv3.1b and Kv3.3 protein is absent in Kv3.1 and Kv3.3 KOs, respectively. A:** Western blot using anti-Kv3.3 antibody on brainstem tissue from P21-22 wildtype, Kv3.3 KO and Kv3.1 KO mice. Each band represents a sample from a different mouse. Kv3.3 expression is significantly lower in the knockout than either WT or Kv3.1 KO (One-way ANOVA & Tukey's post hoc, P values on graph). **B:** Western blot using anti Kv3.1b antibody on the same tissue samples as in A. Kv3.1b expression is significantly lower in the knockout than WT or Kv3.3 KOs (one-way ANOVA & Tukey's post hoc, P-values displayed on graph). All errors plotted are SEM.

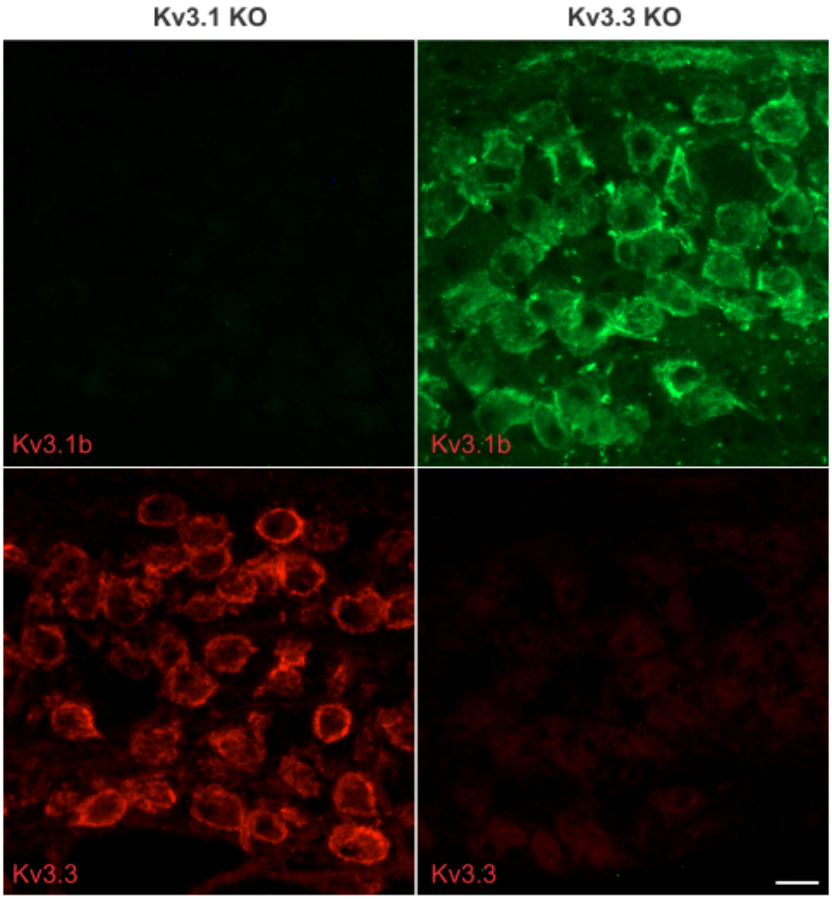

Figure 3.11: **No Kv3.1b or Kv3.3 staining is observed in Kv3.1 and Kv3.3 KO mice, respectively. Left panel:** Kv3.1b (green; dilution 1:1000) and Kv3.3 (red; dilution 1:3000) staining in the MNTB of a P21 Kv3.1 KO mouse. **Right panel:** The same in a Kv3.3 KO mouse. Images taken at 40x magnification. Scale bar = 20μm. Images taken by Michelle Anderson.

3.5 Discussion

High voltage-activated Kv3 currents are vital in the auditory brainstem to rapidly repolarise action potentials, allowing neurons in this system to accurately follow inputs with exceptional temporal precision up to frequencies of ∼800Hz (Macica et al. 2003; Taschenberger and Von Gersdorff 2000; Wu and Kelly 1993). Previous work has identified Kv3.1 as the sole contributor of Kv3 currents in principal neurons of the MNTB, while little work has been published on the subject in LSO neurons (Macica et al. 2003). This chapter demonstrates that, in fact, both Kv3.1 and Kv3.3 subunits are present in the membrane of MNTB and LSO principal neurons and while both of these appear to equally contribute to potassium currents in the MNTB, Kv3.3 is the dominant subunit in the LSO.

3.5.1 MNTB and LSO neurons possess significant Kv3 currents

Here we have confirmed the presence of Kv3 currents in neurons of the MNTB, shown by the sensitivity of potassium currents to low concentrations of TEA (Brew and Forsythe 1995; Macica et al. 2003; Wang et al. 1998) and provided some of the first evidence of functional Kv3 channels in the LSO.

At these concentrations (1mM), TEA is relatively selective for Kv3 channels however, it will also block Kv1.1 homomers (Kd∼0.3mM) and BK channels to some extent (Henney et al. 2009; Grissmer et al. 1994; Coetzee et al. 1999). Block of Kv1.1 homomers by TEA in these cells can be excluded as previous experiments conducted in the lab show the amplitude of TEA-sensitive current is unaffected in the presence of dendrotoxin-I (DTx-I), a specific Kv1 blocker, when sequentially applied to a brain slice (Johnston 2007). Similarly recordings conducted in low calcium do not affect TEA-sensitivity in the MNTB suggesting the absence of BK channels in these cells (Nasreen Choudhury, unpublished). Some change in TEA-sensitivity is seen in the LSO in low-calcium conditions and indeed some TEA sensitive current remains in Kv3.3 KO animals suggesting BK conductances could be present in these neurons, albeit very small (Nasreen Choudhury, unpublished).

Thus the use of TEA in the LSO may lead to an overestimate of overall Kv3 current, however in the MNTB it is possible to conclude that this most likely represents current driven through these channels.

3.5.2 Kv3 subunit composition in the MNTB

The lack of Kv3.2 staining observed in the MNTB and LSO is consistent with a lack of mRNA seen with RNA sequencing and RTPCR studies and suggests the protein is absent from these nuclei. Similarly, the lack of Kv3.4 staining in the membrane suggests that even if this subunit is present it is unlikely to be functional. Thus Kv3 channels in both of these nuclei must be composed of Kv3.1 and Kv3.3 subunits, although composition of channels in different nuclei varies.

In accordance with previous research, Kv3.1b and Kv3.3 proteins were highly expressed in the membrane of MNTB neurons (Wang et al. 1998; Elezgarai et al. 2003; Chang et al. 2007; Grigg, Brew, and Tempel 2000; Li, Kaczmarek, and Perney 2001), suggesting both contribute to functional Kv3 channels in these cells. Indeed, amplitudes of potassium currents in MNTB neurons, in particular the proportion of TEA-sensitive current (Deborah Linley, in press) remains unchanged in both Kv3.1 and Kv3.3 KOs, suggesting compensation for one subunit by the other and thus equal contribution by both to Kv3 channels in wildtype animals.

These results are in contrast to those presented by Macica et al. 2003 in which high-voltage activated potassium currents were vastly diminished in Kv3.1 KOs. The only major experimental difference between the present findings and those in this previous study is that they used a holding potential of -40mV (compared to -60mV used here) in order to inactivate low threshold Kv1 channels (Brew and Forsythe 1995) and isolate Kv3 conductances. This may have also contributed to a small amount of Kv3 inactivation, reducing current amplitudes. However, these experiments were repeated in our lab at a holding of -40mV and no significant differences between WT K^+ currents and those in Kv3.1 KOs were found (Nasreen Choudhury, personal communication). Interestingly only 1 recording from a single neuron was presented in the Macica et al paper and since there are many reasons

for small currents being produced, such as high series resistance and large seal leak, it is likely that if repeated on more neurons, this effect may be lost.

3.5.3 Kv3 subunit composition in the LSO

Similar to the MNTB, principal neurons of the LSO have a high expression of Kv3.3, however Kv3.1b appears to be absent (figure 3.1). This is consistent with mRNA expression previously shown with *in situ* hybridisation (Grigg, Brew, and Tempel 2000; Li, Kaczmarek, and Perney 2001) and with significantly decreased potassium currents in animals lacking Kv3.3 subunits but no change in Kv3.1 KOs, presented here in this study (Figure 3.12).

Thus, in contrast to the MNTB where both subunits appear to equally contribute to Kv3 subunit composition, Kv3.3 appears to be solely responsible for mediating Kv3 current in the LSO and Kv3.1 cannot compensate when Kv3.3 is absent.

3.5.4 Subcellular targeting of Kv3.1b and Kv3.3

While both of these subunits were clearly present in the MNTB, their subcellular distribution differs. Kv3.1b subunits dominated at the axon initial segment (AIS) and nodes of Ranvier in addition to its presence in the somatic membrane, whereas Kv3.3 subunits appeared to be restricted to the soma.

Similarly Kv3.1b was present in the neuropil of the LSO, which consists of axonal segments, synaptic boutons and dendritic compartments. While Kv3.3 was also present in the neuropil it was highly expressed in neuronal somata and proximal dendrites.

These results provide evidence for different subcellular targeting of each of these subunits with Kv3.1b mainly targeted to axonal regions and Kv3.3 abundant in somatodendritric compartments, likely to be determined by sequences in the C-terminus of the proteins (Deng et al. 2005). Indeed, a specific targeting motif has been identified in the C terminus of Kv3.1, which directs this subunit to axons and possibly allows association to ankyrin G, a scaffolding protein present in the AIS (Xu et al. 2007; Ozaita et al. 2002).

3.5.5 Subcellular distribution of Kv3.1 and Kv3.3 may reflect different molecular interactions

Since current kinetics of these subunits are almost identical, with similar activation (-20mV), half-activation (+6.4mV vs +6.7mV for Kv3.3 and Kv3.1, respectively) and inactivation voltages (-19mV vs -12mV in Kv3.3 & Kv3.1) when expressed in CHO cells (chapter 7) these differences in localisation may reflect variation in non-conducting functions of the subunits or proximity to down-stream signalling molecules. Many ion channels have been found to have functions in addition to their role in conducting ions (Kaczmarek 2006).

For example, mutant Kv3.3 subunits cause cellular neurodegeneration in the disease spinocerebellar ataxia type 13 (Waters et al. 2006). There are a number of different mutations which alter the electrical properties of Kv3 channels, some completely abolish the current driven through the channel while some shift the activation voltage (Waters et al. 2006; Duarri et al. 2015; Minassian, Lin, and Papazian 2012). Despite the different effects on channel properties, all of these mutations lead to neurodegeneration in the cerebellum, suggesting these subunits have roles in the cell different from their function of an ion channel. Associations between this subunit and the actin cytoskeleton have recently been identified (Zhang et al. 2016), indicating a possible structural role.

3.5.6 Heteromers vs homomers

It is popular opinion that Kv3.1 and Kv3.3 channels form heteromeric channels in native neurons, based on evidence that other Kv3 subunits heteromerise (Baranauskas et al. 2003), indeed co-immunoprecipitaion performed on cerebellar tissue has shown that the subunits can be associated (Chang et al. 2007). However, here we show that expression of these subunits is unchanged in the absence of the other (figure 3.11), showing that not only are the subunits able to form homomeric channels but they do not require the other subunit to be localised to the membrane or to specific regions of the cell. Additionally, the different subcellular locations in the MNTB, make it unlikely that the entire population of Kv3 channels in these cells are heteromeric.

It seems more likely there is a mix of Kv3.1 homomeric channels in the nodes and AIS and either heteromeric channels or homomeric populations of both subunits in the somatic compartment. As mentioned in section 3.5.4 this may be to maximise the binding abilities of these Kv3 channels to down-stream signalling molecules or may reflect slight differences in subunit function.

In contrast to the MNTB, subunit composition in the LSO principal neurons is likely to be entirely Kv3.3 homomers as Kv3.1b was absent from the somatic membrane of most neurons and had little effect on Kv3 conductivity.

3.5.7 Both Kv3.1 and Kv3.3 contribute to fast AP repolarisation in the MNTB

The somatic and axonal distribution of Kv3.1 and Kv3.3 seen with immunohistochemistry is consistent with the function of Kv3 currents in shaping the action potential (AP) as the AIS is the site of AP generation.

Despite the overall potassium currents being unaffected in the MNTB of both knockouts, they both exhibit small but significant increases in AP duration (0.27ms , 0.41ms & 0.44ms for WT (n=16), Kv3.1 KO (n=11) & Kv3.3 KO (n=18); figure 3.12), highlighting a redundancy in function and thus the importance of Kv3 in these cells (data from myself and Deborah Linley). This suggests that not only are both subunits important for maintaining fast APs in the MNTB, as AP duration is increased in their absence, but their apparent difference in cellular localisation as seen by immunohistochemistry appears to have little effect on their ability to do so.

In contrast, Kv3.3 subunits are solely responsible for repolarising APs in the LSO, with significant increases in AP duration observed in the Kv3.3 KOs compared to both WT and Kv3.1 KO animals (figure 3.12).

3.5.8 Why are expression patterns of Kv3.1 and Kv3.3 in the MNTB and LSO different?

The difference of subunit expression in neurons of these two nuclei may be due to differences in the function of the nuclei themselves.

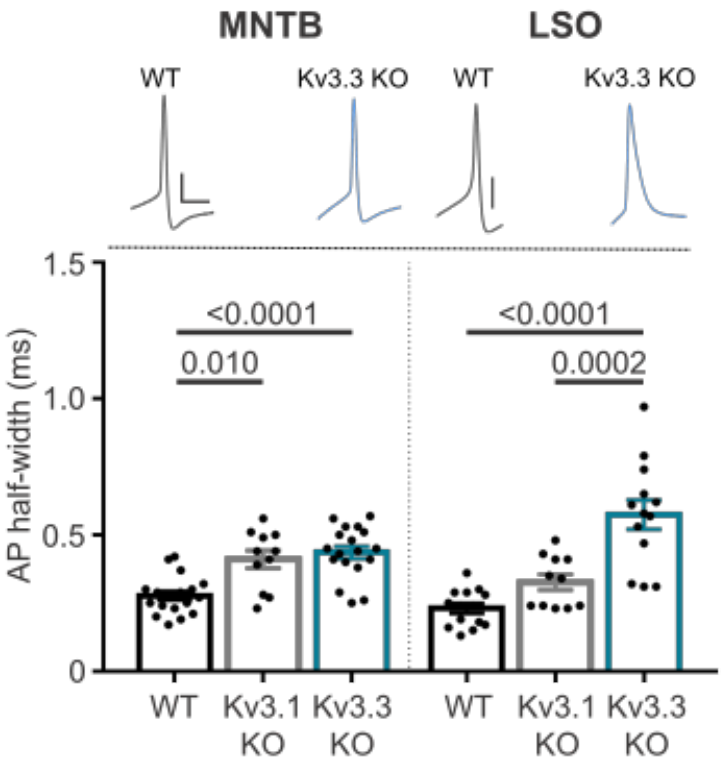

Figure 3.12: **Action potential duration is increased in MNTB and LSO neurons of Kv3.1 KO and Kv3.3 KO mice.** Experiments conducted on brainstem slices from mice aged P17-21, data from myself and Deborah Linley. Each point represents an individual cell. Action potential half-width is significantly longer in Kv3.1 and Kv3.3 KO MNTB compared to WT (one-way ANOVA & Tukey's post hoc, P values on graph). AP half-width in LSO is significantly longer in Kv3.3 KOs compared to WT and Kv3.1 KOs (one-way ANOVA & Tukey's post hoc, P values reported on graph). Representative action potential traces above graph are from WT (black) and Kv3.3 KO (blue) animals in both the MNTB and LSO (data collected by myself). Scale bars = 10mV, 1ms.

The MNTB can reliably fire APs at frequencies over 600Hz (Wu and Kelly 1993). In the MSO where neurons act as coincidence detectors, accurately timed inhibition provided by the MNTB is required to tune temporal sensitivities of neurons in order to process interaural timing differences (Grothe 2003). Neurons in the LSO act as integrators of excitatory inputs from the ipsilateral ear and inhibitory inputs from the contralateral ear and thus these inputs must be precisely timed in order to arrive in the LSO simultaneously (Tsuchitani 1997).

In contrast neurons in the LSO can only fire reliably up to 250Hz (Wu and Kelly 1993). Since these cells act as integrators, the ability to fire at high frequencies is less important since the outputs no longer need to accurately convey absolute information about a sound stimulus, they only need to convey relative information. For example an increase in firing rate from LSO neurons would signify a sound originating closer to the ipsilateral side of the head and a slower firing rate would signify a sound originating closer to the contralateral side of the head. Here, the absolute firing rate is less important, as long as a relative change is perceived.

This difference in function between the MNTB and LSO, i.e the MNTB providing absolute information of sound and the LSO providing relative information may explain the differences in expression of Kv3. The presence of Kv3 thus would be very important in both the soma (Kv3.3) and axon (Kv3.1) in the MNTB in order to keep action potentials as brief as possible during initiation and propagation as well as providing redundancy in the event of dysfunction of one subunit. This would be less important in neurons of the LSO where perhaps somatic Kv3 is adequate.

3.5.9 Contribution by Kv3.1a

This work has ignored the contribution of Kv3.1a subunits due to a lack of a suitable, validated antibody targeting this protein. This subunit is reported to show a developmental decline with adults expressing predominantly Kv3.1b (Perney et al. 1992; Si-qiong and Kaczmarek 1998), although RTPCR done by the Forsythe lab indicates Kv3.1a mRNA is still present in the LSO and MNTB of adult mice (data not shown). It is likely that this subunit complexes with Kv3.1b in the axon (Perney

et al. 1992) and the possibility of an interaction with Kv3.3 can not be discounted.

3.5.10 No functional protein is present in either knockout

There is no Kv3.3 protein detected in brainstem tissue of Kv3.3 KO mice, confirming that these animals do not contain functional Kv3.3 channels. Immunohistochemistry also shows a lack of staining using antibodies directed against Kv3.3, providing validation of both the antibody and the mouse.

Small levels of Kv3.1b protein were detected in brainstem tissue of Kv3.1 KO mice, however lack of fluorescence detected using immunohistochemistry shows this protein is not present in cells of the MNTB or LSO. It is possible that some protein is still made but gets degraded quickly or more likely the antibody is recognising another protein of the same molecular weight.

Importantly, there does not appear to be an upregulation of Kv3 subunits when one subunit is absent, shown by similar protein levels in the knockouts compared to wildtypes. Western blotting however does not give a read out of membrane protein but rather total protein in the cell. In the MNTB where we see compensation of Kv3 currents in the knockouts, this may be due to an increase of membrane expression of the other subunit, despite no increases of overall protein. Likewise it is possible that post-translational modification such as phosphorylation increases the activity of Kv3 channels in the membrane without the need to increase protein (Desai et al. 2008).

3.5.11 Summary

- Kv3.1b and Kv3.3 are widely expressed throughout the superior olivary complex (SOC). Both are present in neurons of the MNTB while only Kv3.3 exists in the soma of LSO neurons.

- Kv3.3 is mainly somatodendritic in subcellular location whereas Kv3.1b is mainly axosomatic.

- Kv3.1 and Kv3.3 equally contribute to Kv3 conductances in the MNTB, where they are likely to form populations of homomeric and heteromeric channels. In comparison only Kv3.3 subunits contribute to Kv3 conductances in the LSO, where they are likely to exist as homomers.

- Kv3.3 and Kv3.1 are equally important in action potential repolarisation in the MNTB, where one subunit can compensate for the other.

- In the LSO, Kv3.3 is the dominant subunit and is solely responsible for fast AP repolarisation.

- This variability in localisation of subunits may reflect a difference in non-conductive functions of individual subunits or in function of the auditory nuclei.

Chapter 4

Kv3 channels in the calyx of Held terminal

The first chapter demonstrated the presence of Kv3-mediated conductances in principal neurons of both the MNTB and LSO and showed the relative subunit contributions to action potential repolarisation. In addition to these principal neurons, Kv3 channels have also been identified in the calyx of Held terminal in the MNTB (Ishikawa et al. 2003; Nakamura and Takahashi 2007). The Calyx is a highly specialised giant synapse, originating from globular bushy cells in the ventral cochlear nucleus, ensheathing principal neurons of the MNTB. The calyx is known to respond to high frequency stimuli with high fidelity and fine temporal precision (Taschenberger and Von Gersdorff 2000). In order to do this, it expresses a diverse range of potassium channels, including low voltage-activated Kv1 channels to set action potential threshold and ensure only one action potential is fired for each stimulus and high voltage-activated Kv3 channels to ensure rapid repolarisation (Dodson et al. 2003; Ishikawa et al. 2003). In this presynaptic terminal, the ability of Kv3 channels to modulate AP waveform, thus calcium influx into the terminal, gives them the potential to indirectly modify transmitter release. While it is known that they exist here, subunit specific contributions at the synapse remains unknown, with previous work again suggesting that Kv3.1 is the likely constituent of presynaptic Kv3 channels based on *in situ* hybridisation and immunohistochemistry (Ishikawa et al. 2003; Ozaita et al. 2002). Here we show that while both Kv3.1 and Kv3.3 are

present in the terminal, Kv3.3 subunits mediate the current and are responsible for fast AP repolarisation.

4.1 Methods

- Mice used for presynaptic recordings were aged P10-12. At this age the calyx structure is still globular, providing a sufficient area for a patch pipette. Thinning and finestration of the terminal occurs after this age and consequently visualisation and identification becomes very difficult (Kandler and Friauf 1993).

- For calyx recordings, 120μm brainstem sections were used to increase the number containing MNTB and therefore the chances of a viable calyx being on the surface, providing better access for the pipette.

- Calyx terminals were identified by their shape, high membrane resistance (>200MΩ), more negative resting potential ($\sim$ -70mV) and lack of spontaneous EPSCs (due to absence of synaptic input).

- Once whole-terminal access was gained, 3 minutes were allowed for equilibration of internal solution (see methods) to occur prior to recordings. Pipette resistances for presynaptic recordings were between 4.5-6MΩ. Any recordings from the terminal with series resistances above 20MΩ were discarded.

- Experiments in which 1mM TEA was used were unpaired due to the technical challenges of retaining a presynaptic recording during perfusion. TEA was dissolved in normal acsf, oxygenated and bath perfused (1ml/min) in a parallel line to normal acsf for at least 5 minutes before recordings were performed. Perfusion of normal acsf was stopped during application of TEA-containing acsf. All solutions were heated to 35^{o}C.

- Due to the delicate nature of the calyx and to prevent movement of the structure, 0.5mL positive pressure was applied (with a 10mL syringe) to the recording pipette when approaching the terminal (compared to 2mL when patching principal neurons). The pipette was moved towards the terminal very slowly using a micromanipulator (Sutter MP-285). Generally the pipette was aimed towards the area of the terminal connected to the axon as this provided a bigger surface area to target, thus the chance of hitting an area which does not cover the end of the pipette was smaller. The success of gaining a good seal and a stable recording with low series resistance was very low at around 50% of attempts compared to a success rate of around 95% with principal neurons.

- Unless otherwise specified all variance is stated as SEM.

4.2 Kv3 currents in the calyx of Held terminal

In order to estimate the proportion of Kv3 current in the presynaptic terminal, whole-cell recordings were made directly from the Calyx in the presence of the Kv blocker TEA (1mM). Figure 4.1A shows potassium currents produced during voltage commands between +30mV and -110mV in control brain slices and those exposed to 1mM TEA. K^+ currents in the terminal were decreased in the presence of TEA, although this was not significant (unpaired t-test, P=0.0810, t=1.921, df=11). At +10mV current amplitudes in WT and 1mM TEA were 9.3 ±1.2nA (n=6) and 7.0 ±0.5nA (n=7), respectively. This TEA-sensitive Kv3 current accounts for around 2.3 ±1.2nA at +10mV.

Voltage clamp recordings were also performed from Kv3.1 KO and Kv3.3 KO mice however, due to the technical challenge of gaining good voltage control of the terminal and the rarity of obtaining knockout mice, n numbers obtained were very low (n=2 for each KO), thus the investigations here used action potential duration as a measure of Kv3 channel activity. APs were recorded in current clamp which does not exhibit the same errors as voltage clamp, thus it was easier to measure small differences in Kv3 function. As the main function of Kv3 channels is action potential repolarisation and given the results of the first chapter, it seemed reasonable to use this as a measure of their activity.

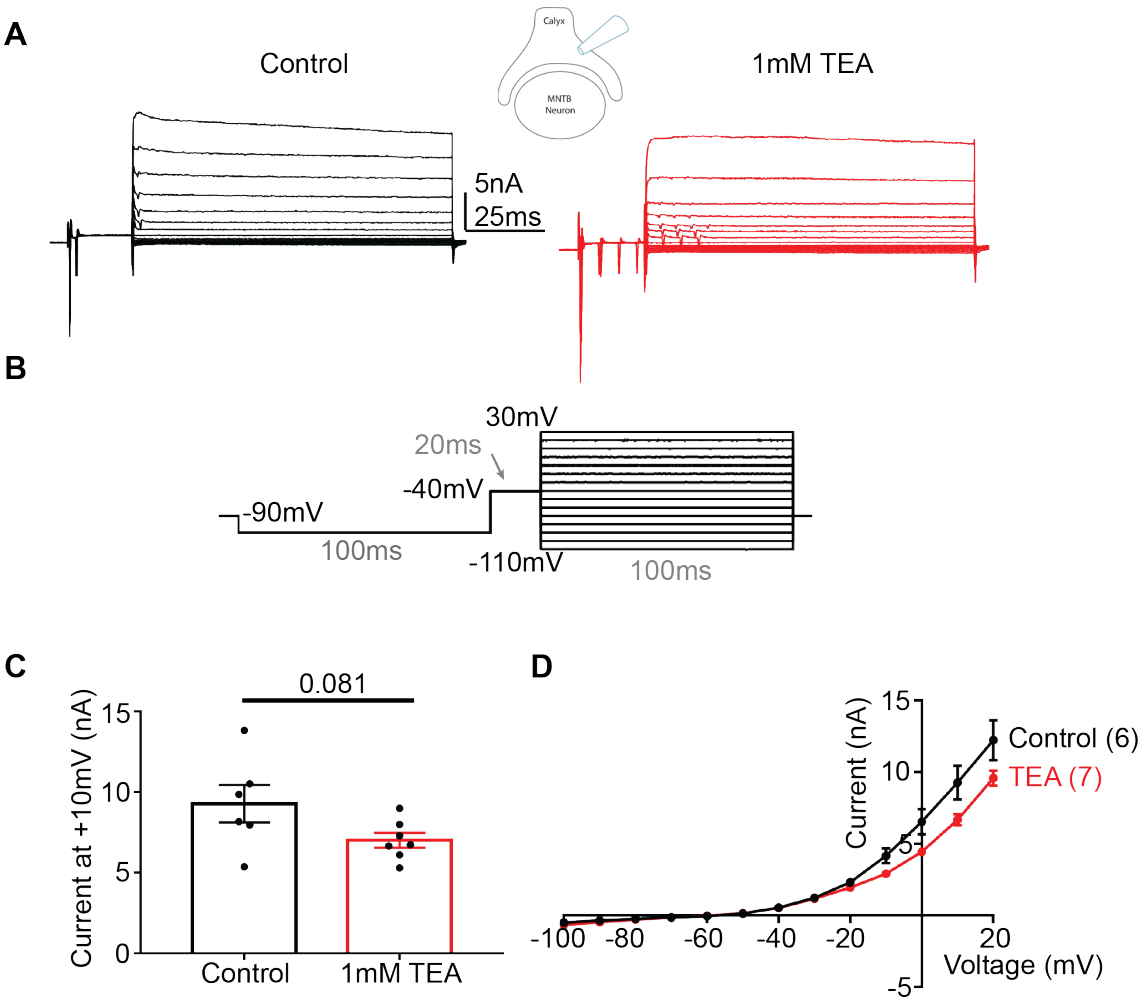

Figure 4.1: **Calyx of Held terminals of mice possess a TEA-sensitive K^+ current. A:** Example current traces in response to step depolarisations as seen in B in terminal from control brain slices and slices perfused with 1mM TEA. Sodium currents are present during the -40mV prestep seen as downward currents. **B:** Voltage command protocol used to elicit currents seen A. From a holding potential of -70mV a 100ms -90mV prestep was followed by 20ms -40mV prestep and 100ms test pulses ranging from +30mV to -110mV in 10mV increments. **C:** Current amplitudes measured between 90-95ms at +10mV. Variance plotted as SEM. There is no significant difference in amplitudes (unpaired t-test, P=0.0810, t=1.921, df=11. **D:** Current-voltage plot of currents measured at 90-95ms of test step. n values are denoted in brackets.

4.3 Kv3 currents modulate presynaptic action potential waveform

To investigate the contribution of Kv3 channel activity to the presynaptic AP waveform, current clamp recordings were conducted from calyces in CBA mice in the presence of the TEA.

Calyces were characterised by their membrane resistance, (typically $> 200\text{M}\Omega$), large hyperpolarisation-activated current (I_h), pronounced afterhyperpolarisation (AHP) and depolarising after-potential (DAP) following an AP (black arrow, figure 4.2). This DAP was obvious when eliciting action potentials using very brief current step injections (0.1ms, 2nA; figure 4.2 top), however the resulting stimulus artefact precluded analysis of AP half-width. Thus these brief pulses were used in identification of presynaptic terminals but longer current step injections (50ms, -50 to 250pA injections in 50pA increments; figure 4.2 bottom) were used to elicit APs for analysis. While DAPs were still present after application of TEA, the fast AHP appeared to be decreased or missing altogether in some recordings (figure 4.2).

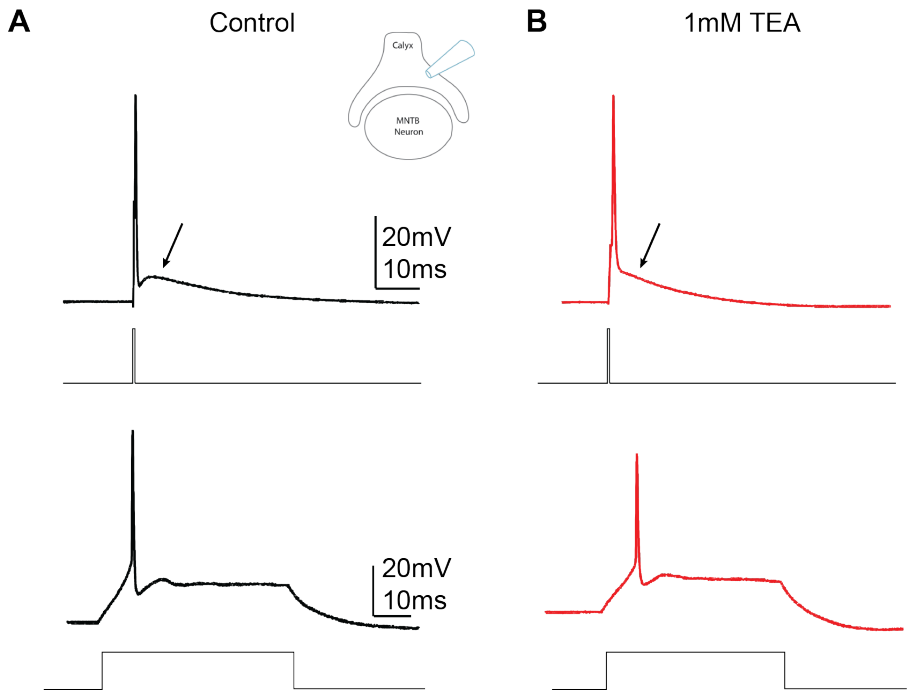

Figure 4.2: **TEA decreases the afterhyperpolarisation amplitude of action potentials at the calyx of Held. A: Top** Action potentials in response to a 2nA, 0.1ms current injection in P10 wildtype mouse. **A: Bottom** Presynaptic action potential in the same cell in response to a 50ms current injection step of 100pA. **B: Top** AP in response to a 2nA, 0.1ms current injection following perfusion with 1mM TEA. **B: Bottom** AP in same cell after perfusion of TEA in response to 150pA current injection for 50ms. Black arrows indicate depolarising after-potential.

Kv3 channels provide the repolarising drive for APs and limit AP duration thus this was measured in the form of half-width to assess the function of Kv3 in the Calyx (figure 4.3).

AP duration was very consistent in control animals and significantly longer in 1mM TEA with average half-width values of 0.3 ±0.01ms (n=10) and 0.5 ±0.04ms (n=7), respectively (unpaired t-test, P= <0.001, t= 7.354, df=16; figure 4.3B). This increase in AP duration was in large part due to an increase in time for the AP to decay from 90-10% of maximum amplitude as shown in figure 4.4 (0.4 ±0.01ms, n=10 in control and 0.7 ±0.06ms, n=7 in TEA; unpaired t-test, P= <0.0001, t= 7.033, df=15). A small but significant increase in AP rise time also occurred in the presence of TEA from 0.15 ±0.01ms in control to 0.17 ±0.01ms in 1mM TEA (unpaired t-test, P=0.042, t=2.219, df= 15; figure 4.4). This increase in rise time may, in part be due to a significant increase in AP amplitude in the presence of TEA (Unpaired t-test, P=0.0132, t=2.788, df=16). AP amplitude increased from 39.5 ±1.4mV in CBA WT to 47.1 ±2.6mV in the presence of 1mM TEA (figure

4.3).

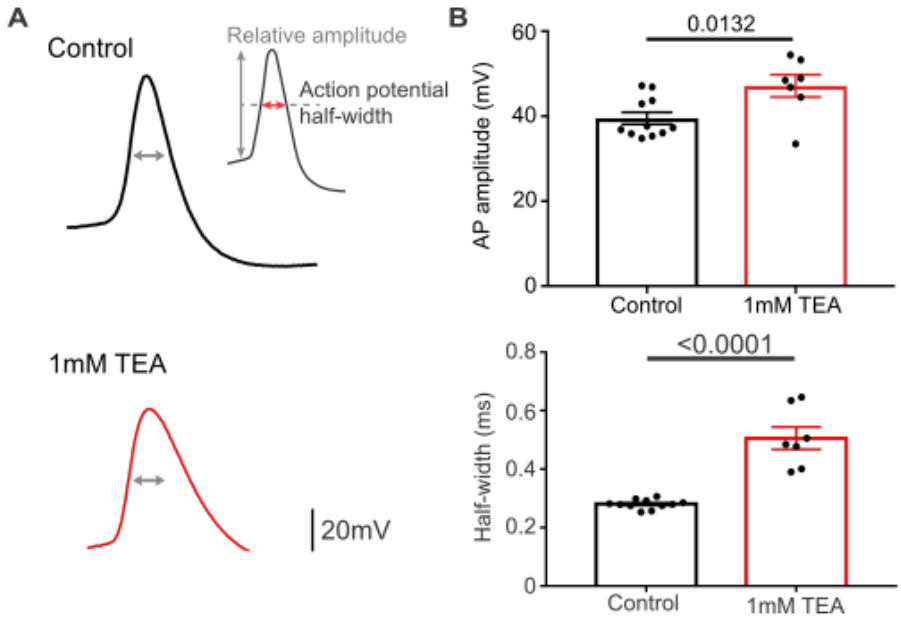

Figure 4.3: **1mM TEA increases action potential duration at the calyx terminal. A:** Example AP traces from mouse calyx of Held in control and after perfusion of 1mM TEA. Holding potential = -70mV. Grey arrow indicates half-width of control AP. **Inset:** Schematic demonstrates how AP relative amplitude and half-width was measured with the grey and red arrows indicating the point of measurement. **B: Top** Relative action potential amplitude as measured in inset. AP amplitude is significantly increased in 1mM TEA (unpaired t-test, P=0.0132, t=2.788, df=16). **B: Bottom** Quantification of AP half width in control and 1mM TEA groups. Half-width is significantly increased in the presence of TEA (unpaired t-test, P= <0.0001, t= 7.354 , df= 16). Variance plotted as SEM.

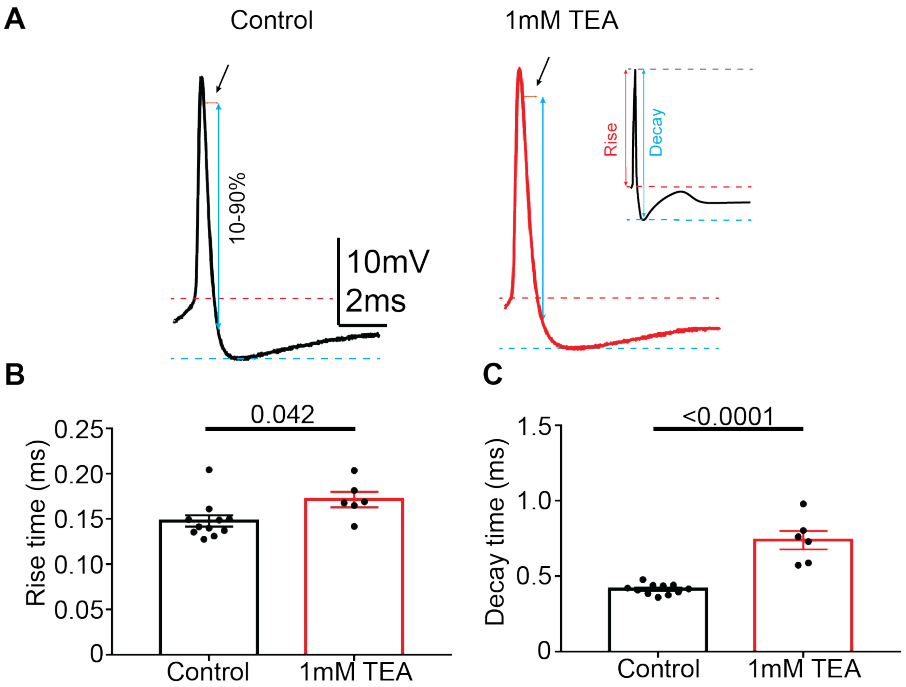

Figure 4.4: **TEA significantly increases AP decay time in the calyx terminal. A:** Example action potential traces from P10 CBA mouse in the absence (control) and presence of 1mM TEA. Terminals were held at -70mV. Black arrow indicates decay time in control. **Inset** Schematic demonstrating how rise and decay time were measured. Red dotted line = start of AP, grey dotted line = AP peak, blue dotted line = AHP peak. Rise time is defined as the time to rise from 10-90% of the distance shown by the red arrows; decay time is the same for the distance indicated by the blue arrow. **B:** Quantification of rise time. Rise time is significantly increased in TEA (t-test, P=0.042, t=2.219, df= 15). **C:** Quantification of AP decay time which is significantly increased in 1mM TEA (t-test, P= <0.0001, t= 7.033, df=15) Variance plotted as SEM, each data point represents a different terminal.

4.4 Kv3.1 and Kv3.3 subunits are present in the calyx of Held terminal

The TEA-sensitive current in the terminal is likely mediated by Kv3 channels. The previous chapter demonstrated that only Kv3.1 and Kv3.3 subunits were present in the MNTB using immunohistochemistry, confirming the absence of Kv3.2 and Kv3.4 mRNA seen with RNA sequencing. From this is can be concluded that only these subunits can contribute to the formation of presynaptic Kv3 channels. In order to identify which of these were present in the terminal and distinguish pre and postsynaptic expression, we used coimmunolabelling of both subunits with the presynaptic marker Vglut1, a vesicular glutamate transporter located on the vesicular membrane, abundant in the calyx (Billups 2005). Sections were post fixed in 4% PFA and antigen retrieval carried out (see methods) as this was the only fixation method in which the Kv3.1b antibody worked. Antibodies were used at dilutions of 1:1000 (Kv3.1b and VGlut1) and 1:3000 (Kv3.3).

Kv3.1b shows diffuse staining throughout the cytoplasm of postsynaptic MNTB neurons as well as more defined, membrane staining (figure 4.5 top left). Vglut has a more defined circular staining pattern consistent with the presence of a synaptic terminal wrapped around the somata of MNTB neurons and shows some degree of overlap with Kv3.1b highlighted by white arrows in figure 4.5 (bottom left). Kv3.3 on the other hand is much more localised to the membrane and shows a high degree of overlap with the presynaptic marker, often where staining of one protein is absent, the other is also missing (highlighted by grey arrows in figure 4.5 bottom right).

It can be difficult to separate the yellow colour from green and red in merged images so to highlight overlap between the subunits and the presynaptic marker the images were processed using image calculator in Fiji with an 'AND' function. This returns an image with grey values only present in pixels that are 'stained' with both proteins. The grey value increases with increased intensity of values in the original images. This shows a large degree of overlap between Vglut staining with both Kv3.1 and Kv3.3 subunits (figure 4.6).

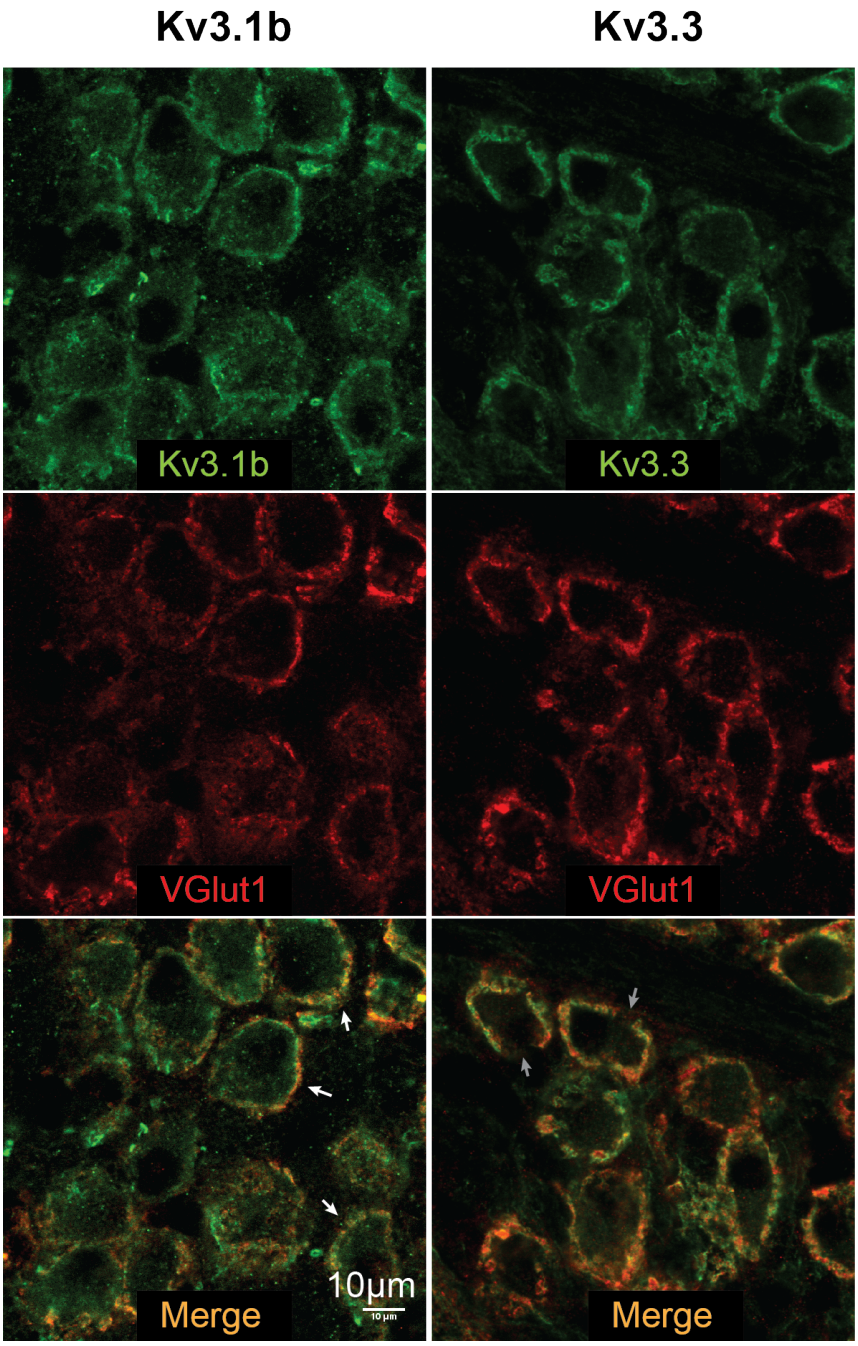

Figure 4.5: **Kv3.1b and Kv3.3 are present in the presynaptic calyx terminal. Top panel:** Kv3.1b (left; dilution 1:1000) and Kv3.3 (right; dilution 1:3000) in the MNTB of a wildtype mouse aged P21. **Middle panel:** Presynaptic marker Vglut in same sections as panel above. **Bottom panel:** Kv3.1b and Vglut merged image on left, Kv3.3 & Vglut merged image on right. White arrows point to areas of apparent colocalisation of Kv3.1b and Vglut. Grey arrows indicate areas where both Kv3.3 and Vglut are absent. Images taken at 63x magnification using a confocal microscope by Michelle Anderson.

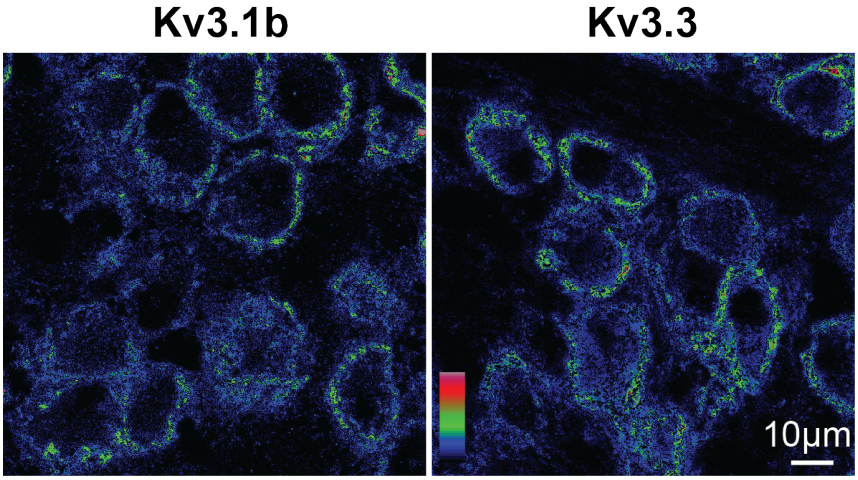

Figure 4.6: **Both Kv3.1b and Kv3.3 colocalise with presynaptic marker.** Colocalisation of Kv3.1b (left) and Kv3.3 (right) with Vglut. Analysis of images in figure 4.5 showing only pixels where overlap of the Kv3 subunit with the presynaptic marker occurs with green-red colours indicating more overlap.

To establish whether one subunit was required for the other to be trafficked to the membrane or for specific subcellular targeting, we also conducted coimmunolabelling on the Kv3.1 and Kv3.3 KO animals. In these animals the pattern of expression did not appear to change with Kv3.1b still showing overlap with Vglut1 in the Kv3.3 KO animals and vice versa (figure 4.7).

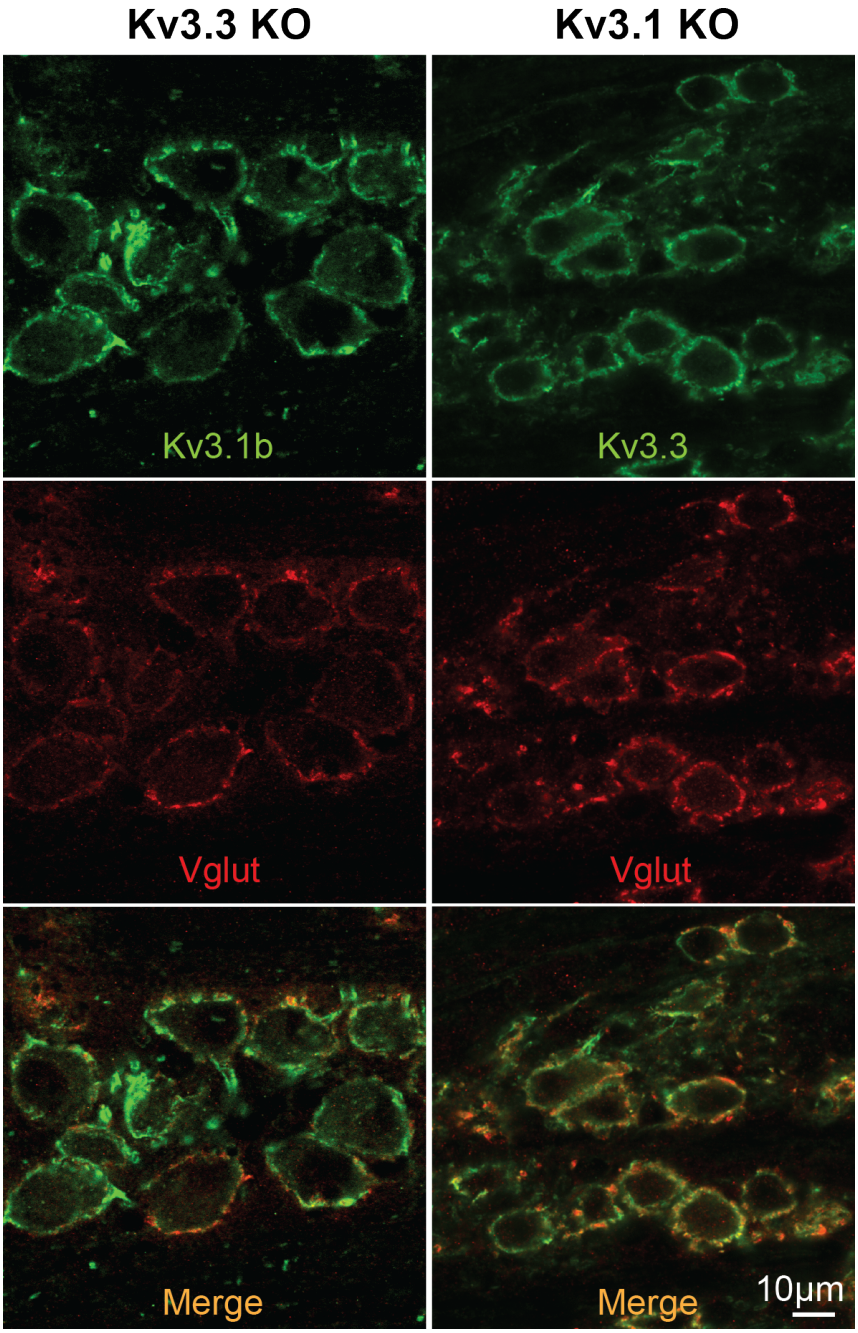

Figure 4.7: **Presynaptic expression of Kv3.1b and Kv3.3 does not change in Kv3.3 and Kv3.1 KO mice, respectively. Top panel:** Kv3.1b (left) in the MNTB of a Kv3.3 KO mouse aged P21. Kv3.3 (right) in MNTB of a Kv3.1 KO mouse aged P21. **Middle panel:** Presynaptic marker Vglut in same sections as panel above. **Bottom panel:** Kv3.1b and Vglut merged image on left, Kv3.3 & Vglut merged image on right. Images taken at 40x magnification using a confocal microscope by Michelle Anderson.

4.5 Contribution of Kv3.1 and Kv3.3 to presynaptic action potential repolarisation

We have established that presynaptic Kv3 currents are present at the calyx of Held synapse and important for action potential repolarisation. Immunohistochemistry shows that both Kv3.1 and Kv3.3 may be present in the terminal but to investigate if either of these were more important in the function of Kv3 channels, whole-cell current clamp recordings from P10-P12 knockout mice lacking either Kv3.1 or Kv3.3 subunits were conducted. Similar to the previous experiments with TEA, short current steps were used to elicit a single action potential for identification purposes and APs generated by longer 50ms step depolarisations were used for analysis (only the first AP generated was analysed. Example traces seen in figure 4.8).

Characteristic depolarising after-potentials were present in presynaptic APs from both knockout mice, however similar to the effect seen with TEA, the AHP amplitude appeared decreased in Kv3.3 KOs (figure 4.8).

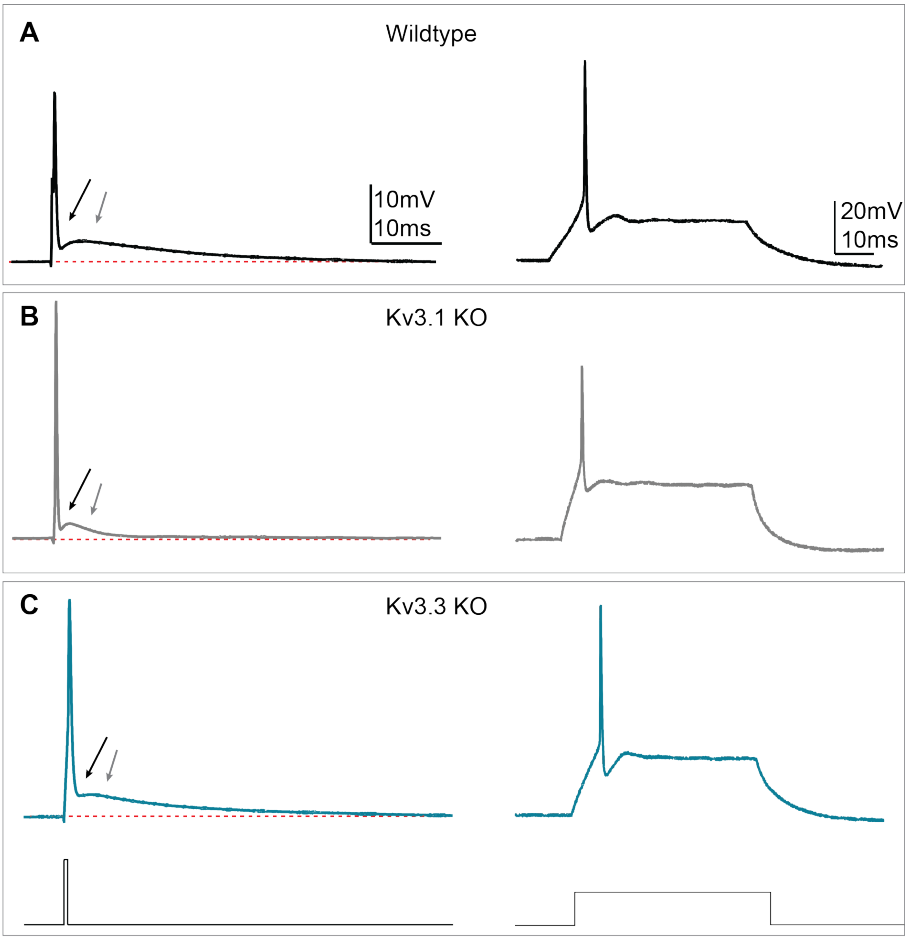

Figure 4.8: **Afterhypolarisation amplitude of action potentials is decreased in Kv3.3 KO mice.** Presynaptic action potential traces from the calyx of Held terminal in wildtype (WT;P10), Kv3.1 KO (P11) and Kv3.3 (P11) mice. **A:** APs in a wildtype calyx in response to a 0.1ms, 2nA current injection (left) or 50ms, 100pA step injection. **B** & **C** APs in a Kv3.1 KO and Kv3.3 KO calyx, respectively, elicited with 0.1ms, 2nA or 50ms, 150pA current injections. Black arrows indicate afterhyperpolarisation (AHP), grey arrows show depolarising after-potential (DAP).

As with TEA, half-width, rise time and decay time of APs were measured in the knockouts in addition to relative amplitude (amplitude from threshold to peak). Data from KOs was compared to both WT and 1mM TEA recordings which represent action potential waveform with and without contribution of Kv3 channel activity, respectively.

Relative AP amplitudes were significantly larger in 1mM TEA compared to WT and Kv3.1 KOs at 47.2 ±3.11mV (n=6) in TEA and 39.5 ±1.42mV (n=11) and 34.9 ±2.25mV (n=5) in WT and Kv3.1 KO (one-way ANOVA, Tukey's post hoc, WT vs TEA P=0.042, Kv3.1 KO vs TEA P=0.0044) (figure 4.9). Amplitudes of APs in both knockouts were similar to WT with those of Kv3.3 KOs slightly raised, although this was not significant (one-way ANOVA, Tukey's post-hoc; WT vs Kv3.3 KO P=0.978; WT vs Kv3.1 KO P=0.396).

AP durations were significantly different between groups (one-way ANOVA, $F(3,25)=29.03$, $P<0.001$) with half-width values much larger in Kv3.3 KOs compared to WT (0.43 ±0.01ms (n=6) & 0.28±0.01ms (n=11), respectively, P= <0.0001; figure 4.9). Interestingly, AP durations in these Kv3.3 KO mice were also significantly longer than those in Kv3.1 KO animals (0.43ms vs 0.32 ±0.01ms (n=5) in Kv3.1 KO, P=0.0148) but similar to those seen in the presence of TEA (0.43ms vs 0.51 ±0.04ms (n=6) in TEA). Kv3.1 KOs were not significantly different to WT (P=0.4995).

This increase in action potential duration in Kv3.3 KO animals is mainly due to an increase in the time taken for the AP to decay from 90-10% of its maximal amplitude (figure 4.9), with no significant changes to the rising phase (one-way ANOVA, Tukey's post hoc, P=0.053). This decay time in Kv3.3 KOs was 0.60 ±0.02ms (n=6) compared to 0.41 ±0.01ms (n=11) in WTs (one-way ANOVA, Tukey's post hoc, P=0.0005). In contrast Kv3.1 KO decay times were not different to those observed in WT (0.52 ±0.03ms (n=5) vs 0.41 (n=11), respectively, P=0.0845).

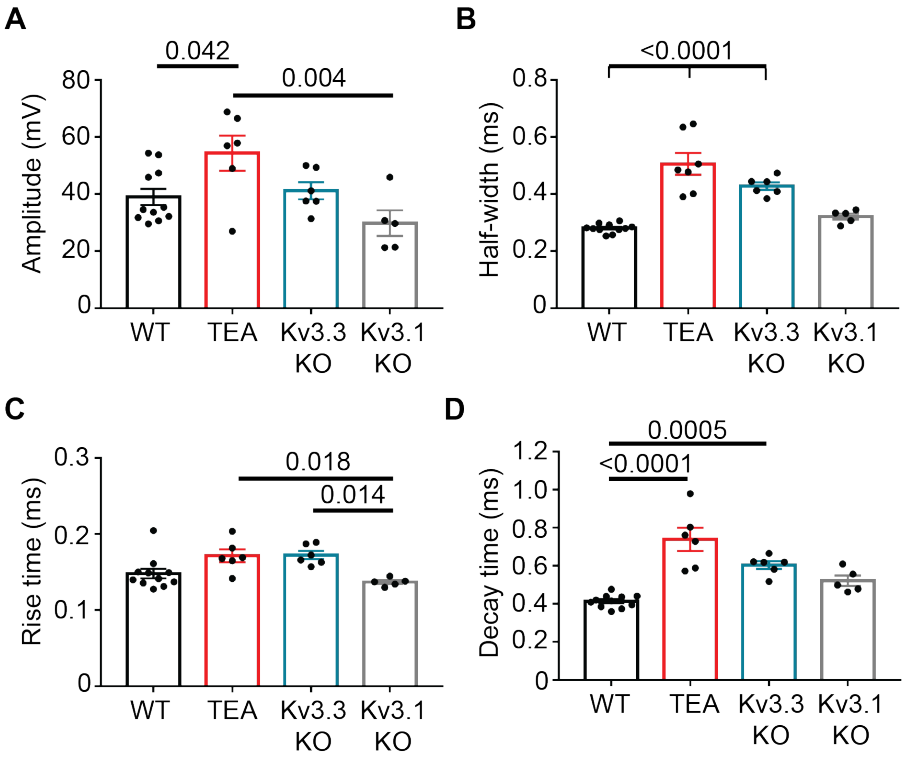

Figure 4.9: **Presynaptic AP duration is significantly increased in Kv3.3 KOs but not Kv3.1 KOs.** Quantification of presynaptic action potential amplitude and duration at the calyx of Held terminal in CBA wildtype (with and without 1mM TEA), Kv3.3 KO and Kv3.1 KO mice aged P10-P12. **A:** Relative amplitude of APs (measured as 'rise' seen in figure4.4 inset). **B:** AP half-width values (measured as in figure 4.3B). **C & D:** AP rise and decay times, measured as in figure 4.4 inset. Each data point represents an individual terminal, variance plotted as SEM. Statistical significance was analysed in all data sets using one-way ANOVA and Tukey's post hoc for multiple comparisons. Significant P values plotted on graphs.

4.6 Discussion

Action potential waveform at the synapse can have a large effect on neurotransmitter release by modulating Ca^{2+} entry into the synaptic terminal and thus calcium-dependent vesicle fusion with the membrane. Therefore, the ability to modify conductances contributing to the AP, principally those driven by Na^+ and K^+ channels, through post-translational modifications such as phosphorylation, or removal of channels from the membrane, provides a cell with a mechanism of finely controlling transmitter release. This is especially important at the calyx of Held synapse in order to ensure faithful transmission at high frequencies and limit the metabolic demands of the synapse. In this chapter we show that Kv3 conductances are present in the calyx of Held terminal and do have an important role in modulating AP waveform. More importantly it appears that Kv3.3 subunits in particular, are critical in the formation and function of these presynaptic Kv3 channels.

4.6.1 Calyces possess TEA-sensitive currents

Here we have confirmed that calyx terminals possess TEA-sensitive currents in accordance with previous data collected from rats (Ishikawa et al. 2003), most of which is mediated by Kv3 channels, although a small contribution by BK conductance may be present (Ishikawa et al. 2003). The contribution of this TEA-sensitive current to overall potassium currents was much smaller in our study ($\sim$ 25% compared to 50%). This is likely to reflect differences in the methods of recording as well as species differences; the previous study used excised patches from the calyx which are likely to have a smaller contribution by other K^+ channels such as Kv1 due to their axonal location (Dodson et al. 2003), making contributions from TEA-sensitive currents appear larger.

4.6.2 Kv3 channels are responsible for modulating presynaptic AP waveform

This Kv3 conductance, much like in the MNTB and LSO principal neurons is responsible for action potential repolarisation in the terminal. This is shown by an increase in AP duration in its absence, primarily due to an increase in the time taken for the AP to repolarise. A small increase in rise time was also observed, although in comparison to the change in decay time this was minimal and unlikely to contribute much to the increased half-width (0.02 ms increase in rise time compared to 0.33ms in decay time with TEA).

The purpose of Kv3 in generating brief action potentials at the terminal is likely to be limiting transmitter release. Long action potentials would result in faster vesicle depletion due to larger release, contributing to much larger synaptic depression and an inability to maintain release at high frequencies (Scheuss, Schneggenburger, and Neher 2002). It may also result in an inability of calcium channels to recover from inactivation between each action potential, compounding the effect on synaptic depression (Forsythe et al. 1998). As vesicle recycling is a metabolically costly process (Heidelberger, Sterling, and Matthews 2002), limiting vesicle release and consequently recycling will also conserve energy, important at this synapse due to the high rate of input stimulation.

In addition to action potential duration, the decreased afterhyperpolarisation seen in the presence of TEA suggests Kv3 channels also contribute to this. This fast AHP is likely required for Na^+ channels to recover from inactivation in preparation for the next AP (Rudy and McBain 2001). This is especially important in the calyx as the large depolarising after-potential (DAP), caused by resurgent sodium channels (Kim, Kushmerick, and Von Gersdorff 2010) remains for several milliseconds after the AP. Without the AHP this depolarised membrane potential caused by the DAP is unlikely to be sufficiently negative to allow all Na^+ channels to recover from inactivation and could lead to action potential failure at higher frequencies (Kuo and Bean 1994).

4.6.3 Subunits forming presynaptic Kv3 channels

Evidence provided in this chapter suggests that while both Kv3.1 and Kv3.3 are present in the terminal (figure 4.5), Kv3.3 is critical for rapid AP repolarisation.

Both Kv3.3 and Kv3.1b appear to show coimmunolocalisation with a presynaptic marker and while it is impossible to really determine whether the protein is present on the post-synaptic or presynaptic membrane with the resolution given with confocal microscopy, these findings are consistent with previous ones showing Kv3.3 immunoreactivity in the terminal (Chang et al. 2007) and the presence of Kv3.1b on the non-release face of the calyx (Elezgarai et al. 2003; Dodson et al. 2003).

Despite both subunits being present in the terminal, the significantly longer AP half-width in Kv3.3 KOs but not Kv3.1 KOs suggests that Kv3.3 subunits are required for proper function of these presynaptic channels. Not only were action potentials significantly longer in Kv3.3 KOs compared to wildtype mice but it was also significantly longer than Kv3.1 KOs, suggesting that, while Kv3.3 can clearly function on its own, similar to LSO neurons, Kv3.1 cannot compensate for the lack of Kv3.3.

There are a number of reasons for which Kv3.3 KOs may show a stronger change in AP, for example, without Kv3.3 present, Kv3.1 may not get trafficked to the terminal membrane however this seems unlikely as the pattern of expression of this subunit is similar when Kv3.3 is absent as compared to wildtype animals (figure 4.7). Additionally, Kv3.1 has been shown to have an axonal targeting motif allowing its localisation to the terminal, suggesting it does not require other subunits to reach the membrane (Ozaita et al. 2002). It is possible the amount of Kv3.3 expression is just much higher in the terminal and Kv3.1 cannot compensate when it is absent.

This leaves the question of why Kv3.1 is present in the terminal at all. It may be that certain signalling molecules can bind to Kv3.1 but not Kv3.3 and thus by incorporating them into heteromeric channels, it allows the activity of the Kv3 channels to be modulated, something we would not see when looking at single action potentials. For example, ancillary proteins such as MiRP 1 and MiRP 2 have been shown to bind to Kv3.1 in CHO cells and change the kinetics of the channel

(Lewis, McCrossan, and Abbott 2004). Additionally, Kv3.3 homomeric channels can show N-type inactivation (chapter 7) and inclusion of Kv3.1 may prevent this from occurring.

Previous research has suggested that Kv3.4 is present at the calyx terminal based on immunohistochemistry (Ishikawa et al. 2003) and current kinetics (Dodson 2003) and indeed has been shown to be present at other synapses in the brain (Rowan and Christie 2017). However the lack of staining seen here with our Kv3.4 antibody (figure 3.2) combined with the lack of an inactivating component in the currents at the terminal (figure 4.1) makes it unlikely that Kv3.4 has a large contribution. Even during the formation of heteromers, Kv3.4 imparts an inactivating component to the potassium current, which is completely absent in our recordings (Baranauskas et al. 2003).

This provides the first evidence that while some Kv3.1/ Kv3.3 heteromers may exist in the terminal, Kv3.3 is the predominant subunit and may even exist in a population of Kv3.3 homomers. Thus when Kv3.1 is absent, there is little change to the function of presynaptic Kv3 channels, however when Kv3.3 subunits are absent, a large proportion of the Kv3 conductance is missing, resulting in significant changes to action potential waveform.

4.7 summary

- TEA-sensitive Kv3 currents are present in the calyx of Held terminal and play a large role in repolarising of the presynaptic action potential, shown by increases in action potential half-width and decay time when absent.

- Action potential duration (half-width and decay time) were significantly increased in Kv3.3 KOs but not Kv3.1 KOs.

- There was no change in Kv3 subunit expression when either subunit was absent, suggesting both Kv3.1b and Kv3.3 can be localised to the presynaptic membrane independently.

- Kv3 channels at the terminal are dominated by Kv3.3 subunits, possibly as homomeric channels. If heteromers are present, Kv3.1 may have a role in binding signalling molecules.

Chapter 5

The role of presynaptic Kv3 channels in modulating synaptic transmission

The previous chapter uncovered an important role for Kv3.3 subunits in modulating the presynaptic action potential waveform. As discussed, this ability of Kv3 conductances to control AP duration provides the synaptic terminal with a potential method of controlling neurotransmitter release indirectly, through regulating calcium influx. As mentioned previously, close coupling between calcium channels and vesicle release machinery means tiny changes to calcium influx can have a large impact on Ca^{2+}-dependent transmitter release (less release with short AP and less calcium; Yang and Wang 2006; Taschenberger and Von Gersdorff 2000; Wang, Neher, and Taschenberger 2008).

The calyx of Held synapse is a well established model for studying synaptic transmission due to its reliability and consistency of release, ease of access for patch pipettes, ability to release at high frequencies and most importantly the fact that a single presynaptic terminal is paired with a single post synaptic cell, thus any changes in postsynaptic responses can be attributed to changes in a single synapse (see review Schneggenburger and Forsythe 2006).

The ability to finely control transmitter release is especially important at this synapse in order to sustain release during high frequency sound stimuli. A number of adaptations enable this synapse to reliably release vesicles upon each stimulus. Firstly, it possesses a large number of release sites and thus ready-releasable

vesicles (Meyer, Neher, and Schneggenburger 2001; Scheuss, Schneggenburger, and Neher 2002; Schneggenburger, Meyer, and Neher 1999). Secondly, there is tight coupling between P-type calcium channels and release machinery within the terminal, permitting vesicle release even during brief calcium transients (Wang, Neher, and Taschenberger 2008; Forsythe et al. 1998). Short-term depression upon prolonged or high frequency stimulation occurs at the synapse, limiting vesicle depletion (Borst, Helmchen, and Sakmann 1995; Schneggenburger, Meyer, and Neher 1999; Wang and Kaczmarek 1998) in addition to rapid activity-dependent replenishment of vesicle pools (Wang and Kaczmarek 1998). Finally, action potential duration at the calyx is particularly brief, limiting calcium influx and thus transmitter release (Taschenberger and Von Gersdorff 2000).

This chapter will discuss the contributions of Kv3.1 and Kv3.3 to modulating synaptic transmission at this calyx of Held synapse, paying particular attention to transmission during high-frequency stimulation since the major role of Kv3 is to permit high-frequency AP firing and the synapse is adapted to sustain transmission during high frequency stimuli (Wang and Kaczmarek 1998). Consistent with evidence presented in the previous chapter of Kv3.3 subunits dominating in the presynaptic terminal, these subunits appear to play a larger role in modulating transmission.

5.1 Methods

- Stimulation experiments were conducted on brainstem slices from mice aged P21-P25. At this age synaptic development in the auditory brainstem has reached near adult maturity (Pilati et al. 2016; Nakamura and Takahashi 2007; Sonntag et al. 2011).

- Brainstem slices of 250μm thickness were used to retain as many synaptic connections as possible.

- A concentric bipolar electrode (bespoke from FHCinc; #CBAD75S) was used with a constant voltage stimulator box (DS2A; Digitimer) in order to stimulate axons of either globular bushy cells or MNTB principal neurons (0.1ms pulse, variable voltage). The stimulator box was connected to a digital output of the digidata and controlled via TTL inputs using Clampex software (Molecular devices). In order to apply input trains and not a constant voltage, an asterix was denoted in the appropriate digital output column within the waveform protocol editor of Clampex.

- For MNTB EPSC recordings, the stimulating electrode was placed at the midline of the brainstem slice and for LSO IPSC recordings it was placed lateral to the MNTB (see figure 5.1).

- Thick-walled glass capillaries (GC150F7.5, Harvard Apparatus) with resistances between 2-4MΩ were filled with a low-chloride patch solution containing (in mM): KGluconate (120), KCl (10), HEPES (40), EGTA (0.2), $MgCl_2$ (1), K_2ATP (2), NaGTP (0.3). Recordings with series resistances over 10MΩ or that increased more than 10% during the recordings were discarded. A low chloride solution was used for this set of experiments due to the direction of Cl^--driven IPSC currents in the LSO changing from inward to outward currents when cells were held at -60mV and the intracellular chloride concentration was 36.5mM (E_{Cl} = -32mV). A low Cl^- solution gave an E_{Cl} of -70mV thus at a holding of -60mV Cl^- ions would always move into the cell, resulting

in hyperpolarisation, preventing this switch from occurring. In addition, this low Cl^- more closely mimics the environment of LSO neurons in adult animals where expression of KCC2 leads to Cl^- extrusion and a consequent low $[Cl^-]_i$ (Kakazu et al. 1999; Balakrishnan et al. 2003).

- After entering whole cell configuration, a -40mV holding potential was applied to inactivate sodium channels and cells were left for 5 minutes to equilibrate prior to recordings. Subsequently 100μs stimulating pulses were given at 0.3Hz in order to assess the voltage threshold required to generate a response. Stimulation voltage was increased between 0 & 20V until a stable reliable EPSC was generated in the MNTB or until an IPSC of maximal amplitude was generated in the LSO. All recordings were done at a holding potential of -40mV, reducing the driving force of ions through AMPA receptors (reversal potential $\sim$0mV; Smith, Wang, and Howe 2000).

- Slices were perfused with oxygenated acsf containing 0.5μM strychnine hydrochloride (Sigma; Stock made in ddH_2O) for recordings of AMPA-mediated EPSCs in the MNTB or 10μM bicuculline (Sigma; stock made with DMSO), 20μM D-(-)-2-Amino-5-phosphonopentanoic acid (D-AP5; Tocris; Stock made in ddH_2O) and 10μM 6,7-Dinitroquinoxaline-2,3-dione (DNQX; Sigma; Stock made in DMSO) for recording glycinergic IPSCs in the LSO. The final concentration of DMSO did not exceed 0.1%.

- All experiments were conducted at 35^{o}C and unless stated otherwise all variances are plotted as SEM.

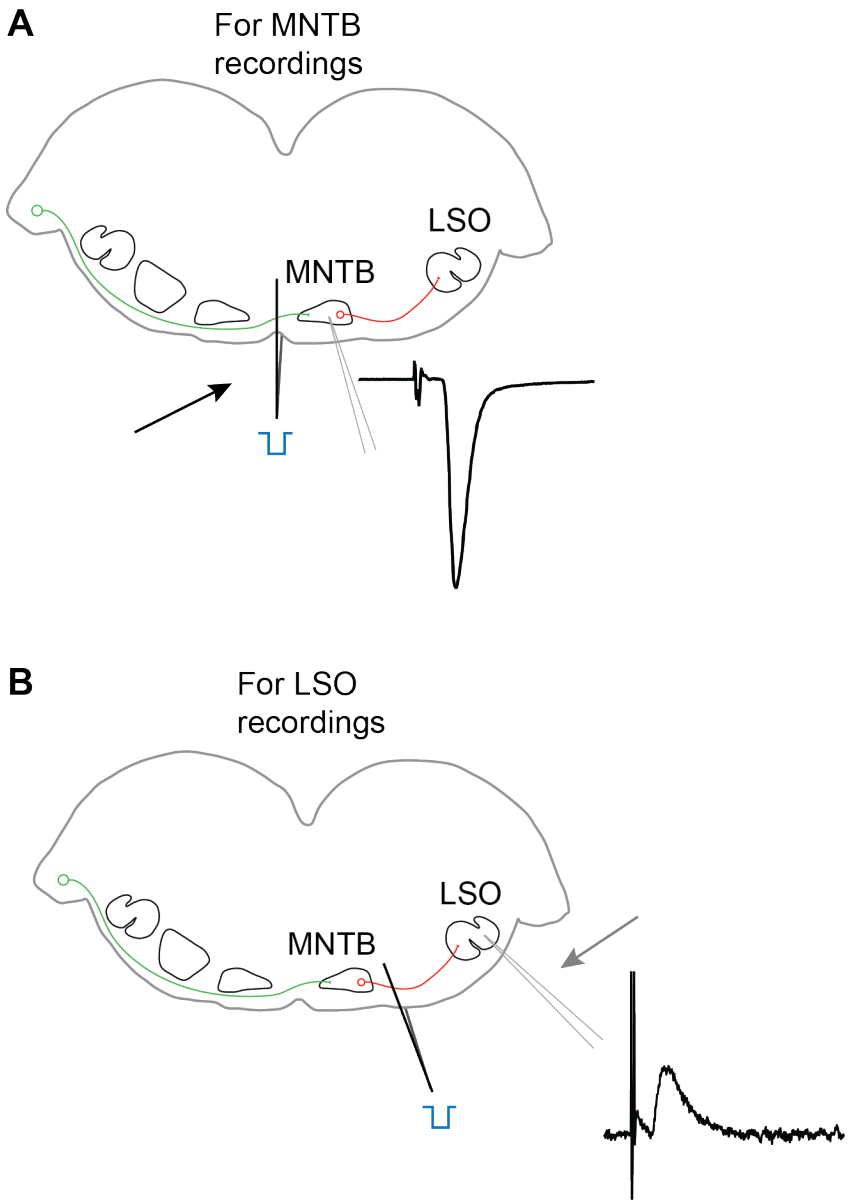

Figure 5.1: **Placement of stimulation electrode for EPSC and IPSC recordings in MNTB and LSO, respectively. A:** Stimulation electrode (black arrow) is placed on the midline to stimulate axons of globular bushy cells, resulting in glutamate release from the calyx of Held, generating EPSCs in MNTB neurons (Black trace). Blue trace shows stimulation voltage waveform. **B:** Electrode is placed immediately lateral to the MNTB to stimulate axons of MNTB principal neurons, resulting in glycinergic release, generating IPSCs in LSO principal neurons (Black trace). Grey arrow indicates placement of recording pipette.

5.2 Simultaneous recordings at the calyx-MNTB synapse

As mentioned previously, the calyx of Held synapse is well studied, primarily owing to the ability to perform simultaneous whole cell patch clamp in the terminal and postsynaptic neuron (figure 5.2). This permits changes in postsynaptic responses to be directly attributed to changes in the terminal. Whilst this is an incredibly powerful technique it is also has limitations. Firstly, as discussed in the previous chapter, presynaptic recordings become much more technically challenging after hearing onset ($\sim$ P12) due to finestration of the terminal and increased myelination (Kandler and Friauf 1993; Borst, Helmchen, and Sakmann 1995). Due to regulations in our animal breeding facility, animals could not be ear-snipped and genotyped until P10, leaving a very limiting window of 2 days for recordings to be performed. Secondly, while the calyx reaches the ability to fire at high frequencies by P14 and becomes 'adult-like' (Sonntag et al. 2011; Chuhma and Ohmori 1998), a number of developmental changes occur after this stage, including an increase in Kv3 expression (RTPCR data from our lab, uncommunicated) and a shortening of the action potential duration (Taschenberger and Von Gersdorff 2000), meaning the results may not be applicable to adult physiology. Lastly, dialysis of the presynaptic terminal would occur during whole cell patch clamp which may dilute important signalling molecules, resulting in artificial physiological changes. For these reasons the rest of the experiments in this chapter were conducted only in adult animals in which recordings were only made from the postsynaptic cell and a stimulating electrode used to evoke APs in the axons of the calyx terminal. Despite not having the ability to directly relate changes in presynaptic action potential to effects in postsynaptic response, this allowed us to conduct experiments in fully developed animals and preserve the internal environment within the terminal (avoiding dialysis).

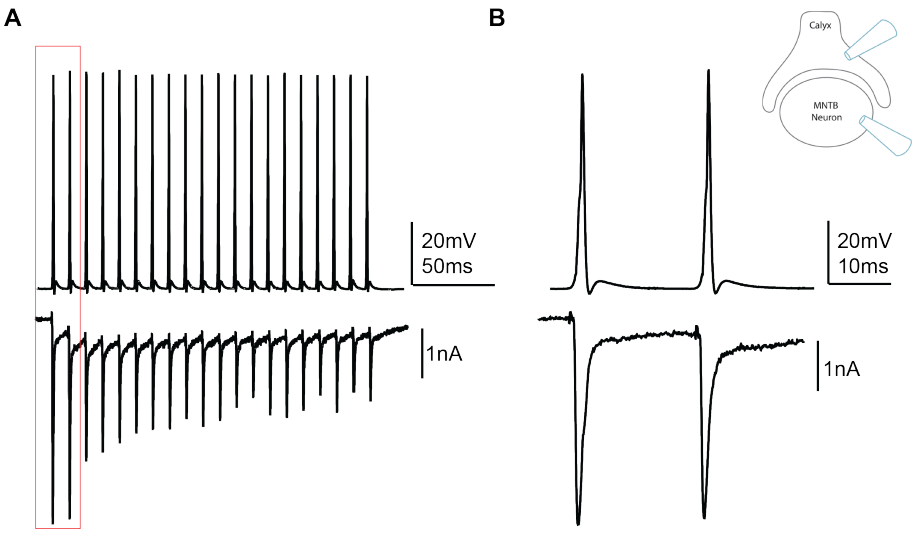

Figure 5.2: **Simultaneous recordings from the calyx of Held terminal and an MNTB principal neuron in a brainstem section of a CBA wildtype mouse aged P11. A:** (Top) Whole-cell current clamp in the calyx terminal held at -70mV. Action potentials were generated using 0.1ms, 2nA current injections given at 200Hz. (Bottom) Resulting EPSCs generated in the postsynaptic MNTB neuron held at -40mV to inactivate sodium channels. **B:** First two action potentials and resulting EPSCs from A (highlighted by orange box) on a larger scale. Paired recording done by myself.

5.3 EPSCs at the MNTB are AMPA-mediated

Glutamate release from the adult calyx of Held results in a large excitatory post synaptic current (EPSC) in the post synaptic MNTB neuron (figure 5.3). These EPSCs are incredibly large to ensure the depolarisation from each stimulus is sufficient to produce an action potential in the post synaptic neuron with average amplitudes in adult CBA wildtype mice of around 13.7nA ±0.40 (n=12; figure5.3). Additionally the decay kinetics are very rapid (0.2 ±0.02ms (n=10); figure 5.3), in order to limit the output of the neuron to a single action potential and allow receptors and ion channels to recover sufficiently between each stimulus during high frequency stimulation (Taschenberger and Von Gersdorff 2000; Futai et al. 2001). These incredibly fast EPSCs are a result of a developmental decrease in NMDA receptor expression and an increase in GluA4 containing AMPA receptors in the membrane of neurons, such that in adults most of the current is driven by AMPA receptors (Futai et al. 2001; Pilati et al. 2016; Caicedo and Eybalin 1999; Mosbacher et al. 1994). The presence of AMPA-driven EPSCs was confirmed in the present study using D-AP5 to block NMDA receptors and DNQX to block AMPA receptors (figure 5.4). DNQX

dramatically attenuated the EPSC amplitude, which was reversed upon washout, whereas D-AP5 has very little to no effect (n=1). It is likely that some NMDA component exists in adult EPSCs, however due to the negative holding potential (-40mV) and presence of Mg^{2+} in both the internal and external solutions, this was not observed in the present study.

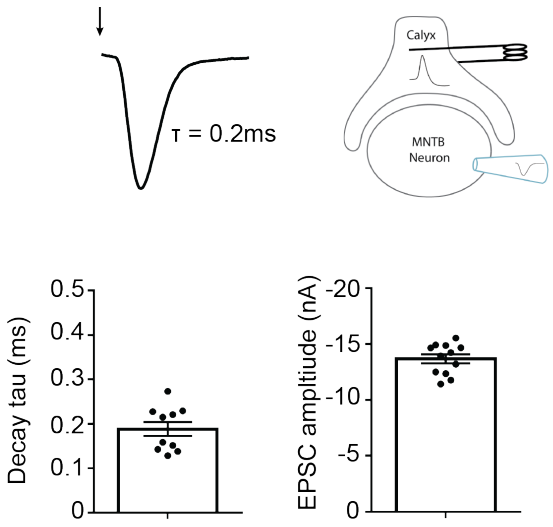

Figure 5.3: **EPSCs recorded from MNTB neurons of adult mice are fast with large amplitudes. Top left:** Example of an EPSC trace recorded from a P22 CBA wildtype mouse with an average decay tau of 0.2ms. Arrow indicates time of stimulation to presynaptic calyx axons. **Top right:** Schematic showing stimulation electrode placed on calyx axons and recording pipette on post synaptic MNTB neuron. **Bottom left:** Decay time constant of EPSCs recorded from mice aged P21-P25. n=10 from 7 animals. Tau taken from an average of 5 EPSCs from each neuron. **Bottom right:** Peak amplitudes for the same EPSCs as those from which decay tau was measured (left). Variance plotted as SEM.

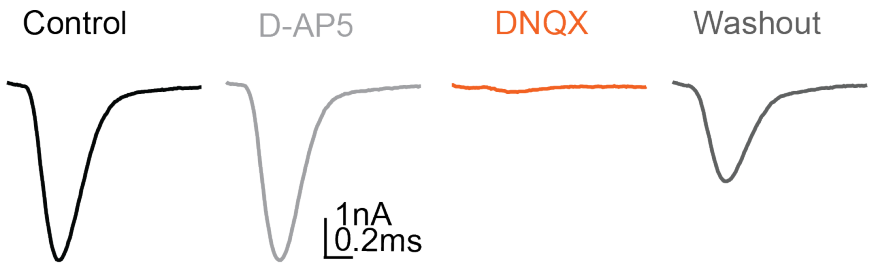

Figure 5.4: **EPSCs recorded from MNTB neurons are AMPA-dependent.** EPSCs recorded from an MNTB neuron during stimulation of the glutamatergic calyx of Held terminal in a P23 wildtype mouse. The neuron was held at -40mV while calyx terminals were stimulated using a concentric bipolar electrode. Traces show EPSC responses in control conditions (black; 5 minutes post break-in), after 10 minutes perfusion of 20μM D-AP5 (NMDA receptor blocker; grey), then 10 minutes perfusion of 10μM DNQX (AMPA receptor blocker; orange) followed by 10 minutes washout with normal acsf. Stimulation was not carried out between each 10 minute recording to avoid activity-dependent changes in amplitude.

5.4 EPSC amplitudes are larger in Kv3.3 KO animals

Simultaneous recordings from the calyx of Held synapse show that increasing presynaptic action potential duration with TEA increases the amplitude of postsynaptic responses (Ishikawa et al. 2003). Given the findings of the previous chapter, indicating that Kv3.3 subunits are the major constituent of presynaptic Kv3 channels and when absent, action potentials are significantly longer, one may predict that EPSC responses would also be increased in animals lacking this subunit. To assess this, whole cell recordings were performed in MNTB neurons of wildtype, Kv3.3 KO and Kv3.1 KO mice whilst axons of the presynaptic calyx terminal were stimulated.

EPSCs recorded from neurons in Kv3.3 KO mice were significantly larger than those in both wildtype and Kv3.1 KO animals (One-way ANOVA and Tukey's post hoc, CBA WT vs Kv3.3 KO P=0.0004; Kv3.1 KO vs Kv3.3 KO P=0.0231). Average amplitudes were -13 ±0.36nA (n=23) for WT, -17 ±1.06nA for Kv3.3 KO (n=20) and -14 ±0.63nA (n=18) for Kv3.1 KOs (figure 5.5). Despite increases in amplitude, there was no change in the decay time constant in either the Kv3.3 KO (0.3 ±0.02ms, n=9) or Kv3.1 KO (0.2 ±0.03ms, n=9) (WT 0.2 ±0.02ms, n=10; One-way ANOVA, $F(2,25)=2.723$, P=0.0851). EPSC amplitudes presented in the above are from a collection of experiments that will be presented throughout the chapter (WT n=22 neurons from 12 animals; Kv3.3 KO n=21 from 9 animals, Kv3.1 KO n=20 from 10 animals) and are taken from the first EPSC response within 100Hz stimulation trains. Decay times were taken only from the most recent experiments (WT n=10 from 7 animals; Kv3.3 KO n=9 from 4 animals; Kv3.1 KO n=9 from 5 animals) and were measured from a single exponential fit to the decay phase of the EPSC.

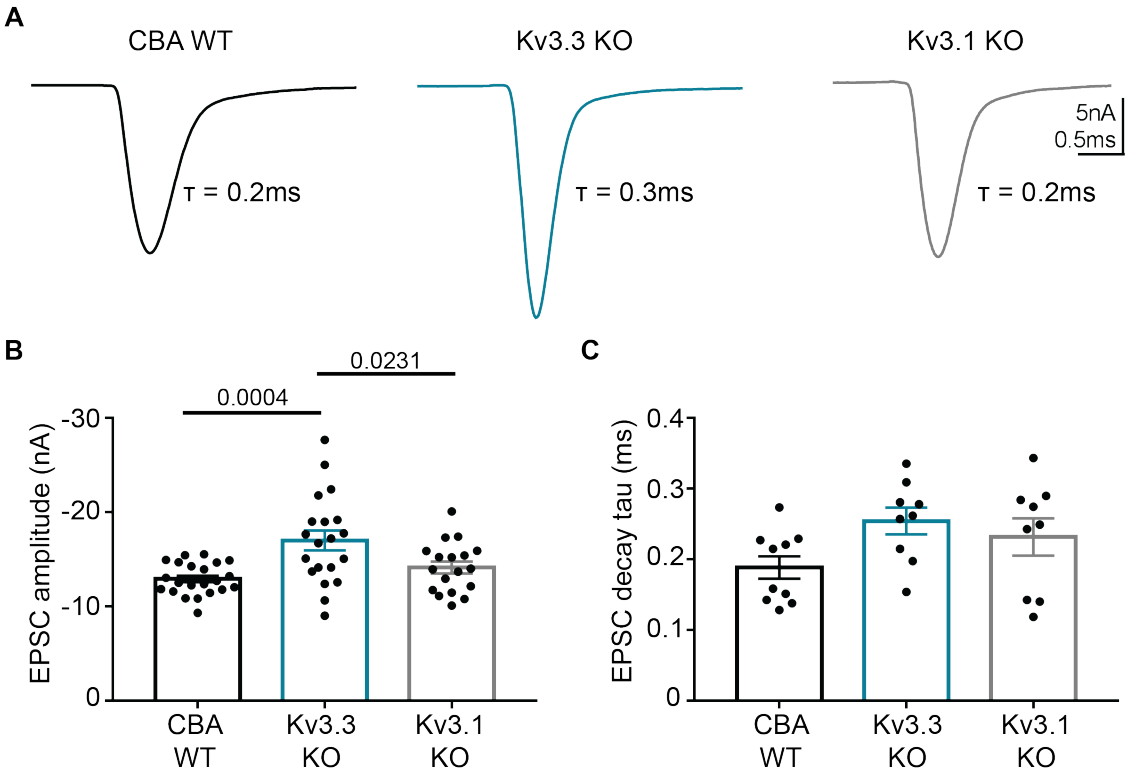

Figure 5.5: **EPSC amplitudes are larger in Kv3.3 KO mice.** Whole cell recordings from MNTB neurons in CBA WT, Kv3.3 KO and Kv3.1 KO mice in response to stimulation of calyx of Held axons. Neurons were held at -40mV to inactivate sodium channels and prevent action potential firing. **A:** Example EPSC traces from CBA WT, Kv3.3 KO and Kv3.1 KO mice. Stimulus artefacts have been removed for clarity. The average decay time constant is stated next to each trace. **B:** Quantification of EPSC amplitude. Each data point represents an average from 5 EPSCs in 1 neuron. Amplitudes were significantly increased in Kv3.3 KO animals compared to WT and Kv3.1 KOs (One-way ANOVA, Tukey's post hoc, P values reported on graph. **C:** EPSC decay constant times for EPSCs. Each data point represents an average from 5 EPSCs in 1 neuron. There were no significant changes in decay tau between groups (one-way ANOVA, $F(2,25) = 2.723$, $P=0.0851$). Variances plotted as SEM.)

5.5 Blocking presynaptic Kv3 has a smaller effect on EPSC amplitude in Kv3.3 KO animals

The previous section revealed increased EPSC amplitudes in animals lacking Kv3.3 subunits, consistent with an increased presynaptic AP duration in these animals seen in the previous chapter. Since the AP is already elongated, we postulated that blocking presynaptic Kv3 channels with 1mM TEA should have little to no impact on postsynaptic response amplitudes.

EPSCs were recorded from MNTB neurons in response to stimulation of axons giving rise to the calyx of Held. Stimulation protocols of 100Hz, 200Hz and 600Hz were applied to the axons three times, each with a rest period of 3 minutes, however only amplitudes of initial responses in 100Hz trains were analysed here (see figure 5.8).

Figure 5.6 shows EPSC responses in single MNTB neurons before and after 13 minutes perfusion of 1mM TEA (paired experiments). EPSC amplitudes were significantly larger in all animals in the presence of TEA (CBA WT before vs after 1mM TEA (n=6), paired t-test, P=0.0023, t=5.696, df=5; Kv3.3 KO before vs 1mM TEA (n=4), paired t-test, P=0.0231, t=4.305, df=3; Kv3.1 KO before vs 1mM TEA (n=4), paired t-test, P=0.0155, t=4.983, df=3; figure 5.6B). While the EPSC amplitudes were larger in all groups, the extent to which they increased was significantly different, with a much smaller increase seen in Kv3.3 KO animals (one-way ANOVA, P=0.0374, F(2,11)=4.497). In wildtype animals, EPSC amplitudes were increased by 57 ±13.0%, 36 ±5.7% in Kv3.1 KOs and only a 14 ±3.1% increase in Kv3.3 KOs (figure 5.6C). The block by TEA was significantly smaller in Kv3.3 KO animals compared to wildtype (Tukey's post hoc P=0.0227).

To ensure changes in EPSC amplitude were not a result of changes at the synapse resulting from repetitive stimulation or duration of experiment, the same experiment was conducted without the addition of TEA (figure 5.6D). Under these conditions there were no significant changes in amplitudes in WT or Kv3.3 KO animals (WT n=4, paired t-test, P=0.1518, t=1.912, df=3; Kv3.3 KO n=4, paired t-test,

P=0.4574, t=0.8507, df=3), however there was a small but significant decrease in Kv3.1 KOs of -11 ±2.18% (n=5; paired t-test, P=0.0197, t=3.766, df=4).

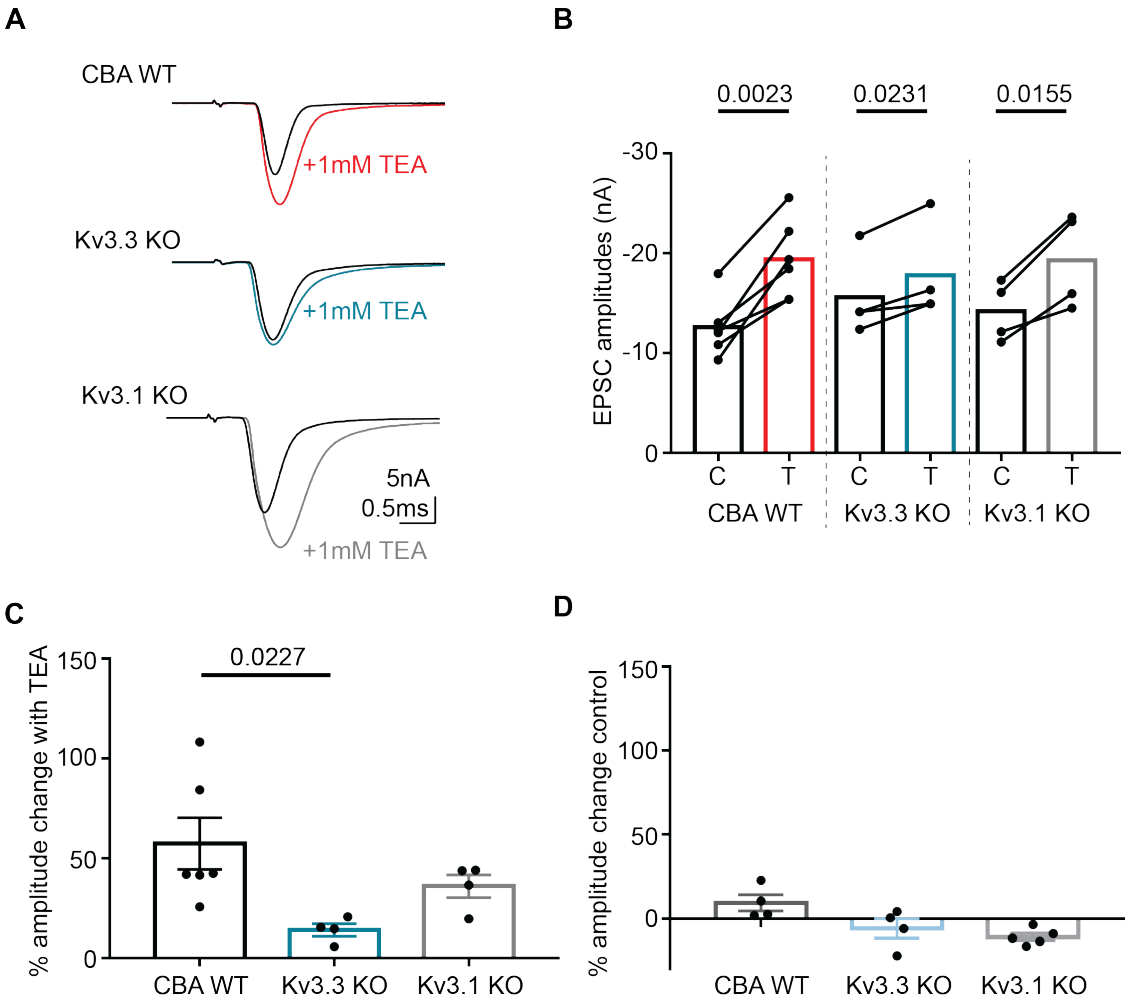

Figure 5.6: **Block of presynaptic Kv3 channels by 1mM TEA is smaller in Kv3.3 KO mice.** EPSCs recorded from MNTB neurons in response to stimulation of the calyx of Held synapse in wildtype, Kv3.3 KO and Kv3.1 KO mice. Neurons were held at -40mV and stimulated every 3 minutes **A:** Example EPSC traces before (black) and after application of 1mM TEA (red, blue and grey in WT, Kv3.3 KO and Kv3.1 KO respectively). **B:** EPSC amplitudes before and after TEA application. C= control, T=TEA. Paired data points from the same neuron are linked by black lines. EPSC amplitudes were significantly increased in the presence of TEA in all groups (paired t-tests, P values reported on graph). **C:** Percent change in EPSC amplitude in TEA compared to control for each genotype (0% represents no change, 100% represents a doubling of amplitude). The magnitude of change was significantly less in Kv3.3 KO animals compared to control (one-way ANOVA, Tukey's post hoc, P value on graph). **D:** Percent change in EPSC amplitude in the absence of TEA. i.e effect of time and repeated stimulation.

As TEA is known to block BK channels at a concentration of 1mM (Coetzee et al. 1999) and BK channels are postulated to be present in the terminal (Ishikawa et al. 2003) we also assessed the effect of a BK specific blocker (50nM iberiotoxin; IC_{50}= $\sim$ 250pM Galvez et al. 1990) on EPSC amplitude. Iberiotoxin had very little effect on EPSC amplitudes. The magnitude of change in the presence of iberiotoxin was similar to that seen when no drugs were applied and much less than that seen in the presence of TEA (9.5 $\pm$4.83% in control n=4, 57 $\pm$12.96% in 1mM TEA (n=6) and -3.7$\pm$9.52% (n=2) in IbTx; figure5.7).

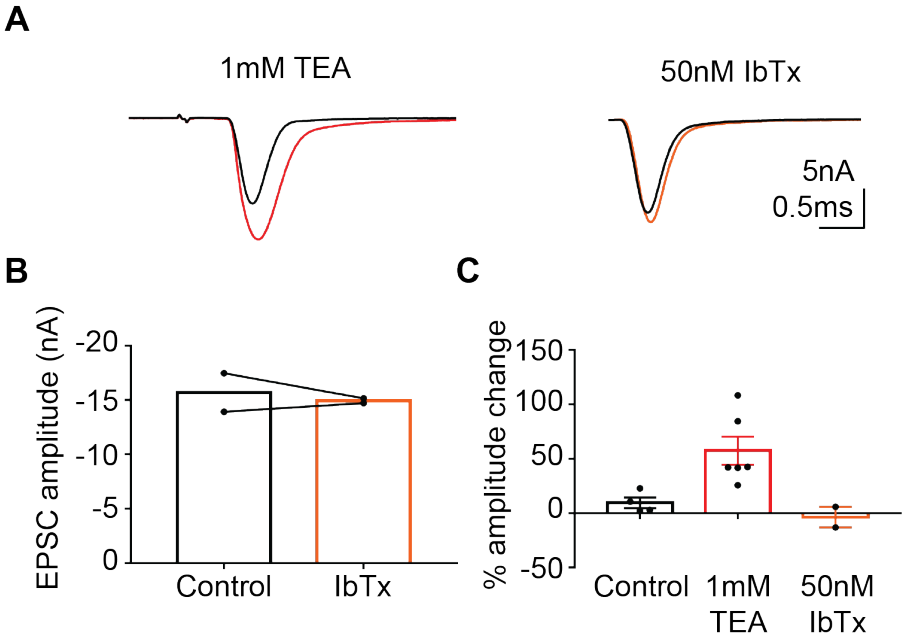

Figure 5.7: **Blocking BK channels has no effect on EPSC amplitude.** EPSC recordings from MNTB neurons of CBA wildtype mice. **A:** Example traces before (black) and after either 1mM TEA (red) or 50nM iberioxoin (IbTx; orange) from a holding potential of -40mV. **B:** EPSC amplitude before and after application of IbTx. **C:** Percent change in EPSC amplitude in conditions where no drug was applied, 1mM TEA was present or 50nM IbTx.

5.6 Short term depression of EPSC amplitudes is much quicker and larger in Kv3.3 KO mice

Evidence from the last two sections has shown that EPSC amplitudes are much larger in Kv3.3 KO animals and blocking presynaptic Kv3 channels with TEA does little to increase them further. This is consistent with findings from the previous chapter, showing that Kv3.3 subunits appear to be the most important subunit for presynaptic AP repolarisation. However, physiologically, a single input would rarely occur within these neurons and since Kv3 channels exist to promote high frequency firing, we wanted to see what would happen to transmitter release during fast stimulation trains. Stimulation trains of 100, 200 and 600Hz were applied to axons giving rise to the calyx of Held; 100 and 200Hz are generally considered to be fairly low frequency at this synapse and have previously been used to assess the effects of TEA and knocking out Kv3.1b subunits on EPSC amplitudes (Wang and Kaczmarek 1998; Macica et al. 2003). While 300Hz has been used as a high frequency stimulus in previous work (Wang and Kaczmarek 1998; Macica et al. 2003), 600Hz was used in the present study to eliminate any ambiguity and to push the synapse to the extreme. Previous work has shown that increased release probability in the presence of TEA results in faster vesicle depletion and short term depression during prolonged stimulation at 200Hz (Wang and Kaczmarek 1998). One may predict that this would also occur in Kv3.3 KO animals as the presynaptic Kv3 currents appears to be vastly reduced, thus mimicking the effect of blocking with TEA.

Due to the low probability of attaining an MNTB neuron which responded to stimulation of the midline (mainly due to severing of axons giving rise to calyces during the brain slicing process), all three stimulation frequencies were performed in one protocol on each neuron (figure 5.8). In each stimulation epoch, 800ms trains of 100Hz were applied 5 times with a rest time of 20s between each, followed by a 30s rest period. This was then repeated with 200 and 600Hz trains. A rest period of 20s was sufficient for EPSC amplitudes to return to baseline (figure 5.17). Three of these such epochs were applied to each cell, the first to attain a baseline EPSC

amplitude, followed by three minutes rest. The second to attain an intermediate recording during drug application (TEA or IbTx), followed by three minutes rest and third to assess the effects of drugs on EPSC amplitudes. Only responses from the first and last stimulation epochs were analysed.

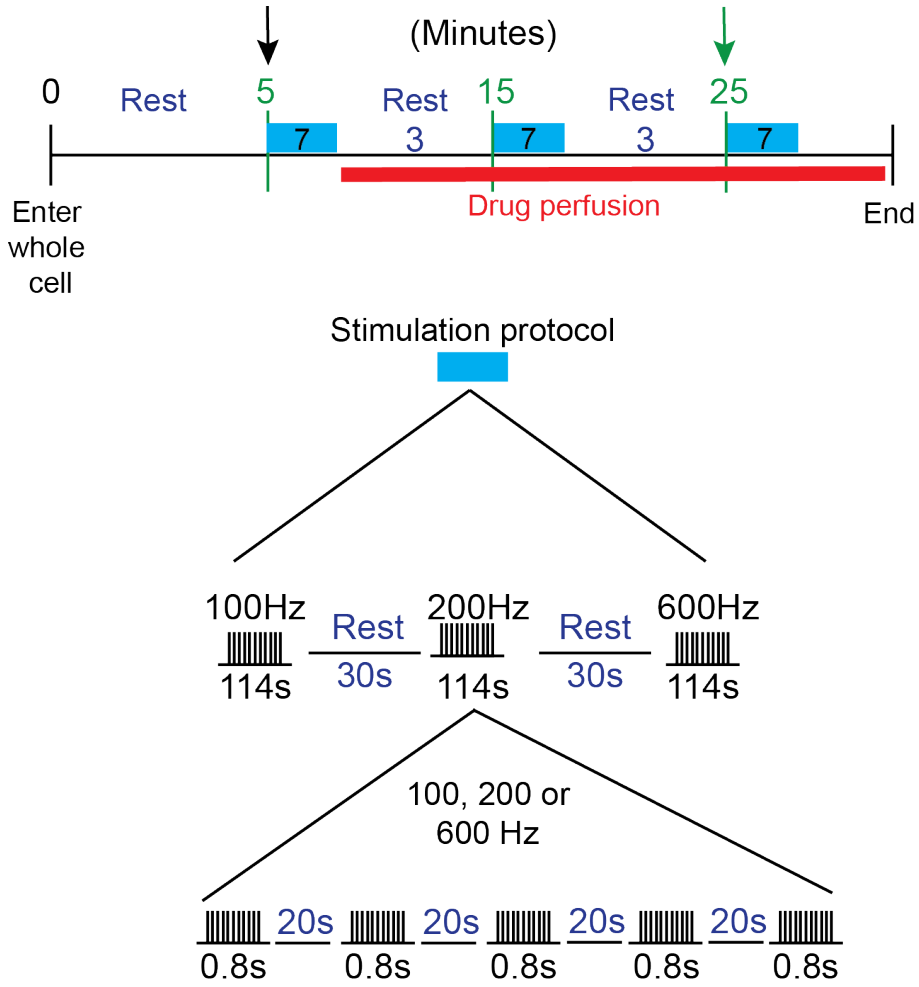

Figure 5.8: **High frequency stimulation train protocol. Top**: Time line of protocol from breaking into the cell until the end of the experiment. Green numbers represent times at which protocol epochs (blue square) are carried out. Red line represent time of drug perfusion in experiments where TEA or IbTx were used. Black arrow indicates epoch used for baseline 'control' recordings. Green arrow indicated epoch used for 'drug' recordings. **Bottom**: Stimulation trains applied in each epoch. (Top row) 100Hz, 200Hz and 600Hz stimulation separated by 30s rest periods. (Bottom row) Each stimulation frequency consists of 5 800ms trains separated by 20s rest periods.

Wildtype, Kv3.3 KO and Kv3.1 KO animals were able to sustain glutamate release at the calyx of Held synapse during stimulation at 100, 200 and 600Hz (figure 5.9). However, following a large initial response, short term depression of EPSC amplitudes appeared to occur much quicker in Kv3.3 KO animals. Surprisingly, this was observed even at 100Hz but was more evident at higher frequencies with EPSC amplitudes reaching a 'plateau' value much quicker than in wildtype neurons in which EPSC responses declined more gradually. Despite responses in Kv3.1 KO animals appearing similar to wildtype at 100Hz, they also exhibited a faster rate of decline at 200 and 600Hz. Additionally, at 600Hz, initial responses in Kv3.3 KO animals did not decay back to baseline before the following stimulus (figure 5.9; black arrow). This was not observed in Kv3.1 KO animals.

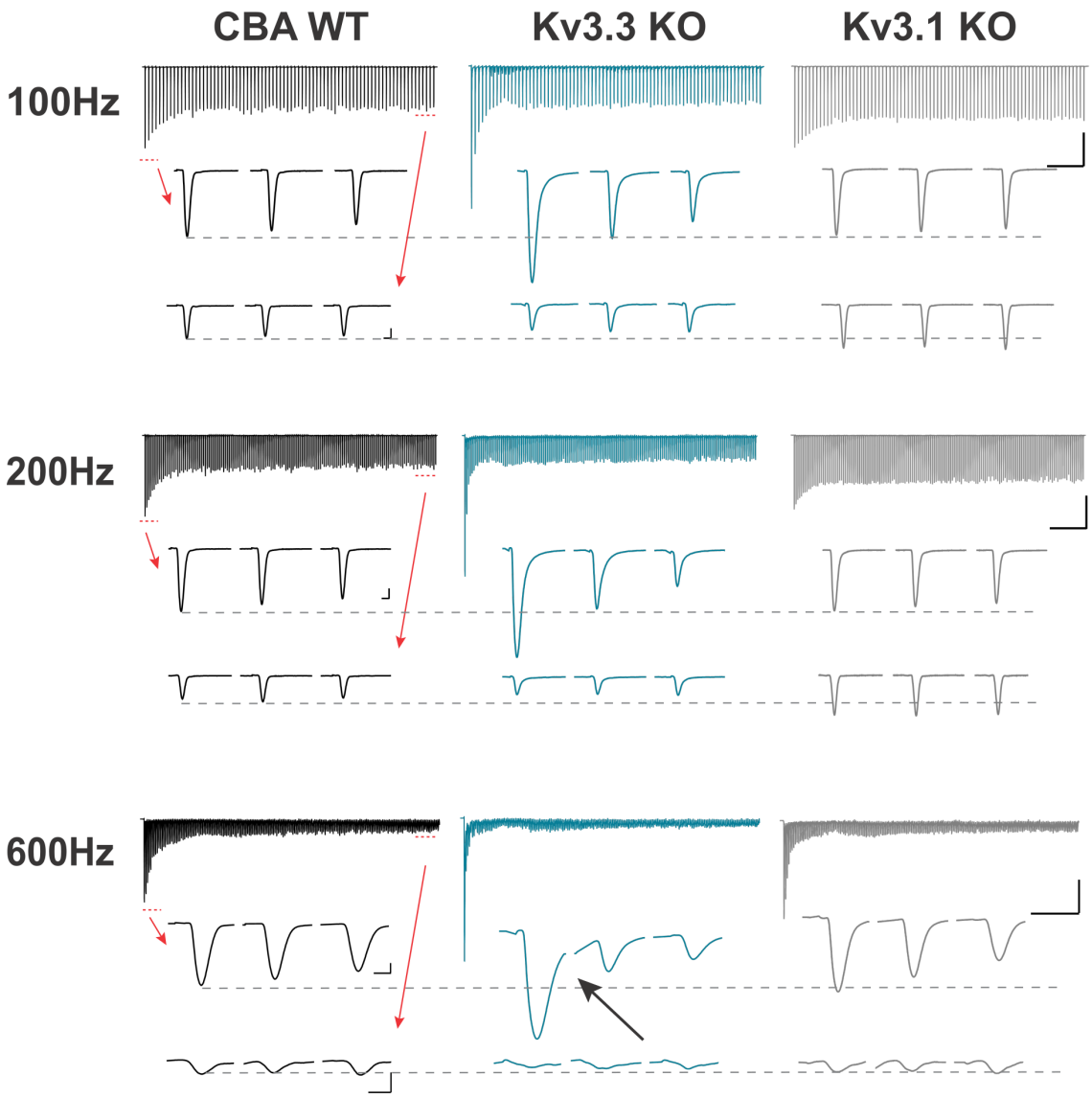

Figure 5.9: **EPSC responses in MNTB neurons of Kv3.3 KO animals show faster short term depression during 100, 200 and 600Hz stimulation. Top** Example EPSC traces from single neurons in the MNTB of wildtype, Kv3.3 KO and Kv3.1 KO in response to 100Hz stimulation at the calyx of Held. Scale bar = 5nA, 100ms. (middle) First 3 EPSC responses from the train are enlarged, with grey dotted line indicating peak amplitude of wildtype responses. (bottom) Last 3 EPSC responses are enlarged, again with the grey line indicating peak amplitudes of wildtype animals. Scale bar = 2nA, 0.5ms. **Centre:** The same for stimulation at 200Hz. **Bottom:** The same for 600Hz stimulation. Scale bar= 5nA, 50ms. The scale of responses at the end of the train were enlarged for clarity (scale bar= 2nA, 0.5ms). Black arrow indicates the initial EPSC failing to return to baseline before the following stimulus in Kv3.3 KO animals.

EPSC amplitudes were measured from each neuron and normalised to the initial responses in order to compare between groups (figure 5.10). A single exponential function was fitted to response trains from each neuron at 100 and 200Hz in order to assess the extent and rate at which short term depression of amplitudes occurred (see table 5.1 'decay rate' and 'plateau'). This was not possible at 600 Hz due to the introduction of another component (possibly due to incorporation of vesicles from the 'reserve' pool into the readily releasable pool) at around the 40th stimulus which resulted in a 'bump', corresponding to an increase in EPSC amplitudes (figure 5.10 bottom).

Responses from neurons of all genotypes showed a characteristic decline in amplitudes which eventually reached a 'plateau' amplitude. At 100Hz, this occurred at around the 20th response, at 200Hz it was observed at ∼50th stimulus. At 600Hz, while amplitudes from the 80th responses were reduced to around 20% of their maximal, they continued to decline throughout the stimulation train.

Interestingly, differences between the knockout animals and wildtype were observed even at 100Hz, despite this being regarded as relatively low frequency (figure 5.10).

At 100, 200 and 600Hz, EPSC responses of Kv3.3 KO animals showed a greater level of short term depression compared to both wildtype and Kv3.1 KO animals (see 'plateau' values, table 5.1). At 200Hz, amplitudes in the 'plateau' phase were significantly decreased compared to wildtype (One-way ANOVA, Tukey's post hoc, P=0.0423; WT n=10, Kv3.3 KO n=10, Kv3.1 KO n=6).

The rate at which this depression of responses occurred was vastly increased in Kv3.3 KO compared to both wildtype and Kv3.1 KOs at both 100 and 200Hz (see table 5.1 'Decay rate'; One-way ANOVA, Tukey's post hoc, 100Hz CBA vs Kv3.3 KO P=<0.0001, Kv3.1 KO vs Kv3.3 KO P=<0.0001; 200Hz CBA vs Kv3.3 KO P=0.0005, Kv3.1 KO vs Kv3.3 KO P=<0.0001). This increase in rate of depression resulted in a characteristic 'dip' in response amplitudes followed by a transient increase at all frequencies (black arrows, figure 5.10). This only occurred in wildtype and Kv3.1 KO neurons at the higher frequencies but was most pronounced at 600Hz.

In contrast to Kv3.3 KO animals, EPSCs appeared to be resistant to short term depression in Kv3.1 KO animals, with very little reduction in amplitude observed throughout trains at both 100 and 200Hz (figure 5.10). Responses during the 'plateau' phase (see table 5.1 'plateau') were significantly increased compared to wildtype (100Hz WT 0.44 ±0.04 n=10; Kv3.1 KO 0.66 ±0.06 n=6; 200Hz WT 0.3 ±0.03; Kv3.1 KO 0.6 ±0.08; one-way ANOVA, Tukey's post hoc, 100Hz P= 0.0021, 200Hz P= 0.0007). The rate at which this depression occurred was similar to that seen in wildtype neurons (table 5.1; 100Hz Kv3.1 KO 0.21 ±0.01, WT 0.23 ±0.02).

Additionally, the absolute EPSC amplitudes of Kv3.1 KOs at the end of the train (last 10 EPSCs; table 5.1) were significantly increased compared to wildtype at both 100 and 200Hz (100Hz Kv3.1 KO -8.6 ±1.29nA (n=6), WT -5.1 ±0.51nA; 200Hz Kv3.1 KO -7.0 ±1.52nA, WT -4.2 ±0.51nA; One way ANOVA, Tukey's post hoc; 100Hz P=0.0108; 200Hz P=0.0135).

Despite most neurons responding to 600Hz stimulation, failures were often observed in neurons of all genotypes. Additionally, there appeared to be an increase in asynchronous release in Kv3.3 KOs that was not observed in wildtype or Kv3.1 KOs (figure 5.11).

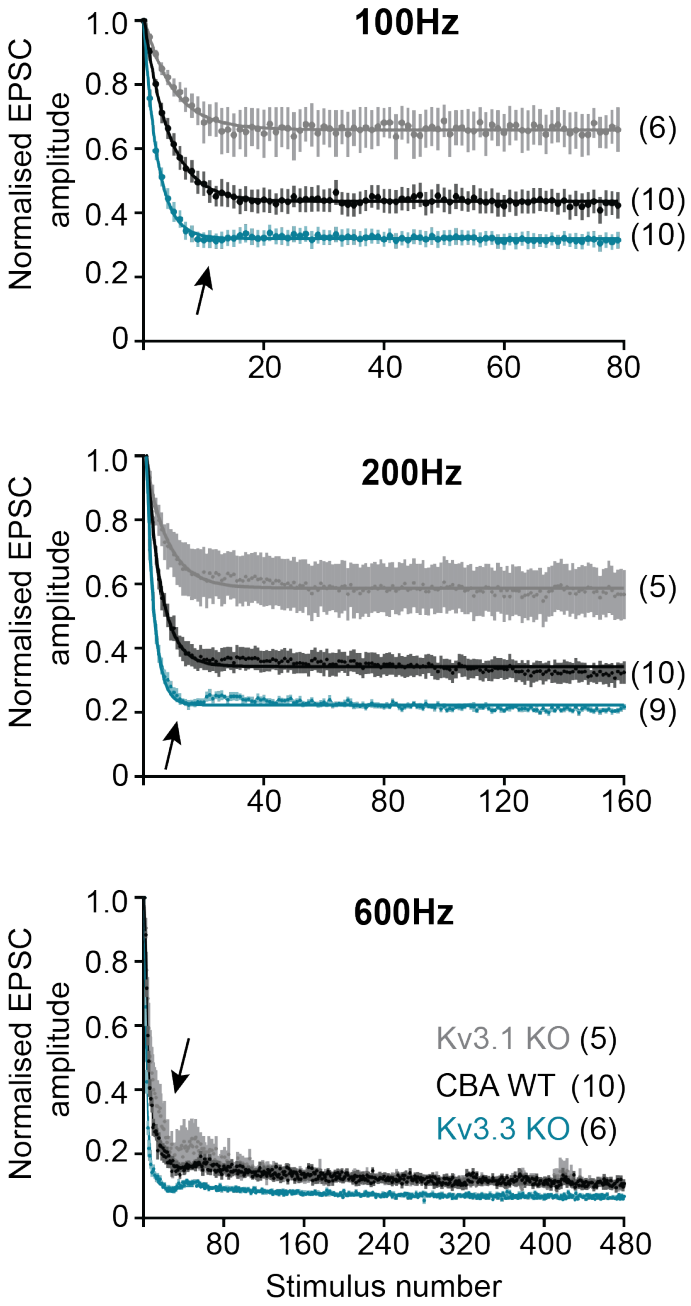

Figure 5.10: **Short term depression of EPSC amplitudes in increased in Kv3.3 KOs and decreased in Kv3.1 KOs. Top:** EPSC amplitudes recorded from MNTB neurons in response to 100Hz stimulation (800ms) of presynaptic axons in CBA wildytpe (black), Kv3.3 KO (blue) and Kv3.1 KO (grey) mice. Amplitudes have been normalised to initial responses. A single exponential fit has been applied to responses in order to measure rate and extent of depression (grey, black and blue lines). n= number of cells, reported in brackets. **Middle:** The same for 200Hz stimulation of presynaptic axons. **Bottom:** Normalised responses to 600Hz stimulation. Black arrows indicate a 'dip' followed by 'bump' in amplitudes in Kv3.3 KO neurons, only seen at 600Hz for wildtype and Kv3.1 KOs. Error bars represent SEM.

Table 5.1: **EPSC parameters in CBA wildtype, Kv3.3 KO and Kv3.1 KO animals in response to 100, 200 or 600Hz stimulation.** (Last EPSC amplitude was an average of the last 10 EPSCs recorded in the train; Decay rate and plateau amplitude refers to a single exponential function fitted to normalised EPSC responses. WT n=10, Kv3.3 KO n=10, Kv3.1 KO n=6. Values in bold are significantly different from WT)

Freq	Parameter	CBA WT	Kv3.3 KO	Kv3.1 KO
100Hz	1st EPSC (nA)	-11.99 ±0.511	-15.88 ±1.662	-12.93 ±1.124
	Last EPSCs (nA)	-5.1 ±0.51	-5.1 ±0.76	**-8.6 ±1.29**
	Decay rate (1/ms)	0.23 ±0.02	**0.46 ±0.04**	0.21 ±0.01
	Plateau amp	0.44 ±0.04	0.32 ±0.03	**0.66 ±0.06**
200Hz	1st EPSC (nA)	-13.0 ±0.76	-16.0 ±1.87	-13.8 ±1.33
	Last EPSCs (nA)	-4.2 ±0.51	-3.4 ±0.37	**-7.0 ±1.52**
	Decay rate (1/ms)	0.21 ±0.02	**0.42 ±0.05**	0.12 ±0.03
	Plateau amp	0.3 ±0.03	**0.2 ±0.01**	**0.6 ±0.08**
600Hz	1st EPSC (nA)	-11.6 ±0.39	-16.0 ±1.59	-13.1 ±1.02
	Last EPSCs (nA)	-1.3 ±0.11	-1.0 ±0.08	-1.3 ± 0.12

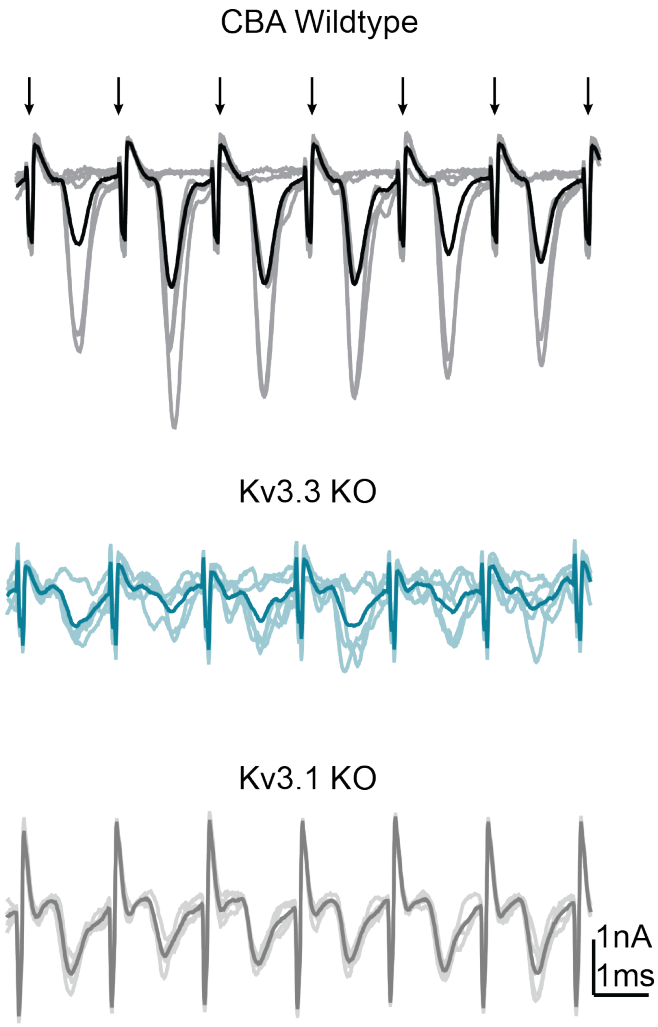

Figure 5.11: **Increase in asynchronous release in Kv3.3 KOs during 600Hz stimulation.** Example traces from single neurons of CBA WT, Kv3.3 KO and Kv3.1 KO mice. 5 individual traces are shown in lighter colours (WT grey, Kv3.3 KO light blue, Kv3.1 KO light grey) and an average of the 5 traces in darker colours. Arrows represents time of stimulus and show corresponding stimulus artefact.

In addition to analysing EPSC amplitudes, one can measure the 'charge' of the response. This is the integral of the EPSC and should reflect total vesicle release due to accounting for both the amplitude, and the duration of the response. The amount of release during 100Hz stimulation was significantly increased in Kv3.1 KOs compared to both CBA wildtypes and Kv3.3 KO mice (One-way ANOVA, Tukey's post hoc; CBA vs Kv3.1 KO P=0.0230; Kv3.3 KO vs Kv3.1 KO P=0.0110). Total charge at the end of the train was 177.7 ±16.81nC in CBA WT (n=8), 162.4 ±30.32nC in Kv3.3 KOs (n=8) and 310.5 ±44.45nC in Kv3.1 KOs (n=8; figure 5.12).

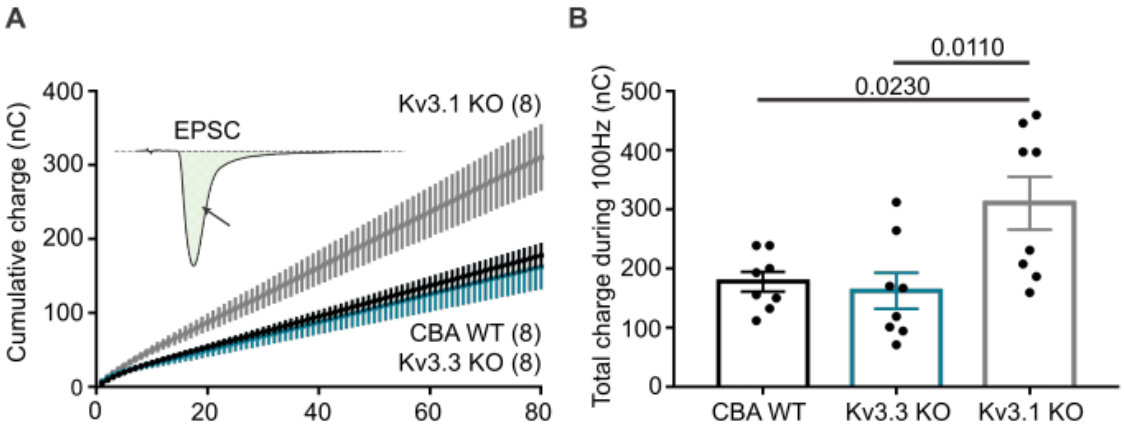

Figure 5.12: **Total vesicle release is increased in Kv3.1 KOs. A:** Cumulative charge of EPSC responses during 100Hz for 800ms in CBA wildtype, Kv3.3 KO and Kv3.1 KO mice. Charge is defined as the integral of the EPSC response (black arrow and green shaded area; inset). n values are in brackets and represent number of neurons. **B:** Total charge during 100Hz stimulation train. Measured by taking cumulative charge value on the last (80th) stimulus. Vesicle release in Kv3.1 KOs is significantly larger than CBA wildtypes and Kv3.3 KOs (one-way ANOVA, Tukey's post hoc, P values on graph). All variances are plotted as SEM.

The ability of Kv3.1 KO animals to sustain such an increased release of neurotransmitter (shown by lack of synaptic depression and increased charge; figures 5.10 & 5.12) suggested that there may be enhanced vesicle recycling in these animals or there was an increase in the readily releasable pool (RRP) of vesicles. To calculate the RRP the charge can also be used, by dividing the charge of each EPSC in the train by charge of single synaptic events (mEPSCs) and using the cumulative results to back-extrapolate to the Y-axis (figure 5.13 left; Schneggenburger, Meyer, and Neher 1999). RRP estimates were 511.2 ±72.35 in CBA WT (n=8), 482.6 ±70.82 in Kv3.3 KOs (n=8) and 517.1 ±89.23 in Kv3.1 KOs (n=8), although there was a lot of variation, there were no significant differences between groups (one-way ANOVA, F(2,21)=0.05615, P=0.9455; figure 5.13).

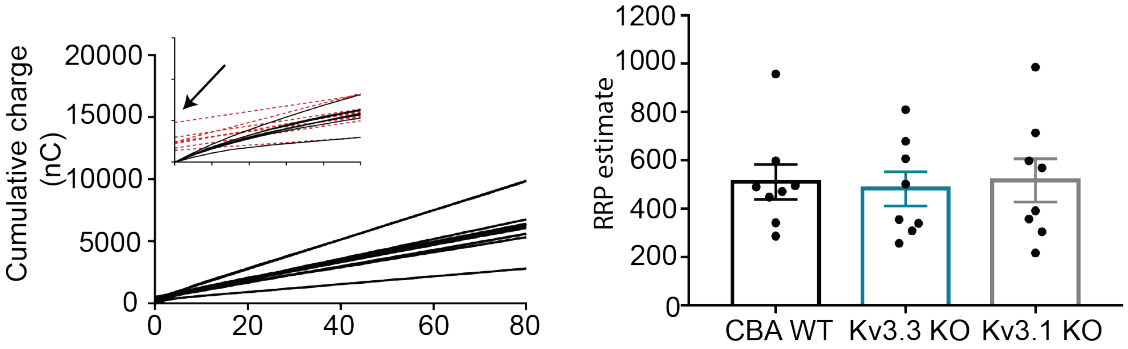

Figure 5.13: **The readily releasable vesicle pool (RRP) is unchanged in Kv3.3 and Kv3.1 KOs. Left:** Cumulative EPSC charges during 100Hz stimulation in 8 single CBA wildtype neurons. (Inset:) linear regressions are fitted to data between the 10th and 30th stimulus and back-extrapolated to the Y-axis. The value at this point (black arrow) indicates RRP size. **Right:** RRP estimates, measured as in A. There are no significant changes in RRP between groups (one-way ANOVA,F(2,21)=0.05615, P=0.9455) Variance plotted as SEM

5.7 Quantal amplitudes are decreased in Kv3.3 KO mice

The last section detailed changes in postsynaptic responses in Kv3.3 KO and Kv3.1 KO mice, in particular, a resistance to short term depression observed in Kv3.1 KO, in comparison to a pronounced depression observed in Kv3.3 KO animals. One would postulate that these changes are purely due to the changes in presynaptic action potential waveform and thus release probability dictated by calcium influx, however, changes in quantal content, number of release sites and postsynaptic AMPA receptor sensitivity may also contribute. This section aims to explore changes in quantal parameters that may result from pre and postsynaptic mechanisms.

Release at this calyx of Held synapse is consistent with the quantal hypothesis (Borst and Sakmann 1996; Meyer, Neher, and Schneggenburger 2001; Scheuss, Schneggenburger, and Neher 2002), meaning that amplitudes of postsynaptic currents linearly correlate with amplitudes of single release events (mEPSCs) and represent the sum of the number of release sites (N), probability of release (p) and quantal content of each vesicle (q; equation 5.1).

$$Mean\ EPSC\ amplitude = N\ *\ p\ *\ q \tag{5.1}$$

This means that quantal analysis can be performed on trains of EPSCs to determine values for these parameters. Previously, reports estimate ∼600-1000 release sites at this synapse (Meyer, Neher, and Schneggenburger 2001; Scheuss, Schneggenburger, and Neher 2002; Schneggenburger, Meyer, and Neher 1999; Barnes-Davies and Forsythe 1995). This is useful as it can provide information on whether pre or postsynaptic mechanisms are responsible for alterations to postsynaptic responses. In particular, changes in the coefficient of variation (S.D/mean EPSC amplitude) suggests modifications in the presynaptic terminal as it depends on N and p (equation 5.2) whereas changes in the variance/mean (variance of EPSC amplitude/mean EPSC amplitude) suggests alterations to either the volume of transmitter within each vesicle or the postsynaptic glutamate receptor sensitivity (equation 5.3).

$$Coefficient\ of\ variation = \sqrt{((1-p)/Np)} \tag{5.2}$$

$$Variance/mean\ = q(1-p) \tag{5.3}$$

This can only be applied using EPSC trains when p is very low (Taschenberger, Scheuss, and Neher 2005), as is the case for immature calyces on which most of these studies have been conducted (Meyer, Neher, and Schneggenburger 2001; Scheuss, Schneggenburger, and Neher 2002). Unfortunately, this was not the case for the present study, highlighted by a non-linear relationship between mean EPSC amplitude and variance of EPSC amplitude (data not shown; Meyer, Neher, and Schneggenburger 2001; Scheuss, Schneggenburger, and Neher 2002). We instead decided to investigate mini EPSCs (mEPSCs) in these neurons. mEPSCs are the result of the contents of a single vesicle of neurotransmitter being released from a presynaptic terminal and binding to postsynaptic receptors. This is an action potential and calcium independent phenomena and thus one may expect that no differences would be present in our knockout animals as Kv3 currents are only active during the action potential due to their high activation voltage.

In order to investigate mEPSCs, a gap free (no voltage commands) protocol was recorded for 30s in neurons of wildtype, Kv3.3 KO and Kv3.1 KO mice at a holding potential of -40mV prior to any other recordings (figure 5.14). Tetrodotoxin (TTx) is often included in acsf during recording of mEPSCs to avoid contamination by spontaneous action potential driven release events, however as AP-driven EPSCs at this synapse are in the magnitude of several nanoamps, it was possible to distinguish between these and miniature events without the need to block APs. mEPSCs were detected using template search and event detection in clampfit software (a template based on 10 mEPSCs chosen manually was used to detect other events).

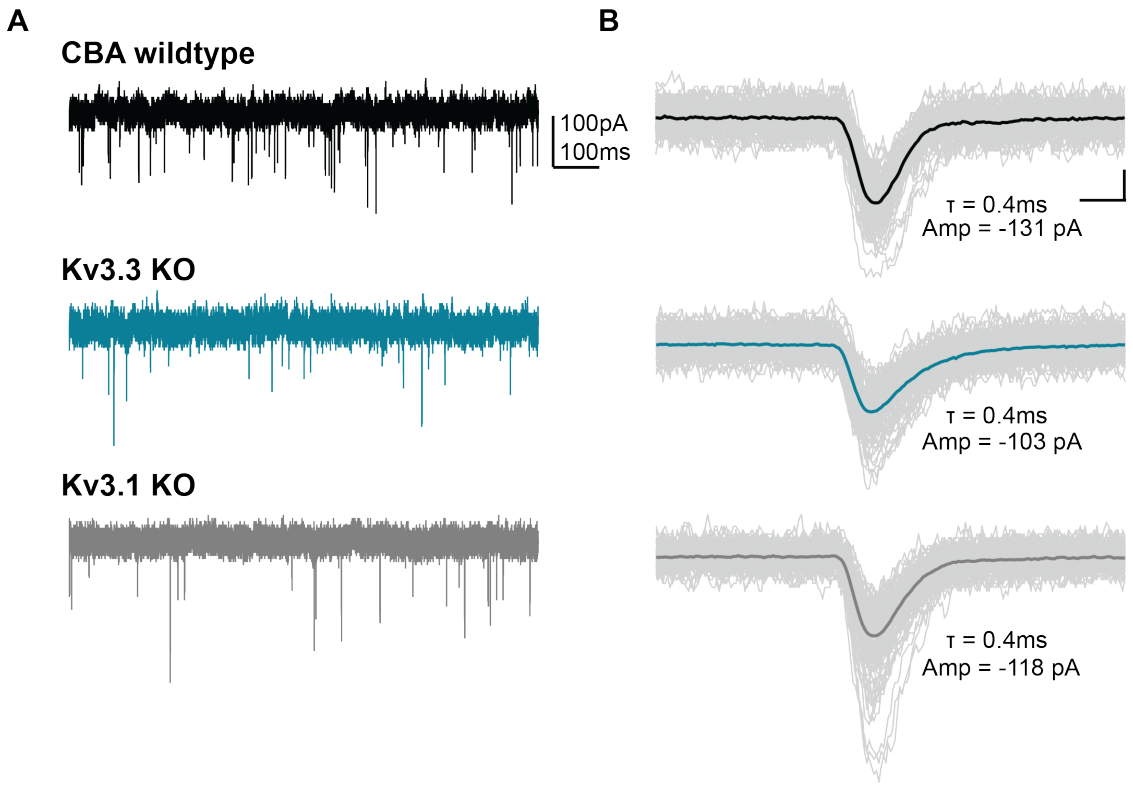

Figure 5.14: **Miniature excitatory post-synaptic currents recorded in MNTB neurons of CBA wildtype, Kv3.3 KO and Kv3.1 KO mice. A:** Example traces from single neurons from each genotype, showing the initial second from a 30s recording. Neurons were held at -40mV. **B:** mEPSC events recorded from same neurons as in A. Dark traces show an average mEPSC from a single neuron during a 30s recording, the lighter colours represent the first 100 single mEPSC events from the same cell. Scale bar = 50pA, 0.2ms. Average amplitudes and decay time constants for all recorded neurons are denoted next to the traces.

Average mEPSC amplitudes were significantly decreased in Kv3.3 KO animals compared to both wildtype and Kv3.1 KO (one-way ANOVA, Tukey's post hoc; CBA WT or Kv3.1 KO vs Kv3.3 KO P=<0.0001; figure 5.15). This was observed both when taking an average of the entire population of mEPSC events from each genotype (figure 5.15A) and when mEPSC amplitudes from a single neuron were averaged before being plotted (One-way ANOVA, Tukey's post hoc; CBA WT vs Kv3.3 KO P=0.0264; figure 5.15B), although absolute amplitudes differed slightly between the two methods. Amplitudes when taking the population as a whole were -117.8 ±0.00pA in WT (n=805), -116.2 ±0.00pA in Kv3.1 KOs (n=492) and -101.8 ±0.00pA in Kv3.3 KOs (n=594). In comparison, amplitudes for CBA wildtypes when taking an average for each neuron was observed to be -130.8 ±6.08pA (n=8), while values for Kv3.1 and Kv3.3 KOs were similar to the population means at -118.5 ±9.40pA (n=8) and -102.8 ±4.76pA (n=8), respectively.

There were no differences observed between either the frequency (WT 14.6 ±2.54, Kv3.3 KO 10.2 ±1.47, Kv3.1 KO 11.0 ±1.34; one-way ANOVA, $F(2,21)=1.552$, P=0.2351) of mEPSC events (calculated by dividing total events by 30s) or in decay time constants (WT 0.39 ± 0.02ms, Kv3.3 KO 0.44 ±0.01ms and Kv3.1 KO 0.42 ±0.02ms; one-way ANOVA, $F(2,20)=1.948$, P=0.1687).

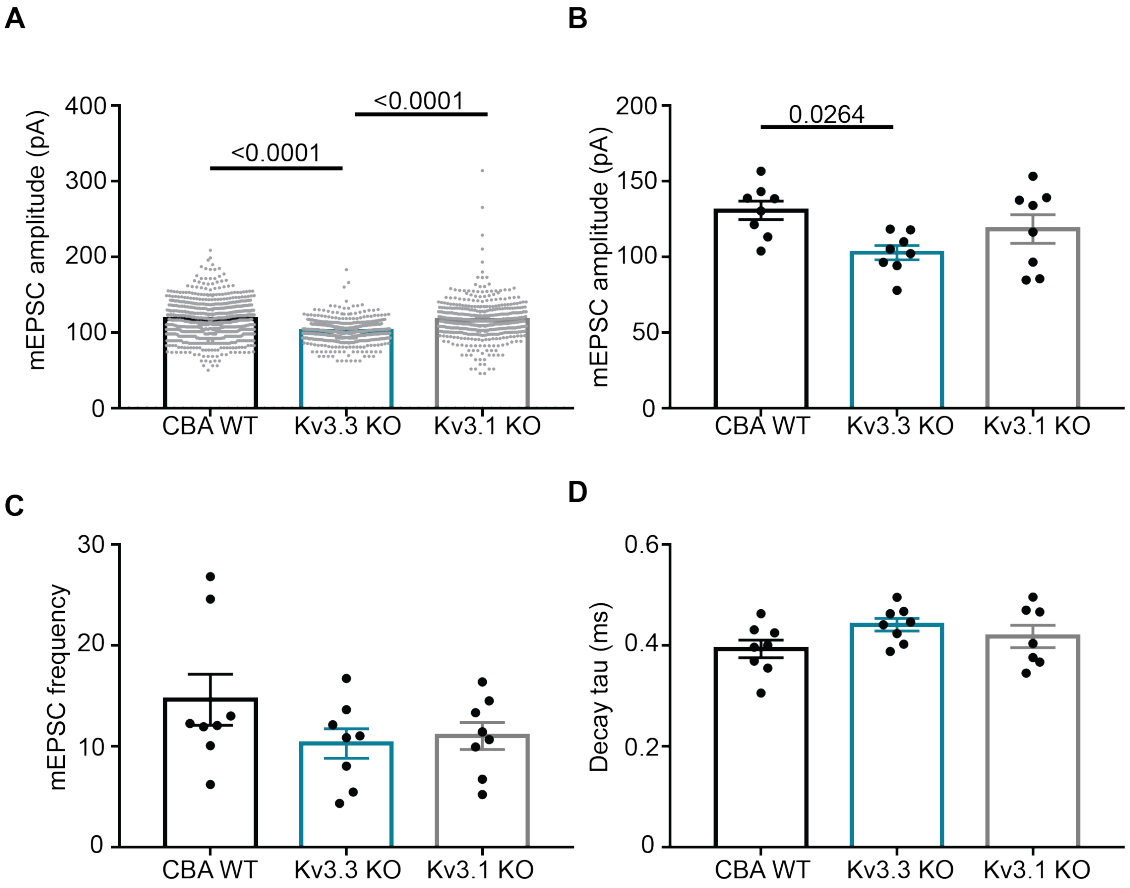

Figure 5.15: **mEPSC amplitude is decreased in Kv3.3 KOs. A:** Amplitudes of mEPSCs during 30s recordings from MNTB neurons in CBA wildtype, Kv3.3 KO and Kv3.1 KO mice. mEPSCs from all neurons were pooled into each genotype (n values; CBA n=805 events from 8 neurons; Kv3.3 KO n=594 from 8 neurons, Kv3.1 KO n=492 events from 8 neurons). mEPSC amplitudes in Kv3.3 KOs were significantly decreased (one-way ANOVA, Tukey's post hoc, P values on graph). **B:** Amplitudes of mEPSCs measured by taking an average amplitude from each neuron. Amplitudes in Kv3.3 KOs were significantly decreased compared to WT (one-way ANOVA, Tukey's post hoc, P=0.0264). **C:** mEPSC frequency during 1s. Measured as number of events in 30s divided by 30. There were no significant differences between groups (one-way ANOVA, $F(2,21)=1.552$, P=0.2351) **D:** Decay time constant of mEPSCs. No significant differences were observed (One-way ANOVA, $F(2,20)=1.948$, P=0.1687). An average was taken for all events in each neuron. For B, C and D, data points represent individual neurons. Variances plotted as SEM.

5.8 Changes in the rate of vesicle replenishment were not observed in Kv3.1 KOs

So far in this chapter we have established that enhanced transmitter release can be sustained at the calyx of Held synapse in Kv3.1 KOs. In contrast enhanced initial release leads to a pronounced synaptic depression in Kv3.3 KOs. While the pronounced depression seen in Kv3.3 KOs may be explained by a faster rate of vesicle depletion (Wang and Kaczmarek 1998), the larger sustained release in Kv3.1 KO is more difficult to explain. It is not due to an increase in the readily releasable pool of vesicles (figure 5.13), nor a change in quantal parameters (figure 5.15). Here we explore the possibility of enhanced vesicle recycling in these animals using recovery curves (Wang and Kaczmarek 1998; Lucas et al. 2018).

It has previously been shown that vesicle recycling is a calcium and thus activity-dependent process. Broadening of presynaptic action potentials with TEA results in faster vesicle recycling, thus one may expect an enhanced rate of vesicle replenishment in Kv3.3 KO animals due to the longer action potentials observed in the presynaptic terminal.

High-frequency stimulation (100Hz) was applied to calyx of Held axons for 1s followed by single stimuli at 50ms, 100ms, 500ms, 1s, 2s, 5s, 10s, 20s and 30s after the train (figure 5.16). This was repeated three times in each neuron with a rest period of 1 minute between each recording. The EPSCs generated in MNTB principal neurons were recorded using voltage clamp. Neurons were held at -40mV to inactivate sodium channels and prevent action potential firing in the postsynaptic neuron. These experiments were conducted in the absence of strychnine.

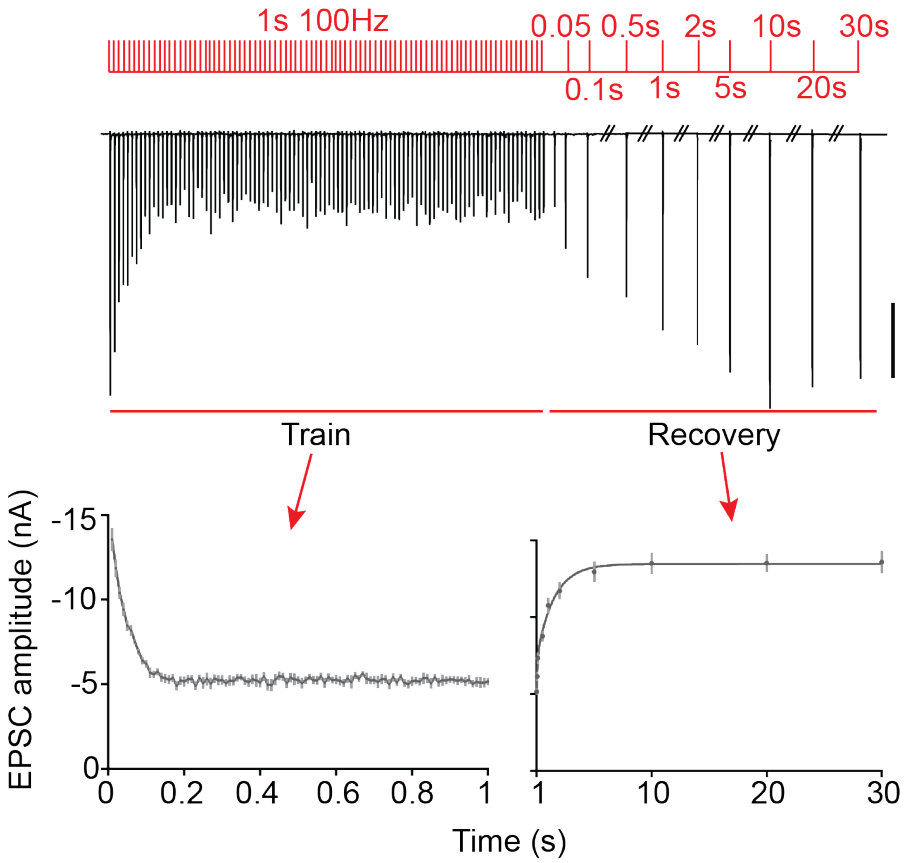

Figure 5.16: **Recovery curve stimulation protocol.** Stimulation protocol shown in red; 100Hz for 1 second followed by stimulation at 50ms, 100ms, 500ms, 1s, 2s, 5s, 10s, 20s and 30s. Example EPSCs recorded from an MNTB neuron in a CBA wildtype mouse in response to stimulation of calyx of Held axons. Scale bar = 5nA. Amplitudes of these EPSCs were measured and plotted into graphs as seen at the bottom. Recovery curves (right) were fit with double exponential functions.

Consistent with results of the previous sections, EPSC amplitudes decline much faster during 100Hz stimulation in Kv3.3 KOs (figure 5.17). Interestingly, although amplitudes in Kv3.1 KOs still showed less depression than wildtypes, this effect was less pronounced in this set of experiments and disappeared altogether when strychnine was added to the external solution (data not shown), despite strychnine being present in the first set of experiments (figure 5.10). This may reflect a smaller number of recordings in the current experiment (6 neurons without strychnine, 5 with strychnine compared to 8 previously) as a larger variability in responses was observed in this genotype and small sample sizes may cause a bias of results.

Amplitudes of EPSCs depressed to 38.92% of the initial value in CBA wildtype, 27.38% in Kv3.3 KOs and 52.97% in Kv3.1 KOs during the 1s 100Hz stimulation train, however they all recovered to their maximum value by 10s after the end of the stimulation, with much of this recovery occurring within the first second (figure 5.17). Fitting this recovery phase with a double exponential (up to 10s; Wang and Kaczmarek 1998) revealed a faster rate of recovery in Kv3.3 KOs compared to both wildtype and Kv3.1 KOs (tau_{fast} 0.16 $\pm$0.06s in Kv3.3 KO (n=5), 0.51 $\pm$0.069s in wildtype (n=6) and 0.57 $\pm$0.05 in Kv3.1 KO (n=6); One-way ANOVA, Tukey's post hoc; Kv3.3 KO vs CBA P=0.0045, Kv3.3 KO vs Kv3.1 KO P=0.0016; figure 5.18).

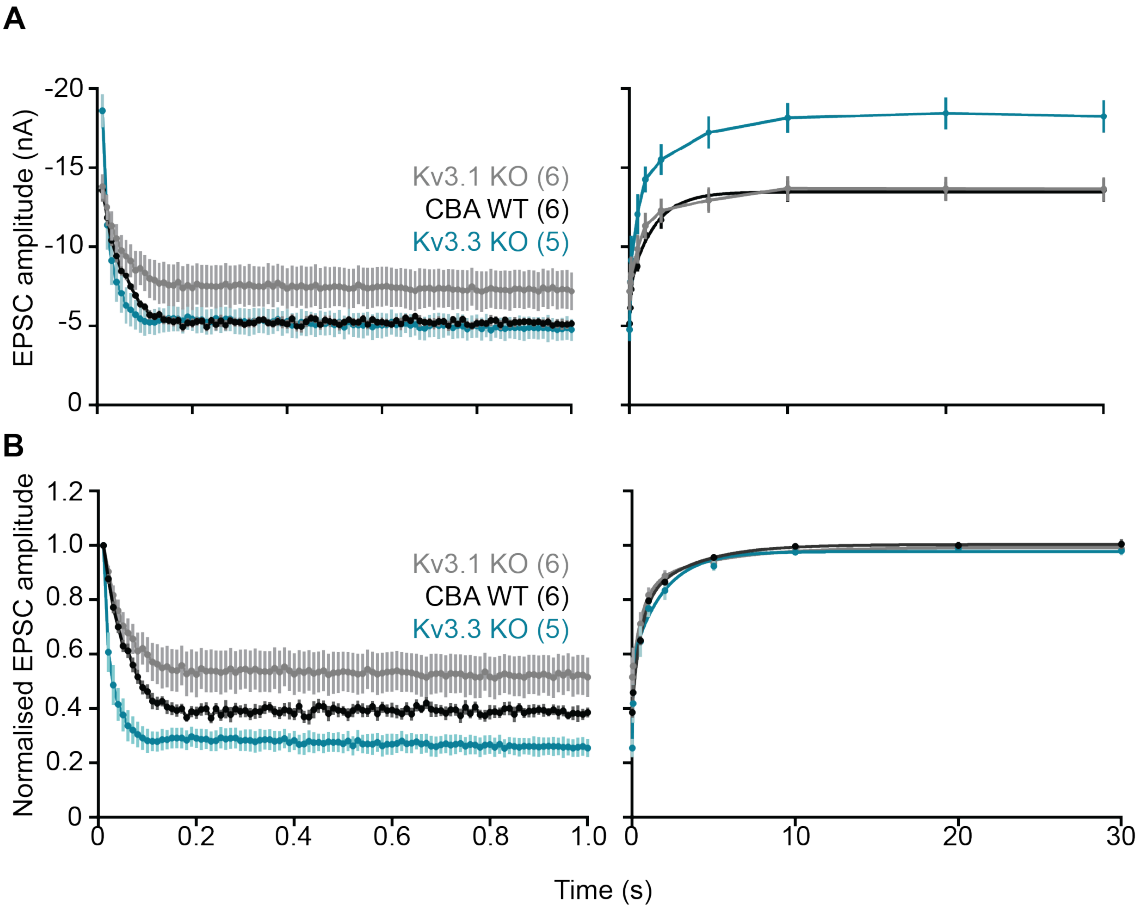

Figure 5.17: **Recovery of EPSC amplitudes after high-frequency stimulation occurs within 10s. A:** Raw EPSC amplitudes recorded in MNTB neurons during 1s stimulation and recovery pulses as described in figure 5.16 in CBA wildtype, Kv3.3 KO and Kv3.1 KO mice. All neurons were held at -40mV. n values represent number of neurons (average from 3 recordings for each neuron) **B:** EPSC amplitudes normalised to the first EPSC in the train. Complete recovery occurs by 10s in all genotypes. All variances plotted as SEM.

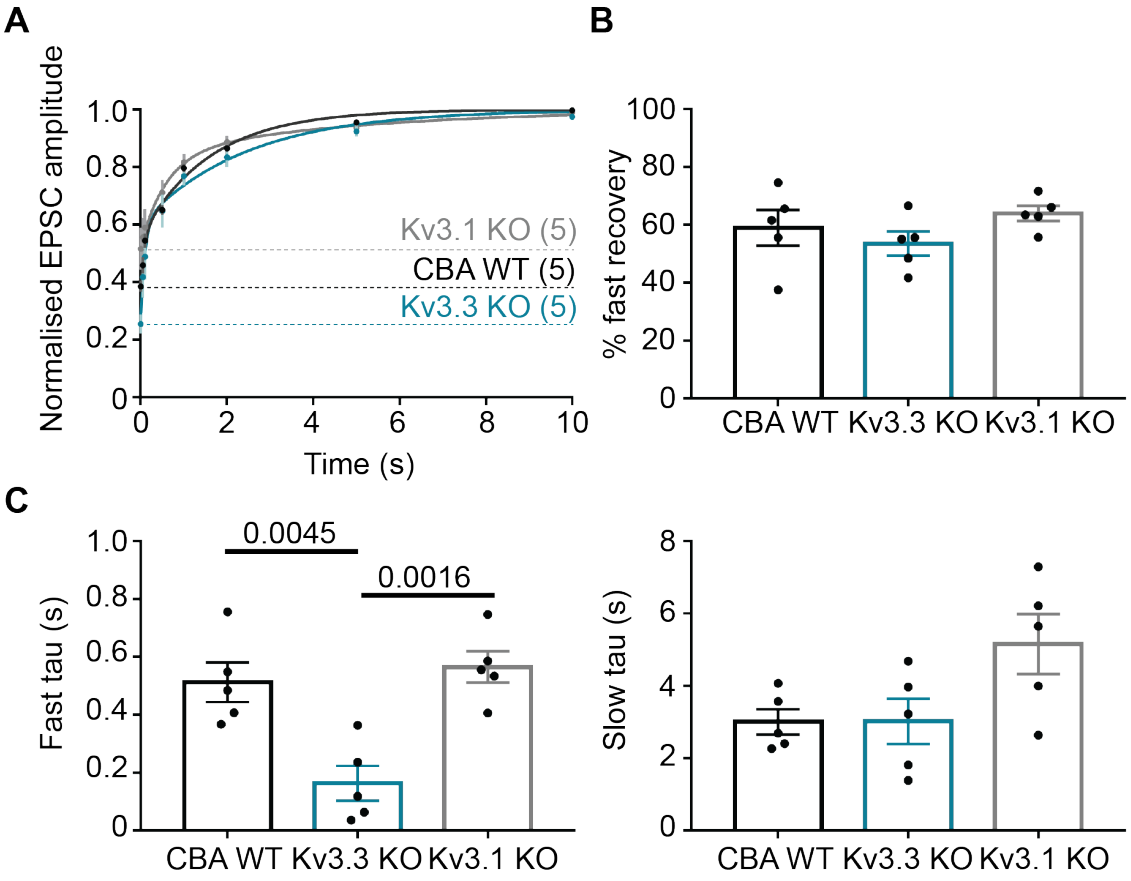

Figure 5.18: **Recovery from short term depression in EPSC amplitude occurs at a faster rate in Kv3.3 KO mice. A:** First 10s of normalised recovery of EPSC amplitudes taken from figure 5.17D. Dotted lines represent values at the end of 1s stimulation trains in CBA wildtype (black), Kv3.3 KO (blue) and Kv3.1 KO (grey), taken as initial values for recovery curves. Double exponential functions were fitted to recovery EPSCs from each neuron during the first 10s of recovery (average curves have been fitted in A for clarity) and time constants were extracted for each genotype in addition to the percent of fast recovery (C & B, respectively). **B:** Percent of fast recovery (% fast tau). There were no significant differences among groups (One-way ANOVA, $F(2,12)=1.322$, $P=0.3028$). **C:** Time constants for the fast and slow exponential components. The fast tau was significantly decreased in Kv3.3 KOs compared to wildtype and Kv3.1 KOs (one-way ANOVA, Tukey's post hoc, P values on graph.). There were no significant differences among the slow time constant (One-way ANOVA, $F(2,12)=3.864$, $P=0.0506$). All variances plotted as SEM. Data points represent individual neurons (average of 3 recordings for each neuron).

5.9 The tonotopic gradient of the MNTB does not influence transmitter release in CBA WT, Kv3.3 KOs or Kv3.1 KOs

Neurons in the MNTB exhibit a tonotopic arrangement, such that cells in the lateral portion have characteristic firing frequencies that are lower than neurons in the medial portion (Sommer, Lingenhöhl, and Friauf 1993). Kv3.1b expression has been shown to follow this tonotopic arrangement with neurons in the medial portion that have higher characteristic firing frequencies expressing more Kv3.1b (Hehn, Bhattacharjee, and Kaczmarek 2004). From this is would be sensible to assume that a similar tonotopic arrangement of Kv3.3 and Kv3.1 exists in the presynaptic terminal and thus the position of a neuron within the MNTB may affect the size of the EPSC recorded, with neurons in lateral portion (with lower Kv3 expression) possibly having larger EPSCs. This would be a potentially confounding variable, thus, to ensure that there was no bias in which neurons were recorded from in the present study, a photograph was taken after each recording and the approximate position of the neuron within the MNTB (medial, middle or lateral) was recorded (see figure 5.19).

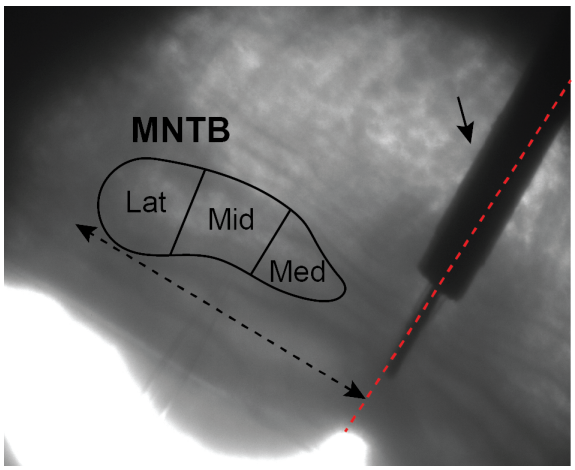

Figure 5.19: **Position of recorded neurons in the tonotopic map of the MNTB.** The MNTB was split into equal thirds with the closest to the midline (red dotted line) labelled 'medial' (med), the middle portion labelled 'middle' (mid) and the portion furthest away from the midline labelled 'lateral' (lat). The black arrow indicates the stimulation electrode.

The majority of neurons recorded in all genotypes were located within the middle portion of the MNTB (45% in wildtype, 60% in Kv3.3 KOs and 70% in Kv3.1 KOs; table 5.2). Very few neurons in the medial portion were recorded from (CBA WT n=2; Kv3.3 KO n=2; Kv3.1 KO n=0). Moreover, the position of the neuron within the tonotopic axis did not have an effect on EPSC amplitude, thus the position of neurons should not represent a confounding variable (table 5.3; one-way ANOVA; CBA, $F(2,8)=1.187$, $P=0.3537$; Kv3.3 KO, $F(2,7)=0.9778$, $P=0.4222$; Unpaired t-test, Kv3.1 KO, $t=0.7313$ $df=8$, $P=0.4855$).

Table 5.2: **Percentage of cells recorded from in each part of the MNTBs tonotopic axis**

Genotype	**% of cells**		
	Medial	**Middle**	**Lateral**
CBA WT	18	45	36
Kv3.3 KO	20	60	20
Kv3.1 KO	0	70	20

Table 5.3: **Initial EPSC amplitudes in cells recorded from the medial, middle and lateral portions of the MNTB**

Genotype	**EPSC amplitudes (nA)**		
	Medial	**Middle**	**Lateral**
CBA WT	-11.78 ± 0.923	-13.71 ± 1.307	-11.44 ± 0.779
Kv3.3 KO	-11.36 ± 2.342	-17.38 ± 2.430	-15.90 ± 1.765
Kv3.1 KO		-15.44 ± 1.438	-13.16 ± 2.060

5.10 Kv3.3 subunits appear to dominate at other auditory synapses

While the calyx of Held synapse provides a great model for studying the role of Kv3 subunits in modulating transmitter release, it is also very specialised and thus data may not always apply to other synapses in the brain. To investigate whether these roles for Kv3 subunits held true at other synapses, we also studied the effects of blocking Kv3 currents on IPSCs within the LSO in CBA, Kv3.3 KO and Kv3.1 KO mice. IPSCs in LSO neurons are generated due to release of glycine during activity within MNTB principal neurons themselves.

Glycinergic IPSCs are mediated by the movement of Cl^- ions into the neuron, thus creating an outward current (as the inside becomes more negative relative to the outside). IPSCs were recorded from LSO principal neurons by stimulating axons of MNTB principal cells (see figure 5.1). Neurons were held at -60mV and 800ms trains of 100Hz stimulation were applied to the axons. As each principal neuron has multiple synaptic inputs, the IPSCs generated are the result of release from several synaptic boutons, possibly from several neurons. For this reason it is difficult to compare absolute amplitudes between genotypes, consequently here we only compare recordings from the same neuron before and after application of 1mM TEA (for 6 minutes). IPSC amplitudes were taken from averages of 3 recordings from each neuron with a rest period of 30s between each. Due to the small size of IPSCs in these neurons and the failures that often occurred, only the first 10 IPSCs in the train have been analysed.

In comparison to the MNTB, short term depression was not observed at this synapse, most likely due to IPSC amplitudes being much smaller than EPSCs recorded at the MNTB (pA rather than nA) and release probability being much lower (paired pulse facilitation was often seen at this synapse; figure 5.20). Despite this, 1mM TEA still increased initial IPSC amplitudes in CBA wildtype and Kv3.1 KO mice, although the extent to which it increased amplitudes was more variable in Kv3.1 KOs. In contrast, initial amplitudes appeared to decrease in the presence

of TEA in Kv3.3 KOs, however due to low n numbers it was not possible to conduct any statistical tests to confirm that this effect was real (figure 5.20).

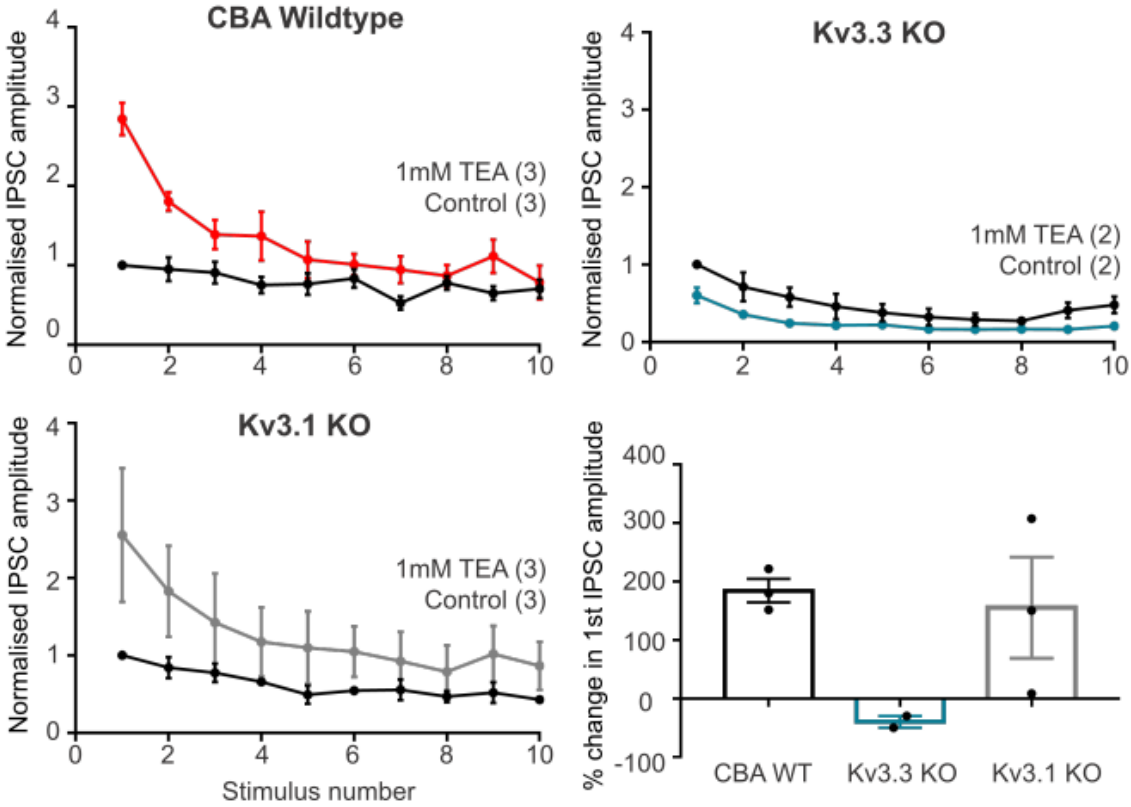

Figure 5.20: **1mM TEA does not affect IPSC amplitudes in Kv3.3 KO mice.** IPSCs recorded from LSO principal neurons during 100Hz stimulation of MNTB axons in CBA wildtype, Kv3.3 KO and Kv3.1 KO mice before and after application of 1mM TEA (6 minutes perfusion). IPSC amplitudes were normalised to the initial amplitude before TEA perfusion. The first 10 responses are plotted. n numbers are indicated in brackets and refers to number of neurons, however these are only from single animals from each genotype. (Bottom right:) Percent change in initial IPSC amplitude after application of 1mM TEA. Variance plotted as SEM.

5.11 Discussion

As discussed in the previous chapter, the ability of Kv3 currents to modulate the presynaptic action potential waveform gives them the potential to modify synaptic transmission by controlling calcium influx into the terminal and thus calcium-dependent vesicle release. This is particularly important at the calyx of Held synapse in order to sustain transmitter release upon high frequency stimulation.

Evidence from the previous chapter suggested that Kv3.3 subunits had a larger influence on action potential duration at the calyx terminal and consequently one may expect that these subunits would also have larger influence on transmission. Here we show that these subunits are required to prevent excess transmitter release upon a given stimulus, thereby preventing depletion of vesicle pools at this synapse and allowing high frequency transmission.

5.11.1 EPSCs in adult MNTB neurons are incredibly rapid

EPSCs generated in MNTB neurons have rapid kinetics in order to limit the output of the neuron to a single AP and allow receptors to recover sufficiently between each stimulus during high frequency stimulation (Taschenberger and Von Gersdorff 2000; Futai et al. 2001). These decay kinetics accelerate with age (Taschenberger and Von Gersdorff 2000) and reach a plateau at around two weeks old in mice, due to a decrease in NMDA receptor expression (Futai et al. 2001), an increase in GluA4 AMPA receptor subunit expression (Caicedo and Eybalin 1999; Pilati et al. 2016) and an decrease in the presynaptic action potential duration (Taschenberger and Von Gersdorff 2000).

In accordance with this previous research, EPSCs recorded from MNTB neurons in the present study had very rapid kinetics. However, EPSC decay times in the current study were slightly faster than those previously reported for adult mice at 0.2 $\pm$0.02ms compared to 0.4ms in P27 animals (Futai et al. 2001). This discrepancy is likely to reflect the difference in the temperature at which recordings were conducted (35^{o}C in the present study compared with room temp), as accelerated AMPA de-

cay kinetics are associated with higher recording temperatures (Postlethwaite et al. 2007).

Despite no significant changes to EPSC decay times in either knockout, both displayed tendencies towards slower decay rates. While these changes may not have a great impact at low frequencies, during high frequency stimulation this resulted in an inability of the initial EPSC to decay back to baseline before the next stimulus in Kv3.3 KO neurons, highlighting a role for these subunits in maintaining accurate timing of transmission by limiting the period over which vesicles are released.

5.11.2 Kv3.3 subunits are required to sustain high frequency transmission at the calyx of Held

Larger EPSCs recorded from Kv3.3 KO mice indicates that these subunits are required for limiting the presynaptic action potential and thus transmitter release, consistent with evidence from the previous chapter that this subunit dominates in the terminal. Furthermore, the reduced effect of TEA on EPSC amplitude in these mice provides further evidence that Kv3.3 is mediating the presynaptic Kv3 current. The fact that small increases in EPSC amplitude were seen in Kv3.3 KOs in the presence of TEA indicates that some Kv3 current is still present in these animals and is likely mediated by Kv3.1 containing channels. The lack of change to EPSC amplitudes seen with IbTx suggests that BK currents contribute very little to modulation of transmitter release during a single stimulus, consistent with slower kinetics of this current preventing contribution of BK to action potential repolarisation (Ishikawa et al. 2003).

Kv3 currents have previously been shown to modulate transmitter release by simultaneous recordings from the calyx of Held and MNTB principal neurons during perfusion of TEA (Ishikawa et al. 2003), however, the present work provides the first evidence of Kv3.3 subunits, in particular, mediating this presynaptic Kv3 current. This is consistent with evidence from the neuromuscular junction, at which Kv3.3 and Kv3.4 subunits appear to be important for modulation of neurotransmission (Brooke et al. 2004).

The importance of Kv3.3 subunits in limiting transmitter release is highlighted during high frequency stimulation, where a larger initial release in animals lacking Kv3.3 subunits results in a larger, faster depression of subsequent responses. While this was more pronounced at 200 and 600Hz, surprisingly, it was still observed at 100Hz, despite previous work showing that action potential firing isn't compromised at this frequency when Kv3 currents are absent (Macica et al. 2003).

A number of mechanisms for short term depression at this synapse have been proposed. AMPA receptor desensitisation has been observed in young animals (Wong et al. 2003) using non-stationary fluctuation analysis (Neher and Sakaba 2001), although this appears to be less important in more mature mice (Wang and Kaczmarek 1998). A more accepted hypothesis is that this depression is due to presynaptic mechanisms, namely the depletion of releasable vesicle pools (Wang and Kaczmarek 1998), although there is still debate about what constitutes a readily releasable vesicle pool and definitions regarding different pools that exist at this synapse (Von Gersdorff and Borst 2002; Neher 2017). It is likely that this is the mechanism for faster, larger short term depression seen in Kv3.3 KO mice as the initial larger release of vesicles is likely to leave fewer vesicles primed for release on subsequent stimuli. Thus, despite the build up of calcium that is likely to occur in the terminal of these animals, due to longer action potentials, and the associated increase in release probability, the amount of vesicles that can be released upon high frequency stimuli remains low. Interestingly, the asynchronous release observed during high-frequency 600Hz stimulation in these animals may be a by-product of a build up of calcium in the terminal, resulting in the recruitment of vesicles from the 'slow-releasing pool' (Sakaba 2006; Neher 2017). This asynchronous release is likely to result in both failure of the EPSCs to depolarise the MNTB neuron sufficiently to generate an action potential and disruption to the timing of action potentials generated. Both of these would exacerbate timing errors in the encoding of auditory stimuli.

This raised intracellular calcium in the terminal is also associated with an increase in the rate of vesicle replenishment following high frequency stimuli, similar to effects previously seen with TEA (Wang and Kaczmarek 1998).

This evidence points towards a requirement of Kv3.3 subunits to limit action potential duration and thus limit transmitter release, in order to maintain an adequate pool of readily releasable or 'primed' vesicles during high frequency stimulation. Additionally, shorter presynaptic action potentials in the presence of Kv3.3 subunits reduces intracellular calcium, ensuring synchronous vesicle release occurs at high frequencies and preventing Ca^{2+}-induced excitotoxicity.

5.11.3 The mystery of resistance to synaptic depression in Kv3.1 KO animals

While the role of Kv3.3 subunits in modulating transmitter release appears clear, the ability of Kv3.1 KO animals to sustain such a large increase in neurotransmitter during high frequency stimulation is rather more puzzling. Not only do these animals show a resistance to synaptic depression but it also appears that the total number of vesicles released during 100Hz stimulation is larger than both wildtype and Kv3.3 KO animals (shown by the increased charge; figure 5.12). A number of factors may contribute to this ability to release more vesicles; one, an increased pool of readily releasable vesicles; two, an increased action potential duration as seen with Kv3.3 KOs; three, an enhanced rate of vesicle recycling or four, changes to the release probability or postsynaptic AMPA receptor expression or sensitivity.

Changes in presynaptic AP duration seems to be an unlikely explanation here as initial EPSC amplitudes are similar to wildtype animals and as seen with Kv3.3 KO animals and previously with TEA (Ishikawa et al. 2003; Wang and Kaczmarek 1998), this would likely result in a more pronounced depression rather than less. Additionally, TEA appeared to increase EPSC amplitudes in these animals to a similar degree as wildtypes. Equally, there does not appear to be a change to the readily releasable pool of vesicles as calculated with cumulative charge (Moulder and Mennerick 2005; Stevens and Williams 2007; Schneggenburger, Meyer, and Neher 1999), suggesting wildtype, Kv3.3 KO and Kv3.1 KO terminals start with the same number of vesicles. Nor does there appear to be a change in release probability or postsynaptic AMPA receptor sensitivity, shown by no change in mEPSC frequency

or amplitude, respectively. In contrast there was a reduction of quantal amplitude observed in Kv3.3 KOs, suggesting a decrease in AMPA receptor expression on the postsynaptic membrane of these mice. This is likely a compensatory mechanism in order to counteract the increase in transmitter release, but may also contribute to enhanced depression seen during high frequency stimulation in these animals. Lastly, there appears to be no differences in the rate of vesicle recycling in these animals compared to wildtype, shown by similar rates of EPSC recovery following 100Hz stimulation (figure 5.18).

So how are these synapses able to continuously release so much transmitter? It is possible that in wildtype neurons Kv3.3 subunits and Kv3.1 subunits form heteromers which are resistant to inactivation whereas in Kv3.1 KOs, Kv3.3 homomeric channels form which inactivate due to the presence of an N-terminal inactivation peptide. This would result in a progressive increase in action potential duration during the train which may cause a larger vesicle release during later stimuli. Estimates of RRP at the calyx are very variable between studies thus the back-extrapolation of cumulative charge method used here may not accurately define the vesicle pools such that an increase in Kv3.1 KOs was missed. Further investigation is required to dissect the mechanisms by which these animals are able to sustain enhanced release but this suggests that Kv3.3 subunits alone are sufficient and Kv3.1 subunits somehow contribute to limiting the amount of transmitter released during repetitive stimulation.

5.12 Importance of Kv3.3 subunits appears to hold true at other auditory synapses

Although the calyx of Held synapse is a great model for studying transmission, it is also highly specialised and unique from other synapses within the brain. This could make generalising results discovered at this synapse rather difficult, however investigation of IPSCs at the MNTB-LSO synapse also reveal decreased block by TEA of presynaptic Kv3 channels in Kv3.3 KO animals and no change in IPSC amplitude, in comparison to significant block in both wildtype and Kv3.1 KO, resulting

in increased IPSC amplitude in these mice. This again suggests that Kv3.3 subunits are important in generating presynaptic Kv3 conductances at other synapses within the brain.

This is an interesting finding as it shows that these subunits have a role in modulating both excitatory and inhibitory transmission. Kv3.1b subunits are restricted to the neuropil in the LSO which consists of synaptic boutons and axonal compartments (chapter 3), suggesting they would have an important role at these synapses, thus it is surprising to observe that synapses in these knockouts behave similar to wildtype. It is possible however that Kv3.1b expression is limited to excitatory synapses within the LSO and thus their function was missed in this present study.

5.13 Consequences on auditory function

As mentioned earlier, Kv3.3 subunits are clearly important in restricting initial transmitter release, thereby allowing the synapse to retain enough 'primed' vesicles for release on subsequent stimuli. This is important in order to generate EPSCs of sufficient magnitude to depolarise the membrane to AP threshold. In addition it appears Kv3.3 subunits are required to maintain synchronous release and thus synchronous AP firing in postsynaptic neurons.

To investigate whether this has any consequences on auditory function in these mice, auditory brainstem responses were measured in collaboration with Sherylanne Newton, in which animals were anaesthetised and subdermal electrodes placed behind the ears and in the centre of the head. Sounds of varying frequencies and intensities were introduced to the animal and activity in the form of compound action potentials was measured. This generated a waveform with a number of peaks (generally 5) that correspond to activity of neurons at different levels of the auditory pathway. Wave I is generally thought to be depolarisation of spiral ganglion neurons, wave II, the cochlea nucleus, wave III and IV, the contralateral MNTB (and possibly SBCs Jalabi et al. 2013; Newton 2017) and superior olivary complex (including MSO and LSO, with a possible contribution from the IC; Land, Burghard, and Kral 2016), respectively. Larger, narrower peaks are associated with highly synchronous

AP firing in a large number of neurons.

Kv3.3 KO animals displayed a decreased wave IV amplitude at high frequencies (24kHz) but not at low frequencies (12kHz) and this wave IV became superimposed on wave III such that it appeared to be a continuous wave with a slight dip in the middle (although this apparent shift in latency of wave IV was not significantly different from WT; figure 5.21). This is consistent with decreased or asynchronous AP firing of neurons in the SOC (MSO, LSO, SPN & IC) and may be caused by a number of factors. Given the results detailed in this chapter of Kv3.3 subunits maintaining sufficient, synchronous transmitter release, and the presence of these subunits in many auditory synapses, it is likely transmitter release within other synapses of the CN and SOC are also affected in Kv3.3 KOs. This may reduce excitatory drive to the SOC and coupled with mistimed inhibition from the MNTB (resulting from mistiming of APs or even AP failures in MNTB neurons due to smaller and irregular EPSCs) and an inability of all of the Kv3.3-containing neurons in this system to follow high frequency stimuli (chapter 3), would lead to fewer output neurons associated with wave IV firing APs in a synchronised manner.

This is likely to have an impact on sound localisation as disruption to AP timing would affect signal integration in both the MSO and LSO, leading to errors in ITD and ILD processing. Indeed, human patients with a mutation in Kv3.3 that renders channels non-functional, display increased thresholds for processing both interaural timing and intensity differences (Middlebrooks et al. 2013).

In contrast to these Kv3.3 KO animals, Kv3.1 KOs display decreased amplitudes at both wave I and wave IV, suggesting an overall decrease in signal reaching the brain, although results among animals in this genotype were much more variable (Newton 2017; figure 5.21).

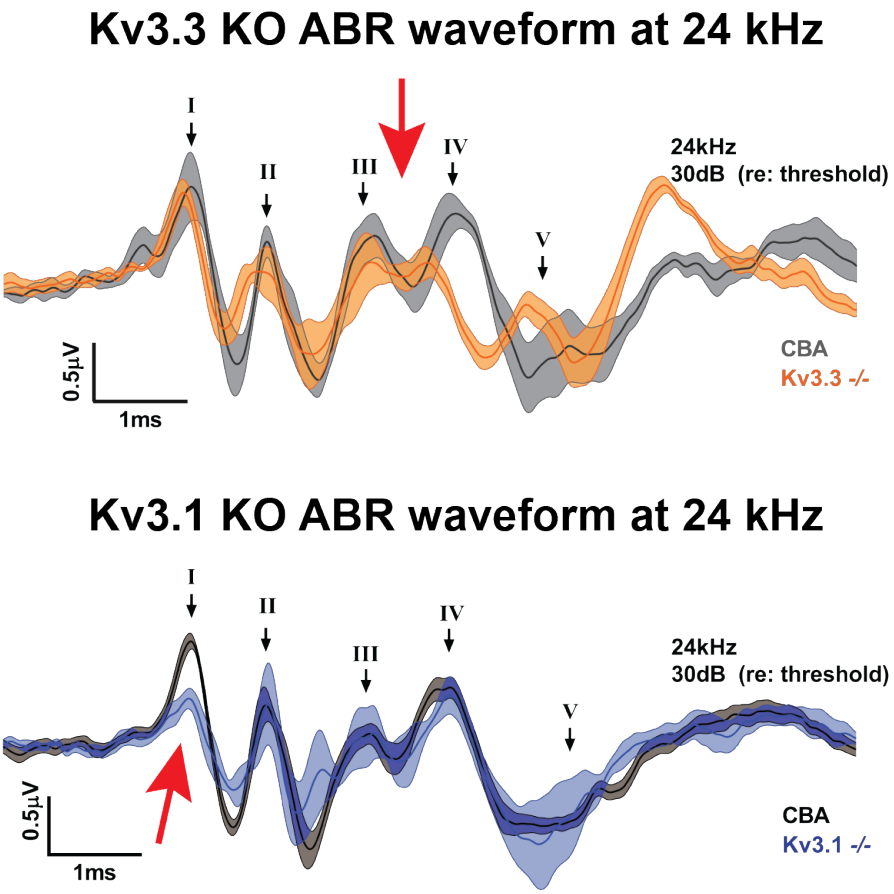

Figure 5.21: **Kv3.3 KO display decreased wave IV amplitude in auditory brainstem response recordings (ABRs) at 24kHz.** (Top) ABR waveforms from CBA wildtype (black) and Kv3.3 KO mice (orange). Red arrow indicates shift of wave IV into wave III in addition to decreased wave IV amplitude. (Bottom) ABR waveforms from CBA wildtype (black) and Kv3.1 KO mice (blue). Red arrow indicates decreased wave I. Adapted from Newton 2017.

5.14 Summary

- Initial EPSC amplitudes are larger in Kv3.3 KO mice compared to wildtype and Kv3.1 KOs.
- Additional blockade of Kv3 channels has little effect on EPSC amplitudes of Kv3.3 KO mice.
- Kv3.3 KOs exhibit faster and larger synaptic depression upon high frequency stimulation
- Kv3.1 KOs show a resistance to short term depression upon high frequency stimulation.
- These effects on synaptic transmission were observed even at lower frequencies (100Hz).
- These changes are purely AP related as no changes were observed in quantal parameters in Kv3.1 KOs and only a decreased quantal amplitude was observed in Kv3.3 KOs.
- Kv3.3 KOs show increased calcium-dependent rate of recovery following high frequency stimulation.
- The impact of Kv3 does not appear to depend on the tonotopic gradient present within the MNTB.
- Auditory function is impaired at high frequencies in Kv3.3 KO mice.

Chapter 6

Kv3.3 and spinocerebellar ataxia type 13 (SCA13)

The last three chapters have hopefully provided evidence that Kv3.3 subunits are just as important as Kv3.1 for the formation and function of Kv3 channels, despite Kv3.1b subunits dominating the focus of previous literature. Emerging evidence of their importance has also come from the discovery of spinocerebellar ataxia type 13 (SCA13), a disease resulting from mutations in the gene encoding Kv3.3 subunits (Waters et al. 2006; Zhang and Kaczmarek 2016). The disease is characterised by cerebellar ataxia as a result of neurodegeneration in the cerebellum.

A number of different mutations (figure 6.1) in the gene are known to cause the disease, some are associated with early onset and others adult onset of symptoms (Waters et al. 2006; Duarri et al. 2015; Minassian, Lin, and Papazian 2012). One particular mutation, R420H, in the voltage sensing domain of the channel has been associated with adult onset ataxia and impaired sound localisation in human patients. Cell lines expressing mutant subunits have no Kv3 current or vastly reduced currents when mutant subunits are co-expressed with wildtype ones (Waters et al. 2006).

In order to investigate the mechanisms by which this mutation can result in impairment of auditory processing, a mouse model harbouring the arginine (R) to histidine (H) mutation was created in the lab by Michelle Anderson, using CRISPR/Cas9 gene editing. This chapter will detail how this mutation affects Kv3 currents

and function in native tissue within neurons of the LSO and MNTB within the sound localisation pathway. As the mutation results in an adult onset of disease symptoms, Kv3 channel function was analysed in two age groups, young (P21-P25) and old (6 months) to determine if changes occur before onset of the disease or get progressively worse with onset of symptoms. Mice homozygous for the mutation will hereafter be referred to as Kv3.3^{R420H}. Unless otherwise stated, all variance is plotted as SEM.

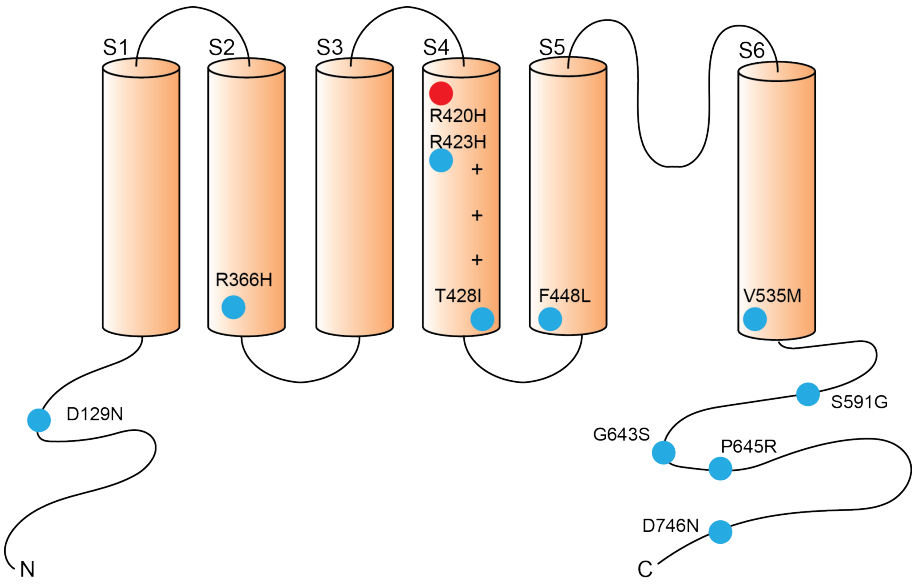

Figure 6.1: **Mutations in the Kv3.3 subunit identified in Spinocerebellar ataxia type 13.** Blue circles show the location of identified mutations within the Kv3.3 subunit. Red circle shows the location of the R420H mutation discussed in this chapter in the voltage sensing domain. Adapted from Zhang and Kaczmarek 2016.

6.1 Potassium currents in MNTB and LSO neurons expressing Kv3.3^{R420H} are similar to those in the Kv3.3 KO

Potassium currents were measured in MNTB and LSO principal neurons from CBA wildtype, Kv3.3 KO and Kv3.3^{R420H} mice aged P21-P25. We observed in the first chapter that neurons of the MNTB express both Kv3.1 and Kv3.3 subunits and had similar current amplitudes in both Kv3.3 and Kv3.1 KOs, suggesting one subunit can compensate for the other, meanwhile in LSO neurons, only Kv3.3 subunits were expressed and current amplitudes in these neurons were dramatically reduced in Kv3.3 KOs.

Currents were compared to both wildtype and Kv3.3 knockouts as Kv3 currents are abolished in cell lines expressing these R420H mutant subunits, thus it is possible that currents in native neurons of Kv3.3^{R420H} mice would also lack a Kv3.3 current and be similar to Kv3.3 KOs. Neurons were held at -60mV, from which a 200ms step to -90mV, a 20ms step to -40mV and 200ms test steps from +40mV to -110mV in 10mV increments were given (refer to figure 3.3). Currents were measured towards the end of the step and plotted in I-V graphs.

Potassium currents in MNTB neurons of Kv3.3^{R420H} mice were similar to both wildtype and Kv3.3 KOs with current amplitudes at +10mV of 9.7 ±1.07nA (n=5) in CBA wildtype, 8.7 ±0.68nA (n=7) in Kv3.3 KOs and 7.8 ±0.45nA (n=12) in Kv3.3^{R420H} (figure 6.2). There were no significant differences between current amplitudes in any of the genotypes (one-way ANOVA, $F(2,21)=2.005$, $P=0.1597$).

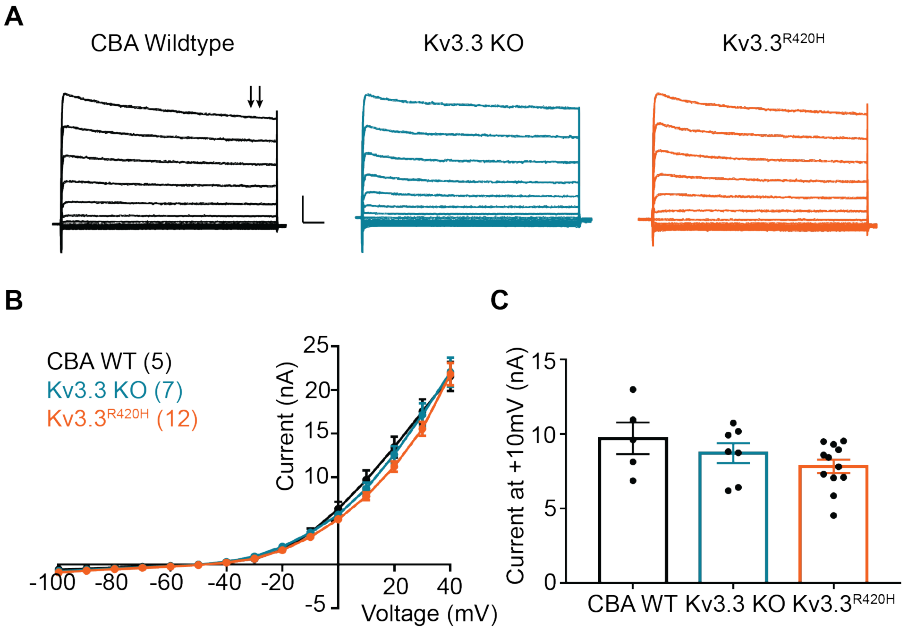

Figure 6.2: **Potassium currents are unchanged in MNTB neurons expressing Kv3.3^{R420H} subunits. A:** Example current traces from single MNTB neurons in wildtype, Kv3.3 KO and Kv3.3^{R420H} mice (P21-25). Neurons were held at -60mV and currents resulting from the following voltage protocol were measured; -90mV for 200ms, -40mV prestep for 20ms, 200ms test pulses from +40mV to -110mV in 10mV increments, followed a a final step to -60mV. Only currents from the test step are shown. Scale bar = 5nA and 20ms. Current amplitudes were measured at the end of the step, (an average was taken over 5ms; black arrows) and plotted into an I-V graph (**B**). N numbers are in brackets and represent number of cells recorded from. **C:** Current amplitudes at +10mV taken from cells in B. There were no significant differences between groups (one-way ANOVA, F(2,21)=2.005), P=0.1597). Variance plotted as SEM.

In contrast to neurons of the MNTB, outward currents measured from LSO neurons were dramatically reduced in comparison to wildtype but similar in amplitude to Kv3.3 KOs (at +10mV, one-way ANOVA, Tukey's post hoc, CBA wildtype vs Kv3.3^{R420H} P= <0.0001). At +10mV amplitudes were 13.7 ±1.15nA (n=11) in wildtype, 5.5 ±0.52nA (n=6) in Kv3.3 KOs and 6.5 ±0.42nA (n=8) in Kv3.3^{R420H} mice (figure 6.3). Current amplitudes were reduced at voltages positive to -20mV, consistent with a reduction in high-voltage activated Kv3 current (which only activates at ∼ -20mV; figure 6.3B).

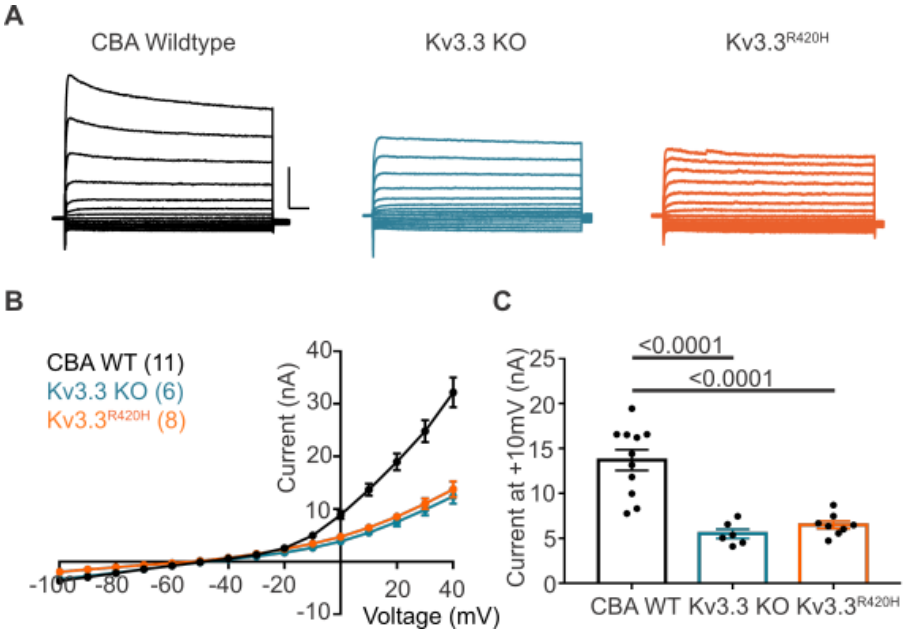

Figure 6.3: **Potassium currents are dramatically reduced in LSO neurons expressing Kv3.3^{R420H} subunits. A:** Example current traces from single LSO neurons in wildtype, Kv3.3 KO and Kv3.3^{R420H} mice (P21-25). Neurons were held at -60mV and currents resulting from the following voltage protocol were measured; -90mV for 200ms, -40mV prestep for 20ms, 200ms test pulses from +40mV to -110mV in 10mV increments, followed a a final step to -60mV. Only currents from the test step are shown. Scale bar = 5nA and 20ms. Current amplitudes were measured at the end of the step and plotted into a current- voltage graph (**B**). N numbers are in brackets and represent number of cells recorded from. **C:** Current amplitudes at +10mV taken from cells in B. Amplitudes in Kv3.3 KO and Kv3.3^{R420H} were significantly reduced compared to wildtype (one-way ANOVA, Tukey's post hoc, P values on graph). Variance plotted as SEM.

6.2 Action potential duration is increased in MNTB and LSO neurons of Kv3.3^{R420H} mice

Data from the previous section suggested that Kv3.3 specific currents are reduced in Kv3.3^{R420H} mice, such that neurons in these animals behave similarly to those in Kv3.3 KO mice. Despite no change in potassium current amplitudes in the MNTB of Kv3.3 KO mice, an increase in AP half-width was still observed (figure 3.12). Since potassium currents in Kv3.3^{R420H} mice appear to behave very similarly to Kv3.3 KOs, one may expect a broadening of the AP in these animals to occur.

To investigate action potential waveform in these mutant mice, currents were injected into the soma of MNTB and LSO neurons in 50pA, 200ms steps via a patch pipette and the resultant changes in voltage were measured. Neurons were held at -60mV and only the first AP to be generated in each neuron was analysed.

Similar to Kv3.3 KOs, AP half-width was significantly increased in MNTB neurons of Kv3.3^{R420H} mice compared to CBA wildtype (one-way ANOVA, Tukey's post hoc, P=0.0126; figure 6.4). AP half-width values were 0.2 ±0.02ms (n=4) in CBA wildtype, 0.4 ±0.04ms (n=7) in Kv3.3 KOs and 0.4 ±0.03ms (n=9) in Kv3.3^{R420H} mice. Whilst there was a significant increase in AP rise time of $\sim$ 0.05ms in these animals compared to wildtype (one-way ANOVA, Tukey's post hoc, P=0.0305; figure 6.4C), much of the change in action potential duration was due to an increased time for the AP to repolarise (figure 6.4D; one-way ANOVA, Tukey's post hoc, CBA wildtype vs Kv3.3^{R420H} P=0.0042). The time taken for the action potential to repolarise was significantly longer, from 0.15 ±0.02ms (n=4) in wildtype to 0.31 ±0.05ms (n=7) in Kv3.3 KOs and 0.37 ±0.03ms (n=9) in Kv3.3^{R420H} mice. Additionally, the after-hyperpolarisation appeared to be reduced in amplitude in these animals, similar to the effect seen with TEA on the presynaptic AP in chapter 4 (figure 6.4A).

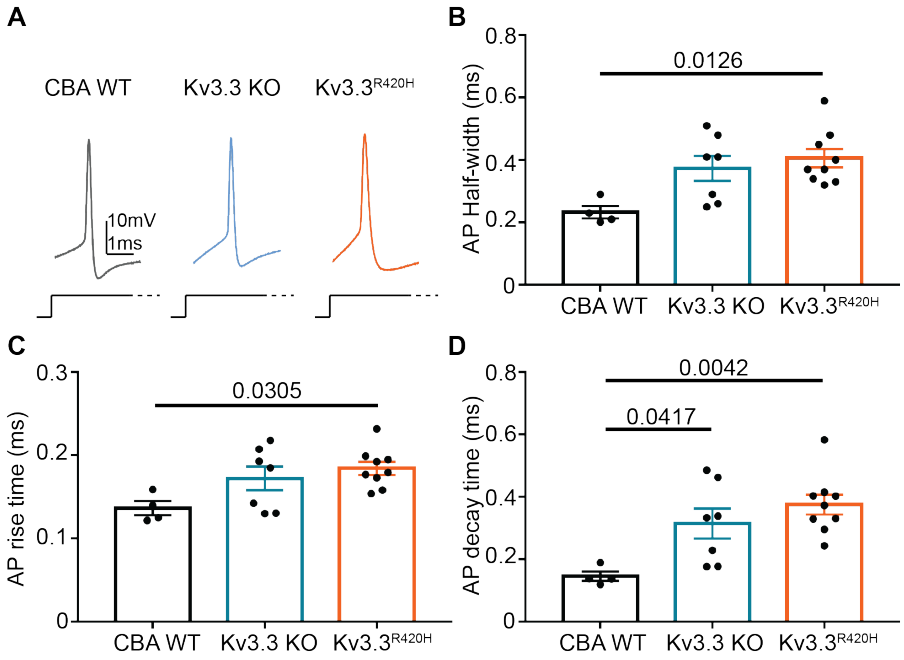

Figure 6.4: **Action potentials are significantly longer in MNTB neurons of Kv3.3^{R420H} mice. A:** Example action potential traces recorded from single MNTB neurons in CBA wildtype, Kv3.3 KO and Kv3.3^{R420H} mice in response to current injection steps. Neurons were held at -60mV. **B:** Action potential half-width measured as shown in figure 4.3. AP half-width is significantly increased in Kv3.3^{R420H} mice (one-way ANOVA, Tukey's post hoc, P=0.0126). **C:** Time taken for action potential to rise from 10-90% of the peak amplitude. Rise time is significantly increased in Kv3.3^{R420H} mice (one-way ANOVA, Tukey's post hoc, P=0.0305). **D:** Time taken for action potential to decay back to 10% of its peak amplitude. Decay time is significantly increased in both Kv3.3 KO and Kv3.3^{R420H} mice (one way ANOVA, Tukey's post hoc, P values on graph). Data points represent recordings from single neurons. Variance plotted as SEM.

Similar to neurons of the MNTB, AP duration is significantly increased in neurons of the LSO in Kv3.3^{R420H} mice compared to wildtype (AP half-width, one-way ANOVA, Tukey's post hoc, P=0.0017; figure 6.5B). The increase in AP duration was much larger in the LSO with half-width values increased from 0.2 ±0.01ms (n=7) in wildtype animals to 0.4 ±0.06ms (n=6) in Kv3.3 KOs and 0.6 ±0.11ms (n=7) in Kv3.3^{R420H} mice (figure 6.5B). This was primarily due to an increase in the time taken for the AP to repolarise (figure 6.5D; AP decay time; one-way ANOVA, tukey's post hoc, CBA wildtype vs Kv3.3^{R420H} P=0.0033). It is worth noting, both half-width and decay times were very variable in Kv3.3^{R420H} mice with some cells showing severe increases and others barely affected. There were no differences in rise time of the action potential in the LSO (one-way ANOVA, F(2,17)= 3.468, P=0.0545; figure 6.5C).

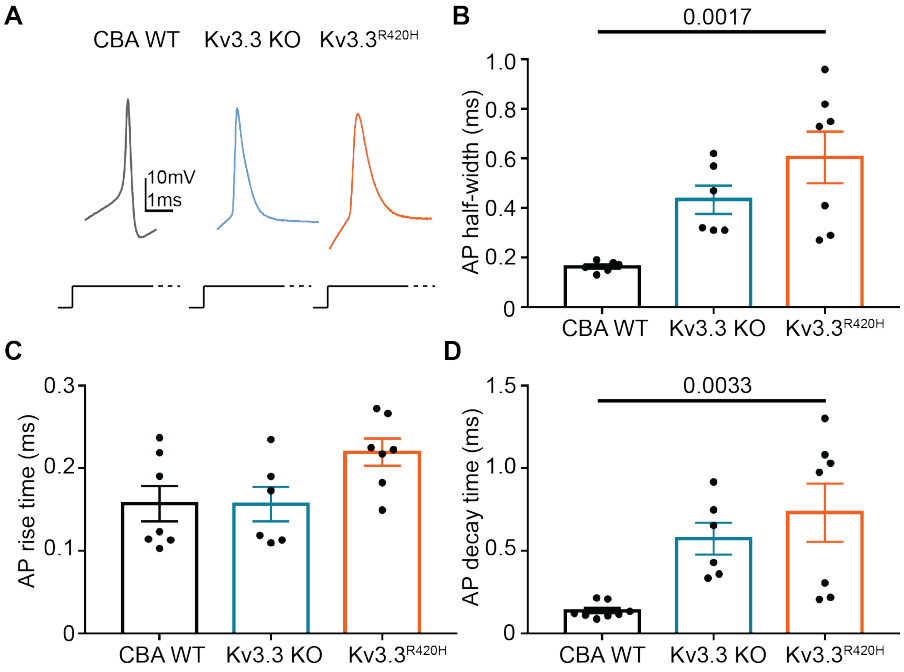

Figure 6.5: **Action potential duration is significantly increased in LSO neurons of Kv3.3^{R420H} mice. A:** Example action potential traces recorded from single LSO neurons in CBA wildtype, Kv3.3 KO and Kv3.3^{R420H} mice in response to current injection steps. Neurons were held at -60mV. **B:** Action potential half-width measured as shown in figure 4.3. AP half-width is significantly increased in Kv3.3^{R420H} mice (one-way ANOVA, Tukey's post hoc, P=0.0017). **C:** Time taken for action potential to rise from 10-90% of the peak amplitude. No significant differences were observed (one-way ANOVA, F(2,17)= 3.468, P=0.0545). **D:** Time taken for action potential to decay back to 10% of its peak amplitude. Decay time is significantly increased in Kv3.3^{R420H} mice (one way ANOVA, Tukey's post hoc, P values on graph). Data points represent recordings from single neurons. Variance plotted as SEM.

6.3 EPSCs at the calyx-MNTB synapse of Kv3.3^{R420H} mice are large and resistant to short term depression

The last section has shown that Kv3 currents in Kv3.3^{R420H} mice are similar to those in Kv3.3 KOs, that is, there appears to be a lack of a Kv3.3 specific current. Since patients with this mutation have impaired sound localisation (Middlebrooks et al. 2013) we wished to examine synaptic transmission at the calyx of Held- MNTB synapse in these animals. This synapse is central to both pathways involved in sound localisation and as raised thresholds were observed for processing of both interaural level and timing differences, it suggests an issue may exist here. As neurons expressing this mutant Kv3.3 subunit appear to behave similar to Kv3.3 KOs, one may postulate that synaptic responses will show pronounced depression during high frequency stimulation trains, as seen in Kv3.3 KOs in the previous chapter.

EPSCs were recorded from MNTB neurons of Kv3.3^{R420H} mice in response to 100Hz stimulation as detailed in the previous chapter (figure 5.17). Data from CBA wildtypes and Kv3.3 KOs in the previous chapter (figure 5.17) is reproduced here in order to compare with the Kv3.3^{R420H} mice. Recordings were performed in the same time-frame (with the absence of strychnine) so control recordings should still be applicable. Neurons were held at -40mV in order to inactivate sodium channels and prevent action potential firing in the postsynaptic MNTB neurons.

EPSC amplitudes recorded from MNTB neurons were significantly increased in Kv3.3^{R420H} mice compared to both wildtype and Kv3.3 KOs at -24 ±1.62nA (n=4)), -14 ±0.68nA (n=6) and -19 ±1.02nA (n=5), respectively (one-way ANOVA, Tukey's post hoc, Kv3.3^{R420H} vs CBA wildtype P=<0.0001; Kv3.3^{R420H} vs Kv3.3 KO P=0.0230; figure 6.6).

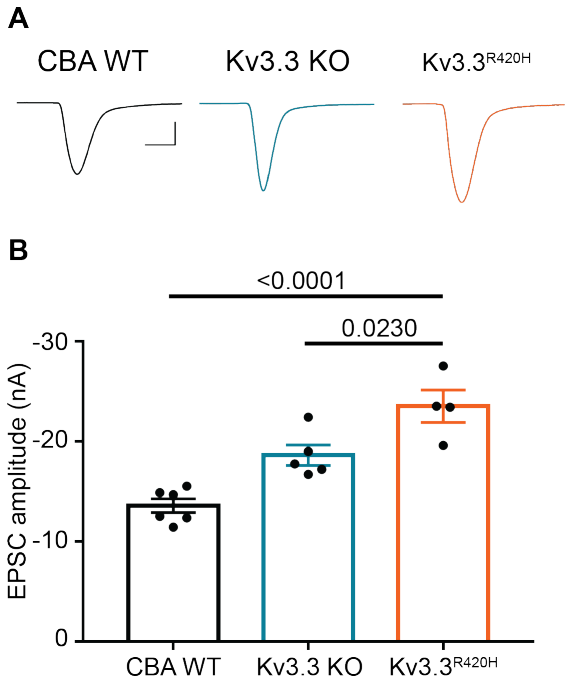

Figure 6.6: **EPSC amplitudes are significantly larger in MNTB neurons of Kv3.3^{R420H} mice. A:** Example EPSC traces from single MNTB neurons in CBA wildtype, Kv3.3 KO and Kv3.3^{R420H}, generated in response to stimulation of calyx of Held fibres. Holding potential = -40mV. Scale bar =5nA, 0.5ms. **B:** Quantification of EPSC amplitudes. Amplitudes were significantly increased in Kv3.3^{R420H} mice compared to both wildtype and Kv3.3 KOs (one-way ANOVA, Tukey's post hoc, P values on graph). Data points represent single neurons. Each point is from an average of 5 recordings from the same neuron. Variance plotted as SEM.

Although EPSC amplitudes in these Kv3.3^{R420H} mice are increased similar to those in Kv3.3 KOs, EPSCs show very little short term depression during 100Hz stimulation (figure 6.7). In fact, such little depression was observed that EPSC amplitudes during the 'plateau' phase were almost twice that of CBA wildtypes at $\sim$ -12nA compared to $\sim$ -5nA (figure 6.7B), much like the effect seen in Kv3.1 KOs. As in the previous chapter, EPSC amplitudes were normalised to that of the initial response and single exponential function fitted to the data points in order to assess the rate and extent of short term depression (this was done for each recording separately however for demonstration purposes a single exponential function has been fitted to average data points in figure 6.7C). As can be observed in both the raw and normalised amplitudes, amplitudes of the 'plateau' phase are significantly increased in Kv3.3^{R420H} mice, reaching around 0.5 $\pm$0.05 of the initial EPSC amplitude compared to Kv3.3 KOs which depress to around 0.3 $\pm$0.04 of their initial amplitude (one-way ANOVA, Tukey's post hoc, Kv3.3^{R420H} vs Kv3.3

KO P=0.0030). They are not significantly different from wildtype, probably owing to the low number of recordings. Despite the extent of depression being reduced, the rate at which it occurs (measured from an exponential fit to EPSC amplitudes) is similar to that in Kv3.3 KOs, and significantly increased compared to wildtype with a decay rate of EPSC amplitudes at 24.01 ±2.3ms compared to 42.4 ±2.71ms in wildtypes (one-way ANOVA, Tukey's post hoc, Kv3.3^{R420H} vs CBA wildtype P=0.0028; figure 6.7).

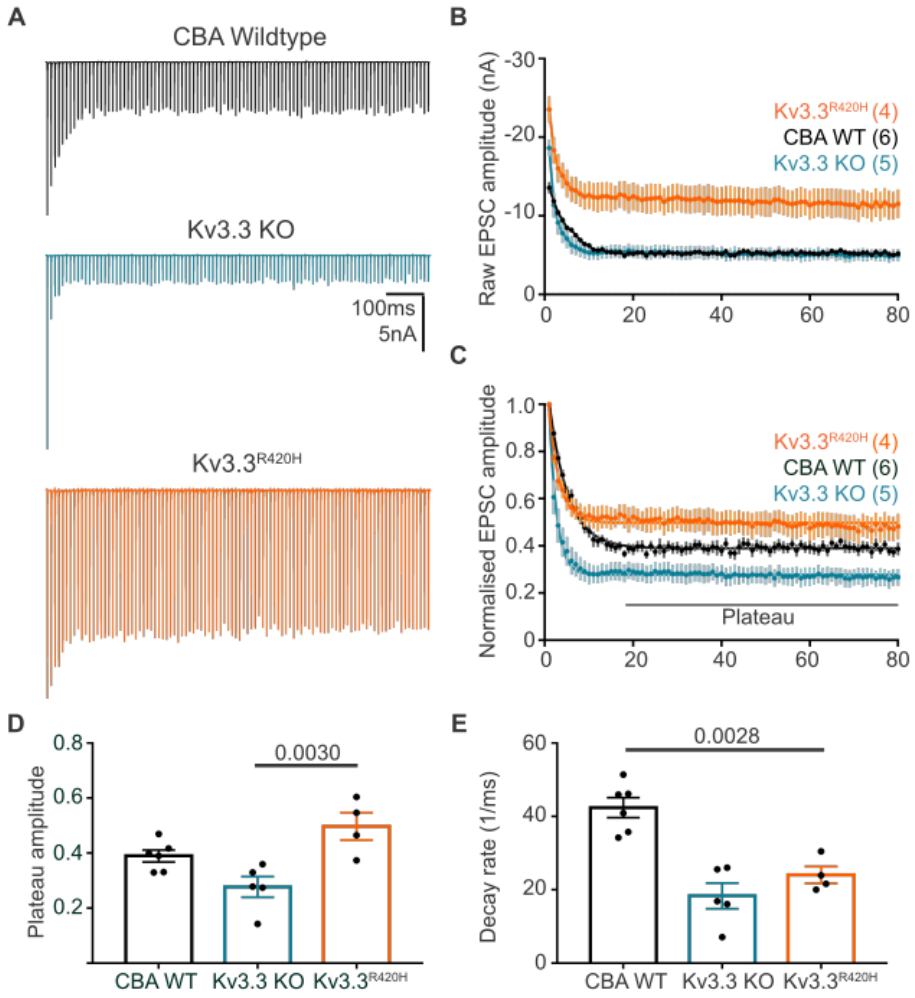

Figure 6.7: **EPSC amplitudes in the MNTB of Kv3.3^{R420H} mice are resistant to short-term depression A:** Example EPSC traces recorded from MNTB neurons in CBA WT, Kv3.3 KO and Kv3.3^{R420H} mice in response to 100Hz stimulation (for 800ms) of presynaptic calyx of Held fibres. Amplitudes of each response were measured and plotted in a graph **(B)**. Numbers in brackets represent number of neurons recorded from. **C:** EPSC amplitudes from B normalised to the initial response. Each data set was fit with a single exponential function to demonstrate the 'plateau' phase in which EPSC responses reach an equilibrium. These exponential fits were used to determine the extent **(D)** and rate **(E)** of short-term depression. Plateau amplitudes were significantly higher in Kv3.3^{R420H} mice compared to Kv3.3 KOs (one-way ANOVA, Tukey's post hoc P=0.0030. The decay rate for depression of EPSC amplitudes was significantly increased in Kv3.3^{R420H} compared to CBA wildtypes (one-way ANOVA, Tukey's post hoc, P=0.0028). Data points represent values from individual neurons. Variance plotted as SEM.

6.4 Potassium currents are increased in MNTB neurons of old Kv3.3^{R420H} mice

The R420H mutation in the Kv3.3 gene results in an adult-onset form of SCA13, suggesting a decline in neuronal function with age. Interestingly, auditory brainstem response recordings from Kv3.3 KO mice also show a progressive worsening with age, with the merging of wave 3 and 4 in addition to the reduction of wave 4 amplitude discussed in the previous chapter becoming much more pronounced. This would suggest that fewer cells are contributing to the compound action potential at wave 4 and action potential firing of neurons in wave 3 have become less synchronised. Thus, further changes in action potential waveform may occur at this age, resulting in a loss of the accurate timing of APs in a population of neurons. For these reasons, potassium currents and action potential duration were examined in mice aged 6 months.

Potassium currents in MNTB neurons of Kv3.3 KOs did not change in old animals, however currents in 6 month old Kv3.3^{R420H} mice were significantly increased compared to their younger counterparts (unpaired t-test, t=3.364 df=19, P=0.0033; young n=12, old n=9; figure 6.8). At +10mV current amplitudes were 7.8 ±0.44nA (n=12) in young animals (P21-P25) compared to 11.7 ±1.20nA (n=9) in older animals (6 months). Increased current amplitudes were observed at voltages above -40mV (I-V plot in figure 6.8B, orange data points), suggesting a possible increase in both low and high-voltage activated potassium currents.

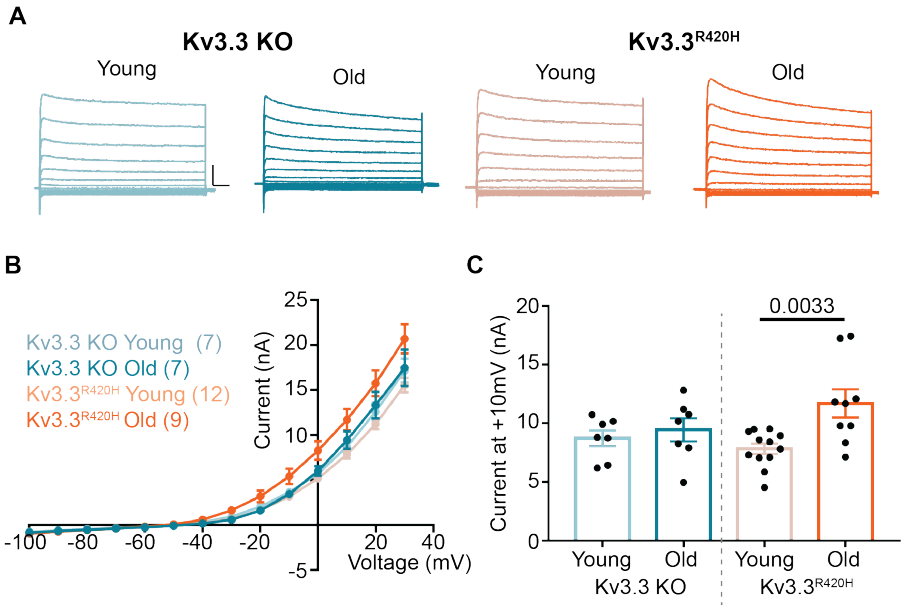

Figure 6.8: **Potassium currents in MNTB neurons of Kv3.3^{R420H} mice were significantly increased at 6 months of age compared to young animals. A:** Example current traces from MNTB neurons of young (P21-P25) and old (6 months) Kv3.3 KO and Kv3.3^{R420H} mice in response to a voltage protocol described in figure 6.2. **B:** Current-voltage plot of potassium currents. n numbers denoted in brackets represent number of neurons recorded from. **C:** Current amplitudes at +10mV taken from B. Current amplitudes are significantly increased in neurons of old Kv3.3^{R420H} mice compared to younger individuals (unpaired t-test, t=3.364 df=19, P=0.0033). Data points represent individual neurons. Variance plotted as SEM.

Similarly, in neurons of the LSO, potassium currents significantly increase with age in Kv3.3^{R420H} mice (at +10mV from 5.5 ±0.42nA (n=8) in young animals to 9.0 ±0.45nA (n=9) in old animals; unpaired t-test, t=4.053 df=15, P=0.0010; figure 6.9C). Interestingly, current amplitudes were also significantly increased in LSO neurons of 6 month old Kv3.3 KOs (at +10mV from 5.5 ±0.52nA (n=6) in young animals to 10.9 ±1.24nA (n=8) in old animals; unpaired t-test, t=3.567 df=12, P=0.0039; figure 6.9C). Whilst slight differences in current amplitudes occur in both animals at voltages positive to -40mV, suggesting an increase in low-voltage activated potassium currents, the biggest changes appear to occur positive to -20mV suggestive of an increased conductance through high-voltage activated channels (figure 6.9B).

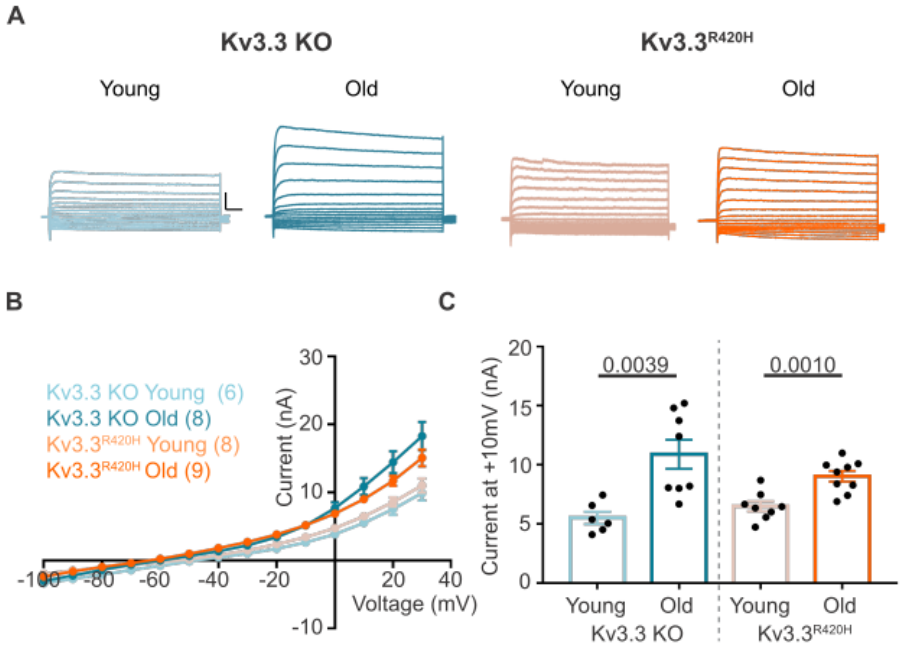

Figure 6.9: **Potassium currents in LSO neurons of Kv3.3^{R420H} and Kv3.3 KO mice were significantly increased at 6 months of age compared to young animals. A:** Example current traces from LSO neurons of young (P21-P25) and old (6 months) Kv3.3 KO and Kv3.3^{R420H} mice in response to a voltage protocol described in figure 6.2. **B:** Current-voltage plot of potassium currents. n numbers denoted in brackets represent number of neurons recorded from. **C:** Current amplitudes at +10mV taken from B. Current amplitudes are significantly increased in neurons of old Kv3.3^{R420H} mice compared to younger individuals (unpaired t-test, t=4.053 df=15, P=0.0010) and in old Kv3.3 KO compared to their younger counterparts (unpaired t-test, t=3.567 df=12, P=0.0039). Data points represent individual neurons. Variance plotted as SEM.

6.5 Action potential duration is unchanged in neurons of the MNTB and LSO of old Kv3.3^{R420H} mice

The previous section showed increases in potassium currents in both MNTB and LSO neurons of Kv3.3^{R420H} mice as well as in LSO neurons of Kv3.3 KOs at 6 months of age, compared to younger individuals. One may expect that this increased potassium conductance would lead to a decrease in action potential duration.

Action potentials were generated in both MNTB and LSO neurons of old (6 month) Kv3.3^{R420H} and Kv3.3 KO mice using current step injections in current clamp (50pA step up to 600pA). Neurons were held at -60mV. Only the first action potential generated was analysed.

Action potential durations were similar in MNTB neurons of both Kv3.3 KOs and Kv3.3^{R420H} mice and did not increase with age (Kv3.3 KO young vs old, unpaired t-test, t=0.5527 df=12, P=0.5906; Kv3.3^{R420H} young vs old, unpaired t-test, t=0.4094 df=15, P=0.6881; figure 6.10B). AP half-widths were 0.4 ±0.06ms (n=7) and 0.4 ±0.04ms (n=7) in Kv3.3 KO young and old animals, respectively and 0.6 ±0.10ms (n=9) and 0.5 ±0.03ms (n=8) in Kv3.3^{R420H} young and old mice, respectively (figure 6.10).

Similarly, despite increased potassium current observed in LSO neurons of both old Kv3.3 KO and Kv3.3^{R420H} mice, there were no differences observed in action potential duration compared to younger individuals (unpaired t-tests, Kv3.3 KO young (n=6) vs old (n=7), t=0.5451 df=11, P=0.5966; Kv3.3^{R420H} young (n=7) vs old (n=7), t=0.7179 df=12, P=0.4866; figure 6.11B). While no changes were observed in action potential duration, the afterhyperpolarisation appeared to be increased in older animals of both genotypes (figure 6.11A).

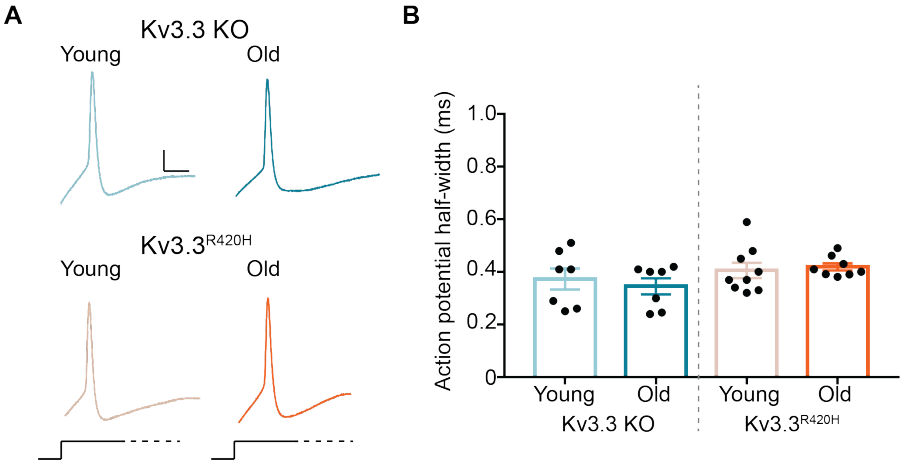

Figure 6.10: **Action potential duration in MNTB neurons does not change in old Kv3.3^{R420H} mice. A:** Example action potential traces from MNTB neurons of young (P21-25) and old (6 months) Kv3.3 KO and Kv3.3^{R420H} mice. Action potentials were measured in current clamp and generated using current step injections of 50pA increments to maximum 600pA. Only the initial action potential generated was analysed. Neurons were held at -60mV. Scale bar= 10mV and 2ms. **B:** Action potential half-width measured as detailed in chapter 1. There were no significant changes between young and old animals of either genotype (Kv3.3 KO young vs old, unpaired t-test, t=0.5527 df=12, P=0.5906; Kv3.3^{R420H} young vs old, unpaired t-test, t=0.4094 df=15, P=0.6881). Data points represent individual neurons. Variance plotted as SEM.

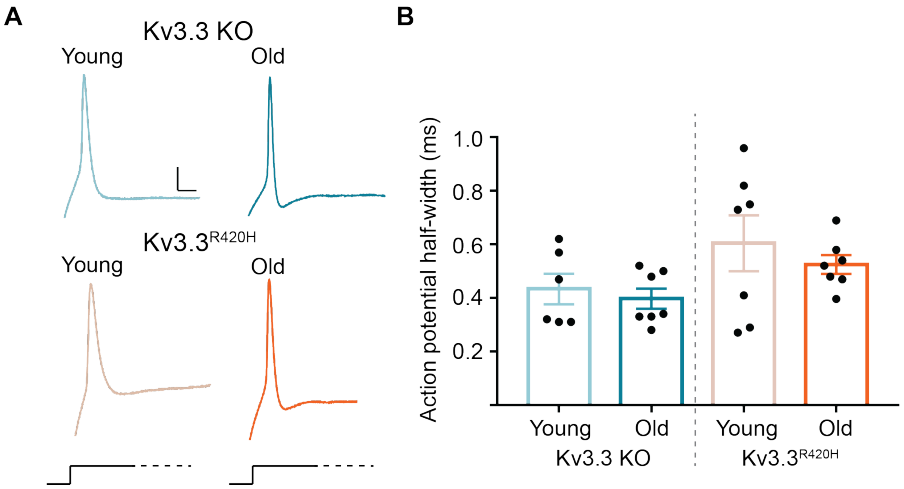

Figure 6.11: **Action potential duration in LSO neurons does not change in old Kv3.3^{R420H} mice. A:** Example action potential traces from LSO neurons of young (P21-25) and old (6 months) Kv3.3 KO and Kv3.3^{R420H} mice. Action potentials were measured in current clamp and generated using current step injections of 50pA increments to maximum 600pA. Only the initial action potential generated was analysed. Neurons were held at -60mV. Scale bar= 10mV and 2ms. **B:** Action potential half-width measured as detailed in chapter 1. There were no significant changes between young and old animals of either genotype (unpaired t-tests, Kv3.3 KO young vs old, t=0.5451 df=11, P=0.5966; Kv3.3^{R420H} young vs old, t=0.7179 df=12, P=0.4866). Data points represent individual neurons. Variance plotted as SEM.

6.6 Kv3.1b and Kv3.3 subunit protein expression increases with age

To assess whether Kv3 subunit expression changed with age, a western blot was performed on CBA wildtype and Kv3.3 KO brainstem tissue from three young animals (P21) and three old (P180) animals. Kv3.3 and Kv3.1b expression was measured, relative to beta-actin in order to normalise for the amount of protein loaded into the gel.

Kv3.3 expression significantly increased between the two age groups in CBA wildtype mice (unpaired t-test, t=2.886 df=4, P=0.0447) from an average of 1.3 $\pm$0.13 (n=3) in young animals to 2.9 $\pm$0.53 (n=3) in older ones (figure 6.12 (top)). No Kv3.3 expression was observed in Kv3.3 KO mice of any age.

Kv3.1b expression was also increased in older CBA wildtype animals (unpaired t-test, t=2.833 df=4, P=0.0472) as well as in older Kv3.3 KO animals (unpaired t-test, t=4.111 df=4, P=0.0147; figure 6.12(bottom)). Although this is significant, there appears to be a difference in Kv3.1b expression in older males and females. While two females showed strong increases to a value of $\sim$ 3, the value from the male was 0.8 (figure 6.12 red circle). Interestingly, Kv3.1b subunit expression in older Kv3.3 KO animals appears less than in CBA wildtypes (figure 6.12 bottom).

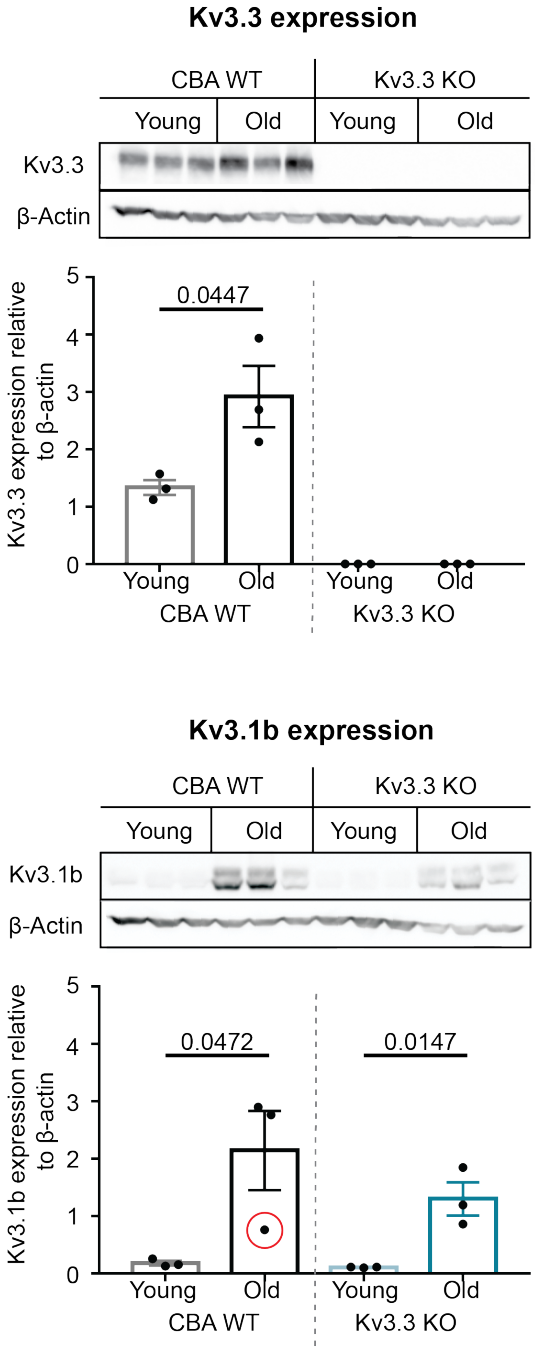

Figure 6.12: **Kv3.3 and Kv3.1b expression increases with age. Top:** Kv3.3 expression in brainstem tissue from CBA wildtype and Kv3.3 KO mice aged P21 (young) or 6 months (old). Samples from three animals of each group were loaded on to the same gel and membranes stained with anti-Kv3.3 and β-actin antibodies. Kv3.3 expression was normalised to that of beta-actin. Kv3.3 expression was significantly increased in old CBA wildtypes compared to younger individuals (unpaired t-test, t=2.886 df=4, P=0.0447). **Bottom:** Kv3.1b expression in brainstem tissue from CBA wildtype and Kv3.3 KO mice aged P21 (young) or 6 months (old). Kv3.1b expression was significantly increased in old CBA wildtypes compared to younger individuals (unpaired t-test, t=2.833 df=4, P=0.0472) and in old Kv3.3 KOs compared to younger animals (unpaired t-test, t=4.111 df=4, P=0.0147). Data points represent individual animals. Variance plotted as SEM.

6.7 Discussion

This chapter provides evidence from the first study into the effect of the R420H mutation on Kv3.3 channel function in native mammal tissue. In cell lines this mutation abolishes Kv3.3 currents mediated by both homomeric channels of mutant subunits as well as heteromeric channels incorporating both mutant and wildtype subunits (Waters et al. 2006). Here, we show that Kv3.3 currents are also attenuated in neurons within the auditory brainstem of mice homozygous for the R420H mutation. Additionally, this occurs in young animals, despite the progressive nature and adult onset of disease symptoms in human patients.

6.7.1 The Kv3.3^{R420H} mutation produces current and action potentials identical to those in Kv3.3 KOs

Potassium currents in MNTB and LSO neurons of Kv3.3^{R420H} mice were similar to those of Kv3.3 KOs. While no difference was observed in current amplitudes within neurons of the MNTB compared to wildtype, action potential duration was increased in these animals to a similar level seen in Kv3.3 KOs. Additionally, current amplitudes in LSO neurons were vastly reduced compared to those in wildtype animals and reached amplitudes indistinguishable from Kv3.3 KOs at voltages positive to -20mV. This was associated with a large increase in action potential duration, again similar to that seen in Kv3.3 KOs. Taken together, this suggests that, consistent with evidence from cell lines, these animals lack a Kv3.3-mediated conductance (Waters et al. 2006).

The findings described here are also consistent with previous work on both this and a related mutation, R423H, which report increased action potential duration and decreased potassium current amplitudes in zebrafish and cultured cerebellar Purkinje neurons expressing the respective mutated Kv3.3 subunits (Issa et al. 2011; Irie et al. 2014). R423H is another mutation present in the voltage sensing domain of the Kv3.3 subunit which forms non-functional channels when expressed in *Xenopus* oocytes. Despite occurring only 3 amino acids away from the mutation in the present

study (R420H) it is associated with a more severe juvenile-onset version of SCA13.

6.7.2 Why is there no Kv3.3 current in Kv3.3^{R420H} mice?

There are a number of reasons for which the Kv3.3 conductance may be lost in these mice, perhaps the mutation results in abnormal folding of the protein such that the channel does not assemble, perhaps channels with the mutation don't get trafficked to the membrane or perhaps the change in amino acid changes the voltage-sensing abilities of the channel such that it never opens upon changes in voltage.

Reduced surface expression of Kv3.3^{R420H} subunits in comparison to wildtype Kv3.3 has been reported previously (Gallego-Iradi et al. 2014; Zhao, Zhu, and Thornhill 2013), in addition to a reduction in the total amount of mutant subunit protein expression (Zhao, Zhu, and Thornhill 2013). Despite a reduction in surface expression, some mutant subunits are still present on the membrane, although post-translational modifications such as glycosylation may be altered on channels incorporating these (Gallego-Iradi et al. 2014).

Kv3.3^{R420H} expression in our mouse model appears to differ in neurons from different nuclei. In neurons of the MNTB, which express both Kv3.3 and Kv3.1b, Kv3.3^{R420H} protein appears to be located in the cytosol and not restricted to the membrane as in wildtypes (figure 6.13 (top left)). In contrast, protein is clearly visible on the membrane of neurons in the LSO, which express only Kv3.3 subunits, in addition to staining throughout the cytosol (figure 6.13 (bottom left)). In accordance with work in cell lines, it appears that less Kv3.3^{R420H} protein is trafficked to the membrane. While there may be a reduction in channels on the membrane, the ones that are incorporated still appear to be non-conducting as Kv3 conductances are equal to Kv3.3 KOs in neurons of the LSO.

Additionally, the presence of functional Kv3.1b subunits appears to prevent Kv3.3^{R420H} subunits reaching the membrane in the MNTB. It has been noted previously that surface expression of Kv3.3^{R420H} subunits cannot be rescued by the presence of Kv3.1b despite wildtype proteins of both forming functional heteromers (Zhao, Zhu, and Thornhill 2013). Here, we show that not only can the expression

of functional Kv3 protein not rescue surface expression of Kv3.3^{R420H} but it seems to prevent it, shown by membrane staining in the LSO (Kv3.3 only) but not MNTB (Kv3.1 and Kv3.3). Moreover, Kv3.1b expression on the membrane does not appear to differ from wildtype, again suggesting that each subunit does not need the other for correct localisation to the membrane, consistent with data from the knock-out animals in chapter one. The fact that no difference in current amplitudes are observed in MNTB neurons also suggests that heteromeric Kv3.1/Kv3.3 channels are not formed. The dominant negative nature of mutant subunits (Waters et al. 2006) on a channel with functional wildtype Kv3 subunits should result in a loss of conductance through both homomeric Kv3.3^{R420H} channels and heteromeric Kv3 channels of Kv3.1 and Kv3.3^{R420H}, reducing overall potassium currents.

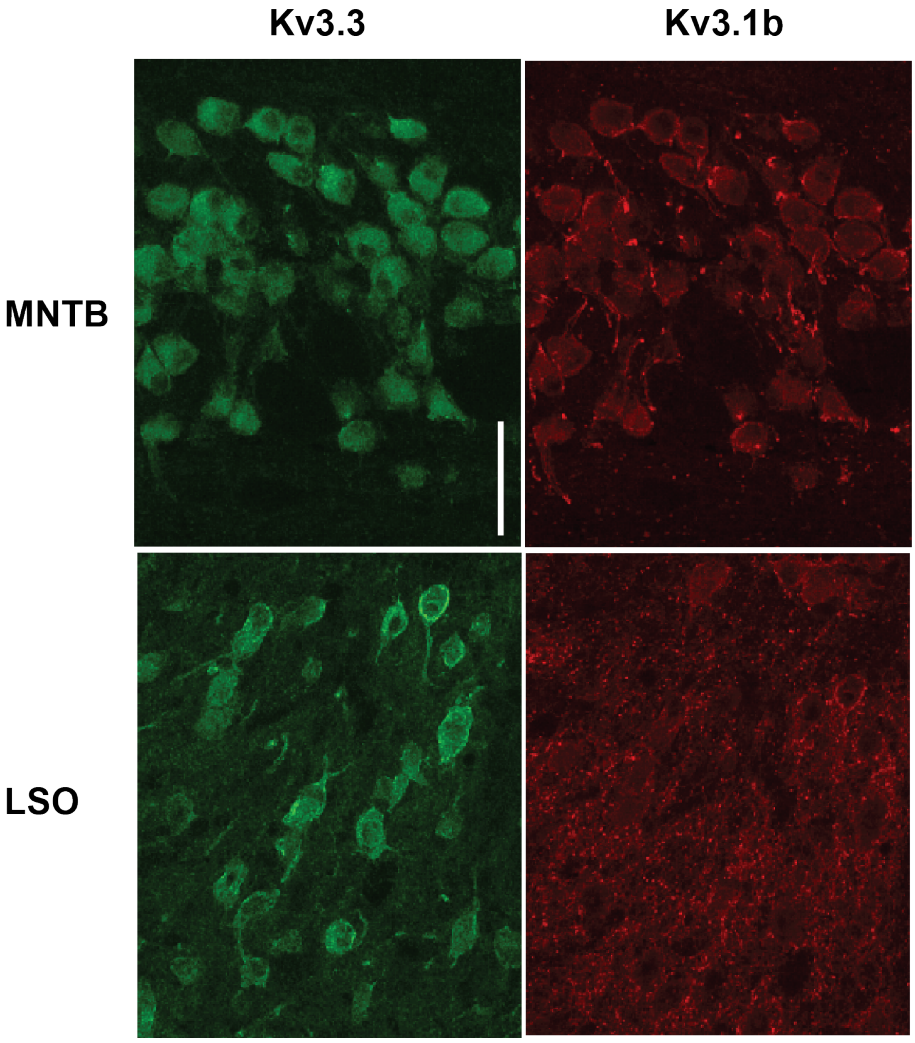

Figure 6.13: **Kv3.3 protein is retained in the cytoplasm of MNTB but not LSO neurons in Kv3.3^{R420H} mice.** Immunohoistochemical staining of Kv3.3 (green; dilution 1:3000) and Kv3.1b (red; 1:1000) in the MNTB and LSO of a homozygous Kv3.3^{R420H} mouse. Immuno and images done by Michelle Anderson.40x magnification; scale bar = 50μm.

6.7.3 Age-dependent changes in Kv3 channels of the MNTB and LSO

Despite the adult-onset of symptoms associated with the R420H mutation in humans (Waters et al. 2006), decreased potassium current amplitudes and increased AP duration were observed in MNTB and LSO neurons of young animals (P20) compared to wildtype and did not appear to deteriorate with age. While current amplitudes increased with age in both mutant and knockout animals, action potential durations stayed constant, most likely due to concurrent increases in sodium conductances.

Interestingly, in addition to these cellular changes in younger animals, mice homozygous for the Kv3.3^{R420H} mutation developed a tremor by the second postnatal week, that was absent from heterozygous mice and did not worsen with age. The mechanism by which this tremor occurred was independent of degeneration of Purkinje neurons as the number of Purkinje neurons was not significantly different in Kv3.3^{R420H} mice compared to wildtype at P21 (unpaired t-test, t=0.9155 df=20, P=0.3708; Michelle Anderson, unpublished). This may indicate that the disease manifests itself slightly differently between mice and humans or that these changes in excitability associated with more subtle symptoms at young ages eventually lead to neurodegeneration of Kv3.3-expressing neurons and cause more severe ataxia in adults. Indeed at 6 months of age there are very few Purkinje neurons left in the cerebellum of Kv3.3^{R420H} mice (Michelle Anderson & Nasreen Choudhury, unpublished). However, a decline in the number of neurons has not been observed within the MNTB or LSO of these mice at either P20 or 6 months of age. Nor was any decline in purkinje or LSO neurons observed in Kv3.3 KOs (figure 6.14), which show similar action potential durations to mutant mice and thus would presumably experience similar levels of calcium influx and the associated excitotoxic effects. Taken together this suggests that neurodegeneration observed in this disease is not merely due to changes in excitability of Kv3.3-expressing neurons but has a much more complex mechanism.

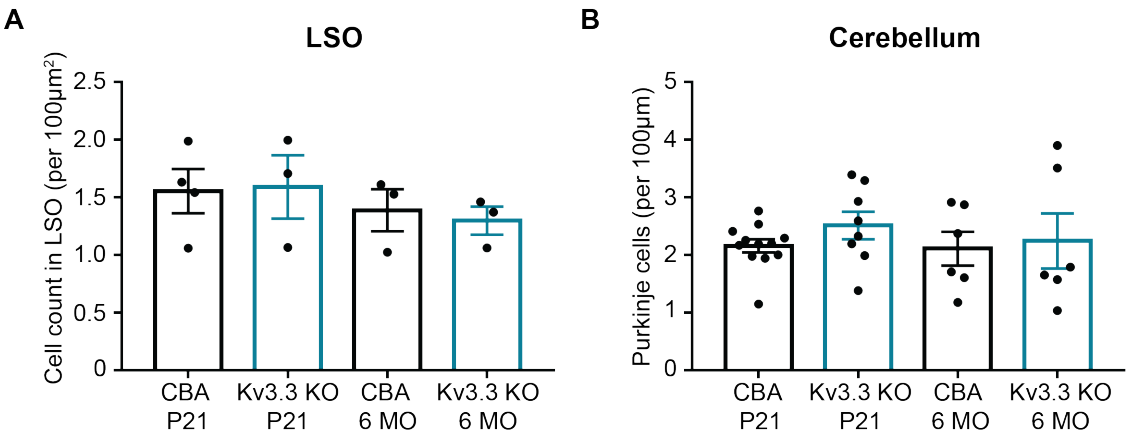

Figure 6.14: **No neurodegeneration is observed in Kv3.3 KOs** Cell counts from LSO and Purkinje neurons of P21 and 6 month old CBA and Kv3.3 KO mice. In LSO counts, brainstem sections were stained with aggrecan while Purkinje neurons were stained with calbindin. Cells were counted in a defined area and normalised to an area of 100um^2 (LSO) or a distance of 100um (Cerebellum). Done in collaboration with Sherylanne Newton.

While changes to action potential duration may not be the cause of neurodegeneration observed in the cerebellum of human patients and in our mouse model, it may still provide a mechanism for the impaired sound localisation seen within some human patients (Middlebrooks et al. 2013) by disrupting the temporal precision of action potential firing within neurons of the MNTB and LSO. Indeed one of the worst affected patients in the Middlebrooks et al. 2013 study was a child that had not yet shown symptoms of ataxia or cerebellar degeneration.

6.7.4 Changes to AP cannot account for decreased auditory function in old Kv3.3 KO mice

As mentioned previously, ABR recordings from old Kv3.3 KO mice show a progressive worsening of auditory function with age. Wave IV amplitudes are decreased further than those seen in young Kv3.3 KOs. Since action potential durations do not change at 6 months of age in Kv3.3 KOs, it is unlikely that changes to synchrony of action potential firing in neurons of both the LSO and MNTB contribute to this decline in auditory function (refer to section 6.4). Additionally, no changes were observed in the number of neurons in either the MNTB or LSO at 6 months of age (data not shown), consequently a decrease in the number of neurons contributing to the compound action potential (wave IV in the ABR) is unlikely to have changed.

Whilst the overall number of neurons may not have changed, it is possible that the proportion with high characteristic frequencies (respond preferentially to high frequency sound stimuli) decreases with age thus fewer cells are recruited during high-frequency sound stimuli.

6.7.5 Age-dependent increase in Kv3 protein expression

Protein expression of both Kv3.1b and Kv3.3 increased in wildtype animals and Kv3.1b increased in Kv3.3 KOs at 6 months of age compared to younger individuals. This is surprising as an age-related decline in hearing has previously been associated with a decrease in Kv3.1b expression (Zettel et al. 2007), although that occurred over a much longer time scale than the present study.

This increase in Kv3.1b is likely to contribute to the increased potassium currents observed in the MNTB of R420H mice in addition to increases in low-voltage activated potassium subunits such as Kv1.1 and 1.2 (Dodson, Barker, and Forsythe 2002). Interestingly, smaller increases in Kv3.1b expression were observed in Kv3.3 KO animals compared to wildtypes which may explain a lack of change in potassium currents in these animals at 6 months of age and may suggest an interaction between the two subunits. Despite increased Kv3.1b expression, it was not able to rescue action potential duration in the older animals of both mutants and Kv3.3 KO.

This increase in Kv3.1b protein is unlikely to have contributed to the increased potassium conductance observed in the LSO of both Kv3.3^{R420H} and Kv3.3 KO mice as these neurons do not express Kv3.1b, at least in the soma.

The fact that Kv3.3 protein also increases with age may result in an accentuated difference between wildtype and Kv3.3 KO ABRs at 6 months of age. This would need further investigation of older wildtype mice.

6.7.6 High frequency transmission is enhanced in Kv3.3^{R420H} mice

Synaptic transmission in Kv3.3^{R420H} appears to have similarities with both Kv3.3 and Kv3.1 KOs. Initial amplitudes and rate of depression are larger, similar to those seen in the Kv3.3 KOs however EPSC amplitudes during sustained high-frequency

stimulation are larger than both wildtype and Kv3.3 KOs, similar to those seen in animals lacking Kv3.1. This is consistent with a lack of both subunits in the terminal and may provide evidence for the dominant negative effect of this mutation on heteromeric channels. The number of recordings are low for Kv3.3^{R420H} mutants however, and more would need to be done to draw any firm conclusions.

While these initial results are exciting, a more in-depth study of cellular physiology and behaviour is required to truly understand the mechanisms by which Kv3.3 subunits can cause neurodegeneration and how changes at the cellular level impact auditory processing. Although, it is clear from these results that Kv3.3 subunits are just as important as Kv3.1 for proper functioning of the brain and while they are often expressed within the same neurons, one cannot always compensate for the other.

6.8 Summary

- Decreases in potassium currents and increased action potential duration occur even in young Kv3.3^{R420H} mice.
- Potassium currents and action potential duration in neurons of the MNTB and LSO of Kv3.3^{R420H} mice are identical to those in Kv3.3 KOs.
- Although potassium currents increase with age, no further changes are seen in action potentials in Kv3.3^{R420H} or Kv3.3 KO mice at 6 months of age.
- The mouse model used in this study shows age-dependent neurodegeneration of purkinje neurons and thus provides a good, accurate model of disease progression in humans.

Chapter 7

Can Kv3 subunits form heteromeric channels?

Different Kv3 subunits are often expressed within the same neurons, for example Kv3.1 and Kv3.3 in the MNTB and cerebellar granular layer (Weiser et al. 1994; Perney et al. 1992), Kv3.1 and Kv3.2 in fast spiking GABAergic interneurons (Chow et al. 1999), Kv3.1 and Kv3.4 in fast spiking neurons (Baranauskas et al. 2003) and Kv3.3 and Kv3.4 in motor nerve terminals (Brooke et al. 2004). This co-expression of multiple subunits supported the belief that Kv3 channels exist as heteromers in these neurons. Indeed, Kv3.1 subunits can be co-immunoprecipitated with both Kv3.3 (Chang et al. 2007) and Kv3.4 (Baranauskas et al. 2003) and kinetics of Kv3 channels formed by co-expression of Kv3.1 and Kv3.4 subunits in HEK293 cells match those seen in fast-spiking neurons (Baranauskas et al. 2003).

There are four Kv3 subunits, Kv3.1 - Kv3.4, each with spliced variants and slightly different kinetics, Kv3.3 and Kv3.4 subunits show levels of inactivation that are absent from Kv3.1 and Kv3.2 (Rudy and McBain 2001). Thus, formation of heteromeric channels provides a mechanism by which Kv3 channels can vary kinetics and downstream signalling pathways to function optimally in a number of different cell types or subcellular locations.

In this chapter, we will explore whether Kv3.3 subunits can form heteromeric channels with other Kv3 subunits when co-expressed in CHO cells. This work was completed during a 3 month industrial placement at Autifony Therapeutics and due

to the limited time-frame, contains some data contribution from Michele Speggiorin, an electrophysiologist at the company. It will be made clear throughout where Michele contributed recordings. Analysis of recordings however, was performed by myself.

7.1 Methods

- All work was carried out on CHO cells cultured at Autifony Therapeutics by myself and Manuela Marabita.

- Kv3.1b and Kv3.4a subunits were transiently expressed in wildtype CHO cells in order to investigate their current kinetics, while Kv3.3 was expressed in a stable CHO cell line. To investigate heteromeric formation Kv3.4a and Kv3.1b were transfected into the Kv3.3 stable cell line. All subunits were co-transfected with GFP for identification of positively transfected cells.

- CHO cells were plated the day prior to recording. Sterile glass coverslips were placed in a well of a sterile 6-well plate under a down-flow cabinet and cells suspended in media were plated at a concentration of $\sim$ 200,000 cells per well.

- On the day of recording, coverslips were removed from media as required and placed in the recording chamber of an electrophysiology rig, perfused with an external acsf solution containing in mM: NaCl (137), KCl (4), Glucose (10), HEPES (10mM), $CaCl_2$ (1.8) and $MgCl_2$ (1), adjusted to pH 7.4 using KOH.

- Glass recording pipettes were pulled to a resistance of 2-3MΩ and filled with a solution containing in mM: KCl (120); EGTA (10); KOH (31.25); MgATP (4); HEPES (10); $CaCl_2$ (5.37) and $MgCl_2$ (1.75). pH = 7.2.

- All recordings were performed at room temperature.

7.2 Kinetics of Kv3.3 channels

Activation and inactivation parameters were assessed in a stable CHO cell line expressing human Kv3.3d subunits. Cells were held at -100mV as a holding of -70mV induced partial inactivation of Kv3.3 currents (figure 7.1).

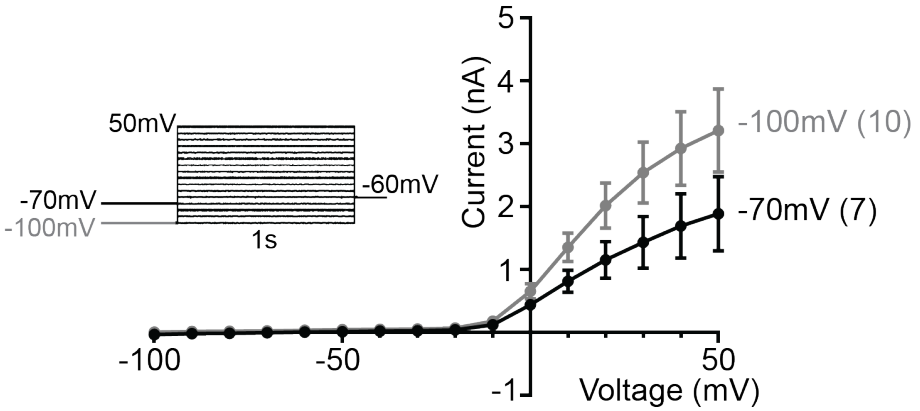

Figure 7.1: **Kv3.3 currents are partially inactivated at a holding potential of -70mV**. Peak Kv3.3 currents recorded from CHO cells from holding potentials of -100mV (grey) and -70mV (black) plotted in a current-voltage graph. Inset: voltage protocol; cells were held at either -100 or -70mV for at least 1 minute prior to recordings followed by sequential 1s voltage steps to +50mV in increments of 10mV before returning to -60mV. Number of cells denoted in brackets. Variance plotted as SEM.

7.2.1 Activation

Kv3.3 currents were generated using the voltage protocol described in figure 7.1, both peak and steady-state currents were measured. These were used to calculate the Kv3.3 conductance using equation 7.1 where G is conductance, I is the current measured at a given voltage (V) and Vrev is the reversal potential for potassium calculated using the Nernst equation and concentrations of K^+ ion present in external and internal solutions (-94mV). Conductances at each voltage were normalised to the maximum (at +50mV) and average data points were fitted with a Boltzmann function in Graphpad Prism 8 (equation 7.2).

$$G = I(V - Vrev) \tag{7.1}$$

$$G = \frac{1}{1 + \exp^{(\frac{V50-V}{Slope(k)})}} \tag{7.2}$$

Kv3.3 channels exhibit slow inactivation when expressed in CHO cells. During the course of 1s, currents decrease from a peak (at +50mV) of 3.2 ±0.66nA to 1.1 ±0.19nA (n=10) at the end of the voltage step (SS; steady-state), a decrease of around 62.1% (figure 7.2B). The activation curve from steady-state currents was shifted to the left of that of peak currents such that the V_{50} changed from 6.4 ±0.8mV at the peak to 2.3 ±0.9mV at steady-state (figure 7.2C), although this difference was not significant (paired t-test, t=2.063 df=8, P=0.0730). In most cells, Kv3.3 channels began to activate at -10mV, with all channels open at ∼ +30mV, although in those with larger currents, the activation voltage appeared to be -20mV (figures 7.3 and 7.2). The voltage at which currents activated was measured manually using current traces, the voltage which first produced a visible current was taken as the activation voltage and this was more obvious in those cells with larger currents, which may explain this variability. The half-maximal activation was observed at 6.4 ±1.6mV and activation slope factor was 6.9 ±0.5mV (figure 7.2B & C). Currents produced at +50mV were fit with an exponential function in order to assess the inactivation time constant. Inactivation of Kv3.3 currents was best fit with a double exponential, the fast time constant of which was 130.0 ±15.9ms and the slow component 471.9 ±55.5ms (figure 7.3D).

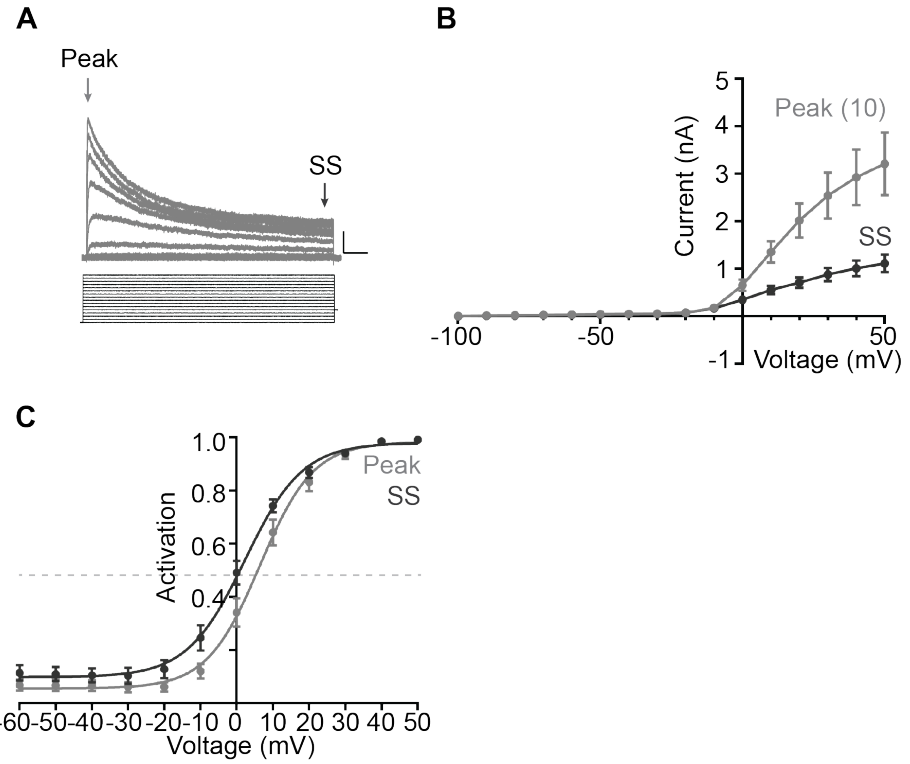

Figure 7.2: **Kv3.3 currents exhibit slow-inactivation in CHO cells A:** Example current trace recorded from a single CHO cell. From a holding potential of -100mV, 1s voltage steps were applied in 10mV increments to +50mV. Arrows denote peak and steady-state (SS) currents that were plotted in (B). Scale bar = 1nA, 100ms. **B:** Current-voltage plot of both peak (light grey) and steady-state (SS; dark grey) currents. Number of cells denoted in brackets. **C:** Activation curve for both peak and steady-state currents plotted in B. Grey dotted line indicates half-maximal point. Variance plotted as SEM.

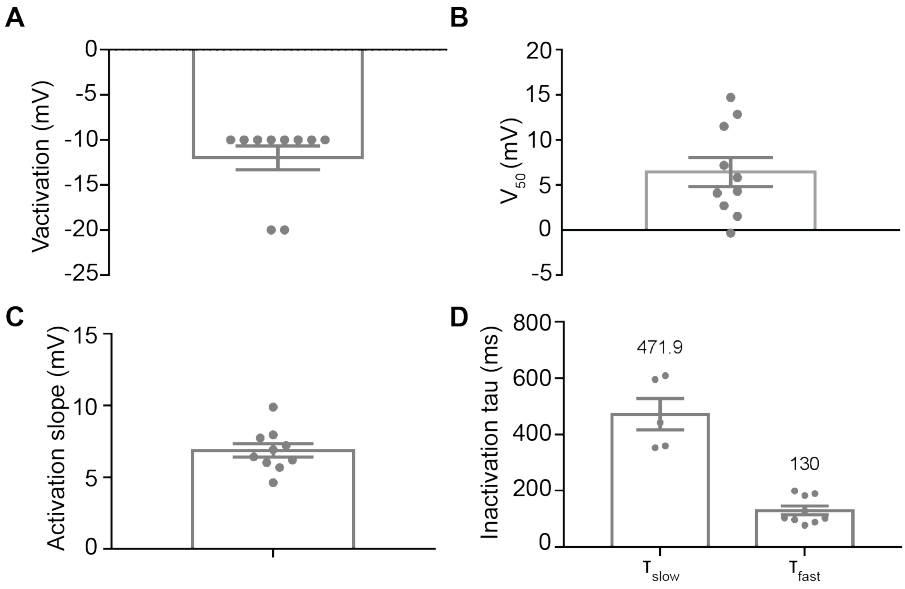

Figure 7.3: **Activation parameters for Kv3.3 channels expressed in CHO cells A:** Activation voltage measured as described in text. **B:** Half-maximal activation of peak Kv3.3 current, measured from activation curves of single cells. **C:** Slope of activation measured from activation curves of single cells. **D:** Inactivation time constant of Kv3.3 currents at +50mV. Current traces were fit with a double exponential function at +50mV. Time constants for tau(slow) and tau(fast) are reported, values above the graph represent the mean. Data points represent individual cells and variance is plotted as SEM.

7.2.2 Steady-state inactivation

Steady-state inactivation of Kv3.3 channels was determined using a 10s voltage pre-step at voltages between -100mV and +40mV in 20mV increments, followed by a 200ms test step to +40mV. A rest period of 1 minute was allowed between each sweep (a sweep consists of pre-step + test step). Currents generated during the test step were measured and normalised to the maximum. Data points were plotted and fit with a Boltzmann function.

Kv3.3 channels showed a steep inactivation which began at -40mV and by -19mV, half of the channels had inactivated (figure 7.4B & C). Full inactivation was not observed, most likely due to the length of the pre-step being inadequate to inactivate all channels. This steady-state inactivation was steep with a slope factor -4.5 ±0.7mV (figure 7.4 D).

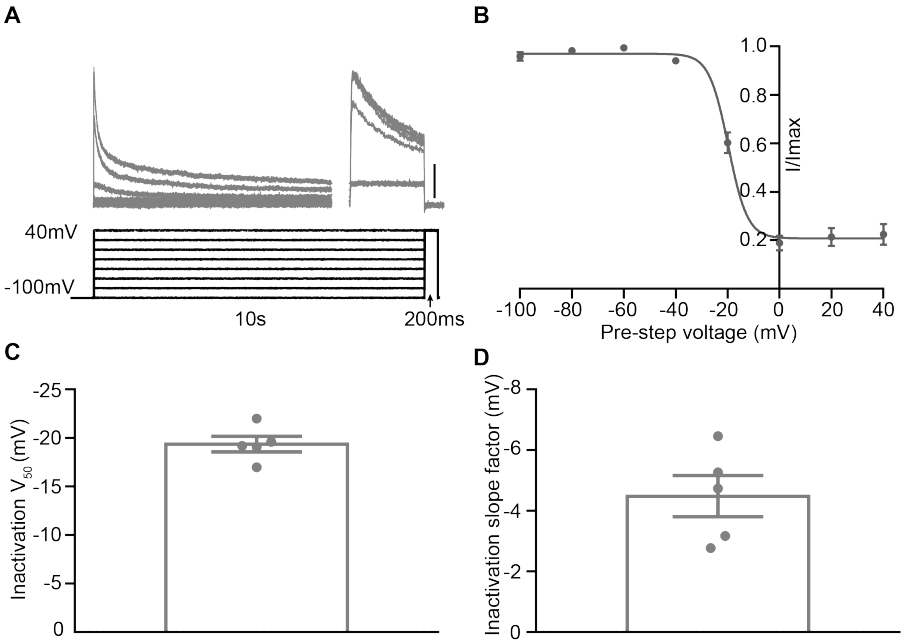

Figure 7.4: **Kv3.3 channels show steep steady-state inactivation in CHO cells A:** Example Kv3.3 current trace recorded from a CHO cell in response to the inactivation protocol described in text. Scale bar = 1nA. **B:** Inactivation curves from normalised currents measured during the test step and plotted against pre-step voltage. Average data plotted from 5 cells and fit with a Boltzmann function. **C:** Half-inactivation voltage (V50) taken from inactivation curves of individual cells. **D:** Slope factor of inactivation taken from inactivation curves of single cells. Data points represent individual cells. Variance plotted as SEM.

7.3 Kinetics of Kv3.1b channels

Human Kv3.1b DNA (1ug) was transfected into CHO K1 cells 48-72 hours prior to electrophysiological recordings. Positively transfected cells were visualised with GFP. Activation and inactivation kinetics were assessed as for Kv3.3 channels. In this section Michele contributed 1 recording for activation and 1 for inactivation.

7.3.1 Activation

In contrast to Kv3.3 channels, Kv3.1b show very little inactivation during the 1s voltage step with peak and steady steady currents at +50mV of 8 ±2nA and 5 ±1nA, respectively (n=11; figure 7.5 A & B). However, the kinetics of activation are very similar to Kv3.3 channels. These channels begin to activate at ∼ -20mV and reach maximum activation by +30mV with a half-maximal activation of 6.7 ±0.9mV, similar to that of Kv3.3 (figures 7.5 & 7.6). The activation curve of the steady-state current is almost identical to that of the peak current, with only a slight shift to negative voltages, producing a half-maximal activation of 3.6 ±1.5mV which was not significantly different from that of the peak (paired t-test, t=2.018 df=9, P=0.0744; figure 7.5C). The activation slope factor observed was 7.9 ±0.39mV, similar to that of Kv3.3 (6.9mV). Inactivation of currents at +50mV could be fit with a single exponential function, yielding an inactivation time constant of 1.2 ±0.2s (figure 7.6D).

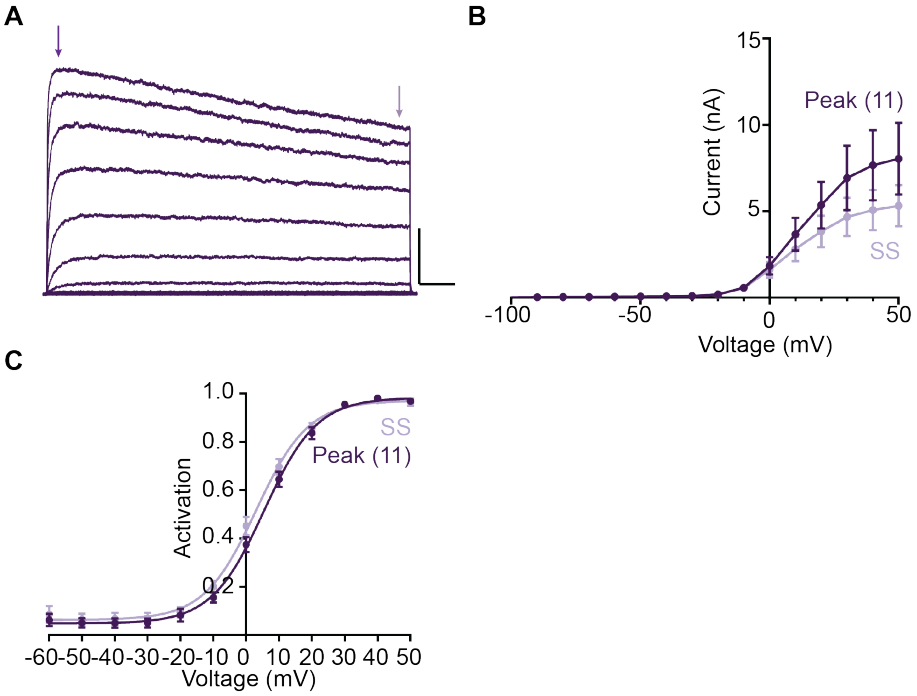

Figure 7.5: **Kv3.1b currents show very little inactivation in CHO cells A:** Example current trace recorded from a single CHO K1 cell transfected with hKv3.1b DNA. From a holding potential of -100mV, 1s voltage steps were applied in 10mV increments to +50mV. Arrows indicate peak and steady-state (SS) currents that were plotted in (B). Scale bar = 1nA. **B:** Current-voltage plot of both peak (Dark purple) and steady-state (SS; light purple) currents. Number of cells denoted in brackets. **C:** Activation curve for both peak and steady-state currents plotted in B. Number of cells denoted in brackets. Variance plotted as SEM.

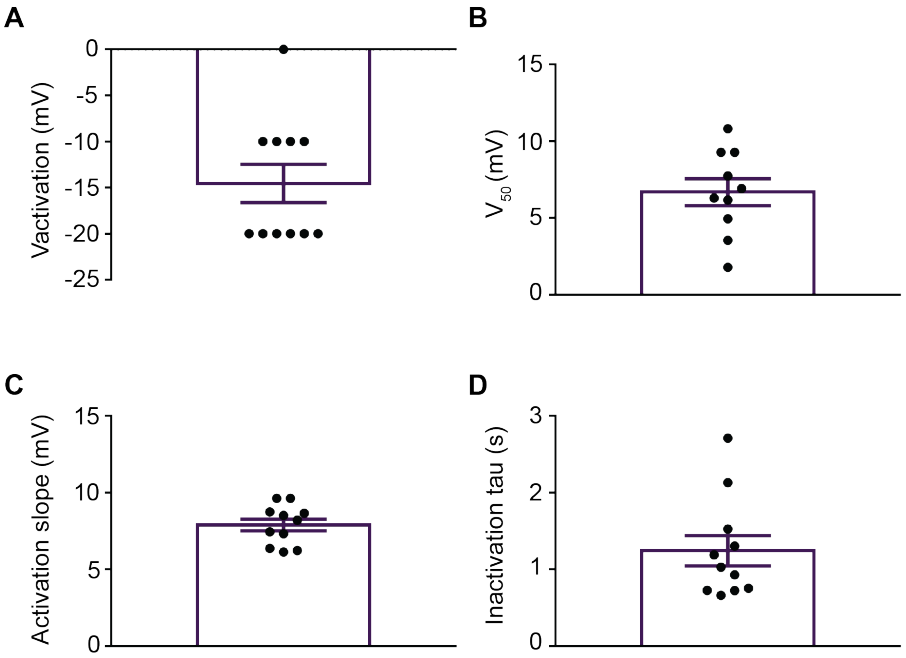

Figure 7.6: **Activation parameters for Kv3.1b channels expressed in CHO cells A:** Activation voltage measured as described in text. **B:** Half-maximal activation of peak Kv3.1 current, measured from activation curves of single cells. **C:** Slope of activation measured from activation curves of single cells. **D:** Inactivation time constant of Kv3.1 currents at +50mV. Current traces were fit with a single exponential function at +50mV and the time constant is reported for each cell. Data points represent individual cells and variance is plotted as SEM.

7.3.2 Steady-state inactivation

Kv3.1b channels begin to inactivate at -40mV and are mostly inactivated by +20mV with a half-inactivation voltage of -12 ±1.67mV, slightly more positive than that of Kv3.3. Similar to Kv3.3, not all Kv3.1b channels had completely inactivated at the end of the 10s pre-step, resulting in the inactivation curve not reaching 0 (figure 7.7B). The slope of inactivation was also very similar to Kv3.3 at -6.7 ±0.30mV.

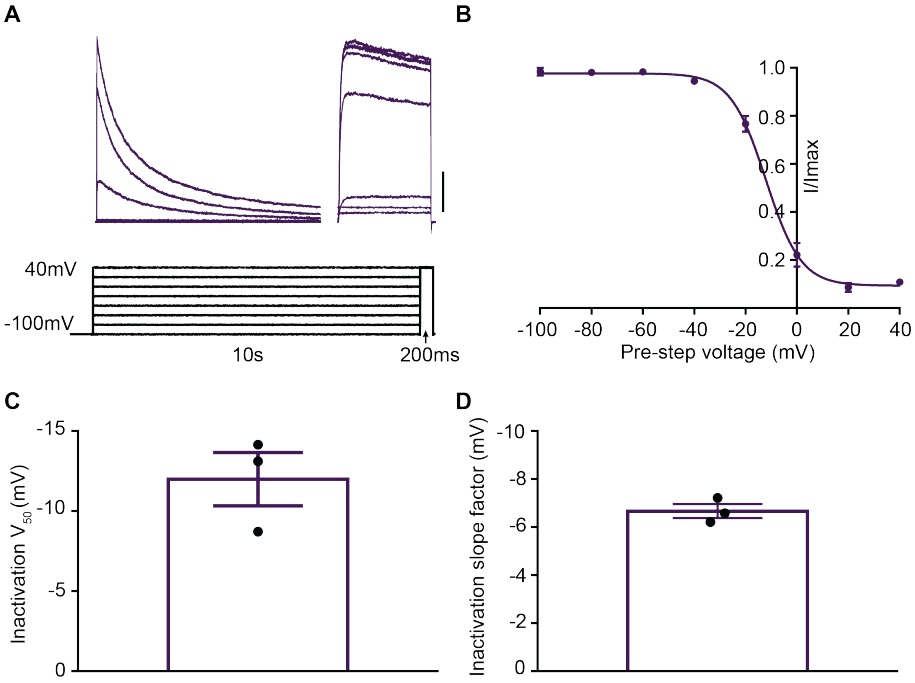

Figure 7.7: **Kv3.1b channels show steep steady-state inactivation in CHO cells A:** Example Kv3.1b current trace recorded from a CHO cells transfected with hKv3.1b in response to the inactivation protocol described in text. Scale bar = 1nA. **B:** Inactivation curves from normalised currents measured during the test step and plotted against pre-step voltage. Average data plotted from 3 cells and fit with a Boltzmann function. **C:** Half-inactivation voltage (V50) taken from inactivation curves of individual cells. **D:** Slope factor of inactivation taken from inactivation curves of single cells. Data points represent individual cells. Variance plotted as SEM.

7.4 Kinetics of Kv3.4a channels

Human Kv3.4a DNA (1ug) was transfected into CHO K1 cells 72hrs prior to electrophysiological recordings. Here, Michele contributed 2 recordings towards activation and 1 towards inactivation.

7.4.1 Activation

Kv3.4a currents exhibit strong inactivation, with full inactivation reached within 250ms of the 1s voltage step (figure 7.8A). Peak Kv3.4a currents measured had an average amplitude of 15 ±6.6nA (at +50mV; n=8) while steady-state currents were close to zero at 0.2 ±0.04nA. Kv3.4a channels begin to activate at much more negative voltages than both Kv3.3 and Kv3.1, at ∼ -40mV (figures 7.8C & 7.9A) with full activation of channels at around +40mV. As currents at steady-state were mostly due to leak, the activation curve showed maximum conductance was reached at -30mV, although this is unlikely to reflect actual channel opening. The slope of activation was less steep compared to both Kv3.3 and Kv3.1 with an average value of 12.9 ±0.8mV (n=8). Inactivation of Kv3.4a currents at +50mV was fit with a double exponential function producing fast and slow time constants of 19.7ms and 179.5ms, respectively.

7.4.2 Steady-state inactivation

Kv3.4a channels begin to inactivate at around -60mV and show complete steady-state inactivation at around -20mV with a half-maximal inactivation voltage of -41 ±2.4mV (figure 7.10B & C). This is around 20mV more negative than both Kv3.3 and Kv3.1 and unlike both of these the 10s pre-step was sufficient to inactivate all channels. While Kv3.4a channels may inactivate at more negative voltages, the slope factor of inactivation was similar to both Kv3.1b and Kv3.3 at -5.5 ±0.9mV.

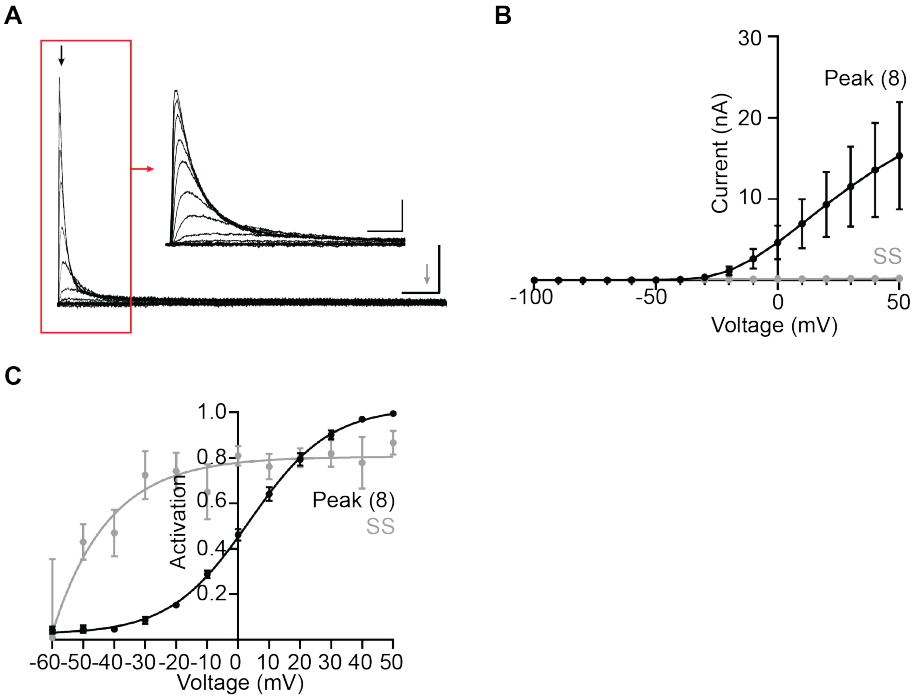

Figure 7.8: **Kv3.4a channels show very fast inactivation when expressed in CHO cells A:** Example current trace recorded from a single CHO K1 cell transfected with hKv3.4a DNA. From a holding potential of -100mV, 1s voltage steps were applied in 10mV increments to +50mV. Arrows indicate peak and steady-state (SS) currents that were plotted in (B). Scale bar = 1nA, 100ms. Inset: Area in red square on a shorter time scale. scale bar = 1nA, 100ms. **B:** Current-voltage plot of both peak (Back) and steady-state (SS; light grey) currents. Number of cells denoted in brackets. **C:** Activation curve for both peak and steady-state currents plotted in B. Number of cells denoted in brackets. Variance plotted as SEM.

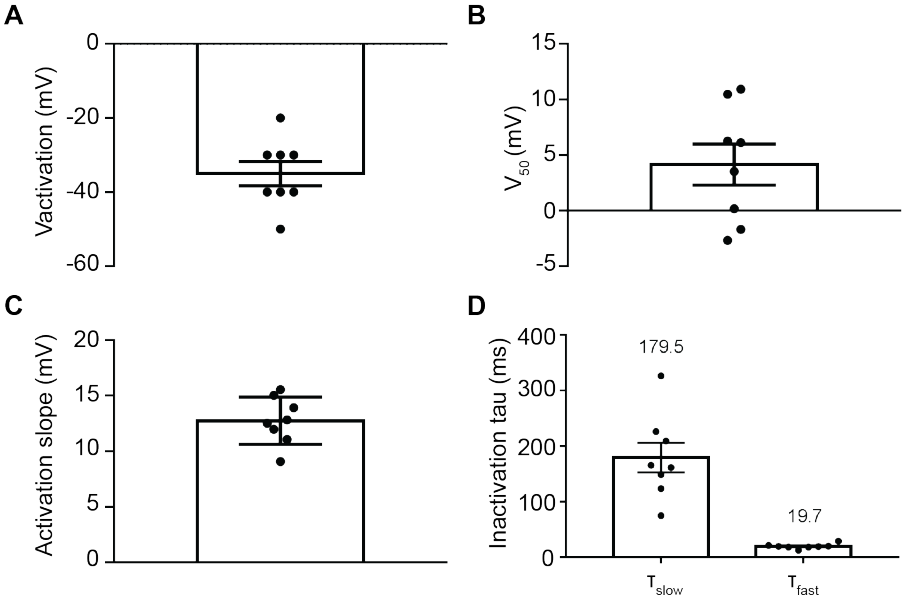

Figure 7.9: **Activation curve parameters for Kv3.4a channels expressed in CHO cells A:** Activation voltage measured as described in text. **B:** Half-maximal activation of peak Kv3.4a current, measured from activation curves of single cells. **C:** Slope of activation measured from activation curves of single cells. **D:** Inactivation time constant of Kv3.4a currents at +50mV. Current traces were fit with a double exponential function at +50mV and the fast (tau_{fast}) and slow (tau_{slow}) time constants are reported for each cell. Data points represent individual cells and variance is plotted as SEM.

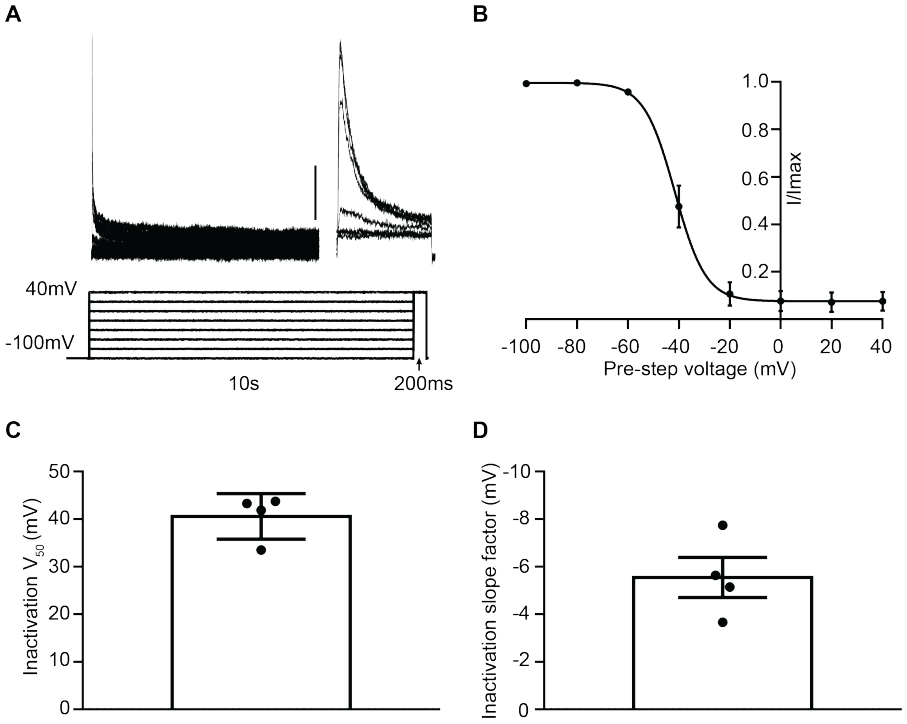

Figure 7.10: **Kv3.4a channels completely inactivate by 0mV in CHO cells A:** Example Kv3.4a current trace recorded from a CHO cell transfected with hKv3.4a in response to the inactivation protocol described in text. Scale bar = 1nA. **B:** Inactivation curves from normalised currents measured during the test step and plotted against pre-step voltage. Average data plotted from 4 cells and fit with a Boltzmann function. **C:** Half-inactivation voltage (V50) taken from inactivation curves of individual cells. **D:** Slope factor of inactivation taken from inactivation curves of single cells. Data points represent individual cells. Variance plotted as SEM.

7.5 Co-expression of Kv3.3 and Kv3.4a

Transfection of Kv3.4a DNA into a Kv3.3-expressing stable CHO line yielded interesting results. Instead of producing a homogeneous population of cells with the same current kinetics, a number of different of current types were observed and cells could be classed into five distinct populations based on these. These were named Kv3.3-like and Kv3.4-like which, as their names suggest, were identical to Kv3.3 and Kv3.4 homomers, respectively, Kv3.3 + Kv3.4 which exhibited currents intermediate to Kv3.3 and Kv3.4 homomers, and Kv3.3/Kv3.4 fast and Kv3.3/Kv3.4 slow, have currents similar to, but not the same as Kv3.4 and Kv3.3, respectively (see figure 7.11). In addition to their difference in appearance, the activation threshold, half-maximal activation and slope of activation differ between groups with Kv3.3-like and Kv3.3/Kv3.4 slow having similar values to Kv3.3 homomers and the other groups having similar values to Kv3.4 homomers (table 7.1). The remaining part of this section will be split into these five groups and their currents will be compared to both Kv3.3 and Kv3.4 homomers to determine which, if any, are generated by heteromeric channels .

Table 7.1: **CHO cells co-expressing hKv3.3 an hKv3.4a can be divided into 5 distinct populations based on their current kinetics.** Activation curve parameters for each population of cells.

Parameter	**Cell type**				
	Kv3.3 like	**Kv3.4 like**	**Kv3.3+ Kv3.4**	**Kv3.3/ Kv3.4 fast**	**Kv3.3/ Kv3.4 slow**
V_{act} (mV)	-3.3 ±2.1	-27.5 ±2.5	-26.7 ±3.3	-30 ±0	-10 ±0
V_{50} (mV)	4.9 ±1.6	2.9 ±4.5	6.2 ±3.1	6.3 ±1.5	9.2 ±0.8
Slope (mV)	6.9 ±0.4	10.5 ±2.2	12.8 ±0.7	11.6 ±0.9	9.7 ±1.3

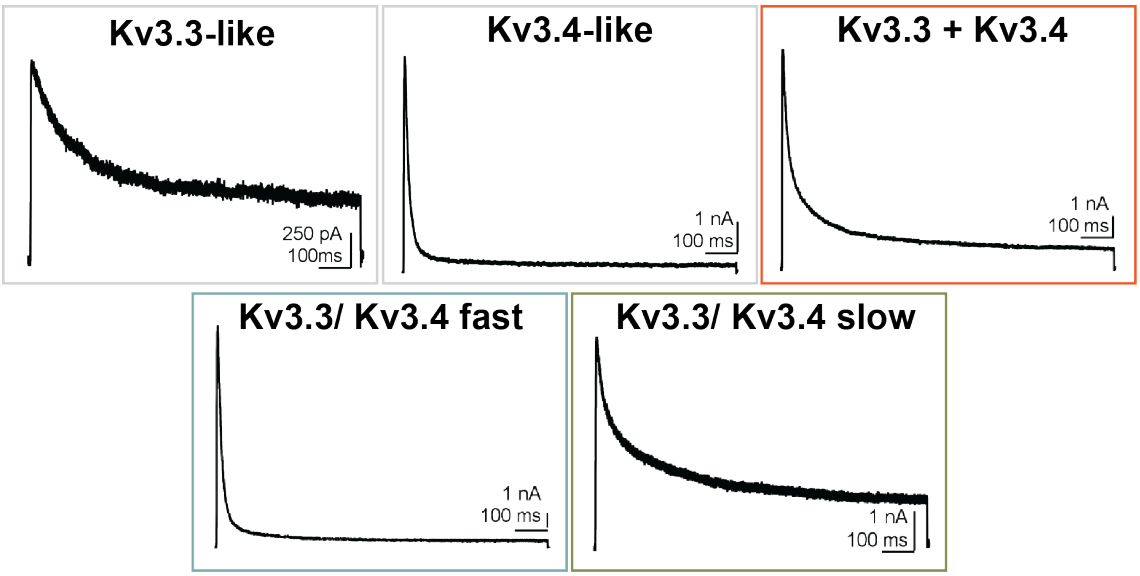

Figure 7.11: **Co-expression of Kv3.3 and Kv3.4 subunits in CHO cells generates five distinct types of Kv3 current.** Example current traces recorded from individual CHO cells expressing human Kv3.3 and Kv3.4a DNA at +50mV. Currents were divided into the above groups based on a number of factors including their inactivation time constants, activation voltage, V50, amplitude of steady-state currents and slope of activation.

7.5.1 Kv3.3-like cells

The first group of cells exhibited currents almost identical to those seen in CHO cells only expressing Kv3.3 subunits, the only difference observed was a more positive activation voltage of -3.3 ±2.1mV (n=6) compared to -13 ± 1.5mV (n=10) in Kv3.3 WT cells (unpaired t-test, t=3.578 df=13, P=0.0034; figure 7.12). As discussed earlier this measure is very subjective and any changes to leak currents or peak amplitudes increases the difficulty of determining the activation voltage. It is evident from the activation curve that these recordings had slightly more leak and thus this may have had an impact on the determined $V_{activation}$ (figure 7.12B). Despite this difference in activation voltage, half-maximal activation voltages (V_{50}), activation slope and inactivation time constants observed in these cells are not significantly different from Kv3.3 WT cells (figure 7.12). In addition, inactivation occurring during the 1s voltage step at +50mV could be fitted with a double exponential, similar to the Kv3.3 WTs (figure 7.12). Despite the presence of GFP in these cells, it is likely that Kv3.4 DNA was not expressed, or at least subunits were not present on the membrane in large enough quantities to carry a sizeable conductance.

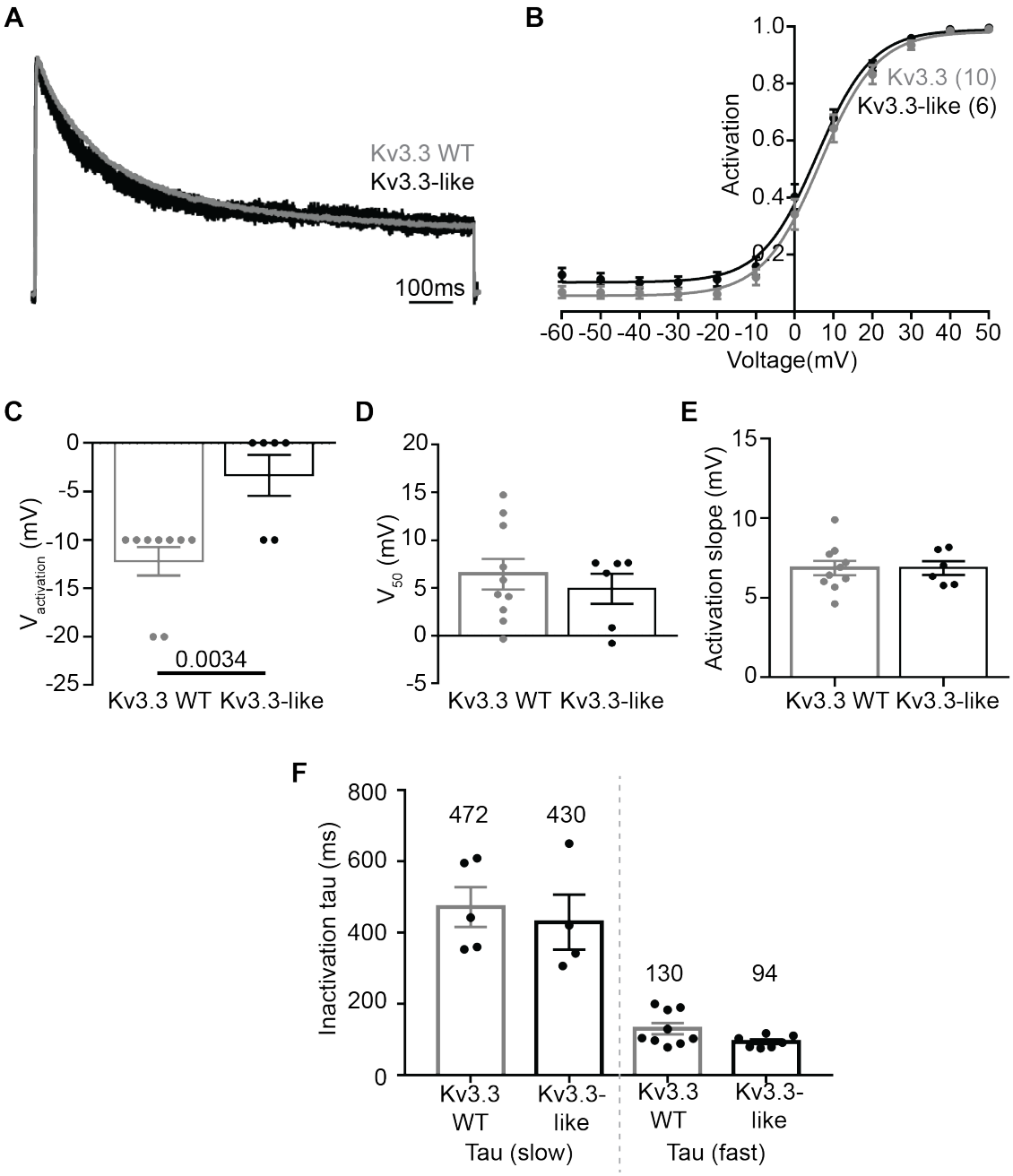

Figure 7.12: **Kv3.3-like cells have near identical currents to Kv3.3 WT. A:** Example current traces recorded from Kv3.3 WT (grey; CHO Kv3.3) and Kv3.3-like cells (black; CHO Kv3.3 transfected with Kv3.4) in response to a 1s +50mV voltage step. Currents have been normalised to the peak. **B:** Activation curve for Kv3.3 WT and Kv3.3-like cells. Number of cells in brackets. **C:** Voltage at which cells begin to activate, measured as described in text. $V_{activation}$ of Kv3.3-like cells is significantly more positive than Kv3.3 WT (t-test, t=3.578 df=13, P=0.0034). **D:** Half-maximal activation voltage (V_{50}). No differences were observed (unpaired t-test, t=0.6418 df=14, P=0.5314). **E:** Slope of activation. No differences were observed (unpaired t-test, t=0.002674 df=14, P=0.9979). **F:** Inactivation time constant. Double exponential functions were fitted to the decaying current at +50mV, fast and slow time constant are reported on graph with average values noted above each column. No differences were observed in either time constant (unpaired t-tests; Tau(slow) t=0.4559 df=7, P=0.6623; tau(fast) t=1.929 df=14, P=0.0743). Variance plotted as SEM.

7.5.2 Kv3.4-like cells

Kv3.4-like cells, in contrast, displayed currents almost identical to Kv3.4a WT cells, inactivating within 250ms with little to no steady-state current (figure 7.13A). Activation curves produced from these currents are the same as Kv3.4 WTs, yielding the same V50 and slope of activation as well as voltage of activation (figure 7.13). Inactivation in these cells at +50mV could be fitted with a double exponential function , which yielded fast and slow time constants very close to those in Kv3.4 WT (figure 7.13F).

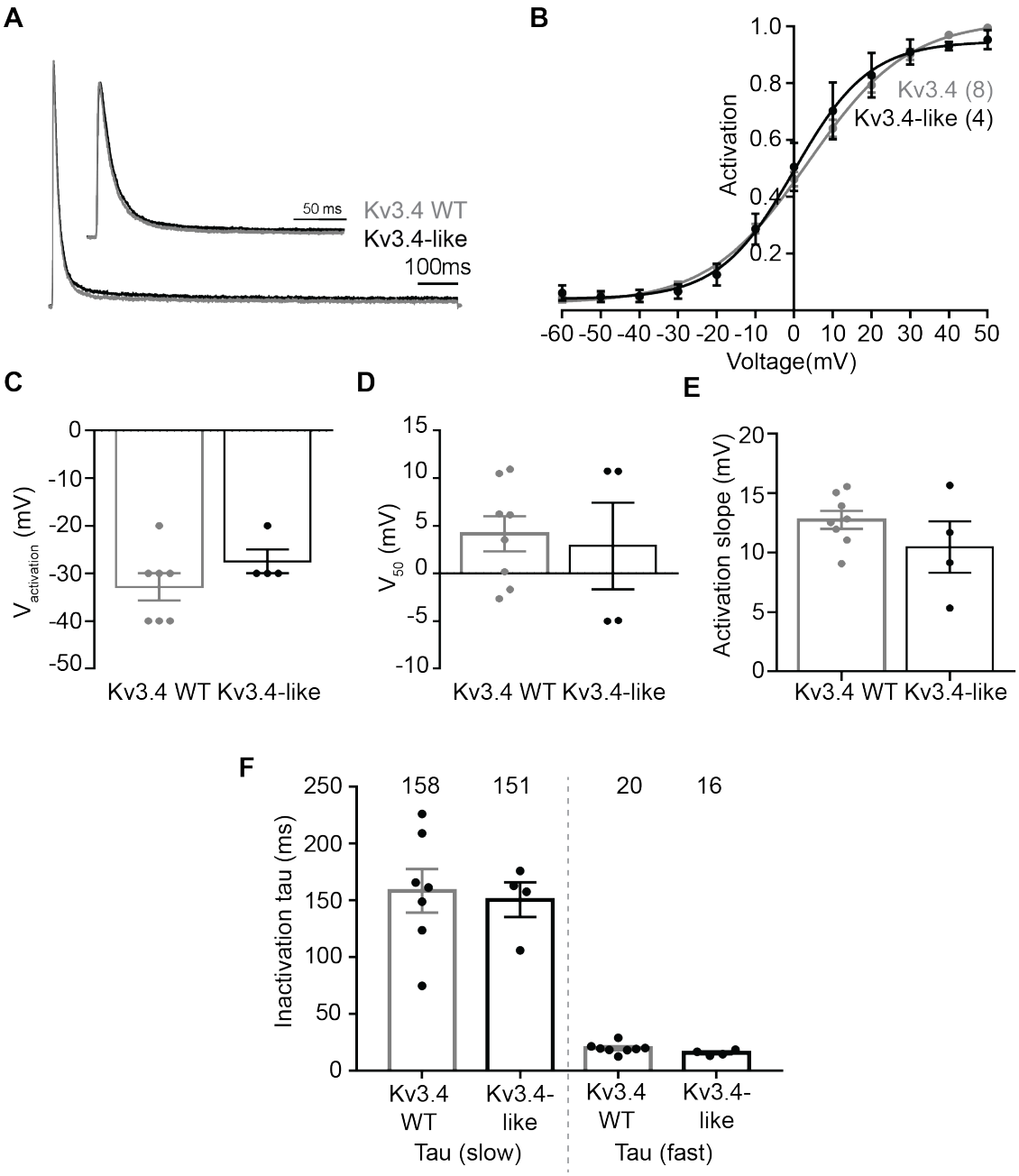

Figure 7.13: **Kv3.4-like cells have identical currents to Kv3.4 WT. A:** Example current traces recorded from Kv3.4 WT (grey; CHO K1 transfected with Kv3.4) and Kv3.4-like cells (black; CHO Kv3.3 transfected with Kv3.4) in response to a 1s +50mV voltage step. Currents have been normalised to the peak. **B:** Activation curves with number of cells in brackets. **C:** Voltage at which cells begin to activate, measured as described in text. No differences were observed (t-test, t=1.254 df=9, P=0.2413). **D:** Half-maximal activation voltage (V_{50}). No differences were observed (unpaired t-test, t=0.3143 df=10, P=0.7597). **E:** Slope of activation. No differences were observed (unpaired t-test, t=1.26 df=10, P=0.2363). **F:** Inactivation time constant. Double exponential functions were fitted to the decaying current at +50mV, fast and slow time constant are reported on graph with average values noted above each column. No differences were observed in either time constant (unpaired t-tests; Tau(slow) t=0.2786 df=9, P=0.7869; tau(fast) t=1.661 df=10, P=0.1278). Variance plotted as SEM.

7.5.3 Kv3.3 + Kv3.4 cells

Cells within this group displayed currents intermediate to both Kv3.3 and Kv3.4 homomers with a fast and slow inactivation phase however, similar to Kv3.3 WTs, these currents did not fully inactivate. This could be interpreted as the sum of two components (Kv3.3 and Kv3.4). Activation curves produced from these cells were more similar to Kv3.4 WT cells; the slope of activation was significantly increased in both Kv3.4 and Kv3.3 + Kv3.3 cells compared to Kv3.3 WT (6.9mV (n=8), 12.8mV (n=5) and 12.4mV (n=10), respectively; one-way ANOVA, Tukey's post hoc; Kv3.3 WT vs Kv3.4 WT and Kv3.3 WT vs Kv3.3 + Kv3.4 P=<0.0001; figure 7.14E). No difference was observed in V_{50} between any of the groups, however, the voltage of activation was significantly more negative in Kv3.3 + Kv3.4 cells compared to Kv3.3 WT and significantly more positive than Kv3.4 WT (one-way ANOVA; Tukey's post hoc; Kv3.3 WT vs Kv3.3 + Kv3.4, P= 0.0085; Kv3.3 + Kv3.4 vs Kv3.4 WT, P= 0.0499; figure 7.14C).

Despite having similar characteristics to Kv3.4 WTs, inactivation of these currents at +50mV could only be fitted with a triple exponential function (figure 7.15A). This made it difficult to compare activation to Kv3.3 and Kv3.4 wildtypes (which were fitted by a double), thus both double and triple exponential functions were fitted to all groups.

When fitted with a triple exponential the only difference observed between groups was an increased fast tau in Kv3.4 WT and Kv3.3 + Kv3.4 cells compared to Kv3.3 WT, however values in Kv3.3 WTs were very close to zero due to the absence of a very fast component making this comparison unfair.

When fitted with a double exponential, the slow time constant of Kv3.3 + Kv3.4 cells was intermediate to, and significantly different from both Kv3.3 and Kv3.4 WT cells (one-way-ANOVA; Tukey's post hoc, Kv3.3 (n=10) WT vs Kv3.3 + Kv3.4 (n=5) P= 0.0129; Kv3.4 WT (n=8) vs Kv3.3 + Kv3.4 P= 0.0393; figure 7.15). In addition, the fast time constant of Kv3.3 + Kv3.4 was similar to Kv3.4 WT, consistent with the presence of a fast inactivation phase and was significantly faster than that observed in Kv3.3 WT (one-way ANOVA; Tukey's post hoc, P=0.0002;

figure 7.15B).

Steady-state (plateau) currents were analysed in these cells. As Kv3.4 WT do not produce a plateau current, one may expect plateau currents of homomeric populations of Kv3.3 and Kv3.4 to be the same as Kv3.3 WT. Any difference in these cells compared to Kv3.3 WT may suggest a Kv3.4 component and thus the presence of heteromers, however currents measured at the end of the 1s voltage step are very similar to those observed in Kv3.3 WT cells, with no differences observed in the V50 or slope of activation (figure 7.16).

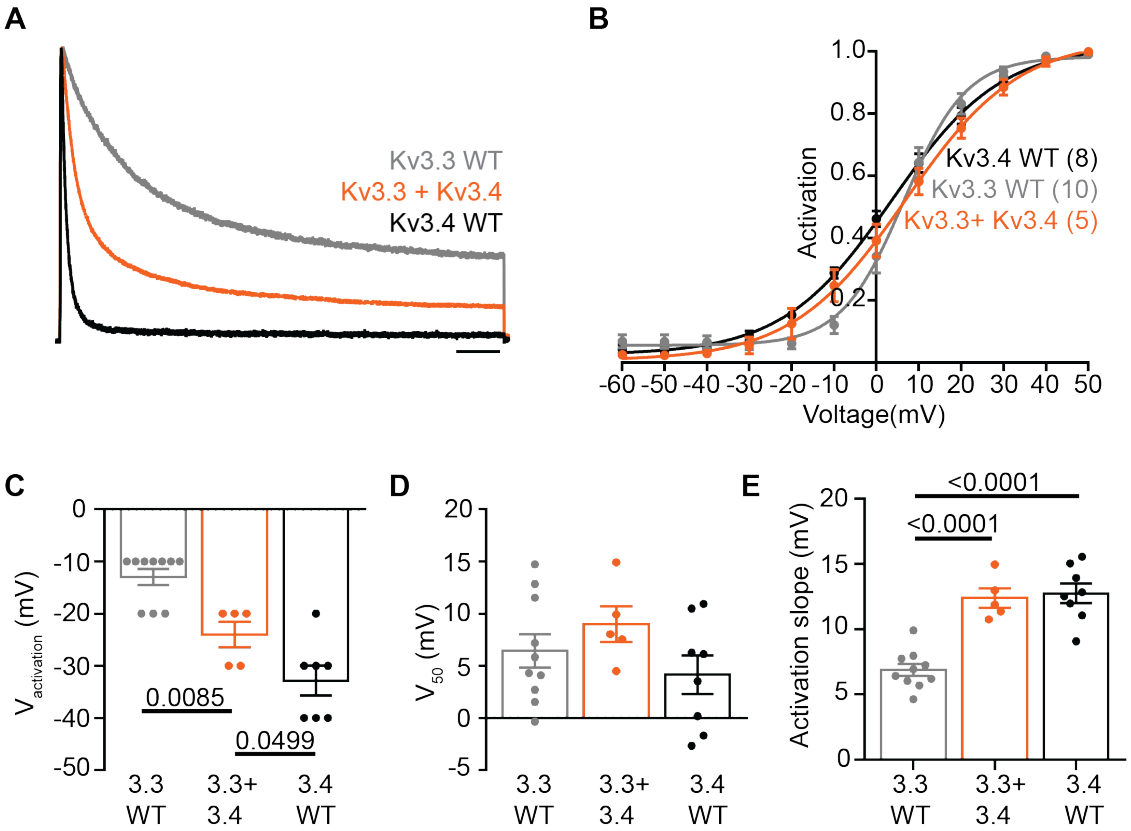

Figure 7.14: **Kv3.3 + Kv3.4 cells display current kinetics intermediate to both Kv3.3 and Kv3.4 WT A:** Example current traces recorded from Kv3.3 WT (grey; CHO Kv3.3), Kv3.4 WT (black; CHO K1 transfected with Kv3.4) and Kv3.3 + Kv3.4 cells (orange; CHO Kv3.3 transfected with Kv3.4) in response to a 1s +50mV voltage step. Currents have been normalised to the peak. **B:** Activation curves with number of cells in brackets. **C:** Voltage at which cells begin to activate. $V_{activation}$ in Kv3.3 + Kv3.4 cells is significantly different from both Kv3.3 and Kv34 WT (one-way ANOVA, Tukey's post hoc, P values on graph). **D:** Half-maximal activation voltage (V_{50}). No differences were observed (one-way ANOVA; $F(2,20)=1.518$; $P=0.2434$). **E:** Slope of activation. Significantly increased in both Kv3.3 + Kv3.4 and Kv3.4 WT compared to Kv3.3 WT (one-way ANOVA, Tukey's post hoc, P values on graph). Variance plotted as SEM.

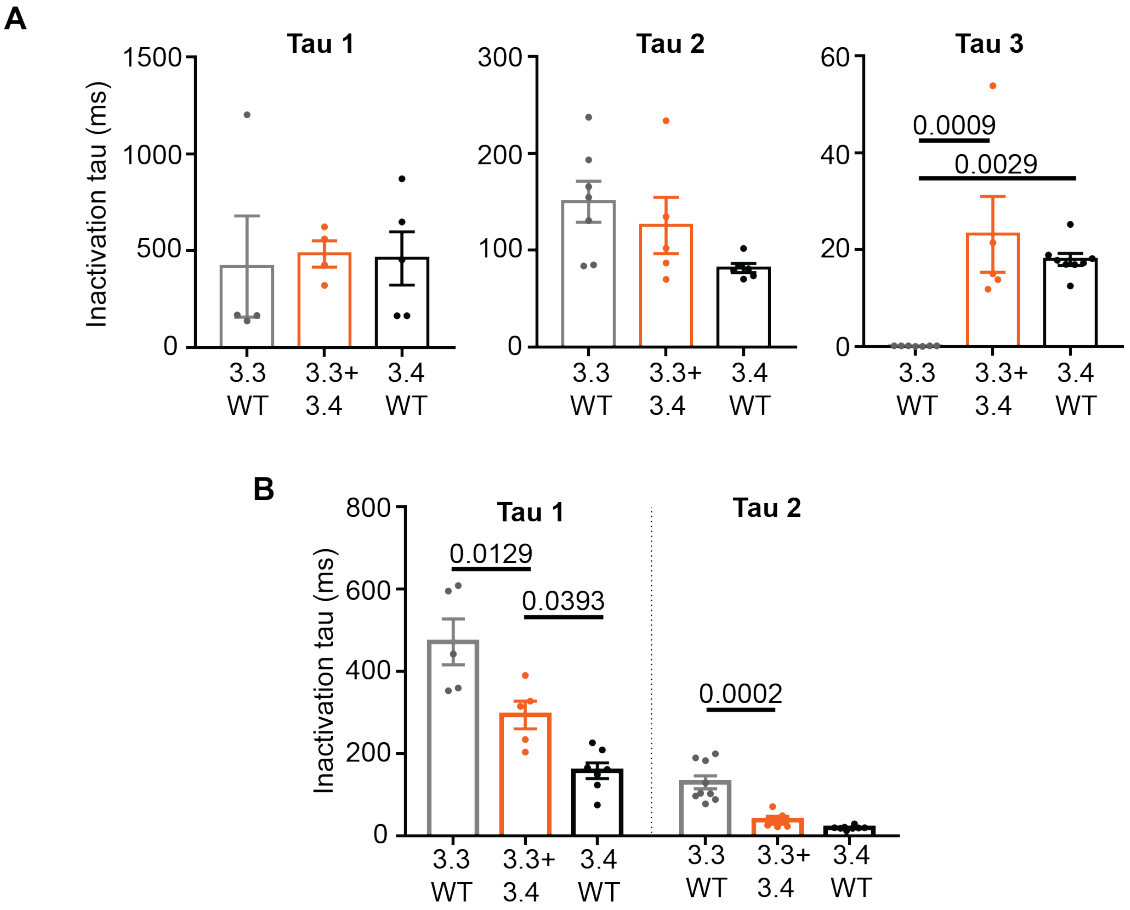

Figure 7.15: **Inactivation of Kv3.3 + Kv3.4 currents at +50mV has three components** Inactivation of Kv3.3 + Kv3.4 currents, Kv3.3 WT and Kv3.4 WT were each fitted with triple and double exponential functions. **A:** Inactivation time constant. Triple exponential functions were fitted to the decaying current at +50mV, three time constants are reported on graph. Tau 3 was significantly slower in Kv3.3 + Kv3.4 and Kv3.4 WT compared to Kv3.3 WT (one-way ANOVA, Tukey's post hoc, P values on graph. **B:** Inactivation time constant. Double exponential function fitted to decaying phase of current. The slow time constant of Kv3.3 + Kv3.4 was significantly different from both Kv3.3 and Kv3.4 WT and the fast constant of Kv3.3 + Kv3.4 was significantly faster than that observed in Kv3.3 WT (one-way ANOVA, Tukey's post hoc, P values on graph). Variance plotted as SEM.

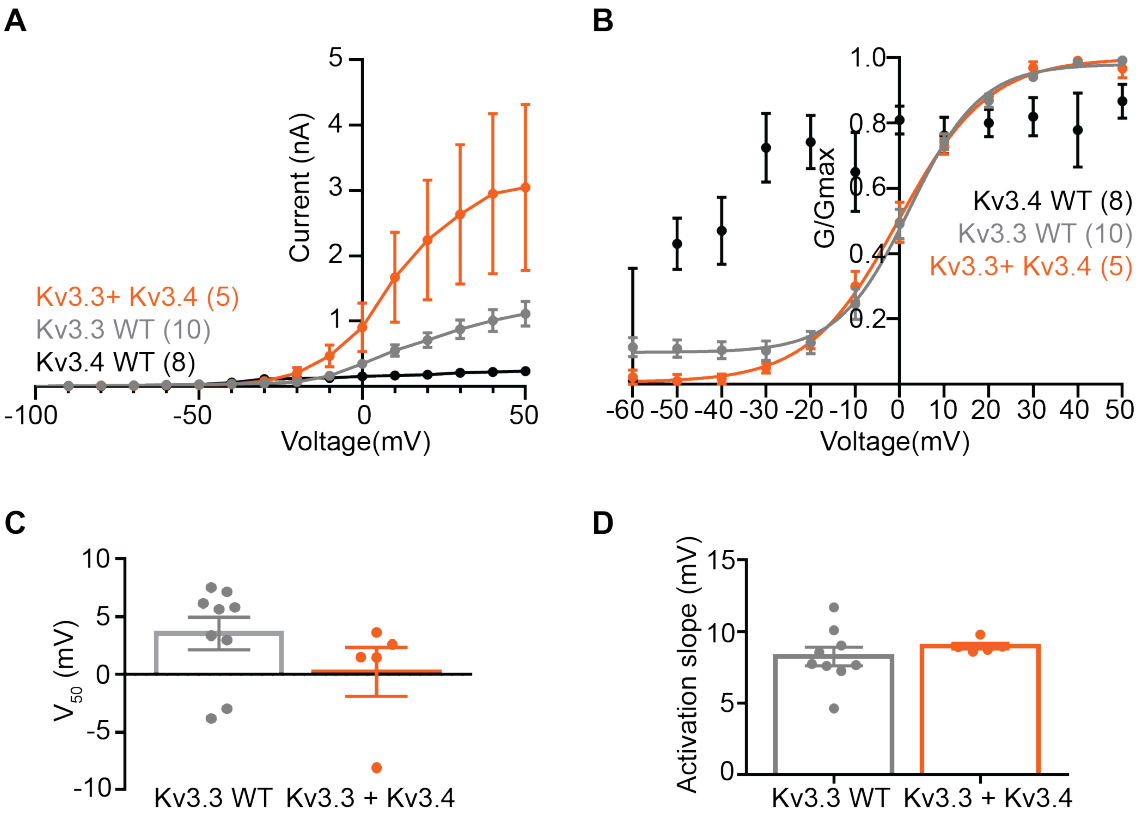

Figure 7.16: **Steady-state currents of Kv3.3 + Kv3.4 cells are not different to those in Kv3.3 WT A:** I-V plot of currents measured at the end of a 1s voltage protocol as seen in figure 7.1. **B:** Activation curves for these steady-state currents. Conductance was calculated and normalised to the maximum value. Data was fitted with a Boltzmann function. **C:** Half-maximal activation measured from activation curves fitted to individual cells. No differences were observed (unpaired t-test; t=1.356 df=12, P=0.2001). **D:** Slope of activation. No differences were observed (unpaired t-test; t=0.8173 df=12, P=0.4297). Variance plotted as SEM.

7.5.4 Kv3.3/Kv3.4 fast

Cells in this category possess currents very similar to those in Kv3.4 WTs, with a large, fast inactivating component, similar activation voltages, V_{50} and slope of activation (figure 7.17). Inactivation at +50mV, however, can only be fit with a triple exponential, similar to Kv3.3 + Kv3.4 cells from the previous section (figure 7.18). These properties are consistent with either the formation of heteromers in a 3:1 Kv3.4:Kv3.3 ratio or the formation of homomers with a larger population of Kv3.4 channels.

Consistent with their similarity to Kv3.4 WT, these cells have a $V_{activation}$ much more negative than Kv3.3 WT (-30mV vs -12mV in Kv3.3 WT; one-way ANOVA, Tukey's post hoc, P=<0.0001) in addition to a significantly narrower slope of activation (12mV (n=6) vs 6.9mV (n=10) in Kv3.3 WT; one-way ANOVA, Tukey's post hoc, P=0.0003). No differences were observed in V_{50} compared to either Kv3.3 or Kv3.4 WT (figure 7.17).

As the inactivating components of these currents (at +50mV) could only be fit with a triple exponential, as in the previous section, all groups were fit with both triple and double exponential functions. When fit with a triple exponential, the fastest component of inactivation (tau 3) in Kv3.3/Kv3.4 fast cells is significantly faster than Kv3.4 WT (one-way ANOVA, Tukey's post hoc, P=0.0015; figure 7.18). The middle component (tau 2) was also significantly faster than Kv3.3 WT (one-way ANOVA, Tukey's post hoc, P=0.0012), but no different to Kv3.4 WT. When fitted with a double exponential function, time constants of Kv3.3/Kv3.4 fast cells were similar to those of Kv3.4 but both fast and slow time constants were significantly faster than those observed in Kv3.3 WT (one-way ANOVA, Tukey's post hoc; tau (slow) P=0.0002; tau(fast) P=<0.0001; figure 7.18B).

Similar to Kv3.4 WT, little to no steady state current was observed from cells in this category.

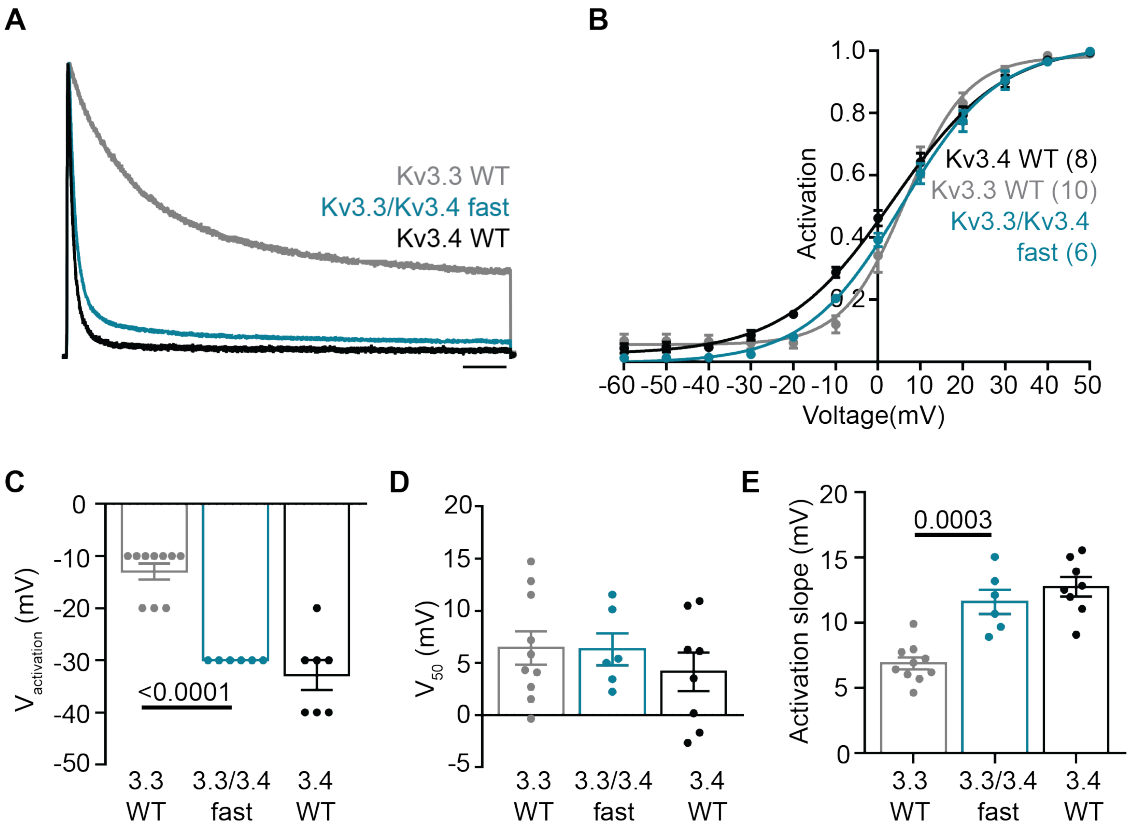

Figure 7.17: **Kv3.3/Kv3.4 fast cells display current kinetics similar to Kv3.4 WT A:** Example current traces recorded from Kv3.3 WT (grey; CHO Kv3.3), Kv3.4 WT (black; CHO K1 transfected with Kv3.4) and Kv3.3/Kv3.4 fast cells (blue; CHO Kv3.3 transfected with Kv3.4) in response to a 1s +50mV voltage step. Currents have been normalised to the peak. **B:** Activation curves with number of cells in brackets. **C:** Voltage at which cells begin to activate. $V_{activation}$ in Kv3.3/Kv3.4 fast cells was significantly more negative than Kv3.3 WT (one-way ANOVA, Tukey's post hoc, P=<0.0001). **D:** Half-maximal activation voltage (V_{50}). No differences were observed (one-way ANOVA; F(2, 21)=0.5722; P=0.5728). **E:** Slope of activation. Significantly increased in Kv3.3/Kv3.4 fast compared to Kv3.3 WT (one-way ANOVA, Tukey's post hoc, P=0.0003). Variance plotted as SEM.

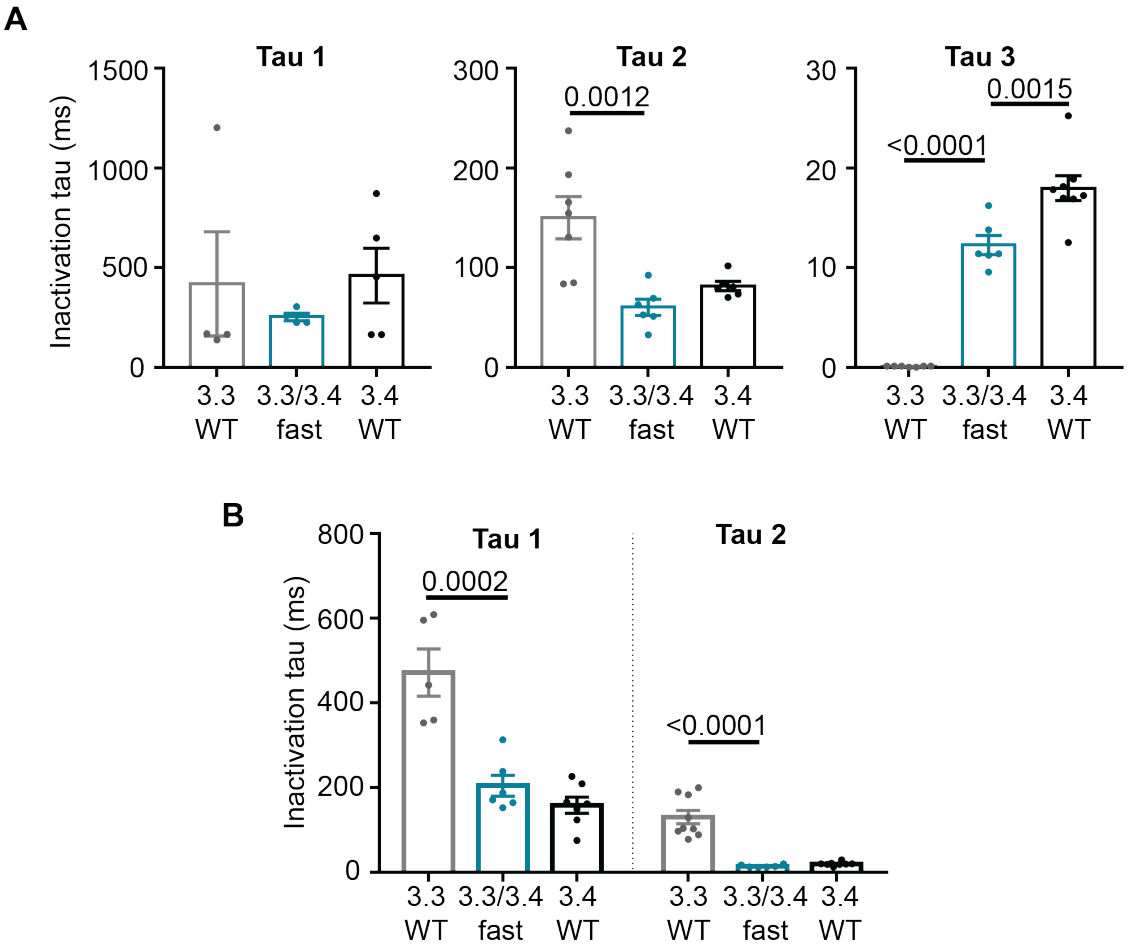

Figure 7.18: **Inactivation of Kv3.3/Kv3.4 fast currents at +50mV has three components.** Inactivation of Kv3.3/Kv3.4 fast currents, Kv3.3 WT and Kv3.4 WT were each fitted with triple and double exponential functions. **A:** Inactivation time constant. Triple exponential functions were fitted to the decaying current at +50mV, three time constants are reported on graph. Tau 3 was significantly slower in Kv3.3/Kv3.4 fast and Kv3.4 WT compared to Kv3.3 WT (one-way ANOVA, Tukey's post hoc, P values on graph. **B:** Inactivation time constant. Double exponential function fitted to decaying phase of current. Both the slow (tau 1) and fast (tau 2) time constants of Kv3.3/Kv3.4 fast cells were significantly faster than Kv3.3 WT (one-way ANOVA, Tukey's post hoc, P values on graph). Variance plotted as SEM.

7.5.5 Kv3.3/Kv3.4 slow cells

Kv3.3/Kv3.4 slow cells had currents very similar to Kv3.3 WT, however a distinct fast-inactivating component was present, that was never observed in Kv3.3 WT cells (figure 7.19). Current properties in these cells are suggestive of either heteromers in a 3:1 Kv3.3:Kv3.4 ratio or homomers with a larger population of Kv3.3 channels.

These cells had activation curves, activation voltages and V_{50}s similar to Kv3.3 WT, although the slope of activation was significantly different from both Kv3.3 and Kv3.4 WT (one-way ANOVA, Tukey's post hoc; Kv3.3/Kv3.4 slow vs Kv3.3 WT P=0.0487; Kv3.3/Kv3.4 slow vs Kv3.4 WT P=0.0411; figure 7.19). Additionally the voltage of activation was significantly more positive than Kv3.4 WT (one-way ANOVA, Tukey's post hoc, P=<0.0001).

Similar to the other two categories, the inactivation of these currents at +50mV was fit best with a triple exponential, yielding a fast (tau 3) tau that was significantly slower than both Kv3.3 and Kv3.4 WTs (Kv3.3 WT 0.1 ±0.02ms, n=10; Kv3.3/Kv3.4 slow 24.2 ±1.6ms n=5; Kv3.4a 18.0 ±1.2ms n=8; one-way ANOVA, Tukey's post hoc, vs Kv3.3 WT P=<0.0001, vs Kv3.4 WT P=0.0035; figure 7.20) in addition to a middle time constant that was slower than Kv3.4 but similar to Kv3.3 WT (Kv3.3 WT 150 ± 21ms; Kv3.3/Kv3.4 slow 161 ± 28.2ms; Kv3.4 WT 82 ±4.5ms; one-way ANOVA, Tukey's post hoc, vs Kv3.4 WT P=0.0406). When fitted with a double exponential these cells had a slow time constant that was significantly slower than Kv3.4 WT but similar to Kv3.3 WT (Tau_{slow}, Kv3.3 WT 472 ±55ms; Kv3.3/Kv3.4 slow 329 ±50.7ms; Kv3.4 WT 158 ±19.2ms; one-way ANOVA, Tukey's post hoc, vs Kv3.4 WT P=0.0229) and a fast time constant that was significantly faster than Kv3.3 WT but similar to Kv3.4 WT (Tau_{fast}, Kv3.3 WT 130 apm15.9ms; Kv3.3/Kv3.4 slow 34.5 ±3.1ms; Kv3.4 WT 19.7 ±1.6ms; one-way ANOVA, Tukey's post hoc, vs Kv3.3 P=<0.0001).

These cells also had large steady-state currents that were of similar amplitudes to those observed in Kv3.3 WT (figure 7.21). Activation curves produced from these currents were similar to Kv3.3 WT, yielding a similar V50 and slope of activation (figure 7.21).

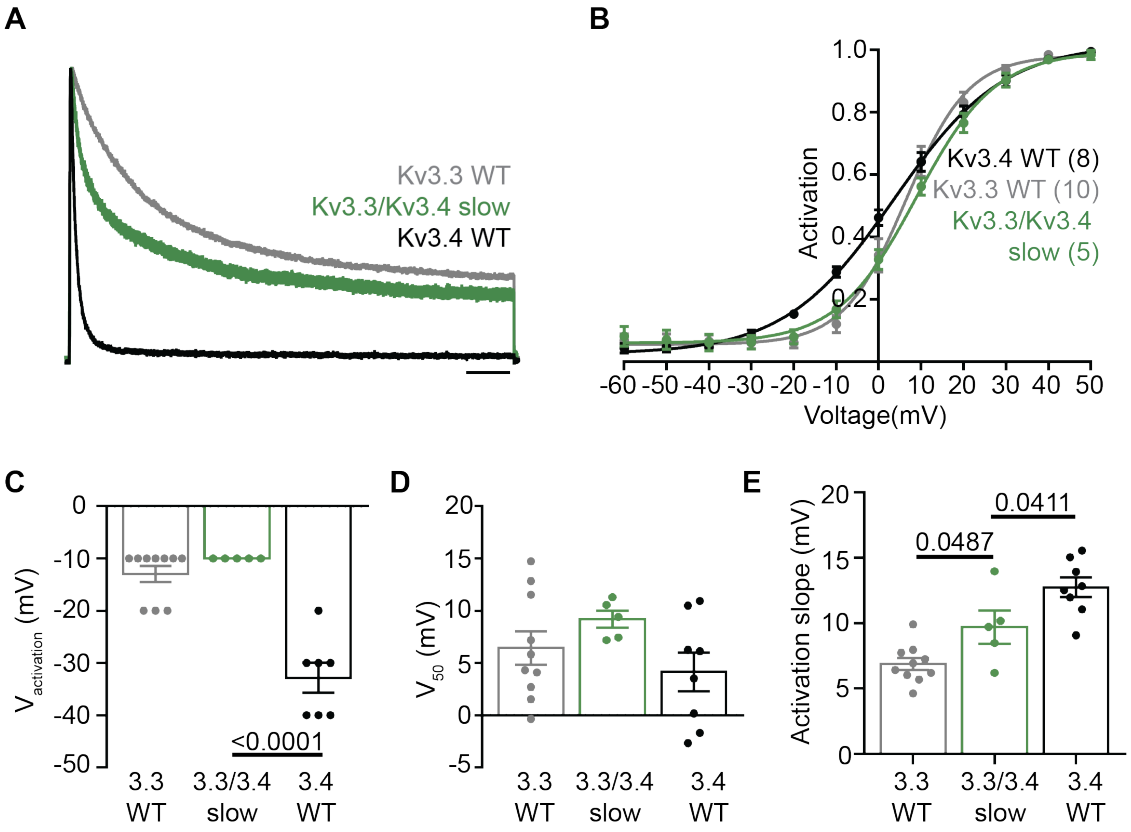

Figure 7.19: **Kv3.3/Kv3.4 slow cells display current kinetics similar to Kv3.3 WT A:** Example current traces recorded from Kv3.3 WT (grey; CHO Kv3.3), Kv3.4 WT (black; CHO K1 transfected with Kv3.4) and Kv3.3/Kv3.3 fast cells (green; CHO Kv3.3 transfected with Kv3.4) in response to a 1s +50mV voltage step. Currents have been normalised to the peak. **B:** Activation curves with number of cells in brackets. **C:** Voltage at which cells begin to activate. $V_{activation}$ in Kv3.3/Kv3.4 slow cells was significantly more positive than Kv3.4 WT (one-way ANOVA, Tukey's post hoc, P=<0.0001). **D:** Half-maximal activation voltage (V_{50}). No differences were observed (one-way ANOVA; F(2,20)=1.807; P=0.1899). **E:** Slope of activation. Significantly different in Kv3.3/Kv3.4 slow compared to both Kv3.3 and Ks3.4 WTs (one-way ANOVA, Tukey's post hoc, P values on graph). Variance plotted as SEM.

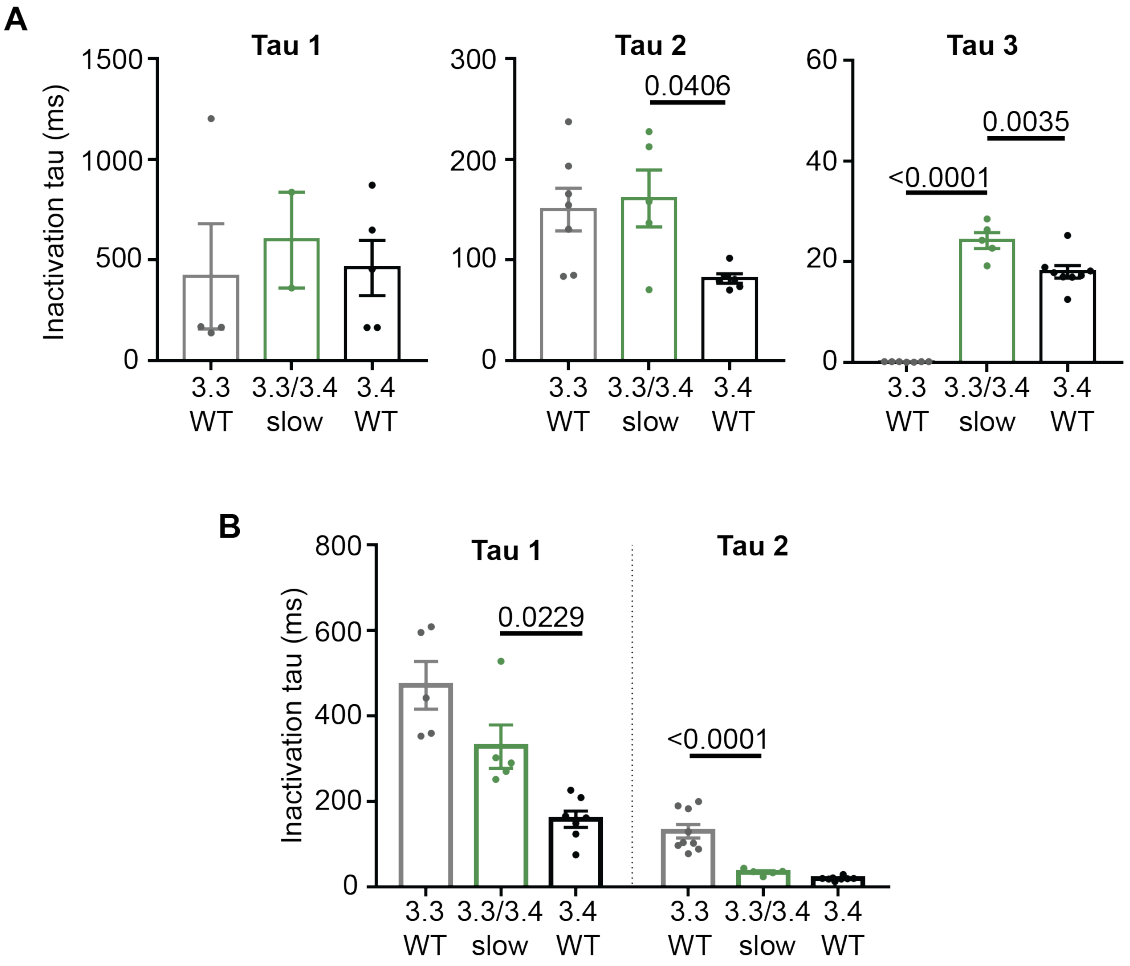

Figure 7.20: **Inactivation of Kv3.3/Kv3.4 slow currents at +50mV has three components.** Inactivation of Kv3.3/Kv3.4 slow currents, Kv3.3 WT and Kv3.4 WT were each fitted with triple and double exponential functions. **A:** Inactivation time constant. Triple exponential functions were fitted to the decaying current at +50mV, three time constants are reported on graph. Tau 3 was significantly slower in Kv3.3/Kv3.4 slow compared to Kv3.3 WT and Kv3.4 WT (one-way ANOVA, Tukey's post hoc, P values on graph. **B:** Inactivation time constant. Double exponential function fitted to decaying phase of current. Slow time constants (tau 1) of Kv3.3/Kv3.4 slow were significantly slower than Kv3.4 WT and fast (tau 2) time constants of Kv3.3/Kv3.4 slow cells were significantly faster than Kv3.3 WT (one-way ANOVA, Tukey's post hoc, P values on graph). Variance plotted as SEM

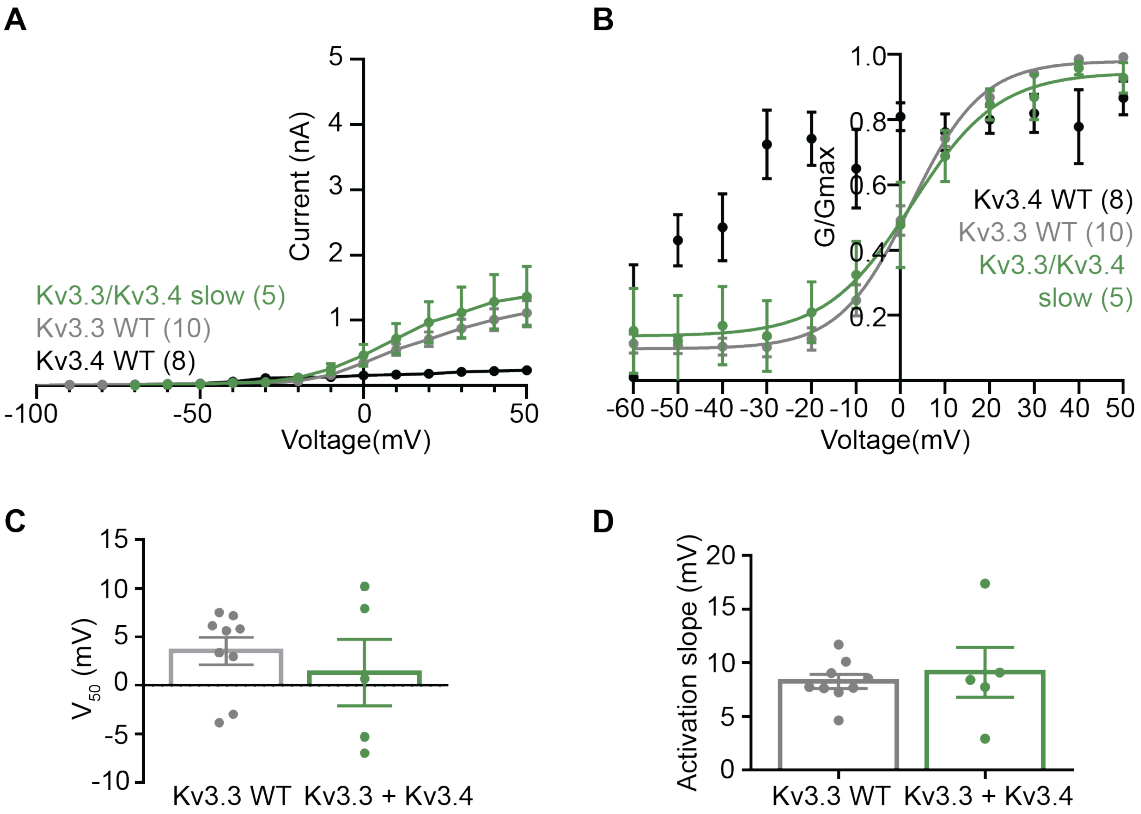

Figure 7.21: **Steady-state currents of Kv3.3/Kv3.4 slow cells are not different to those in Kv3.3 WT. A:** I-V plot of currents measured at the end of a 1s voltage protocol as seen in figure 7.1. **B:** Activation curves for these steady-state currents. Conductance was calculated and normalised to the maximum value. Data was fitted with a Boltzmann function. **C:** Half-maximal activation measured from activation curves fitted to individual cells. No differences were observed (unpaired t-test; t=0.7116 df=12, P=0.4903). **D:** Slope of activation. No differences were observed (unpaired t-test; t=0.4513 df=12, P=0.6598). Variance plotted as SEM.

7.5.6 Kv3.4 does not co-immunoprecipitate with Kv3.3

While this electrophysiological data was interesting, it was difficult to determine whether these subunits were actually forming heteromeric channels or whether these changes in currents were due to different sized populations of homomeric Kv3.3 and Kv3.4 WT channels. In order to gain some clarity, co-immunoprecipitation studies were performed on these CHO Kv3.3 cells transfected with Kv3.4a DNA to determine whether these subunits do indeed interact. Cells were transfected with 1μg Kv3.4a DNA 72 hours prior to the co-immunoprecipitation procedure to allow sufficient time for channels to be expressed. This also matched with one time point at which electrophysiological recordings were made. Isotype control antibodies were also used to highlight non-specific binding of the primary antibody to proteins in the sample. These antibodies are raised in the same species as the primary antibodies, in this case rabbit (anti-Kv3.3) and sheep (anti-Kv3.4a) but lack specificity to target protein.

Kv3.3 protein was successfully immunoprecipitated and produced a band at $\sim$ 80KDa when the membrane was exposed to an anti-Kv3.3 antibody. Similarly, Kv3.4a protein was successfully immunoprecipitated using a Kv3.4a specific antibody and produced a band at $\sim$ 85KDa when the membrane was incubated with an anti-Kv3.4a antibody. However, Kv3.4 was not co-immunoprecipitated with Kv3.3 nor was Kv3.3 protein co-immunoprecipitated with Kv3.4 (figure 7.22). Upon a higher exposure, a faint band was seen with the Kv3.4a antibody in the Kv3.3 immunoprecipitate (figure 7.22), however this was not seen when the co-immunoprecipitation protocol was repeated, nor was it seen when cells were lysed at 24 or 48 hours post-transfection.

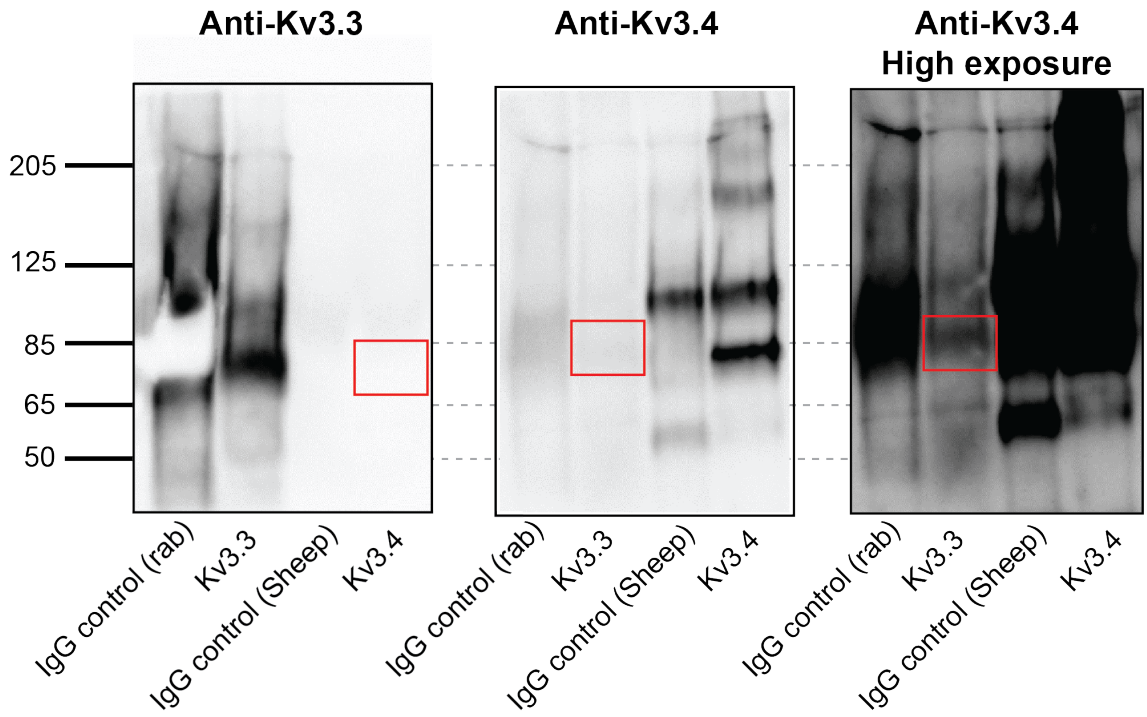

Figure 7.22: **Kv3.4 protein does not co-immunoprecipitate with Kv3.3.** Kv3.3 expressing CHO cells were transfected with Kv3.4a DNA 72hrs prior to protein extraction. **Left:** Western blot with anti-Kv3.3 antibody on a membrane containing protein samples from immunoprecipitation with an rabbit IgG isotype control, Kv3.3, sheep IgG isotype control and Kv3.4 antibodies. Molecular weights determined using a prestained protein ladder are indicated on the left. **Middle** The western blot membrane stained with an anti-Kv3.3 antibody was stripped and re-incubated with an anti-Kv3.4a antibody. This is shown with a higher exposure on the right. Red squares indicate the expected position of a co-immunoprecipitated band.

7.5.7 Kv3.3 and Kv3.4 are not colocalised

To corroborate results of co-immunoprecipitation, immunohistochemistry was also carried out on CHO cells expressing both Kv3.3 and Kv3.4. All cells appeared to express both subunits, suggesting a 100% transfection success, although the presence of Kv3.3-like and Kv3.4-like cells detected with electrophysiology suggests that the protein may not be forming functional channels on the membrane, even if it is present. While the subunits did appear to co-localise in some areas of cells (white arrow figure 7.23), more often than not fluorescence did not overlap. Interestingly, Kv3.4a subunits often showed a highly polarised expression, with high densities in one side of the cell, whereas Kv3.3 expression was more uniform across each cell (figure 7.23).

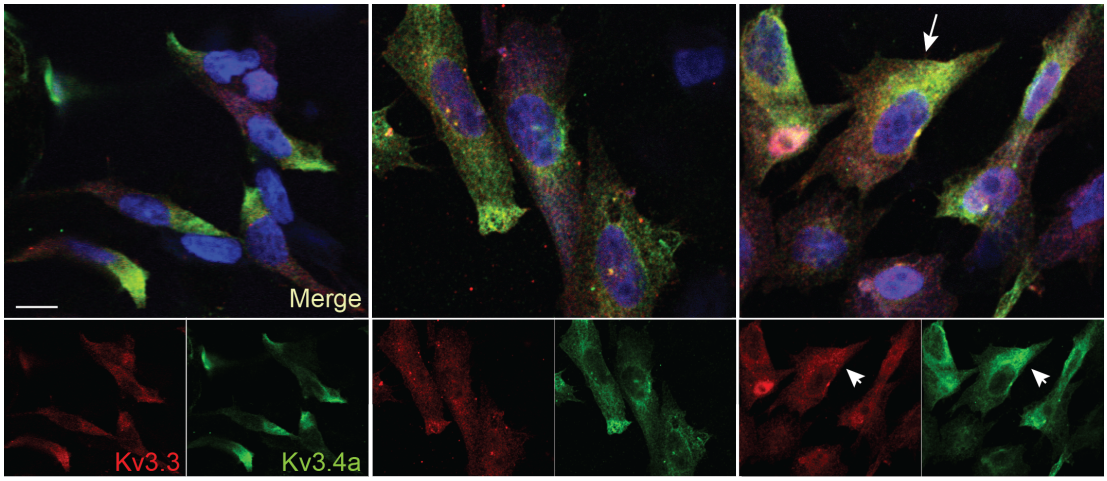

Figure 7.23: **Kv3.3 and Kv3.4 subunits do not co-localise.** Immunohistochemical staining of Kv3.3 CHO cells transfected with Kv3.4 DNA. Red=Kv3.3. Green=Kv3.4a. Each image was taken from a separate coverslip on which CHO cells were grown. Scale bar=10μm. Photos by Angela Chiavegato.

7.6 Co-expression of Kv3.3 and Kv3.1b

In contrast to co-expression of Kv3.4 and Kv3.3, transfecting CHO cells with Kv3.1b DNA yielded only two types of current which have been named Kv3.1/Kv3.3 fast and Kv3.1/Kv3.3 slow which are similar to, but not the same as, Kv3.3 and Kv3.1 WTs, respectively. Kv3.3 WT and Kv3.1 WT cells have currents with remarkably similar features (figure 7.24), with the only observable difference being the extent and rate at which channels inactivate during a 1s voltage step to +50mV (figure 7.25).

The similarities between the two wildtype channels meant that few differences were observed between wildtype cells and cells co-expressing Kv3.3 and Kv3.1b. Activation curves for all cells were remarkably similar and yielded very similar activation voltages, V_{50}s and slopes of activation (figure 7.24). Despite this, differences were observed in the rate of inactivation of these channels.

Kv3.1/Kv3.3 slow channels exhibited inactivation at +50mV similar to Kv3.1b WT channels, and consequently could be fit with a single exponential that yielded a time constant that was significantly slower than Kv3.3 WT cells (Tau, Kv3.3 WT 219 ±2.4ms (n=10); Kv3.1/Kv3.3 slow 481 ±98.7 (n=8); Kv3.1 WT 1216 ±216ms (n=10); one-way ANOVA, Tukey's post hoc, P=0.0043; figure 7.25A). In contrast, Kv3.1/Kv3.3 fast inactivation was best fit with a double exponential and yielded a fast time constant that was significantly different from both Kv3.1 and Kv3.3 WTs (Tau_{fast}, Kv3.3 WT 130 ±15.9ms (n=9); Kv3.1/Kv3.3 fast 88.9 ±3.5ms; Kv3.1 WT 0.09 ±3.5ms; one-way ANOVA, Tukey's post hoc, Vs Kv3.1 WT P=<0.0001; vs Kv3.3 WT P=0.0234; figure 7.25B). In addition the contribution of this fast component to the overall inactivation is significantly lower than in Kv3.3 WTs (Kv3.3 WT 40.5 ±4.2%; Kv3.1/Kv3.3 fast 26.6 ±3.9%; unpaired t-test, t=2.44 df=15, P=0.0276; figure 7.25D). Despite Kv3.1/Kv3.3 slow cells showing an inactivation time constant similar to Kv3.1 WT, currents in both these and Kv3.1/Kv3.3 fast cells inactivate to a larger extent during the 1s voltage step compared to Kv3.1b WT (one-way ANOVA, Tukey's post hoc, Kv3.1/Kv3.3 slow vs Kv3.1 WT P=0.0010;

Kv3.1/Kv3.3 fast vs Kv3.1 WT P=<0.0001; figure 7.25C).

Steady-state currents in both Kv3.1/Kv3.3 slow and fast were similar in amplitude to Kv3.3 WT and smaller than Kv3.1 WT however, activation curves produced from these currents were similar in all groups and yielded no significant differences in V50s and slopes of activation (figure 7.26).

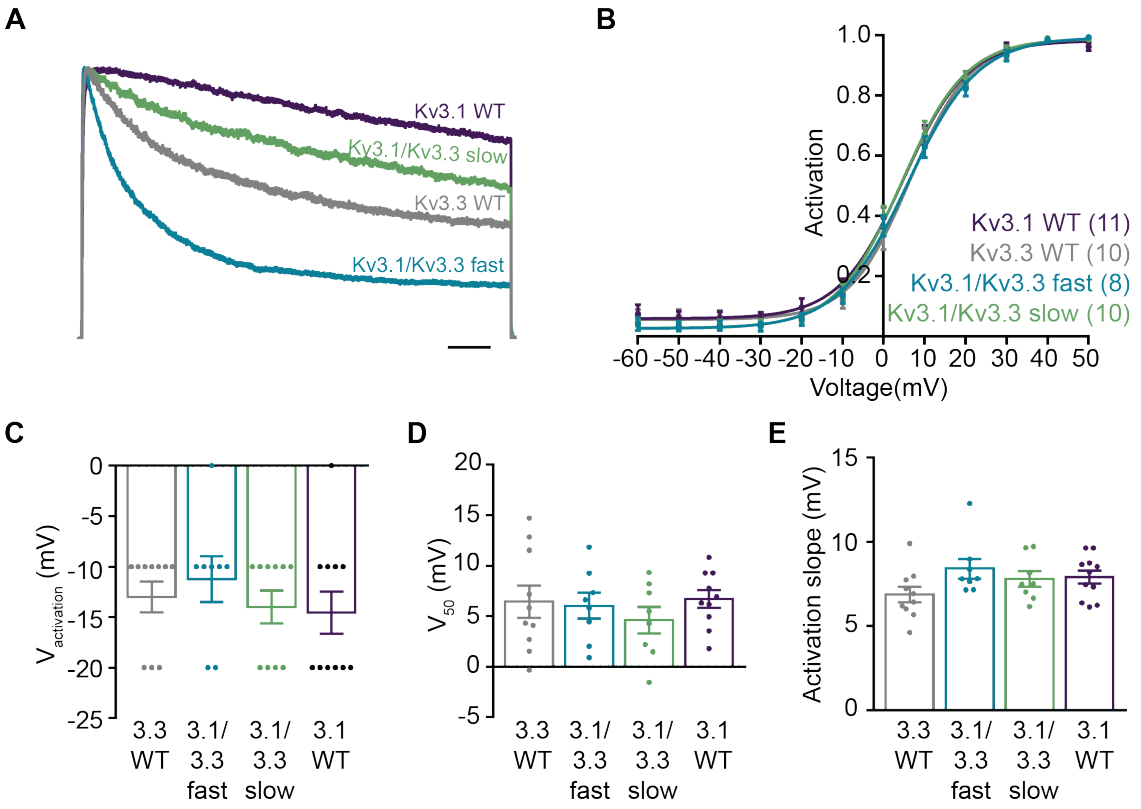

Figure 7.24: **Kv3.1/Kv3.3 slow and fast cells display current kinetics similar to both Kv3.3 and Kv3.1 WT A:** Example current traces recorded from Kv3.3 WT (grey; CHO Kv3.3), Kv3.1 WT (purple; CHO K1 transfected with Kv3.1), Kv3.1/Kv3.3 fast (blue; CHO Kv3.3 transfected with Kv3.1) and Kv3.1/Kv3.3 slow cells (green; CHO Kv3.3 transfected with Kv3.1b) in response to a 1s +50mV voltage step. Currents have been normalised to the peak. **B:** Activation curves with number of cells in brackets. **C:** Voltage at which cells begin to activate. No differences were observed between groups (one-way ANOVA, F(3,35)=0.5441, P=0.6554). **D:** Half-maximal activation voltage (V_{50}). No differences were observed (one-way ANOVA; F(3,32)=0.4894; P=0.6921). **E:** Slope of activation. No differences observed (one-way ANOVA, F(3,33)=1.849, P=0.1575). Variance plotted as SEM. 6 data points contributed by Michele.

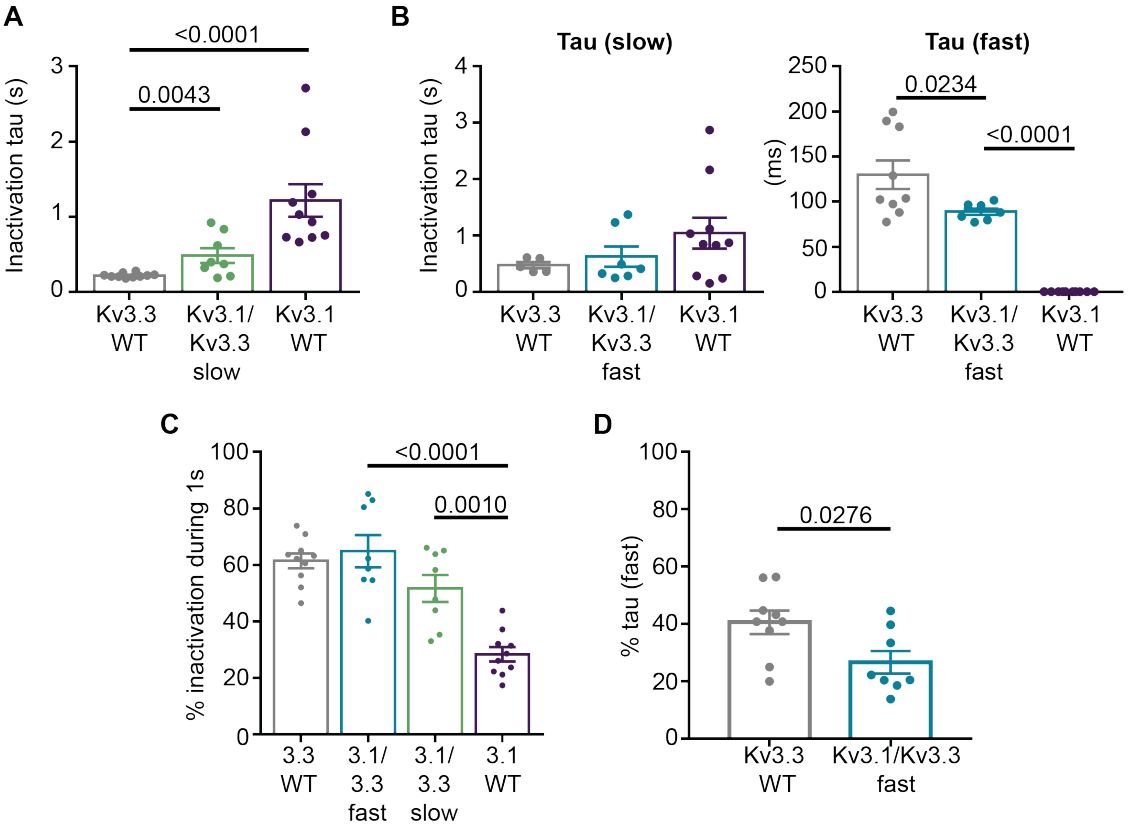

Figure 7.25: **Kv3.1/Kv3.3 slow cells have a similar inactivation time constant to Kv3.1 WT and Kv3.1/Kv3.3 fast cell have similar time constants to Kv3.3 WT. A:** Inactivation time constant for Kv3.1/Kv3.3 slow cells. Inactivation of Kv3.1/Kv3.3 slow currents at +50mV were fit with a single exponential and were significantly slower than Kv3.3 WT (one-way ANOVA, Tukey's post hoc, P values on graph). **B:** Inactivation time constant for Kv3.1/Kv3.3 fast cells. Inactivation of Kv3.1/Kv3.3 fast currents at +50mV were fit with a double exponential and had a fast time constant that was significantly different from both Kv3.3 and Kv3.1 WT (one-way ANOVA, Tukey's post hoc, P values on graph). **C:** Percent of inactivation, measured as steady-state current amplitudes at +50mV as a percentage of peak current amplitudes. Both Kv3.1/Kv3.3 slow and fast cells exhibit higher levels of inactivation compared to Kv3.1 WT (one-way ANOVA, Tukey's post hoc, P values on graph. **D:** Percent contribution of fast tau to inactivation in Kv3.1/Kv3.3 and Kv3.3 WT cells. This is significantly lower in Kv3.1/Kv3.3 fast cells (unpaired t-test, t=2.44 df=15, P=0.0276). Variance plotted as SEM.

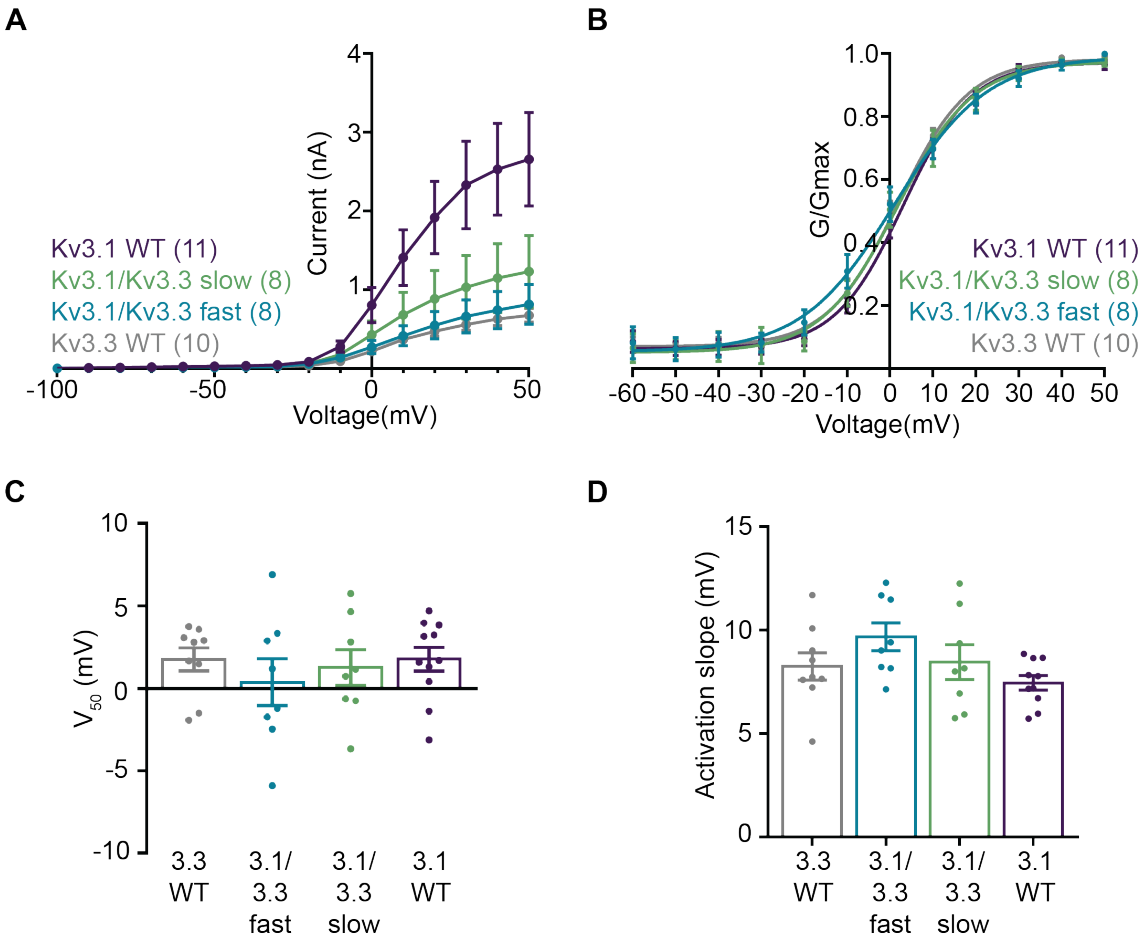

Figure 7.26: **Steady-state currents of Kv3.1/Kv3.3 slow and fast cells are not different to those in Kv3.3 or Kv3.1 WT A:** I-V plot of currents measured at the end of a 1s voltage protocol as seen in figure 7.1. **B:** Activation curves for these steady-state currents. Conductance was calculated and normalised to the maximum value. Data was fitted with a Boltzmann function. **C:** Half-maximal activation measured from activation curves fitted to individual cells. No differences were observed (one-way ANOVA; $F(3,32)=0.4364$, $P=0.7284$). **D:** Slope of activation. No differences were observed (one-way ANOVA; $F(3,31)=2.147$, $P=0.1144$). Variance plotted as SEM.

7.6.1 Steady-state inactivation

While few differences were observed between activation parameters in Kv3.1/Kv3.3 slow and fast cells, differences were present in steady-state inactivation. Inactivation curves produced from both of these groups were shifted negatively compared to both Kv3.3 and Kv3.1 WT cells (figure 7.27B). Inactivation V50s observed were significantly more negative in both groups than Kv3.1b WT at -25 ±2.7mV (n=3) in Kv3.1/Kv3.3 fast (n=3) and -24 ±1.9mV in Kv3.1/Kv3.3 slow (n=2) compared to -19 ±0.8mV in Kv3.3 WT (n=5) and -12 ±1.7mV in Kv3.1 WT (one-way ANOVA, Tukey's post hoc, Kv3.1/Kv3.3 fast vs Kv3.1b P=0.0025; Kv3.1/Kv3.3 slow vs Kv3.1 P=0.0085; figure 7.27C). However, due to low n number these results have to be taken with caution.

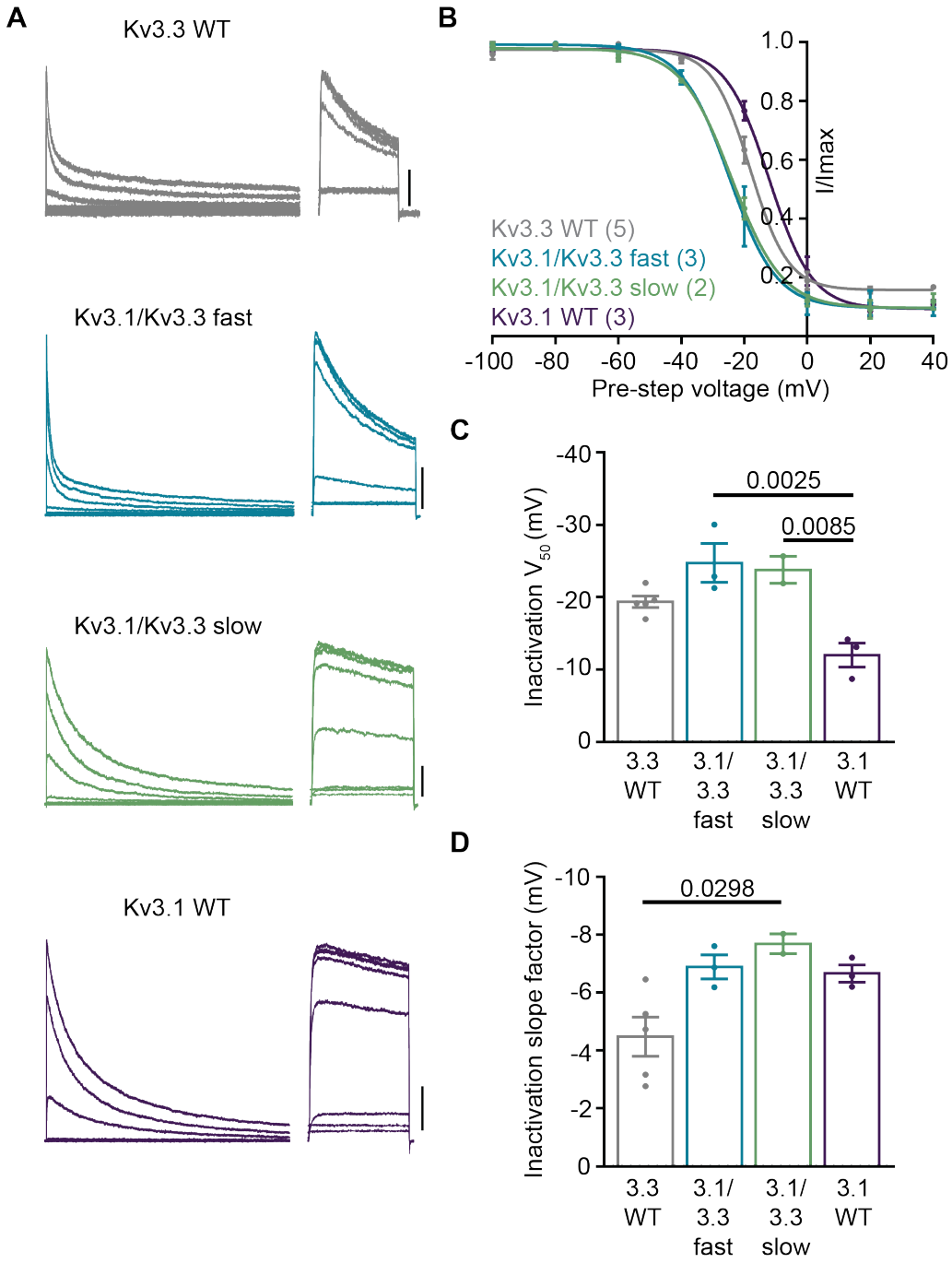

Figure 7.27: **Inactivation curves of Kv3.1/Kv3.3 fast and slow cells are shifted to more negative potentials compared to both Kv3.3 and Kv3.1 WT cells. A:** Example traces recorded from CHO cells expressing Kv3.3, Kv3.1 or co-expressing both subunits in response to an inactivation voltage protocol described in text. Scale bar= 1nA. **B:** Inactivation curves from normalised currents measured during the test step and plotted against pre-step voltage. Average data plotted from cells and fit with a Boltzmann function. Number of cells in brackets. **C:** Half-inactivation voltage (V_{50}). V_{50} is at significantly more negative voltages in Kv3.1/Kv3.3 fast and slow cells compared to WT (one-way ANOVA, Tukey's post hoc, P values on graph). **D**: Slope of inactivation, significantly steeper in Kv3.3 WT compared to Kv3.1/Kv3.3 fast cells (one-way ANOVA, Tukey's post hoc, P=0.0298). Variance plotted as SEM. Michele contributed 2 data points.

7.6.2 Kv3.1 co-immunoprecipitates with Kv3.3

To determine whether Kv3.1b and Kv3.3 interact, co-immunoprecipitation was carried out on CHO Kv3.3 cells tranfected with Kv3.1b. Kv3.1b DNA (1ug) was transfected into CHO Kv3.3 cells 48hrs prior to protein extraction for the co-immunoprecipitation protocol. Antibodies were also tested on samples containing only Kv3.3, Kv3.1 and both Kv3.3 and Kv3.1 to ensure that both the anti-Kv3.1b and anti-Kv3.3 antibodies did not recognise the other subunit. While no band was seen in samples containing only Kv3.3 when incubated with the Kv3.1b antibody (data not shown), a band did appear in samples containing only Kv3.1b when membranes were incubated with a anti-Kv3.3 antibody, suggesting that the Kv3.1b antibody is specific for Kv3.1b but the Kv3.3 antibody may recognise both Kv3.3 and Kv3.1b.

Kv3.1b was immunoprecipitated with our Kv3.1b antibody, indicated by a band at ∼85KDa when samples were loaded on a western blot and incubated with an anti-Kv3.1b antibody. Interestingly, a band was also produced with the anti-Kv3.1b antibody when Kv3.3 was immunoprecipitated, suggesting Kv3.1b was pulled down with Kv3.3 (figure 7.28 red square on left).

Kv3.3 protein was also immunoprecipitated with our Kv3.3 antibody and produced a band on a western blot at ∼80KDa when incubated with an anti-Kv3.3 antibody (figure 7.28 right). A band was also produced with the anti-Kv3.3 antibody in the Kv3.1b immunoprecipitated sample, again suggesting that Kv3.3 was pulled down with Kv3.1b (figure 7.28 red square on right).

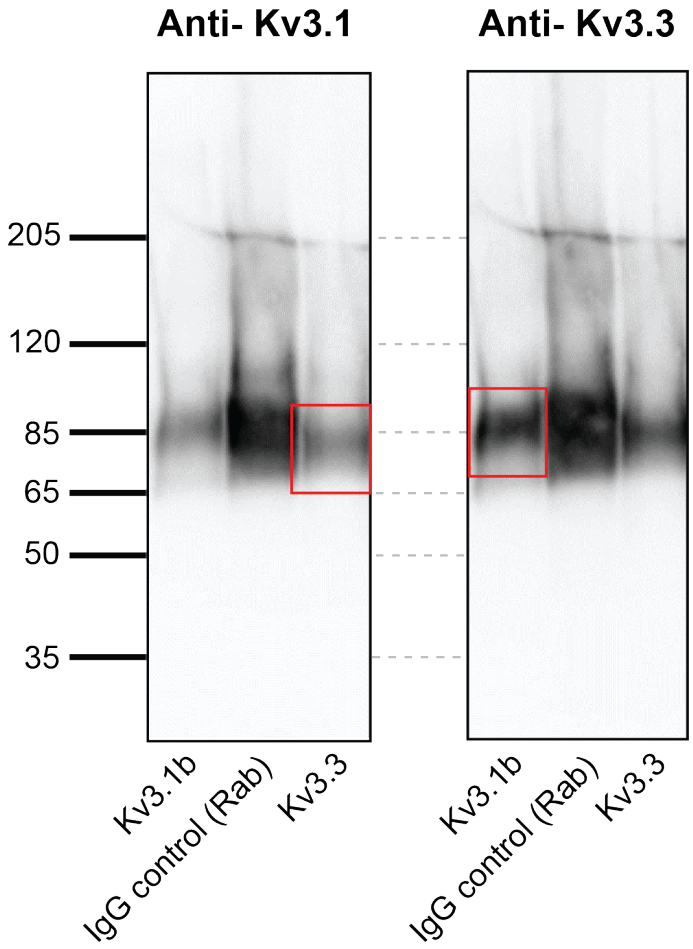

Figure 7.28: **Kv3.1b is co-immunoprecipitated with Kv3.3 in CHO cells. Left:** Western blot incubated with anti-Kv3.1b antibody. 50uL samples were loaded containing CHO Kv3.3 transfected with Kv3.1b DNA immunoprecipitated with anti Kv3.1b (left lane), rabbit igG isotype control antibody (middle lane) and anti-Kv3.3 (right lane). **Right:** Western blot incubated with anti-Kv3.3 antibody. The blot incubated with Kv3.1b was stripped and re-incubated with an anti-Kv3.3 antibody. Red squares indicates expected position of co-immunoprecipitated band.

7.7 Discussion

The formation of heteromeric ion channels has often been used to explain discrepancies between biophysical properties of homomeric Kv3 channels expressed in cell lines and those encountered in native tissue. Despite this, little practical evidence exists showing that different Kv3 subunits can associate and form functional channels. In this chapter we explored whether heteromeric Kv3 channels can indeed form in CHO cell lines, using electrophysiology and co-immunoprecipitation of Kv3.3 stable CHO cell lines transfected with Kv3.4a or Kv3.1b subunit DNA. The results presented here suggest that while Kv3.3 and Kv3.1b appear to interact, this doesn't seem to be the case with Kv3.3 and Kv3.4a subunits.

7.7.1 Properties of Kv3.3, Kv3.1b and Kv3.4a homomeric channels

Biophysical properties of Kv3.3 and Kv3.1b channels were remarkably similar when subunits were expressed alone in CHO cells, with the only observable difference being faster inactivation of Kv3.3 homomers during prolonged depolarisation. In contrast, Kv3.4 channels activated and inactivated at more negative voltages than both Kv3.1 and Kv3.3 as well as having a weaker voltage-dependence of activation and fully inactivating within 250ms of prolonged depolarisation.

It is important to note that inactivation observed in Kv3.3 WT cells is isoform-specific, governed by the presence of an N-terminal inactivation peptide (Fernandez et al. 2003). There is no evidence of an inactivating component in potassium currents recorded from either MNTB or LSO neurons, suggesting that this isoform is not present in these cells within mice.

Half-maximal activation values observed in the current study were slightly more negative than those in published literature at +6mV for Kv3.1b compared to +21mV (Macica et al. 2003) and +5mV for Kv3.3 compared to 19-30mV (Zhang et al. 2016; Desai et al. 2008), although this is likely to reflect differences in the species from which the subunit DNA was cloned (mouse Kv3.3 and Kv3.1b in published literature and human in the present study).

Interestingly, the more negative activation voltage observed in Kv3.4a WTs may also be isoform-specific as both Kv3.4b and c activate at voltages similar to Kv3.1 and Kv3.3 (Baranauskas et al. 2003; Rudy and McBain 2001).

This not only shows the importance of different Kv3 subunits but also isoforms in determining the biophysical properties of functional channels in native neurons. Although, the subtle differences observed between Kv3.1 and Kv3.3 subunits here makes it unlikely that the formation of heteromeric channels with these subunits would lead to big changes in potassium conductance and as discussed in chapter 1 may instead dictate the binding of second messengers.

7.7.2 Do Kv3.3 subunits form heteromeric channels?

Evidence for the formation of Kv3 heteromers is scarce, partially due to the difficulty of interpreting electrophysiological data gained from expressing two different subunits in an expression system. Determining whether the results are due to different sized populations of homomers, the formation of heteromers or a mixture of the two is incredibly difficult, especially when only subtle differences are observed between homomeric channels of the two subunits. By combining electrophysiology with co-immunoprecipitation and immunohistochemistry in this study we have attempted to consolidate results and provide clearer answers.

The presence of so many different populations of cells possessing different current properties when Kv3.4a is transfected into CHO Kv3.3 cells suggests that even if Kv3.4/Kv3.3 heteromeric channels do form, they are clearly not the 'favoured' confirmation. This is consolidated by the absence of a band in the co-immunoprecipitation study and the lack of overlap between the subunits observed with immunohistochemistry. While some heteromeric channels may exist, the changes in activation of channels when both Kv3.4 and Kv3.3 are expressed can likely be explained by the presence of homomers in different ratios (1:1 in Kv3.3 + Kv3.4 cells; 1:3 Kv3.3 to Kv3.4 in Kv3.3/Kv3.4 fast and 3:1 in Kv3.3/Kv3.4 slow) with the kinetics of highest expressed subunit dominating the overall current.

This is in contrast to Kv3.3 cells transfected with Kv3.1b. Not only were fewer

populations of cells produced but both groups (Kv3.1/Kv3.3 slow and fast) displayed a negative shift in steady-state inactivation that could not be explained by populations of homomeric channels. Additionally both subunits could be co-immunopreciptated with the other, suggesting interactions between them do occur.

While Kv3.3 subunits may form heteromeric channels with Kv3.1b, it is unlikely this is the case with Kv3.4a. That is not to say that other Kv3.3 and Kv3.4 isoforms do not interact, nor does the interaction between Kv3.1 and Kv3.3 observed here necessarily mean that this occurs in native mammalian neurons, although Kv3.1 subunits have previously been shown to interact with both Kv3.3 and Kv3.4 in rodent neurons (Chang et al. 2007; Baranauskas et al. 2003).

7.8 Summary

- Kv3.1b currents activate at ∼-10mV and show little inactivation during prolonged depolarisation
- Kv3.3 currents activate at ∼-20mV and show slow, partial inactivation.
- Kv3.4a currents activate at ∼-40mV and display rapid, full inactivation.
- Co-expressing Kv3.3 and Kv3.4a subunits yields 5 distinct populations of cells with different current kinetics, all intermediate to Kv3.3 and Kv3.4a homomers.
- Kv3.4a is not co-immunoprecipitated with Kv3.3, nor do the subunits co-localise.
- Co-expressing Kv3.3 and Kv3.1b yields two populations of cells with activation properties intermediate to Kv3.3 and Kv3.1b homomers and steady-state inactivation properties distinctly different to homomeric channels.
- Kv3.1b is co-immunoprecipitated with Kv3.3 subunits.

Chapter 8

Final conclusions and future directions

The aim of this thesis was to assess contributions of individual subunits to the formation and function of Kv3 potassium channels, using the auditory pathway as a model. In particular, we wished to study the composition of presynaptic Kv3 channels at the calyx of Held and investigate the role these channels play in modulating neurotransmission.

Furthermore, we sought to identify changes to electrical excitability of neurons in mice carrying a Kv3.3^{R420H} mutation within the KCNC3 gene and examine changes during the time-course of disease progression.

While the presence of Kv3 channels in auditory brainstem neurons has previously been described (Brew and Forsythe 1995; Wang et al. 1998; Macica et al. 2003), the contributions of individual subunits is relatively unknown. This work is the first to identify particular roles of Kv3.1 and Kv3.3 in the MNTB, LSO and calyx of Held and also provides the first experimental evidence describing the effects of the Kv3.3^{R420H} mutation on Kv3 channel function in an intact mammalian model.

8.1 Main findings

- Kv3.1 and Kv3.3 are equally important for AP repolarisation in MNTB neurons; Kv3.3 dominates in LSO neurons and at the calyx of Held.
- Kv3.3 limits transmitter release from the calyx of Held ensuring reliable release during high frequency.
- Transmitter release at the calyx of Held is enhanced in Kv3.1 KOs during high frequency stimulation.
- Kv3.3 is non-functional in mice harbouring an SCA13 (R420H) mutation.
- Kv3.3 subunits associate with Kv3.1 but not with Kv3.4.

8.2 Role of Kv3 channels in cell excitability

Kv3 channels are particularly important in producing brief action potentials, preventing prolonged inactivation of sodium channels, resulting in neurons that can fire high frequency APs (Wang et al. 1998; Macica et al. 2003). Despite previous reports identifying Kv3.1 as the sole contributor to Kv3 currents in the MNTB (Macica et al. 2003) we show that Kv3.3 also has an important role. Indeed, both Kv3.1 and Kv3.3 equally contribute to Kv3 currents in the MNTB shown by increased action potential duration in MNTB neurons of both Kv3.1 and Kv3.3 KOs (chapter 3 discussion). In addition, Kv3.3 subunits appear to mediate the majority of Kv3 current in the LSO and calyx of Held terminal with dramatic increases in AP duration observed in both areas and little to no increase seen in Kv3.1 KOs (chapter 3 and 4, respectively).

Kv3.3 is not only essential for maintaining normal AP waveform in the brainstem but the involvement of Kv3.3 subunits in SCA13 highlights just how important this subunit is throughout the brain. Similar to LSO neurons, Kv3 currents in Purkinje cells of the cerebellum are dominated by Kv3.3 where it is required for complex spiking (Hurlock, McMahon, and Joho 2008) and normal motor function. An absence of Kv3.3 results in drastic changes to AP waveform, consistent with the effect observed in the LSO and indicates that, like the LSO, other Kv3 subunits cannot compensate for the lack of Kv3.3 in these neurons. Thus, a disruption to Kv3.3 subunits leads to a vastly reduced Kv3 current in these neurons, creating severe motor abnormalities. While the auditory phenotype associated with the loss of Kv3.3 in the brainstem is much less severe, disruption of precise AP timing in this region likely explains sound localisation deficits seen in SCA13 patients (Middlebrooks et al. 2013).

8.3 Role of Kv3 in modulating transmission

Small changes in action potential waveform can have a large impact on calcium entry into a presynaptic terminal and consequently, transmitter release from the synapse (Sabatini and Regehr 1997; Yang and Wang 2006).

The present study has highlighted a particular role of Kv3.3 subunits in maintaining brief action potentials at the calyx of Held terminal, limiting transmitter release and thus maintaining faithful transmission during high frequency stimulation. Kv3.3 KOs display long presynaptic action potentials, associated with large initial EPSCs in postsynaptic MNTB neurons and increased short term depression of EPSC amplitude during high frequency stimulation (chapter 4).

The role of Kv3.1 subunits in the presynaptic terminal is less clear. Kv3.1 KO mice display similar initial EPSC amplitudes to wildtype mice but subsequent EPSCs during high frequency stimulation appear to show less short term depression, resulting in a larger number of quanta (vesicle) released during a stimulation train in comparison to both Kv3.3 and WT mice. It is possible that Kv3.3 homomeric channels (only seen in Kv3.1 KOs) inactivate over time, increasing AP duration and thus increase transmitter release during sustained stimulation. If this were true, Kv3.1 subunits may be incorporated into heteromeric channels to prevent inactivation, again acting to limit transmitter release upon sustained stimulation of GBCs and conserve vesicle pools and energy stores. Further investigation would be required to understand the mechanism by which these Kv3.1 KO mice are able to sustain such large amount of release.

Furthermore, the dominant role of Kv3.3 subunits appears to apply at both excitatory and inhibitory synapses within the brainstem. The inability of TEA to increase IPSC amplitude at the inhibitory MNTB-LSO synapse (chapter 5) implies very little Kv3 is present within boutons of Kv3.3 KO animals. Thus it is possible that this holds true in other areas of the brain, most importantly, in synapses of the cerebellum. Kv3.1 and Kv3.3 are present in cerebellar granule cell- purkinje cell synapses (Matsukawa et al. 2003) and if Kv3.3 is the dominant subunit, similar to brainstem synapses, transmitter release is likely to be increased in SCA13 patients (due to a lack of functional Kv3.3). Here the ability to sustain release at high frequencies is much less important but increased transmitter release, thus excitatory drive, coupled with altered electrical excitability in Purkinje cells themselves (Hurlock, McMahon, and Joho 2008) may contribute to neurodegeneration observed in

SCA13 patients through excitotoxicity.

8.4 Kv3 channel composition in auditory brainstem neurons

This study has highlighted the diversity of Kv3 subunit expression between not only neuronal types but subcellular compartments. While LSO principal neurons appeared to be dominated by Kv3.3 subunits, both Kv3.1 and Kv3.3 were observed in calyx of Held terminals (chapter 4) and in somata of MNTB principal neurons (chapter 3). In MNTB neurons, where both subunits were expressed, the subcellular localisation of subunits differed with Kv3.3 expression limited to the soma while Kv3.1 was highly abundant not only in the soma but also the axon initial segment (AIS; figure 3.1). Kv3.1b is also present in the nodes of Ranvier (NoR), while Kv3.3 is not (Devaux et al. 2003; Chang et al. 2007). Consistent with expression patterns, it is likely that Kv3 channel composition varies with neuronal type and possibly subcellular compartment.

Given the results of chapter 7, primarily that Kv3.1 and Kv3.3 can be co-immunopreciptated when expressed in CHO cells and co-transfection of both subunits results in a shift in the inactivation curve compared to homomeric channels of both, it is likely that these subunits associate and can form heteromeric channels *in vivo*. While heteromeric Kv3 channels may form in the MNTB and calyx of Held in wildtype animals, it is important to note that both Kv3.1 and Kv3.3 subunits can be correctly localised and form functional homomeric channels. This was shown by a wildtype-like expression pattern of the remaining subunit in each knockout (as well as wildtype Kv3.1b expression in the Kv3.3^{R420H} mouse), observed with immunohistochemistry, as well as only minor changes to action potential waveform and no change to potassium current amplitudes in MNTB neurons when either subunit is lacking (chapter 3). This ability of both subunits to form functional homomeric channels and be targeted to the correct cellular location, thus compensating for the lost subunit would explain why double Kv3.1/Kv3.3 knockouts display severe ataxic phenotypes whereas single knockouts display only very mild motor abnormalities

(Ho, Grange, and Joho 1997; Sánchez et al. 2000; Joho et al. 2006).

So it appears that these subunits most likely exist as both homomers and heteromers depending on neuronal type and subcellular location. However, the ability to form heteromers may not be true for all subunits as Kv3.3 CHO cells transfected with Kv3.4 did not appear to yield heteromeric channels (chapter 7). Indeed the only current evidence for formation of heteromeric channels comes from investigation of Kv3.1 with other subunits (Baranauskas et al. 2003; Chang et al. 2007), thus it may be that this subunit is required for heteromerisation to occur.

8.5 SCA13 mouse model

As mentioned, the work in this thesis conducted on Kv3.3^{R420H} mice is the first from a mammalian model. The R420H mutation harboured by this mouse causes adult-onset progressive SCA13 in humans with severe cerebellar neurodegeneration and associated ataxia (Waters et al. 2006). Moreover some patients also exhibit impaired sound localisation, although unlike ataxia the penetrance for this is not ∼100% (Middlebrooks et al. 2013; Waters et al. 2006). Importantly, the mutation is dominant negative and almost all human sufferers are heterozygous for the mutated gene.

Kv3.3^{R420H} when expressed in cell lines results in a complete absence of Kv3.3 current (Waters et al. 2006). Results from the current study show this is true in our mammalian model with MNTB and LSO neurons displaying similar potassium current amplitudes and AP durations to Kv3.3 KO mice, albeit with increased variability. Decreased Kv3.3 conductance in these animals is likely to, in part, be caused by retention of mutated subunits within the cytoplasm of neurons, as shown by increased cytoplasmic staining of Kv3.3 in MNTB neurons.

Interestingly, changes in cell excitability were observed in young animals (P21-25), despite the adult-onset nature of the disease and did not change with increasing age (6 months). While the motor abilities of these mice have not yet been assessed, a tremor can be observed in homozygous mice from around two weeks of age which is not seen in heterozygous or wildtype mice. Although neurons of these mice have

currents identical to Kv3.3 KOs, Kv3.3 KOs do not have an overt motor-related phenotype, nor do they show Purkinje cell degeneration, suggesting the mutation may have an effect unrelated to electrical excitability of neurons, the mechanism of which requires future exploration.

Thus, this mouse appears to be a good model of SCA13 caused by the R420H mutation and should provide clues to the mechanism by which this particular mutation can result in neurodegeneration as well as providing a system to assess the impact of this mutation on auditory function. It is important to note that within this study we focussed on homozygous mice however, since heterozygous humans are affected, changes to cellular physiology should also be investigated in heterozygous mice.

8.6 Limitations

While the mouse provides a good model for studying auditory physiology, key differences between rodents and humans may make the work conducted on human mutations in mouse models difficult to apply to other mammals. Humans have a low-frequency hearing range of around 20Hz - 20KHz (Reynolds et al. 2010) while mice hear optimally at much higher frequencies (16-100KHz) which is likely to have a large impact on the relative importance of different auditory nuclei. Thus the significant role that Kv3.3 plays in limiting action potential duration in LSO neurons of mice may become less important in humans, which primarily use ITDs and thus the MSO for sound localisation. However, it has been shown that murine MSO neurons also contain Kv3 channels (Fischl et al. 2016) and thus it is sensible to assume Kv3.3 may play a similar role here. Indeed, the fact that humans carrying SCA13 mutations show disrupted sound localisation suggest these channels are likely to be important throughout the entire auditory brainstem. Secondly, while electrophysiological data gathered at the cellular level in mice may be used to imply reasons behind this disrupted sound localisation in humans, it is incredibly difficult to investigate this behaviour in the mouse model. Despite these challenges, the mouse still provides an excellent model for investigating the function of these channels with

and without mutations in native tissue and allows examination of their connection with other cellular processes such as neurotransmission.

8.7 Future directions

The study of individual Kv3 subunits has previously been hampered by the lack of subunit-specific blocking compounds. While knockouts are a useful tool to study subunit specific contributions to Kv3 channels, they come with drawbacks, primarily compensation by other subunits. The knockouts used in the present study have provided some interesting insights into the roles of Kv3.1 and Kv3.3 in the auditory brainstem, however they produce an artificial system in which homomeric channels are produced that may not necessarily form in wildtype animals. To negate this problem, the lab is currently developing a subunit-specific blocker by means of optically controlled tethered drugs. Specifically a TEA moiety which can be bound to particular subunits via a cysteine-dependent tether. This tethered TEA molecule can then be controlled using different wavelengths of lights to either extend and block the pore of channels incorporating the subunit or to shrink and leave the channel in the open configuration (Fortin et al. 2011). This should provide a better method to study subunit-specific currents in a wildtype configuration and by using a focussed laser on specific portions of the cell, should allow assessment of the function of these channels in specific cellular compartments.

8.7.1 Chapter 3

Chapter three outlined the contribution of Kv3.1 and Kv3.3 to the total potassium current in neurons of the MNTB and LSO and briefly described changes to single action potential duration in knockout animals. Since the role of Kv3 is to enable these neurons to fire at high frequencies it would be pertinent to investigate the ability of neurons in the MNTB and LSO of knockout animals to follow high frequency stimuli. Would the elongated AP in Kv3.3 KO LSO neurons impair its ability to fire successive APs? Are there any consequences of the slightly increased duration in MNTB neurons of both knockouts?

8.7.2 Chapter 4 and 5

Chapters 4 and 5 examined Kv3.1 and Kv3.3 contributions to presynaptic action potential waveform and consequent transmitter release. Further voltage clamp experiments should be conducted to examine potassium currents in the presynaptic terminal of knockout animals, perhaps using excised patches to increase the quality of voltage clamp.

Additionally, calcium transients in the presynaptic terminal of wildtype and knockout animals should be investigated to confirm that larger EPSCs observed in Kv3.3 KOs is due to increased calcium influx into the calyx in response to a longer AP. This may be done either by calcium imaging or using electrophysiology, measuring Ca^{2+} currents in response to an action potential waveform voltage protocol (taken from WT and KOs).

The functional consequences of decreased EPSC amplitude during sustained activity in Kv3.3 KOs also requires further investigation. Do these really fail to cause action potentials in the postsynaptic MNTB neuron? This would require measuring changes in voltage in MNTB neurons in response to stimulation of the calyx with current clamp.

Finally, more experiments are required assessing the effect of TEA on IPSC amplitude in LSO neurons of wildtype and KO mice to ensure the lack of effect observed in Kv3.3 KO mice is real.

8.7.3 Chapter 6

Chapter 6 briefly described changes to potassium currents and action potential duration in MNTB and LSO neurons of mice carrying a Kv3.3^{R420H} mutation. While this provided interesting insights, a thorough exploration of these mice is required including behavioural testing of motor and auditory function in both homozygous and heterozygous mice; a more detailed investigation of disease progression with age including monitoring of Purkinje cell loss as well as possible neuronal cell loss in the auditory brainstem; analysis of changes to synaptic function and possible morphological changes to neurons that may be associated with eventual neuronal

death.

8.7.4 Chapter 7

Lastly, chapter 7 aimed to investigate whether expression of two different Kv3 subunits in CHO cells would result in formation of heteromeric channels. A number of experiments could be done here including the assessment of inactivation in Kv3.3/Kv3.4 expressing cells as well as increasing the number of recordings in Kv3.3/Kv3.1 expressing cells; co-transfection of two subunits into a WT CHO cell rather than transfection of one subunit into a stable CHO Kv3.3 line; or transfection of concatamers of two different subunits, forcing the production of heteromers; transfection of different isoform and subunit combinations to investigate whether Kv3.1 is needed for heteromerisation; repetition of co-immunoprecipitation experiments for both Kv3.1/Kv3.3 and Kv3.3/Kv3.4 experiments and finally conducting immunohistochemistry of Kv3.1 and Kv3.3.

Chapter 9

References

Albrecht, O., Dondzillo, A., Mayer, F., Thompson, J. A., and Klug, A. (2014). "Inhibitory projections from the ventral nucleus of the trapezoid body to the medial nucleus of the trapezoid body in the mouse". In: *Frontiers in neural circuits* 8, p. 83.

Balakrishnan, V., Becker, M., Löhrke, S., Nothwang, H. G., Güresir, E., and Friauf, E. (2003). "Expression and function of chloride transporters during development of inhibitory neurotransmission in the auditory brainstem". In: *Journal of Neuroscience* 23.10, pp. 4134–4145.

Baranauskas, G., Tkatch, T., Nagata, K., Yeh, J. Z., and Surmeier, D. J. (2003). "Kv3. 4 subunits enhance the repolarizing efficiency of Kv3. 1 channels in fast-spiking neurons". In: *Nature neuroscience* 6.3, p. 258.

Barbour, B. (2011). *Electronics for electrophysiologists*.

Barnes-Davies, M. and Forsythe, I. D. (1995). "Pre-and postsynaptic glutamate receptors at a giant excitatory synapse in rat auditory brainstem slices." In: *The Journal of physiology* 488.2, pp. 387–406.

Beck, E. J., Sorensen, R. G., Slater, S. J., and Covarrubias, M. (1998). "Interactions between multiple phosphorylation sites in the inactivation particle of a K+ channel: insights into the molecular mechanism of protein kinase C action". In: *The Journal of general physiology* 112.1, pp. 71–84.

Billups, B. (2005). "Colocalization of vesicular glutamate transporters in the rat superior olivary complex". In: *Neuroscience letters* 382.1-2, pp. 66–70.

Borst, J. G., Helmchen, F., and Sakmann, B. (1995). "Pre-and postsynaptic whole-cell recordings in the medial nucleus of the trapezoid body of the rat." In: *The Journal of physiology* 489.3, pp. 825–840.

Borst, J. G. G. and Sakmann, B. (1996). "Calcium influx and transmitter release in a fast CNS synapse". In: *Nature* 383.6599, p. 431.

Boudreau, J. C. and Tsuchitani, C. (1968). "Binaural interaction in the cat superior olive S segment." In: *Journal of neurophysiology* 31.3, pp. 442–454.

Brew, H. M. and Forsythe, I. D. (1995). "Two voltage-dependent K+ conductances with complementary functions in postsynaptic integration at a central auditory synapse". In: *Journal of Neuroscience* 15.12, pp. 8011–8022.

Brew, H. M., Hallows, J. L., and Tempel, B. L. (2003). "Hyperexcitability and reduced low threshold potassium currents in auditory neurons of mice lacking the channel subunit Kv1. 1". In: *The Journal of physiology* 548.1, pp. 1–20.

Brooke, R. E., Moores, T. S., Morris, N. P., Parson, S. H., and Deuchars, J. (2004). "Kv3 voltage-gated potassium channels regulate neurotransmitter release from mouse motor nerve terminals". In: *European Journal of Neuroscience* 20.12, pp. 3313–3321.

Brown, M., El-Hassar, L., Zhang, Y., Alvaro, G., Large, C. H., and Kaczmarek, L. K. (2016). "Physiological modulators of Kv3. 1 channels adjust firing patterns of auditory brain stem neurons". In: *Journal of neurophysiology* 116.1, pp. 106–121.

Caicedo, A. and Eybalin, M. (1999). "Glutamate receptor phenotypes in the auditory brainstem and mid-brain of the developing rat". In: *European Journal of Neuroscience* 11.1, pp. 51–74.

Cant, N. B. and Hyson, R. L. (1992). "Projections from the lateral nucleus of the trapezoid body to the medial superior olivary nucleus in the gerbil". In: *Hearing research* 58.1, pp. 26–34.

Cao, X.-J., Shatadal, S., and Oertel, D. (2007). "Voltage-sensitive conductances of bushy cells of the Mammalian ventral cochlear nucleus". In: *Journal of neurophysiology* 97.6, pp. 3961–3975.

Catterall, W. A. (2010). "Ion channel voltage sensors: structure, function, and pathophysiology". In: *Neuron* 67.6, pp. 915–928.

Chan, E. (1997). "Regulation and function of Kv3. 3". PhD thesis. Rockefeller University.

Chang, S. Y., Zagha, E., Kwon, E. S., Ozaita, A., Bobik, M., Martone, M. E., Ellisman, M. H., Heintz, N., and Rudy, B. (2007). "Distribution of Kv3. 3 potassium channel subunits in distinct neuronal populations of mouse brain". In: *Journal of Comparative Neurology* 502.6, pp. 953–972.

Chow, A., Erisir, A., Farb, C., Nadal, M., Ozaita, A., Lau, D., Welker, E., and Rudy, B. (1999). "K+ channel expression distinguishes subpopulations of parvalbumin- and somatostatin-containing neocortical interneurons". In: *Journal of Neuroscience* 19.21, pp. 9332–9345.

Chuhma, N. and Ohmori, H. (1998). "Postnatal development of phase-locked high-fidelity synaptic transmission in the medial nucleus of the trapezoid body of the rat". In: *Journal of Neuroscience* 18.1, pp. 512–520.

Coetzee, W. A., Amarillo, Y., Chiu, J., Chow, A., Lau, D., McCormack, T., Morena, H., Nadal, M. S., Ozaita, A., Pountney, D., et al. (1999). "Molecular diversity of K+ channels". In: *Annals of the New York Academy of Sciences* 868.1, pp. 233–255.

Covarrubias, M., Wei, A., Salkoff, L., and Vyas, T. B. (1994). "Elimination of rapid potassium channel inactivation by phosphorylation of the inactivation gate". In: *Neuron* 13.6, pp. 1403–1412.

De Lange, R. P. J., De Roos, A. D. G., and Borst, J. G. G. (2003). "Two modes of vesicle recycling in the rat calyx of Held". In: *Journal of Neuroscience* 23.31, pp. 10164–10173.

Deng, Q., Rashid, A. J., Fernandez, F. R., Turner, R. W., Maler, L., and Dunn, R. J. (2005). "A C-terminal domain directs Kv3. 3 channels to dendrites". In: *Journal of Neuroscience* 25.50, pp. 11531–11541.

Desai, R., Kronengold, J., Mei, J., Forman, S. A., and Kaczmarek, L. K. (2008). "Protein kinase C modulates inactivation of Kv3. 3 channels". In: *Journal of Biological Chemistry* 283.32, pp. 22283–22294.

Devaux, J., Alcaraz, G., Grinspan, J., Bennett, V., Joho, R., Crest, M., and Scherer, S. S. (2003). "Kv3. 1b is a novel component of CNS nodes". In: *Journal of Neuroscience* 23.11, pp. 4509–4518.

Diochot, S., Schweitz, H., Béress, L., and Lazdunski, M. (1998). "Sea anemone peptides with a specific blocking activity against the fast inactivating potassium channel Kv3. 4". In: *Journal of Biological Chemistry* 273.12, pp. 6744–6749.

Dodson, P. D. (2003). "The role of voltage-gated potassium channels in regulating excitability at a central synapse". PhD thesis. Cell Physiology.

Dodson, P. D., Barker, M. C., and Forsythe, I. D. (2002). "Two heteromeric Kv1 potassium channels differentially regulate action potential firing". In: *Journal of Neuroscience* 22.16, pp. 6953–6961.

Dodson, P. D., Billups, B., Rusznák, Z., Szûcs, G., Barker, M. C., and Forsythe, I. D. (2003). "Presynaptic rat Kv1. 2 channels suppress synaptic terminal hyperexcitability following action potential invasion". In: *The Journal of physiology* 550.1, pp. 27–33.

Doyle, D. A., Cabral, J. M., Pfuetzner, R. A., Kuo, A., Gulbis, J. M., Cohen, S. L., Chait, B. T., and MacKinnon, R. (1998). "The structure of the potassium channel: molecular basis of K+ conduction and selectivity". In: *science* 280.5360, pp. 69–77.

Duarri, A., Nibbeling, E. A., Fokkens, M. R., Meijer, M., Boerrigter, M., Verschuuren-Bemelmans, C. C., Kremer, B. P., Warrenburg, B. P. van de, Dooijes, D., Boddeke, E., et al. (2015). "Functional analysis helps to define KCNC3 mutational spectrum in Dutch ataxia cases". In: *PLoS One* 10.3, e0116599.

Elezgarai, I., Diez, J., Puente, N., Azkue, J. J., Benitez, R., Bilbao, A., Knöpfel, T., Donate-Oliver, F., and Grandes, P. (2003). "Subcellular localization of the voltage-dependent potassium channel Kv3. 1b in postnatal and adult rat medial nucleus of the trapezoid body". In: *Neuroscience* 118.4, pp. 889–898.

Fernandez, F. R., Morales, E., Rashid, A. J., Dunn, R. J., and Turner, R. W. (2003). "Inactivation of Kv3. 3 potassium channels in heterologous expression systems". In: *Journal of Biological Chemistry* 278.42, pp. 40890–40898.

Figueroa, K. P., Minassian, N. A., Stevanin, G., Waters, M., Garibyan, V., Forlani, S., Strzelczyk, A., Bürk, K., Brice, A., Dürr, A., et al. (2010). "KCNC3: phenotype, mutations, channel biophysics — a study of 260 familial ataxia patients". In: *Human mutation* 31.2, pp. 191–196.

Fischer, A. U., Müller, N. I., Deller, T., Del Turco, D., Fisch, J. O., Griesemer, D., Kattler, K., Maraslioglu, A., Roemer, V., Xu-Friedman, M. A., et al. (2019). "GABA is a modulator, rather than a classical transmitter, in the medial nucleus of the trapezoid body–lateral superior olive sound localization circuit". In: *The Journal of physiology* 597.8, pp. 2269–2295.

Fischl, M. J., Burger, R. M., Schmidt-Pauly, M., Alexandrova, O., Sinclair, J. L., Grothe, B., Forsythe, I. D., and Kopp-Scheinpflug, C. (2016). "Physiology and anatomy of neurons in the medial superior olive of the mouse". In: *Journal of neurophysiology* 116.6, pp. 2676–2688.

Forsythe, I. D. (1994). "Direct patch recording from identified presynaptic terminals mediating glutamatergic EPSCs in the rat CNS, in vitro." In: *The Journal of physiology* 479.3, pp. 381–387.

Forsythe, I. D. and Barnes-Davies, M. (1993). "The binaural auditory pathway: excitatory amino acid receptors mediate dual timecourse excitatory postsynaptic currents in the rat medial nucleus of the trapezoid body". In: *Proceedings of the Royal Society of London. Series B: Biological Sciences* 251.1331, pp. 151–157.

Forsythe, I. D., Tsujimoto, T., Barnes-Davies, M., Cuttle, M. F., and Takahashi, T. (1998). "Inactivation of presynaptic calcium current contributes to synaptic depression at a fast central synapse". In: *Neuron* 20.4, pp. 797–807.

Fortin, D. L., Dunn, T. W., Fedorchak, A., Allen, D., Montpetit, R., Banghart, M. R., Trauner, D., Adelman, J. P., and Kramer, R. H. (2011). "Optogenetic photochemical control of designer K+ channels in mammalian neurons". In: *Journal of neurophysiology* 106.1, pp. 488–496.

Futai, K., Okada, M., Matsuyama, K., and Takahashi, T. (2001). "High-fidelity transmission acquired via a developmental decrease in NMDA receptor expression at an auditory synapse". In: *Journal of Neuroscience* 21.10, pp. 3342–3349.

Gallego-Iradi, C., Bickford, J. S., Khare, S., Hall, A., Nick, J. A., Salmasinia, D., Wawrowsky, K., Bannykh, S., Huynh, D. P., Rincon-Limas, D. E., et al. (2014). "KCNC3R420H, a K+ channel mutation causative in spinocerebellar ataxia 13 displays aberrant intracellular trafficking". In: *Neurobiology of disease* 71, pp. 270–279.

Galvez, A., Gimenez-Gallego, G., Reuben, J. P., Roy-Contancin, L., Feigenbaum, P., Kaczorowski, G. J., and Garcia, M. L. (1990). "Purification and characterization of a unique, potent, peptidyl probe for the high conductance calcium-activated potassium channel from venom of the scorpion Buthus tamulus." In: *Journal of Biological Chemistry* 265.19, pp. 11083–11090.

Grigg, J. J., Brew, H. M., and Tempel, B. L. (2000). "Differential expression of voltage-gated potassium channel genes in auditory nuclei of the mouse brainstem". In: *Hearing research* 140.1-2, pp. 77–90.

Grissmer, S., Nguyen, A. N., Aiyar, J., Hanson, D. C., Mather, R. J., Gutman, G. A., Karmilowicz, M. J., Auperin, D. D., and Chandy, K. G. (1994). "Pharmacological characterization of five cloned voltage-gated K+ channels, types Kv1. 1, 1.2, 1.3, 1.5, and 3.1, stably expressed in mammalian cell lines." In: *Molecular pharmacology* 45.6, pp. 1227–1234.

Grothe, B. (2003). "New roles for synaptic inhibition in sound localization". In: *Nature Reviews Neuroscience* 4.7, p. 540.

Grothe, B. and Pecka, M. (2014). "The natural history of sound localization in mammals–a story of neuronal inhibition". In: *Frontiers in neural circuits* 8, p. 116.

Grothe, B., Pecka, M., and McAlpine, D. (2010). "Mechanisms of sound localization in mammals". In: *Physiological reviews* 90.3, pp. 983–1012.

Hamann, M., Billups, B., and Forsythe, I. D. (2003). "Non-calyceal excitatory inputs mediate low fidelity synaptic transmission in rat auditory brainstem slices". In: *European Journal of Neuroscience* 18.10, pp. 2899–2902.

Hehn, C. A. A. von, Bhattacharjee, A., and Kaczmarek, L. K. (2004). "Loss of Kv3. 1 tonotopicity and alterations in cAMP response element-binding protein signaling in central auditory neurons of hearing impaired mice". In: *Journal of Neuroscience* 24.8, pp. 1936–1940.

Heidelberger, R., Sterling, P., and Matthews, G. (2002). "Roles of ATP in depletion and replenishment of the releasable pool of synaptic vesicles". In: *Journal of Neurophysiology* 88.1, pp. 98–106.

Helfert, R. H. and Schwartz, I. R. (1987). "Morphological features of five neuronal classes in the gerbil lateral superior olive". In: *American journal of anatomy* 179.1, pp. 55–69.

Henney, N. C., Li, B., Elford, C., Reviriego, P., Campbell, A. K., Wann, K. T., and Evans, B. A. J. (2009). "A large-conductance (BK) potassium channel subtype affects both growth and mineralization of human osteoblasts". In: *American Journal of Physiology-Cell Physiology* 297.6, pp. C1397–C1408.

Ho, C. S., Grange, R. W., and Joho, R. H. (1997). "Pleiotropic effects of a disrupted K+ channel gene: reduced body weight, impaired motor skill and muscle contraction, but no seizures". In: *Proceedings of the National Academy of Sciences* 94.4, pp. 1533–1538.

Hodgkin, A. L. and Huxley, A. F. (1952). "A quantitative description of membrane current and its application to conduction and excitation in nerve". In: *The Journal of physiology* 117.4, pp. 500–544.

Hoshi, T., Zagotta, W. N., and Aldrich, R. W. (1990). "Biophysical and molecular mechanisms of Shaker potassium channel inactivation". In: *Science* 250.4980, pp. 533–538.

Hurlock, E. C., McMahon, A., and Joho, R. H. (2008). "Purkinje-cell-restricted restoration of Kv3. 3 function restores complex spikes and rescues motor coordination in Kcnc3 mutants". In: *Journal of Neuroscience* 28.18, pp. 4640–4648.

Irie, T., Matsuzaki, Y., Sekino, Y., and Hirai, H. (2014). "Kv3. 3 channels harbouring a mutation of spinocerebellar ataxia type 13 alter excitability and induce cell death in cultured cerebellar Purkinje cells". In: *The Journal of physiology* 592.1, pp. 229–247.

Ishikawa, T., Nakamura, Y., Saitoh, N., Li, W.-B., Iwasaki, S., and Takahashi, T. (2003). "Distinct roles of Kv1 and Kv3 potassium channels at the calyx of Held presynaptic terminal". In: *Journal of Neuroscience* 23.32, pp. 10445–10453.

Issa, F. A., Mazzochi, C., Mock, A. F., and Papazian, D. M. (2011). "Spinocerebellar ataxia type 13 mutant potassium channel alters neuronal excitability and causes locomotor deficits in zebrafish". In: *Journal of Neuroscience* 31.18, pp. 6831–6841.

Iwasaki, S. and Takahashi, T. (1998). "Developmental changes in calcium channel types mediating synaptic transmission in rat auditory brainstem". In: *The Journal of physiology* 509.2, pp. 419–423.

Jalabi, W., Kopp-Scheinpflug, C., Allen, P. D., Schiavon, E., DiGiacomo, R. R., Forsythe, I. D., and Maricich, S. M. (2013). "Sound localization ability and glycinergic innervation of the superior olivary complex persist after genetic deletion of the medial nucleus of the trapezoid body". In: *Journal of Neuroscience* 33.38, pp. 15044–15049.

Jeffress, L. A. (1948). "A place theory of sound localization." In: *Journal of comparative and physiological psychology* 41.1, p. 35.

Jenkins, W. M. and Masterton, R. B. (1982). "Sound localization: effects of unilateral lesions in central auditory system." In: *Journal of Neurophysiology* 47.6, pp. 987–1016.

Johnston, J. (2007). "On the composition, properties and physiological roles of K+ currents found at a central auditory synapse". PhD thesis. Cell Physiology and Pharmacology.

Johnston, J., Forsythe, I. D., and Kopp-Scheinpflug, C. (2010). "SYMPOSIUM REVIEW: Going native: voltage-gated potassium channels controlling neuronal excitability". In: *The Journal of physiology* 588.17, pp. 3187–3200.

Johnston, J., Griffin, S. J., Baker, C., Skrzypiec, A., Chernova, T., and Forsythe, I. D. (2008). "Initial segment Kv2. 2 channels mediate a slow delayed rectifier and maintain high frequency action potential firing in medial nucleus of the trapezoid body neurons". In: *The Journal of physiology* 586.14, pp. 3493–3509.

Joho, R. H., Street, C., Matsushita, S., and Knöpfel, T. (2006). "Behavioral motor dysfunction in Kv3-type potassium channel-deficient mice". In: *Genes, Brain and Behavior* 5.6, pp. 472–482.

Joris, P. X., Smith, P. H., and Yin, T. C. T. (1998). "Coincidence detection in the auditory system: 50 years after Jeffress". In: *Neuron* 21.6, pp. 1235–1238.

Joshi, I. and Wang, L.-Y. (2002). "Developmental profiles of glutamate receptors and synaptic transmission at a single synapse in the mouse auditory brainstem". In: *The Journal of physiology* 540.3, pp. 861–873.

Kaczmarek, L. K. (2006). "Non-conducting functions of voltage-gated ion channels". In: *Nature Reviews Neuroscience* 7.10, p. 761.

Kakazu, Y., Akaike, N., Komiyama, S., and Nabekura, J. (1999). "Regulation of intracellular chloride by cotransporters in developing lateral superior olive neurons". In: *Journal of Neuroscience* 19.8, pp. 2843–2851.

Kandler, K. and Friauf, E. (1993). "Pre-and postnatal development of efferent connections of the cochlear nucleus in the rat". In: *Journal of Comparative Neurology* 328.2, pp. 161–184.

— (1995). "Development of glycinergic and glutamatergic synaptic transmission in the auditory brainstem of perinatal rats". In: *Journal of Neuroscience* 15.10, pp. 6890–6904.

Kanemasa, T., Gan, L., Perney, T. M., Wang, L. Y., and Kaczmarek, L. K. (1995). "Electrophysiological and pharmacological characterization of a mammalian Shaw channel expressed in NIH 3T3 fibroblasts". In: *Journal of Neurophysiology* 74.1, pp. 207–217.

Kapfer, C., Seidl, A. H., Schweizer, H., and Grothe, B. (2002). "Experience-dependent refinement of inhibitory inputs to auditory coincidence-detector neurons". In: *Nature neuroscience* 5.3, p. 247.

Kim, J. H., Kushmerick, C., and Von Gersdorff, H. (2010). "Presynaptic resurgent Na+ currents sculpt the action potential waveform and increase firing reliability at a CNS nerve terminal". In: *Journal of Neuroscience* 30.46, pp. 15479–15490.

Kopp-Scheinpflug, C., Fuchs, K., Lippe, W. R., Tempel, B. L., and Rübsamen, R. (2003). "Decreased temporal precision of auditory signaling in Kcna1-null mice: an electrophysiological study in vivo". In: *Journal of Neuroscience* 23.27, pp. 9199–9207.

Kopp-Scheinpflug, C., Tozer, A. J. B., Robinson, S. W., Tempel, B. L., Hennig, M. H., and Forsythe, I. D. (2011). "The sound of silence: ionic mechanisms encoding sound termination". In: *Neuron* 71.5, pp. 911–925.

Kotak, V. C., Korada, S., Schwartz, I. R., and Sanes, D. H. (1998). "A developmental shift from GABAergic to glycinergic transmission in the central auditory system". In: *Journal of Neuroscience* 18.12, pp. 4646–4655.

Kramer, J. W., Post, M. A., Brown, A. M., and Kirsch, G. E. (1998). "Modulation of potassium channel gating by coexpression of Kv2. 1 with regulatory Kv5. 1 or Kv6. 1 α-subunits". In: *American Journal of Physiology-Cell Physiology* 274.6, pp. C1501–C1510.

Kreusch, A., Pfaffinger, P. J., Stevens, C. F., and Choe, S. (1998). "Crystal structure of the tetramerization domain of the Shaker potassium channel". In: *Nature* 392.6679, p. 945.

Kuo, C.-C. and Bean, B. P. (1994). "Na+ channels must deactivate to recover from inactivation". In: *Neuron* 12.4, pp. 819–829.

Kuwabara, N., DiCaprio, R. A., and Zook, J. M. (1991). "Afferents to the medial nucleus of the trapezoid body and their collateral projections". In: *Journal of Comparative Neurology* 314.4, pp. 684–706.

Kuwabara, N. and Zook, J. M. (1992). "Projections to the medial superior olive from the medial and lateral nuclei of the trapezoid body in rodents and bats". In: *Journal of Comparative Neurology* 324.4, pp. 522–538.

Land, R., Burghard, A., and Kral, A. (2016). "The contribution of inferior colliculus activity to the auditory brainstem response (ABR) in mice". In: *Hearing research* 341, pp. 109–118.

Lauer, A. M., Connelly, C. J., Graham, H., and Ryugo, D. K. (2013). "Morphological characterization of bushy cells and their inputs in the laboratory mouse (Mus musculus) anteroventral cochlear nucleus". In: *PloS one* 8.8, e73308.

Lee, J. S., Ho, W. K., and Lee, S. H. (2012). "Actin-dependent rapid recruitment of reluctant synaptic vesicles into a fast-releasing vesicle pool". In: *Proceedings of the National Academy of Sciences* 109.13, E765–E774.

Lewis, A., McCrossan, Z. A., and Abbott, G. W. (2004). "MinK, MiRP1, and MiRP2 diversify Kv3. 1 and Kv3. 2 potassium channel gating". In: *Journal of Biological Chemistry* 279.9, pp. 7884–7892.

Li, W., Kaczmarek, L. K., and Perney, T. M. (2001). "Localization of two high-threshold potassium channel subunits in the rat central auditory system". In: *Journal of Comparative Neurology* 437.2, pp. 196–218.

Linley, D. M. (2017). "The Influence of acoustic over-exposure on central auditory processing". PhD thesis. Department of Neuroscience, Psychology and Behaviour.

Liu, P., Jo, S., and Bean, B. P. (2012). "Modulation of neuronal sodium channels by the sea anemone peptide BDS-I". In: *Journal of neurophysiology* 107.11, pp. 3155–3167.

Llinas, R., Sugimori, M., and Silver, R. B. (1992). "Microdomains of high calcium concentration in a presynaptic terminal". In: *Science* 256.5057, pp. 677–679.

Long, S. B., Campbell, E. B., and MacKinnon, R. (2005). "Crystal structure of a mammalian voltage-dependent Shaker family K+ channel". In: *Science* 309.5736, pp. 897–903.

Lucas, S. J., Michel, C. B., Marra, V., Smalley, J. L., Hennig, M. H., Graham, B. P., and Forsythe, I. D. (2018). "Glucose and lactate as metabolic constraints on presynaptic transmission at an excitatory synapse". In: *The Journal of physiology* 596.9, pp. 1699–1721.

Macica, C. M., Von Hehn, C. A. A., Wang, L.-Y., Ho, C.-S., Yokoyama, S., Joho, R. H., and Kaczmarek, L. K. (2003). "Modulation of the kv3. 1b potassium channel isoform adjusts the fidelity of the firing pattern of auditory neurons". In: *Journal of Neuroscience* 23.4, pp. 1133–1141.

Masterton, B., Diamond, I. T., Harrison, J., and Beecher, M. (1967). "Medial superior olive and sound localization". In: *Science* 155.3770, pp. 1696–1697.

Matsukawa, H., Wolf, A. M., Matsushita, S., Joho, R. H., and Knöpfel, T. (2003). "Motor dysfunction and altered synaptic transmission at the parallel fiber-Purkinje cell synapse in mice lacking potassium channels Kv3. 1 and Kv3. 3". In: *Journal of Neuroscience* 23.20, pp. 7677–7684.

McCrossan, Z. A., Lewis, A., Panaghie, G., Jordan, P. N., Christini, D. J., Lerner, D. J., and Abbott, G. W. (2003). "MinK-related peptide 2 modulates Kv2. 1 and Kv3. 1 potassium channels in mammalian brain". In: *Journal of Neuroscience* 23.22, pp. 8077–8091.

Meinrenken, C. J., Borst, J. G. G., and Sakmann, B. (2002). "Calcium secretion coupling at calyx of Held governed by nonuniform channel–vesicle topography". In: *Journal of Neuroscience* 22.5, pp. 1648–1667.

Meyer, A. C., Neher, E., and Schneggenburger, R. (2001). "Estimation of quantal size and number of functional active zones at the calyx of held synapse by nonstationary EPSC variance analysis". In: *Journal of Neuroscience* 21.20, pp. 7889–7900.

Middlebrooks, J. C., Nick, H. S., Subramony, S., Advincula, J., Rosales, R. L., Lee, L. V., Ashizawa, T., and Waters, M. F. (2013). "Mutation in the kv3. 3 voltage-gated potassium channel causing spinocerebellar ataxia 13 disrupts sound-localization mechanisms". In: *PloS one* 8.10, e76749.

Minassian, N. A., Lin, M.-C. A., and Papazian, D. M. (2012). "Altered Kv3. 3 channel gating in early-onset spinocerebellar ataxia type 13". In: *The Journal of physiology* 590.7, pp. 1599–1614.

Misonou, H., Mohapatra, D. P., and Trimmer, J. S. (2005). "Kv2. 1: a voltage-gated k+ channel critical to dynamic control of neuronal excitability". In: *Neurotoxicology* 26.5, pp. 743–752.

Moore, M. J. and Caspary, D. M. (1983). "Strychnine blocks binaural inhibition in lateral superior olivary neurons". In: *Journal of Neuroscience* 3.1, pp. 237–242.

Moreno, H., Kentros, C., Bueno, E., Weiser, M., Hernandez, A., De Miera, E. V.-S., Ponce, A., Thornhill, W., and Rudy, B. (1995). "Thalamocortical projections have a K+ channel that is phosphorylated and modulated by cAMP-dependent protein kinase". In: *Journal of Neuroscience* 15.8, pp. 5486–5501.

Mosbacher, J., Schöpfer, R., Monyer, H., Burnashev, N., Seeburg, P. H., and Ruppersberg, J. P. (1994). "A molecular determinant for submillisecond desensitization in glutamate receptors". In: *Science* 266.5187, pp. 1059–1062.

Moulder, K. L. and Mennerick, S. (2005). "Reluctant vesicles contribute to the total readily releasable pool in glutamatergic hippocampal neurons". In: *Journal of Neuroscience* 25.15, pp. 3842–3850.

Muona, M., Berkovic, S. F., Dibbens, L. M., Oliver, K. L., Maljevic, S., Bayly, M. A., Joensuu, T., Canafoglia, L., Franceschetti, S., Michelucci, R., et al. (2015). "A recurrent de novo mutation in KCNC1 causes progressive myoclonus epilepsy". In: *Nature genetics* 47.1, p. 39.

Nabekura, J., Katsurabayashi, S., Kakazu, Y., Shibata, S., Matsubara, A., Jinno, S., Mizoguchi, Y., Sasaki, A., and Ishibashi, H. (2004). "Developmental switch from GABA to glycine release in single central synaptic terminals". In: *Nature neuroscience* 7.1, p. 17.

Nabel, A. L., Callan, A. R., Gleiss, S., Leibold, C., and Felmy, F. (2019). "Distinct distribution patterns of potassium channel sub-units in somato-dendritic compartments of neurons of the medial superior olive". In: *Frontiers in cellular neuroscience* 13, p. 38.

Nakamura, Y. and Takahashi, T. (2007). "Developmental changes in potassium currents at the rat calyx of Held presynaptic terminal". In: *The Journal of physiology* 581.3, pp. 1101–1112.

Nascimento, F. A. and Andrade, D. M. (2016). "Myoclonus epilepsy and ataxia due to potassium channel mutation (MEAK) is caused by heterozygous KCNC1 mutations". In: *Epileptic Disorders* 18.s2, S135–S138.

Neher, E. (2017). "Some subtle lessons from the calyx of Held synapse". In: *Biophysical journal* 112.2, pp. 215–223.

Neher, E. and Sakaba, T. (2001). "Combining deconvolution and noise analysis for the estimation of transmitter release rates at the calyx of Held". In: *Journal of Neuroscience* 21.2, pp. 444–461.

Newton, S. (2017). "Noise-induced Hearing Loss: Changes in Gene Expression in the Auditory Pathway". PhD thesis. Department of Neuroscience, Psychology and Behaviour.

Nordeen, K. W., Killackey, H. P., and Kitzes, L. M. (1983). "Ascending auditory projections to the inferior colliculus in the adult gerbil, Meriones unguiculatus". In: *Journal of Comparative Neurology* 214.2, pp. 131–143.

Ogden, D. (1994). *Microelectrode techniques. The Plymouth workshop handbook*. The Company of Biologists Ltd.

Olsen, T., Capurro, A., Pilati, N., Large, C. H., and Hamann, M. (2018). "Kv3 K+ currents contribute to spike-timing in dorsal cochlear nucleus principal cells". In: *Neuropharmacology* 133, pp. 319–333.

Ottschytsch, N., Raes, A., Van Hoorick, D., and Snyders, D. J. (2002). "Obligatory heterotetramerization of three previously uncharacterized Kv channel α-subunits identified in the human genome". In: *Proceedings of the National Academy of Sciences* 99.12, pp. 7986–7991.

Ozaita, A., Martone, M., Ellisman, M., and Rudy, B. (2002). "Differential subcellular localization of the two alternatively spliced isoforms of the Kv3. 1 potassium channel subunit in brain". In: *Journal of neurophysiology* 88.1, pp. 394–408.

Perney, T. M., Marshall, J., Martin, K. A., Hockfield, S., and Kaczmarek, L. K. (1992). "Expression of the mRNAs for the Kv3. 1 potassium channel gene in the adult and developing rat brain". In: *Journal of Neurophysiology* 68.3, pp. 756–766.

Pilati, N., Linley, D. M., Selvaskandan, H., Uchitel, O., Hennig, M. H., Kopp-Scheinpflug, C., and Forsythe, I. D. (2016). "Acoustic trauma slows AMPA receptor-mediated EPSCs in the auditory brainstem, reducing GluA4 subunit expression as a mechanism to rescue binaural function". In: *The Journal of physiology* 594.13, pp. 3683–3703.

Post, M. A., Kirsch, G. E., and Brown, A. M. (1996). "Kv2. 1 and electrically silent Kv6. 1 potassium channel subunits combine and express a novel current". In: *FEBS letters* 399.1-2, pp. 177–182.

Postlethwaite, M., Hennig, M. H., Steinert, J. R., Graham, B. P., and Forsythe, I. D. (2007). "Acceleration of AMPA receptor kinetics underlies temperature-dependent changes in synaptic strength at the rat calyx of Held". In: *The Journal of physiology* 579.1, pp. 69–84.

Si-qiong, J. L. and Kaczmarek, L. K. (1998). "The expression of two splice variants of the Kv3. 1 potassium channel gene is regulated by different signaling pathways". In: *Journal of Neuroscience* 18.8, pp. 2881–2890.

Rettig, J., Heinemann, S. H., Wunder, F., Lorra, C., Parcej, D. N., Dolly, J. O., and Pongs, O. (1994). "Inactivation properties of voltage-gated K+ channels altered by presence of β-subunit". In: *Nature* 369.6478, p. 289.

Reynolds, R. P., Kinard, W. L., Degraff, J. J., Leverage, N., and Norton, J. N. (2010). "Noise in a laboratory animal facility from the human and mouse perspectives". In: *Journal of the American association for laboratory animal science* 49.5, pp. 592–597.

Rietzel, H.-J. and Friauf, E. (1998). "Neuron types in the rat lateral superior olive and developmental changes in the complexity of their dendritic arbors". In: *Journal of Comparative Neurology* 390.1, pp. 20–40.

Rizzoli, S. O. and Betz, W. J. (2005). "Synaptic vesicle pools". In: *Nature Reviews Neuroscience* 6.1, p. 57.

Rosato-Siri, M. D., Zambello, E., Mutinelli, C., Garbati, N., Benedetti, R., Aldegheri, L., Graziani, F., Virginio, C., Alvaro, G., and Large, C. H. (2015). "A novel modulator of Kv3 potassium channels regulates the firing of parvalbumin-positive cor-

tical interneurons". In: *Journal of Pharmacology and Experimental Therapeutics* 354.3, pp. 251–260.

Rowan, M. J. and Christie, J. M. (2017). "Rapid state-dependent alteration in Kv3 channel availability drives flexible synaptic signaling dependent on somatic subthreshold depolarization". In: *Cell reports* 18.8, pp. 2018–2029.

Rudy, B., Chow, A., Lau, D., Amarillo, Y., Ozaita, A., Saganich, M., Moreno, H., Nadal, M. S., Hernandez-Pineda, R., Hernandez-Cruz, A., et al. (1999). "Contributions of Kv3 channels to neuronal excitability". In: *Annals of the New York Academy of Sciences* 868.1, pp. 304–343.

Rudy, B. and McBain, C. J. (2001). "Kv3 channels: voltage-gated K+ channels designed for high-frequency repetitive firing". In: *Trends in neurosciences* 24.9, pp. 517–526.

Sabatini, B. L. and Regehr, W. G. (1997). "Control of neurotransmitter release by presynaptic waveform at the granule cell to Purkinje cell synapse". In: *Journal of Neuroscience* 17.10, pp. 3425–3435.

Sakaba, T. (2006). "Roles of the fast-releasing and the slowly releasing vesicles in synaptic transmission at the calyx of held". In: *Journal of Neuroscience* 26.22, pp. 5863–5871.

Sakaba, T. and Neher, E. (2001). "Calmodulin mediates rapid recruitment of fast-releasing synaptic vesicles at a calyx-type synapse". In: *Neuron* 32.6, pp. 1119–1131.

Sánchez, J. A., Ho, C. S., Vaughan, D. M., Garcia, M. C., Grange, R. W., and Joho, R. H. (2000). "Muscle and motor-skill dysfunction in a K+ channel-deficient mouse are not due to altered muscle excitability or fiber type but depend on the genetic background". In: *Pflügers Archiv* 440.1, pp. 34–41.

Sätzler, K., Söhl, L. F., Bollmann, J. H., Borst, J. G. G., Frotscher, M., Sakmann, B., and Lübke, J. H. R. (2002). "Three-dimensional reconstruction of a calyx of Held and its postsynaptic principal neuron in the medial nucleus of the trapezoid body". In: *Journal of Neuroscience* 22.24, pp. 10567–10579.

Scheuss, V., Schneggenburger, R., and Neher, E. (2002). "Separation of presynaptic and postsynaptic contributions to depression by covariance analysis of successive EPSCs at the calyx of held synapse". In: *Journal of Neuroscience* 22.3, pp. 728–739.

Schneggenburger, R. and Forsythe, I. D. (2006). "The calyx of Held". In: *Cell and tissue research* 326.2, pp. 311–337.

Schneggenburger, R., Meyer, A. C., and Neher, E. (1999). "Released fraction and total size of a pool of immediately available transmitter quanta at a calyx synapse". In: *Neuron* 23.2, pp. 399–409.

Schneggenburger, R. and Neher, E. (2000). "Intracellular calcium dependence of transmitter release rates at a fast central synapse". In: *Nature* 406.6798, p. 889.

Seidl, A. H. and Rubel, E. W. (2016). "Systematic and differential myelination of axon collaterals in the mammalian auditory brainstem". In: *Glia* 64.4, pp. 487–494.

Sento, S. and Ryugo, D. K. (1989). "Endbulbs of held and spherical bushy cells in cats: morphological correlates with physiological properties". In: *Journal of Comparative Neurology* 280.4, pp. 553–562.

Sinclair, J. L., Fischl, M. J., Alexandrova, O., Heβ, M., Grothe, B., Leibold, C., and Kopp-Scheinpflug, C. (2017). "Sound-evoked activity influences myelination of brainstem axons in the trapezoid body". In: *Journal of Neuroscience* 37.34, pp. 8239–8255.

Smith, A. J., Owens, S., and Forsythe, I. D. (2000). "Characterisation of inhibitory and excitatory postsynaptic currents of the rat medial superior olive". In: *The Journal of Physiology* 529.3, pp. 681–698.

Smith, P. H., Joris, P. X., and Yin, T. C. T. (1993). "Projections of physiologically characterized spherical bushy cell axons from the cochlear nucleus of the cat: evidence for delay lines to the medial superior olive". In: *Journal of Comparative Neurology* 331.2, pp. 245–260.

Smith, P. H., Joris, P. X., and Yin, T. C. T. (1998). "Anatomy and physiology of principal cells of the medial nucleus of the trapezoid body (MNTB) of the cat". In: *Journal of neurophysiology* 79.6, pp. 3127–3142.

Smith, T. C., Wang, L.-Y., and Howe, J. R. (2000). "Heterogeneous conductance levels of native AMPA receptors". In: *Journal of Neuroscience* 20.6, pp. 2073–2085.

Sommer, I., Lingenhöhl, K., and Friauf, E. (1993). "Principal cells of the rat medial nucleus of the trapezoid body: an intracellular in vivo study of their physiology and morphology". In: *Experimental brain research* 95.2, pp. 223–239.

Song, P., Yang, Y., Barnes-Davies, M., Bhattacharjee, A., Hamann, M., Forsythe, I. D., Oliver, D. L., and Kaczmarek, L. K. (2005). "Acoustic environment determines phosphorylation state of the Kv3. 1 potassium channel in auditory neurons". In: *Nature neuroscience* 8.10, p. 1335.

Sonntag, M., Englitz, B., Typlt, M., and Rübsamen, R. (2011). "The calyx of held develops adult-like dynamics and reliability by hearing onset in the mouse in vivo". In: *Journal of Neuroscience* 31.18, pp. 6699–6709.

Spirou, G. A., Brownell, W. E., and Zidanic, M. (1990). "Recordings from cat trapezoid body and HRP labeling of globular bushy cell axons". In: *Journal of neurophysiology* 63.5, pp. 1169–1190.

Steinert, J. R., Postlethwaite, M., Jordan, M. D., Chernova, T., Robinson, S. W., and Forsythe, I. D. (2010). "NMDAR-mediated EPSCs are maintained and accelerate in time course during maturation of mouse and rat auditory brainstem in vitro". In: *The Journal of physiology* 588.3, pp. 447–463.

Sterenborg, J. C., Pilati, N., Sheridan, C. J., Uchitel, O. D., Forsythe, I. D., and Barnes-Davies, M. (2010). "Lateral olivocochlear (LOC) neurons of the mouse LSO receive excitatory and inhibitory synaptic inputs with slower kinetics than LSO principal neurons". In: *Hearing research* 270.1-2, pp. 119–126.

Stevens, C. F. and Williams, J. H. (2007). "Discharge of the readily releasable pool with action potentials at hippocampal synapses". In: *Journal of neurophysiology* 98.6, pp. 3221–3229.

Südhof, T. C. (2012). "The presynaptic active zone". In: *Neuron* 75.1, pp. 11–25.

Sun, J.-Y. and Wu, L.-G. (2001). "Fast kinetics of exocytosis revealed by simultaneous measurements of presynaptic capacitance and postsynaptic currents at a central synapse". In: *Neuron* 30.1, pp. 171–182.

Taschenberger, H., Leão, R. M., Rowland, K. C., Spirou, G. A., and Von Gersdorff, H. (2002). "Optimizing synaptic architecture and efficiency for high-frequency transmission". In: *Neuron* 36.6, pp. 1127–1143.

Taschenberger, H., Scheuss, V., and Neher, E. (2005). "Release kinetics, quantal parameters and their modulation during short-term depression at a developing synapse in the rat CNS". In: *The Journal of physiology* 568.2, pp. 513–537.

Taschenberger, H. and Von Gersdorff, H. (2000). "Fine-tuning an auditory synapse for speed and fidelity: developmental changes in presynaptic waveform, EPSC kinetics, and synaptic plasticity". In: *Journal of Neuroscience* 20.24, pp. 9162–9173.

Tollin, D. J. (2003). "The lateral superior olive: a functional role in sound source localization". In: *The neuroscientist* 9.2, pp. 127–143.

Tollin, D. J. and Yin, T. C. (2005). "Interaural phase and level difference sensitivity in low-frequency neurons in the lateral superior olive". In: *Journal of Neuroscience* 25.46, pp. 10648–10657.

Trimmer, J. S. (2015). "Subcellular localization of K+ channels in mammalian brain neurons: remarkable precision in the midst of extraordinary complexity". In: *Neuron* 85.2, pp. 238–256.

Tsuchitani, C. (1997). "Input from the medial nucleus of trapezoid body to an interaural level detector". In: *Hearing research* 105.1-2, pp. 211–224.

Von Gersdorff, H. and Borst, J. G. G. (2002). "Short-term plasticity at the calyx of Held". In: *Nature Reviews Neuroscience* 3.1, p. 53.

Wadel, K., Neher, E., and Sakaba, T. (2007). "The coupling between synaptic vesicles and Ca2+ channels determines fast neurotransmitter release". In: *Neuron* 53.4, pp. 563–575.

Wang, L.-Y., Gan, L., Forsythe, I. D., and Kaczmarek, L. K. (1998). "Contribution of the Kv3. 1 potassium channel to high-frequency firing in mouse auditory neurones". In: *The Journal of physiology* 509.1, pp. 183–194.

Wang, L.-Y. and Kaczmarek, L. K. (1998). "High-frequency firing helps replenish the readily releasable pool of synaptic vesicles". In: *Nature* 394.6691, p. 384.

Wang, L.-Y., Neher, E., and Taschenberger, H. (2008). "Synaptic vesicles in mature calyx of Held synapses sense higher nanodomain calcium concentrations during action potential-evoked glutamate release". In: *Journal of Neuroscience* 28.53, pp. 14450–14458.

Waters, M. F., Minassian, N. A., Stevanin, G., Figueroa, K. P., Bannister, J. P., Nolte, D., Mock, A. F., Evidente, V. G. H., Fee, D. B., Müller, U., et al. (2006). "Mutations in voltage-gated potassium channel KCNC3 cause degenerative and developmental central nervous system phenotypes". In: *Nature genetics* 38.4, p. 447.

Weiser, M., De Miera, E. V.-S., Kentros, C., Moreno, H., Franzen, L., Hillman, D., Baker, H., and Rudy, B. (1994). "Differential expression of Shaw-related K+ channels in the rat central nervous system". In: *Journal of Neuroscience* 14.3, pp. 949–972.

Wong, A. Y., Graham, B. P., Billups, B., and Forsythe, I. D. (2003). "Distinguishing between presynaptic and postsynaptic mechanisms of short-term depression during action potential trains". In: *Journal of Neuroscience* 23.12, pp. 4868–4877.

Wu, L.-G., Westenbroek, R. E., Borst, J. G. G., Catterall, W. A., and Sakmann, B. (1999). "Calcium channel types with distinct presynaptic localization couple differentially to transmitter release in single calyx-type synapses". In: *Journal of Neuroscience* 19.2, pp. 726–736.

Wu, S. H. and Kelly, J. B. (1993). "Response of neurons in the lateral superior olive and medial nucleus of the trapezoid body to repetitive stimulation: intracellular and extracellular recordings from mouse brain slice". In: *Hearing research* 68.2, pp. 189–201.

Xu, M., Cao, R., Xiao, R., Zhu, M. X., and Gu, C. (2007). "The axon–dendrite targeting of Kv3 (Shaw) channels is determined by a targeting motif that associates with the T1 domain and ankyrin G". In: *Journal of Neuroscience* 27.51, pp. 14158–14170.

Yang, Y.-M. and Wang, L.-Y. (2006). "Amplitude and kinetics of action potential-evoked Ca2+ current and its efficacy in triggering transmitter release at the developing calyx of held synapse". In: *Journal of Neuroscience* 26.21, pp. 5698–5708.

Yellen, G., Sodickson, D., Chen, T.-Y., and Jurman, M. E. (1994). "An engineered cysteine in the external mouth of a K+ channel allows inactivation to be modulated by metal binding". In: *Biophysical Journal* 66.4, pp. 1068–1075.

Yeung, S. Y. M., Thompson, D., Wang, Z., Fedida, D., and Robertson, B. (2005). "Modulation of Kv3 subfamily potassium currents by the sea anemone toxin BDS: significance for CNS and biophysical studies". In: *Journal of Neuroscience* 25.38, pp. 8735–8745.

Zettel, M. L., Zhu, X., O'Neill, W. E., and Frisina, R. D. (2007). "Age-related decline in Kv3. 1b expression in the mouse auditory brainstem correlates with functional deficits in the medial olivocochlear efferent system". In: *Journal for the Association for Research in Otolaryngology* 8.2, pp. 280–293.

Zhang, Y. and Kaczmarek, L. K. (2016). "Kv3. 3 potassium channels and spinocerebellar ataxia". In: *The Journal of physiology* 594.16, pp. 4677–4684.

Zhang, Y., Zhang, X.-F., Fleming, M. R., Amiri, A., El-Hassar, L., Surguchev, A. A., Hyland, C., Jenkins, D. P., Desai, R., Brown, M. R., et al. (2016). "Kv3. 3 channels bind Hax-1 and Arp2/3 to assemble a stable local actin network that regulates channel gating". In: *Cell* 165.2, pp. 434–448.

Zhao, J., Zhu, J., and Thornhill, W. B. (2013). "Spinocerebellar ataxia-13 Kv3. 3 potassium channels: arginine-to-histidine mutations affect both functional and protein expression on the cell surface". In: *Biochemical Journal* 454.2, pp. 259–265.